

AD-A012 269

INVESTIGATION OF BRITTLE FRACTURES IN GRAPHITE-
EPOXY COMPOSITES SUBJECTED TO IMPACT

L. B. Greszczuk, et al

McDonnell Douglas Astronautics Company

Prepared for:

Army Air Mobility Research and Development
Laboratory

May 1975

DISTRIBUTED BY:

NTIS

National Technical Information Service
U. S. DEPARTMENT OF COMMERCE

204069

USAAMRDL-TR-75-15



**INVESTIGATION OF BRITTLE FRACTURES IN GRAPHITE-EPOXY
COMPOSITES SUBJECTED TO IMPACT**

McDonnell Douglas Astronautics Company
5301 Bolsa Avenue
Huntington Beach, Calif. 92647

AD A012269

May 1975

Final Report

Approved for public release;
distribution unlimited.

Prepared for

EUSTIS DIRECTORATE

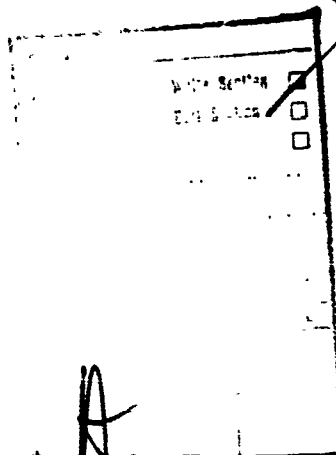
U. S. ARMY AIR MOBILITY RESEARCH AND DEVELOPMENT LABORATORY
Fort Eustis, Va. 23604

Reproduced by
**NATIONAL TECHNICAL
INFORMATION SERVICE**
U.S. Department of Commerce
Springfield, VA. 22151

EUSTIS DIRECTORATE POSITION STATEMENT

This report describes an analytical technique for determining impact damage in multilayer composite plates having different fiber orientations. The analysis was verified by a test program. The analytical technique can be used to determine impact resistance of new composite materials that are proposed for Army aircraft structures.

Duane M. Saylor of the Technology Applications Division served as project engineer for this effort.



DISCLAIMERS

The findings in this report are not to be construed as an official Department of the Army position unless so designated by other authorized documents.

When Government drawings, specifications, or other data are used for any purpose other than in connection with a definitely related Government procurement operation, the United States Government thereby incurs no responsibility nor any obligation whatsoever; and the fact that the Government may have formulated, furnished, or in any way supplied the said drawings, specifications, or other data is not to be regarded by implication or otherwise as in any manner licensing the holder or any other person or corporation, or conveying any rights or permission, to manufacture, use, or sell any patented invention that may in any way be related thereto.

Trade names cited in this report do not constitute an official endorsement or approval of the use of such commercial hardware or software.

DISPOSITION INSTRUCTIONS

Destroy this report when no longer needed. Do not return it to the originator.

Unclassified

SECURITY CLASSIFICATION OF THIS PAGE (When Data Entered)

| REPORT DOCUMENTATION PAGE | | READ INSTRUCTIONS BEFORE COMPLETING FORM |
|---|-----------------------|---|
| 1. REPORT NUMBER USAAMRDL-TR-75-15 | 2. GOVT ACCESSION NO. | 3. RECIPIENT'S CATALOG NUMBER ADA-2201 |
| 4. TITLE (and Subtitle) Investigation of Brittle Fractures in Graphite-Epoxy Composites Subjected to Impact | | 5. TYPE OF REPORT & PERIOD COVERED Final Report |
| | | 6. PERFORMING ORG. REPORT NUMBER MDC G5656 |
| 7. AUTHOR(s) L. B. Greszczuk H. Chao | | 8. CONTRACT OR GRANT NUMBER(s) DAAJ02-74-C-0009 |
| 9. PERFORMING ORGANIZATION NAME AND ADDRESS McDonnell Douglas Astronautics Company 5301 Bolsa Avenue Huntington Beach, California 92647 | | 10. PROGRAM ELEMENT, PROJECT, TASK AREA & WORK UNIT NUMBERS 62208A 1F262208AH90 02 003 EK |
| 11. CONTROLLING OFFICE NAME AND ADDRESS Eustis Directorate U. S. Army Air Mobility R&D Laboratory Fort Eustis, VA. 23604 | | 12. REPORT DATE May 1975 |
| 14. MONITORING AGENCY NAME & ADDRESS (if different from Controlling Office) | | 13. NUMBER OF PAGES 217 |
| | | 15. SECURITY CLASS. (of this report) Unclassified |
| | | 15a. DECLASSIFICATION/DOWNGRADING SCHEDULE |
| 16. DISTRIBUTION STATEMENT (of this Report) proved for public release; distribution unlimited. | | |
| 17. DISTRIBUTION STATEMENT (of the abstract entered in Block 20, if different from Report) | | |
| 18. SUPPLEMENTARY NOTES | | |
| PRICES SUBJECT TO CHANGE | | |
| 19. KEY WORDS (Continue on reverse side if necessary and identify by block number) Impact Impact Damage Composites Impact Theory Graphite Fibers Hybrid Composites Brittle Fracture | | |
| 20. ABSTRACT (Continue on reverse side if necessary and identify by block number) The principal objectives of this program were (1) to establish how the brittle fracture characteristics of graphite-epoxy composites subjected to impact are influenced by such parameters as fiber and matrix properties, fiber orientation, stacking sequence, laminate thickness, curvature effects and interleaving effects and (2) to recommend solutions to the brittle fracture problem. To accomplish these objectives, a three-phase program was conducted. Phase I involved a literature survey on the experimental and theoretical work on the brittle fracture of composites subjected to impact as well as a literature | | |

DD FORM 1 JAN 73 1473 EDITION OF 1 NOV 65 IS OBSOLETE

Unclassified

SECURITY CLASSIFICATION OF THIS PAGE (When Data Entered)
540-76

Unclassified

SECURITY CLASSIFICATION OF THIS PAGE(When Data Entered)

survey on failure theories for brittle, orthotropic, and anisotropic materials. In Phase II, available computer solutions such as SAAS III, ASAAS and CYLINDER were modified and/or extended to the problems of determining the impact response of multilayer, generally orthotropic solids and multilayer orthotropic cylinders subjected to impact by an impactor in a form of a body of revolution. The quas. dynamic approach employed in studying the impact response of generally orthotropic plates involved (1) determination of the surface pressure in the composite target material caused by the impactor; (2) determination of the internal triaxial stresses due to the surface pressure; (3) determination of failure modes (local and overall) due to these stresses; and (4) determination of coupling between impact velocity, properties of target and failure modes. In studying the impact response of composite cylinders, a computer program capable of handling stress wave effects was used. The analytical techniques that were developed were used to study the influence of the following parameters on impact response: fiber and matrix properties, fiber layup and stacking sequence, thickness effects, curvature effects and hybridization. At the end of Phase II a test plan was prepared. In Phase III the test plan was implemented, which involved fabrication and impact testing of specimens. Types of graphite fibers used in the experimental program included Thornel 300, Modmor II and Celion GY-70. Types of resins investigated included 5208 epoxy, ERLA 4617 and polysulfone. Fiber layups investigated included unidirectional, 2:1 bidirectional, 1:1 bidirectional and tridirectional (pseudo-isotropic). In the case of tridirectional composites, three different stacking sequences were used to establish how the latter influences the impact response. Two types of hybrid composites that were investigated included Thornel 300/Fiberglass/5208 and Thornel 300/Kevlar 49/5208.

The investigation of the influence of specimen geometry included fabrication and impact testing of composite plates of three different thicknesses (0.066 in., 0.139 in. and 0.260 in.) and fabrication and testing of 3-in. - and 6-in. -diameter bidirectional Thornel 300/5208 composite cylinders. The important results of the theoretical and experimental studies were as follows: (1) Resistance to impact damage increases as the strength of the graphite fibers increases and the modulus of the fibers decreases; of the three fibers investigated, composites made with Thornel 300 showed best resistance to impact damage. (2) Resistance to impact damage increases as the Young's modulus of the matrix decreases and the strength of the matrix increases. The energy level required to cause visible damage in composites made with polysulfone matrix and Thornel 300 fibers was almost an order of magnitude higher than that for composites made with other resins; the mechanical properties of the Thornel 300/polysulfone matrix were poor, however. (3) Bidirectional layup was more efficient in resisting impact damage than tridirectional or unidirectional layup. (4) Construction employing complete dispersion of layers (having different fiber orientation) through the thickness was more resistant to impact damage than construction in which the layers were not dispersed. (5) Effects of Hybridization on impact damage were inconclusive because of poor-quality test specimens. (6) Impact of a spherical impactor into cylindrical target or a flat target having unidirectional fiber layup resulted in an elliptical area of contact; whereas in plates having 1:1 bidirectional or tridirectional fiber layup, the area of contact was circular. (7) The visible damage resulting from impact consisted of transverse cracks, running parallel to the fibers, on the back face of the plates or cylinders. (8) Theoretical predictions of impact damage in composites showed fair correlation with test results; however, further refinement of the theory appears desirable.

Unclassified

SECURITY CLASSIFICATION OF THIS PAGE(When Data Entered)

PREFACE

This is the final report on the work performed under Eustis Directorate, U. S. Army Air Mobility Research and Development Laboratory Contract DAAJ02-74-C-0009, entitled "Investigation of Brittle Fractures in Graphite-Epoxy Composites." The report covers the period 7 November 1973 to 20 December 1974. The principal investigator for this study was L. B. Greszczuk. The U. S. Army Project Officer was Mr. D. Saylor. Significant contributions to this program were made by the following individuals. H. Toellner and R. Palmer of Douglas Aircraft Company in fabricating the composite specimens; A. Puetz and R. Snell in impact testing; H. Chane in analysis of impact response of cylinders; J. Desrosiers in mechanical properties testing of composites.

TABLE OF CONTENTS

| | Page |
|---|------|
| PREFACE | 3 |
| LIST OF ILLUSTRATIONS | 6 |
| LIST OF TABLES | 13 |
| INTRODUCTION | 16 |
| SECTION I - LITERATURE SURVEY RELATIVE TO IMPACT BEHAVIOR AND BRITTLE FRACTURE IN GRAPHITE-EPOXY COMPOSITES | 17 |
| SECTION II - THEORY DEVELOPMENT FOR PREDICTING THE RESPONSE OF COMPOSITES TO IMPACT LOADING | 25 |
| SECTION III - THEORY APPLICATION | 65 |
| SECTION IV - DESCRIPTION OF MATERIALS AND SPECIMENS USED IN THE TEST PROGRAM | 127 |
| SECTION V - EXPERIMENTAL STUDIES ON IMPACT RESPONSE OF COMPOSITES | 138 |
| SECTION VI - EVALUATION OF RESULTS, CONCLUSIONS, AND RECOMMENDATIONS | 194 |
| REFERENCES | 201 |
| BIBLIOGRAPHY | 208 |
| LIST OF SYMBOLS | 213 |

Preceding page blank

LIST OF ILLUSTRATIONS

| Figure | | Page |
|--------|--|------|
| 1 | Essential Features of the Approach | 26 |
| 2 | Values of Parameters m , n , and s | 28 |
| 3 | Actual and Approximate Shape of the Area of Contact Resulting From an Indentation or Impact of a Rigid Spherical Body Into Generally Orthotropic Composite Material | 33 |
| 4 | Planar or Transversely Isotropic Multilayer Material . | 36 |
| 5 | Internal Stress Distribution in Semi-Infinite Multilayer Planar Isotropic Material Resulting From Surface Pressure Caused by Foreign Object Impact ($E_1/E_2 = 0.35$) | 37 |
| 6 | Internal Stress Distribution in Semi-Infinite Multilayer Planar Isotropic Material Resulting From Surface Pressure Caused by Foreign Object Impact ($E_1/E_2 = 2.86$) | 38 |
| 7 | Generally Orthotropic Multilayer Material | 39 |
| 8 | Comparison of Solutions for Deflections in a Circular Isotropic Plate Subjected to Uniform Surface Pressure. | 44 |
| 9 | Variation of Young's Moduli and Shear Modulus as a Function of β | 45 |
| 10 | Variation of Poisson's Ratios as a Function of β | 46 |
| 11 | Comparison of Solutions for Deflections in a Circular Orthotropic Plate Subjected to Uniform Surface Pressure | 47 |
| 12 | Comparison of Solutions for Stresses in a Circular Orthotropic Plate Subjected to Uniform Surface Pressure | 49 |

LIST OF ILLUSTRATIONS (Continued)

| Figure | | Page |
|--------|--|------|
| 13 | Sample Problem Used in Modified ASAAS Code. | 52 |
| 14 | Model Used in the Cylinder Code | 56 |
| 15 | Area of Contact and Pressure/Load Distribution. . . . | 57 |
| 16 | Actual and Computer Idealization of Pressure-Time Distribution | 57 |
| 17 | Variation of Impact-Induced Stresses (at $s = 0$) as a Function of Time and Axial Coordinate, x | 58 |
| 18 | Variation of Impact-Induced Stresses (at $x = 0$) as a Function of Time and Circumferential Coordinate, s . | 60 |
| 19 | Variation of Stresses at $x = 0$, $s = 0$ as a Function of Time | 61 |
| 20 | Initiation and Growth of Failure in a Multilayer Composite Cylinder Subjected to Impact | 62 |
| 21 | Failure in Various Layers at $t = 15.4 \mu\text{sec}$ When Critical Damage Occurs (Failure of Layer Number 1 in the Fiber Direction | 63 |
| 22 | Test-Theory Comparison of Tensile Strength and Young's Modulus of Pseudo-Isotropic Composites Made of Various Fiber-Matrix Combinations. | 72 |
| 23 | Correlation Between Compressive Strength and Compressive Modulus of Epoxy Resins | 74 |
| 24 | Correlation Between Transverse Young's Modulus and Transverse Compressive Strength of Graphite-Epoxy Composites | 77 |
| 25 | Maximum Surface Pressure Versus Impact Velocity. . | 80 |
| 26 | Contact Duration Between Target and Impactor Versus Impact Velocity | 81 |
| 27 | Nondimensional Contact Radius as a Function of Impact Velocity | 82 |
| 28 | Grid Used in the Computer Solution. | 84 |

LIST OF ILLUSTRATIONS (Continued)

| Figure | | Page |
|--------|--|------|
| 29 | Equivalent Stress Contours for Celion GY70-Epoxy (Material No. 2) Subjected to $q_0 = 100$ ksi | 85 |
| 30 | Equivalent Stress Contours for Thornel 300-Epoxy (Material No. 6) Subjected to $q_0 = 100$ ksi | 86 |
| 31 | Damage Resulting From a 100-In. /Sec Impact of a 0.15-In. -Diameter Steel Sphere Into Semi-Infinite Composite Targets Made of Thornel 300 Fibers and Different Resins | 90 |
| 32 | Radial Stress At Center of Circular Plate ($D = \text{constant}$) | 92 |
| 33 | Radial Stress At Center of Plate ($H = \text{constant}$). | 93 |
| 34 | Influence of Plate Thickness on Local and Plate Bending Deformations at the Edge of the Area of Contact | 95 |
| 35 | Influence of Plate Radius on Local and Plate Bending Deformations at the Edge of the Area of Contact | 96 |
| 36 | Influence of Plate Thickness on Maximum Surface Pressure at Which Failure Initiates at a Point in a Plate | 97 |
| 37 | Influence of Plate Radius on Maximum Surface Pressure at Which Failure Initiates at a Point in a Plate. | 98 |
| 38 | Increase of Maximum Surface Pressure With Time | 99 |
| 39 | Increase in Damage Zone (Shaded Area) With Increasing Surface Pressure or Time (See Figure 38) in a Semi-Infinite Target. | 100 |
| 40 | Initiation and Growth of Failure Zone with Increasing Surface Pressure (or Increasing Impact Velocity) | 102 |
| 41 | Increase in Damage Zone as a Function of Increasing Surface Pressure and/or Increasing Impact Velocity ($R/H = \text{Constant}$). | 103 |
| 42 | Influence of Plate Boundary Conditions on Impact Response ($v = 50$ In. /Sec, $q_0 = 102$ ksi). | 105 |

LIST OF ILLUSTRATIONS (Continued)

| Figure | | Page |
|--------|--|------|
| 43 | Foreign Object Impact-Induced Damage in Unidirectional Thornel 300-Epoxy Composite | 107 |
| 44 | Foreign Object Impact-Induced Damage in 1:1 Bidirectional Thornel 300-Epoxy Composite | 108 |
| 45 | Foreign Object Impact-Induced Damage in Tridirectional Thornel 300-Epoxy Composite (Material In-Plane Pseudo-Isotropic) | 109 |
| 46 | Foreign Object Impact Damage in a Tridirectional Thornel 300-Epoxy Composite Subjected to 50-In./Sec Impact by a 1.5-In.-Diameter Steel Sphere. | 110 |
| 47 | Foreign Object Impact-Induced Damage in a Bidirectional Thornel 300-Epoxy Plate Having Nine-Layer Dispersed Construction | 112 |
| 48 | Foreign Object Impact-Induced Damage in a Bidirectional Thornel 300-Epoxy Plate Having Three-Layer Construction | 113 |
| 49 | Impact Damage on the Top Surface (Impacted Surface) of a Nine-Layer Bidirectional Thornel 300-Epoxy Plate | 114 |
| 50 | Surface Damage Caused by Impact of a 1.5-In.-Diameter Steel Ball | 115 |
| 51 | Material Configurations for Studying the Influence of Hybridization on Impact Response | 116 |
| 52 | Damage Zone in 3-In.-Diameter Glass-Epoxy-Thornel 300-Epoxy Hybrid Composite Plates Subjected to 30-In./Sec Impact by a 1.5-In.-Diameter Steel Impactor | 117 |
| 53 | Damage Zone in 3-In.-Diameter Hybrid Composite Plates Subjected to 50-In./Sec Impact by a 1.5-In.-Diameter Steel Impactor. | 118 |
| 54 | Damage Zone in 3-in.-Diameter PRD 49-Epoxy/Thornel 300-Epoxy Hybrid Composite Plates Subjected to 30-In./Sec Impact by a 1.5-In.-Diameter Steel Impactor | 121 |

LIST OF ILLUSTRATIONS (Continued)

| Figure | | Page |
|--------|---|------|
| 55 | Damage Zone in 3-In. -Diameter PRD 49-Epoxy/ Thornel 300-Epoxy Hybrid Composite Plates Subjected to 50-In. /Sec Impact by a 1.5-In. -Diameter Steel Impactor | 122 |
| 56 | Cylinder Geometry and Material Distribution Through the Wall Thickness of the Cylinder | 123 |
| 57 | Test Specimens for Measuring the Mechanical Properties of Thornel 300-5208 Unidirectional Composite | 132 |
| 58 | Failed Specimens (Typical Results) | 133 |
| 59 | Test Setup for Low-Velocity Impact | 139 |
| 60 | Test Setup and Instrumentation | 140 |
| 61 | Test Specimens and Supports | 141 |
| 62 | Cylindrical Test Specimens | 142 |
| 63 | Oscilloscope Traces From Instrumented Aluminum Plate Impacted at 100 In. /Sec With a 1.5-In. -Diameter Steel Sphere | 145 |
| 64 | Back Face Impact Damage in Composite Plates Made With Three Different Reinforcing Fibers | 147 |
| 65 | Impact Site and Corresponding Damage on the Back Surface in Composite Plates Made With Thornel 300 Fibers and ERLA 4617 (Specimen 1.2a) or APCO Resin. | 151 |
| 66 | Impact Damage in Thornel 300-Polysulfone as a Function of Impact Velocity | 153 |
| 67 | Damage on the Top Face in Thornel 300-Polysulfone Composite Plate | 155 |
| 68 | Impact Damage in Composite Plates Having Different Fiber Orientations | 159 |

LIST OF ILLUSTRATIONS (Continued)

| Figure | | Page |
|--------|--|------|
| 69 | Impact Damage in Composite Plates Having Different Fiber Stacking Sequences | 163 |
| 70 | Impact Damage in 0.066-In. - Thick Thornel 300-5208 Composite Plates | 164 |
| 71 | Impact Damage in 0.25-In. - Thick Thornel 300-5208 Composite Plates as a Function of Increasing Impact Velocity | 165 |
| 72 | Impact Damage in Thornel 300-APCO Resin Composite Plate | 167 |
| 73 | Ultrasonic Attenuation Through the Impacted Regions . | 169 |
| 74 | Change in Longitudinal Wave Velocity Through the Impacted Regions | 169 |
| 75 | Impact Damage in Thornel 300-Fiberglass-5208 Epoxy Hybrid Composite Having Dispersed Construction . . . | 171 |
| 76 | Impact Damage in Three-Layer Thornel 300-Fiberglass-5208 Epoxy Hybrid Composite Plate. | 173 |
| 77 | Resin Surface Cracks in Thornel 300-Kevlar 49 Hybrid Composite Plate Prior to Testing; (Cracks are in Kevlar 49) | 175 |
| 78 | Impact Damage in Thornel 300-Kevlar 49-5208 Epoxy Hybrid Composite Plate Having Dispersed Construction | 176 |
| 79 | Impact Damage in Three-Layer Thornel 300-Kevlar 49-5208 Epoxy Hybrid Composite Plates | 177 |
| 80 | Shape of the Area of Contact Resulting From a 100-In. /Sec Impact of a 1.5-In. - Diameter Steel Sphere into Cylindrical Targets. | 181 |
| 81 | Impact Damage on the Inner Surface of 6-In. - Diameter Cylinders. | 182 |
| 82 | Impact-Induced Strains in Pseudo-Isotropic Modmor II-5208 Composite Plate (Specimen 1.1c) at $r = 0$ | 184 |

LIST OF ILLUSTRATIONS (Continued)

| Figure | | Page |
|--------|--|------|
| 83 | Impact-Induced Strains in Pseudo-Isotropic Modmor II-5208 Composite Plate (Specimen 1.1c) at $r = R/4$ and $r = R/2$ | 185 |
| 84 | Impact-Induced Strains in Pseudo-Isotropic Thornel 300-5208 Composite Plate (Specimen 1.1b) at $r = 0$ | 186 |
| 85 | Influence of Repeated Impacts on Strain-Time Response (Thornel 300-5208 Pseudo-Isotropic Laminate Designated 1.1b). | 187 |
| 86 | Impact-Induced Strains in 2:1 Bidirectional Thornel 300-5208 Composite Plate (Specimen 1.3c) Subjected to 100-In./Sec Impact | 188 |
| 87 | Impact-Induced Strains in 6-In. - Diameter, 2:1 Bidirectional Thornel 300-5208 Composite Cylinder | 192 |
| 88 | Impact-Induced Strains in 3-In. - Diameter, 2:1 Bidirectional Thornel 300-5208 Composite Cylinder | 193 |
| 89 | Influence of Plate Thickness on Impact-Induced Pressure Which Initiates Bending Failure at the Back Face of the Plate. | 195 |

LIST OF TABLES

| Tables | Page |
|--|------|
| I Normal Stresses in Orthotropic Solid | 50 |
| II Radial Stresses in Orthotropic Solid | 51 |
| III Yarn, Tow and Filament Properties | 66 |
| IV Properties of Fibers and Composites | 67 |
| V Properties of Thornel 300 Graphite-Fiber Composites. | 68 |
| VI Properties of the Candidate Groups of Composites . . | 69 |
| VII Properties of Pseudo-Isotropic Laminates (Calculated) | 71 |
| VIII Properties of the Candidate Composite Materials . . . | 73 |
| IX Properties of Candidate Resins (Estimated) | 75 |
| X Properties of Unidirectional Composites (Calculated) . | 75 |
| XI Properties of Transversely Isotropic Composite Materials Made With Resins Having Different Moduli . | 78 |
| XII Values of k_2 for Different Composites (Based on Properties Data Shown in Table VIII) | 79 |
| XIII Damage Zone for a Constant Surface Pressure ($q_0 = 100$ ksi). | 87 |
| XIV Damage Zone for a Constant Impact Velocity ($v = 100$ In. /Sec). | 87 |
| XV Relative Impact Velocities to Initiate Shear Failure at a Point Within the Target | 89 |
| XVI Relative Impact Velocity to Initiate Tensile Failures (at $r/a = 1$). | 89 |

LIST OF TABLES (Continued)

| Table | | Page |
|--------|--|------|
| XVII | Influence of Resin on Size of Damage Zone in Composites Made With Thornel 300 Fibers. | 89 |
| XVIII | Influence of Plate Boundary Conditions on Dimensions of Damage Zone Caused by 30 In. /Sec Impact by a 1.5-In. -Diameter Steel Sphere | 104 |
| XIX | Influence of Plate Boundary Conditions on Dimensions of Damage Zone Caused by 50 In. /Sec Impact by a 1.5-In. -Diameter Steel Impactor | 104 |
| XX | Influence of Combining Materials on the Size of Damage Zone Resulting From a 30-In. /Sec Impact by a 1.5-In. -Diameter Steel Sphere | 119 |
| XXI | Influence of Combining Materials on the Size of Damage Zone Resulting From a 50-In. /Sec Impact by a 1.5-In. -Diameter Steel Sphere. | 120 |
| XXII | Influence of Target Curvature on Impact Parameters . | 125 |
| XXIII | Failure Mode, Location and Sequence in 3-In. - and 6-In. -Diameter Cylinders. | 126 |
| XXIV | Reinforcement and Matrix Materials | 128 |
| XXV | Mechanical Properties Data From QC Tests | 129 |
| XXVI | Average Mechanical Properties for Thornel 300-5208 Unidirectional Composites (Measured Data). | 134 |
| XXVII | Description of Fiber and Resin Materials and Fiber Patterns in Various Panels and Cylinders | 135 |
| XXVIII | Test Variables and Specimens for Investigating | 136 |
| XXIX | Description of Composite Specimens | 137 |
| XXX | Specimen Instrumentation | 144 |
| XXXI | Influence of Fiber Properties on Experimentally Observed Impact Damage | 149 |

LIST OF TABLES (Continued)

| Table | | Page |
|---------|---|------|
| XXXII | Influence of Resin Properties on Experimentally Observed Impact Damage | 156 |
| XXXIII | Influence of Fiber Orientation on Experimentally Observed Impact Damage | 158 |
| XXXIV | Influence of Stacking Sequence on Experimentally Observed Impact Damage | 161 |
| XXXV | Influence of Plate Thickness on Experimentally Observed Impact Damage | 162 |
| XXXVI | Impact Damage in Hybrid Composites | 170 |
| XXXVII | Influence of Curvature on Experimentally Observed Impact Damage. | 179 |
| XXXVIII | Test Data From Instrumented Composite Plate Tests . | 191 |

INTRODUCTION

During the past decade, significant progress has been made in developing advanced composites possessing high strength, high modulus, and low density, and in understanding their behavior under certain types of loading. As a result, composites such as boron-epoxy and graphite epoxy have been successfully employed as structural materials in aircraft, missiles, and space vehicles, and have satisfactorily demonstrated their performance through extensive ground testing and in flight. Moreover, the application of these composite materials to various structural components of aerospace vehicles has demonstrated significant (10 to ~50%) weight savings over comparable components made of conventional metals.

Despite the tremendous advantages that advanced composites have over metals in applications requiring high strength, high stiffness, and low weight, in applications where impact by foreign objects is a design consideration, the advantages inherent in composites are overshadowed by their poor resistance to impact loading. The severity of this problem was demonstrated when a major aerospace company attempted to use graphite-epoxy turbine blades in one of its production engines. During a test flight through a rain storm, the turbine blades were severely damaged and eroded and, although the plane landed safely, the near-disaster created an impetus for an in-depth understanding of the problem and a search for means to overcome it. Numerous other reports in the open literature dealing with the response of advanced composites to various types of impact have further increased the need for a better understanding of the problem so that the survivability of composites under various types of impact loading can be increased.

The studies presented in this report are oriented toward this need; that is, toward understanding brittle fracture in graphite-epoxy composites subjected to foreign-object impact. The approach used in studying the problem consists of experimental and theoretical efforts and is discussed in detail in the sections that follow.

SECTION I

LITERATURE SURVEY RELATIVE TO IMPACT BEHAVIOR AND BRITTLE FRACTURE IN GRAPHITE-EPOXY COMPOSITES

A literature survey was conducted on brittle fracture in graphite-epoxy composites subjected to impact loading, and a bibliography was compiled on the subject. In order for the results obtained from the literature survey to be of maximum benefit to this program, papers and publications dealing with the following areas were sought, reviewed, and evaluated:

1. Brittle fracture of composites under static loading, including strength prediction from given loading.
2. Behavior of composites under impact loading (experimental and theoretical work).
3. Brittle fracture of composites under impact loading (experimental and theoretical work).
4. Test methods, specimens, and condition, for assessment of impact response of brittle composites.
5. Material design concepts for improving impact resistance of composites (hybrid composites, protective coatings, etc.).
6. Other pertinent work on the subject such as stress-wave response of composites and failure in brittle materials under impact.

The results of the literature survey are presented under three main subheadings: (1) Behavior of Composites Under Impact Loading, (2) Failure Criteria for Brittle, Orthotropic, Anisotropic, and Composite Materials, and (3) Stress-Wave Response of Composite Materials.

BEHAVIOR OF COMPOSITES UNDER IMPACT LOADING

Material dealing with the behavior of composites subjected to impact loading has only recently begun appearing in the literature. The amount of literature in this area is still quite limited. Brief summaries of the more pertinent papers related to impact response of composites and anisotropic materials are presented below.

A number of papers on the behavior of composites, including graphite-epoxy composites, subjected to various types of impact loading were presented at a recent ASTM Symposium on Foreign Object Behavior of Composites, held in Philadelphia, Pennsylvania, in September 1973. The papers that were presented will appear as an ASTM Special Technical Publication (STP), which will also include some papers that were not presented at the symposium. *

The symposium focused on the understanding of the foreign-body impact failure mechanism of filamentary composites, identification of suitable tests for impact response studies, experimental studies on performance of composite laminates and sandwich construction under impact conditions, and the selection and evaluation of suitable protective coating materials or design techniques for increasing the survivability of composites in impact-type environments.

Several of the papers that contained data and results directly applicable to this program are briefly described below.

In a paper by Oplinger and Slepetz¹, test results are presented on the behavior of sandwich panels with faces made of different composites and subjected to falling-weight impact tests. The variables in this study were different types of composite materials, fiber orientation and layup, sandwich core density, and loading parameters. Strength measurements were made on the initial test specimens and also on specimens that were subjected to impact loading. Sandwich panels made with graphite-epoxy faces were shown to be more susceptible to impact damage than similar panels made with S-glass-epoxy faces. The poor impact strength of graphite-epoxy composites was attributed to their low strains to failure.

The investigation described by Broutmen, Rotem, and Zych⁶ involved impact testing of various composites using an instrumented drop-weight impact machine and a more conventional instrumented Charpy impact machine. Various failure modes were discussed, as well as the influence of composite materials and lamination on the failure modes caused by impact. Instrumented Charpy testing was also used in the studies

*References 1 through 12, listed on page 201, are the papers that were presented at the ASTM Symposium. References 13 and 14 are the papers that were not presented. Individual references will be cited throughout where discussed.

¹Oplinger, D. W., and Slepetz, J. M., IMPACT DAMAGE TOLERANCE OF GRAPHITE/EPOXY SANDWICH PANELS, U.S. Army Materials and Mechanics Research Center, Watertown, Mass., September 1973.

⁶Broutmen, L. J., Rotem, A., and Zych, J., IMPACT ENERGY OF GLASS FIBER AND GLASS-CARBON FIBER HYBRID COMPOSITES, Illinois Institute of Technology, Chicago, Illinois, September 1973.

reported by Beaumont, Riewald, and Zweben⁷. The instrumentation was such that both the impact loads and the impact energy histories were measured. Types of materials investigated included unidirectional E-glass-epoxy, PRD-49-epoxy, and graphite-epoxy composites. Impact behavior of hybrid composites consisting of high-modulus graphite and PRD-49 fibers in epoxy matrix was also investigated. Hybridization was shown to increase the "impact strength" by a factor of 10 in comparison to that of all-graphite composites.

The paper by Greszczuk¹⁰ presents theoretical studies on the response of isotropic and composite materials to particle impact. Solutions are given therein for the magnitude and distribution of the time-dependent pressure resulting from particle impact, internal triaxial stresses in the target caused by the surface pressure, and the target failure modes caused by the internal stresses. Types of composite materials for which results are presented include glass-, boron-, and graphite-epoxy. It is shown that the impact resistance of materials is governed by elastic and strength properties of the target materials, and that the sequence of failure modes changes as the mechanical properties of the composite are changed.

In addition to papers described above, a number of other papers and publications were found concerning the behavior of composites under impact loading.

A paper by Chamis, Hanson, and Serafini¹⁵ contains theoretical and experimental studies on the impact resistance of unidirectional composites made with S-glass, PRD-49, and various types of graphite fibers, as well as on the impact resistance of hybrid composites. Miniature Izod and longitudinal impact tests were used in the experimental portion of this investigation to evaluate the impact resistance of unidirectional composites in the longitudinal and transverse directions. Impact resistance for the shear loading is also investigated experimentally. Experimental and theoretical results are also presented on failure modes associated with impact loading of specimens described above. Types of failures observed in various types of composites include

⁷Beaumont, P. W., Riewald, P. G., and Zweben, C., THE IMPACT FRACTURE CHARACTERISTICS OF SOME FIBER-STRENGTHENED EPOXY RESIN SYSTEMS, E. I. duPont de Nemours and Company, Incorporated, Wilmington, Delaware, September 1973.

¹⁰Greszczuk, L. B., RESPONSE OF ISOTROPIC AND COMPOSITE MATERIALS TO PARTICLE IMPACT, McDonnell Douglas Astronautics Company, Huntington Beach, California, September 1973.

¹⁵Chamis, C. C., Hanson, M. P., and Serafini, T. T., IMPACT RESISTANCE OF UNIDIRECTIONAL FIBER COMPOSITES, IN COMPOSITE MATERIALS: TESTING AND DESIGN, American Society for Testing and Materials, ASTM STP 497, February 1972, pp. 324-349.

cleavage, fiber debonding and pullout, delaminations, matrix fracture, and fiber splitting. Impact strength in the transverse direction is shown to increase with increasing fiber tensile strength and decreasing fiber modulus.

A paper by Novak and DeCrescente¹⁶ presents Charpy impact strength for unidirectional graphite-, boron-, and glass-resin composites tested in the fiber direction. The impact strength of glass-resin is shown to be significantly higher than that of either the boron or the graphite composites. The mechanisms by which resin-matrix composites absorb energy are studied, and it is found that the tensile stress-strain characteristics of the fibers are of primary importance in determining the level of composite impact resistance. The toughness of the resin matrix is shown to represent a small contribution to composite impact energy. Increasing the impact strength of boron and graphite composites by the inclusion of glass fibers is discussed.

A recent report by Friedrich and Preston¹⁷ presents studies on impact resistance of composite blades used in aircraft turbine engines. Impact damage caused by steel, gelatin, and ice projectiles was investigated experimentally. Types of composites investigated included S-glass-epoxy, boron-epoxy, PRD-49-epoxy, various types of graphite-epoxy, and hybrid composites. Impact tests were performed on cantilevered flat plates and simulated fan-blade specimens consisting of cantilevered double-tapered specimens. Other variables investigated included mass and size of the projectile, impact velocity, impact angle, and material layup. Photomicrographs showing internal damage caused by impact onto various composite materials are also presented. The test results indicate that the most important factor in improving the impact resistance is to increase the transverse tensile strength of composites. A paper based on the above-described work was presented at the ASTM Symposium by Preston and Cook¹².

¹⁶Novak, R. C., and DeCrescente, M. A., IMPACT BEHAVIOR OF UNIDIRECTIONAL RESIN MATRIX COMPOSITES TESTED IN FIBER DIRECTION, IN COMPOSITE MATERIALS: TESTING AND DESIGN, American Society for Testing and Materials, ASTM STP 497, February 1972, pp. 311-323.

¹⁷Friedrich, A. L., and Preston, J. L., Jr., IMPACT RESISTANCE OF FIBER COMPOSITE BLADES USED IN AIRCRAFT TURBINE ENGINES, Pratt and Whitney Aircraft, Division of United Aircraft Corporation; NASA Technical Report CR-134502, National Aeronautics and Space Administration, NASA Lewis Research Center, Cleveland, Ohio, May 1973.

¹²Preston, J. L., Jr., and Cook, T. S., IMPACT RESPONSE OF GRAPHITE-EPOXY COMPOSITES TO SIMULATED AIRCRAFT ENGINE FOREIGN OBJECT DAMAGE ENVIRONMENTS, Pratt and Whitney Aircraft Corporation, Division of United Aircraft, East Hartford, Conn., Sept. 1973.

Another publication in the area of the response of graphite-epoxy turbofan blades subjected to impact is a report by Coppa¹⁸. Coppa describes experimental studies on the effects of simulated bird-carcass impact on graphite-epoxy turbofan blades, including test facilities and instrumentation that were utilized and the results that were obtained. Such quantities as energy and momentum transferred to the blades, blade impact forces, vibration frequencies, damping factors, dynamic tip deflections, and bending moments were evaluated.

A paper by Sayers and Harris¹⁹ is another recent publication related to application of graphite-epoxy composites to turbofan engine blades. The paper presents test results on the interlaminar shear strength of graphite-epoxy composites subjected to impact loading. Both static and drop-ball-impact interlaminar shear tests were conducted on unidirectional and cross-ply graphite-epoxy composites. The interlaminar shear strength from the impact tests was found to be about 70 percent of the static interlaminar shear strength. The static and impact tests lasted approximately 50 and 0.0007 seconds, respectively.

A paper by Bradshaw, Dorey, and Sidey²⁰ describes the various types of fracture observed in graphite-epoxy composites subjected to impact. These are discussed in terms of the fracture energies and the stresses to cause fracture. Experiments are described showing how component geometry and material variables affect both the elastic strain energy before fracture and the type and extent of impact fracture damage. Failure and design criteria for different applications are discussed. Suggested impact tests include threshold drop-weight or ballistic tests for determining the resistance against handling or repeated low-energy impact, and Izod or Charpy tests for containment. An assessment is made of the various material modifications for optimizing impact performance. These include fiber, matrix, interface, mixed carbon-glass fibers, and three-dimensional reinforcement.

¹⁸Coppa, A. P., MEASUREMENT OF TURBOFAN BLADE RESPONSE TO SIMULATED BIRD-CARCASS IMPACT, General Electric Report, 71 SD 266, December 1971.

¹⁹Sayers, K. H., and Harris, B., INTERLAMINAR SHEAR STRENGTH OF A CARBON FIBER REINFORCED COMPOSITE MATERIAL UNDER IMPACT CONDITIONS, J. Composite Materials, Vol. 7, January 1973, pp. 129-133.

²⁰Bradshaw, F. J., Dorey, G., and Sidey, G. R., IMPACT RESISTANCE OF CARBON FIBER REINFORCED PLASTICS, Royal Aircraft Establishment Technical Report 72240, March 1973.

A more recent paper by Dorey²¹ discusses fracture processes by which graphite-epoxy composites fail under impact loading and also gives the residual strengths and stiffnesses of several composites that have been subjected to drop-weight and ball-gun impact. Material modification aimed at minimizing certain types of impact damage are also described therein.

A recent report by Moon²² presents calculations for stresses and displacements induced in anisotropic plates by short-duration impact forces. The theoretical model attempts to model the response of fiber composite turbine fan blades to impact by foreign objects such as stones and hailstones. In this model, Hertzian impact theory is used in determining the impact force. The plate response treats the laminated blade as an equivalent anisotropic material, using a form of Mindlin's theory for crystal plates. The analysis makes use of a computational tool called the "fast Fourier transform." Results are presented in the form of stress contour plots in the plane of the plate for various times after impact. Examination of the maximum stresses due to impact versus ply layup angle reveals that the $\pm 15^\circ$ layup angle gives lower flexural stresses than 0° , $\pm 30^\circ$, and $\pm 45^\circ$ cases.

In another publication, Moon presents a survey of papers on wave propagation and impact response in composite materials.²³ The major portion of the references presented therein are on various wave propagation problems in composite materials.

²¹Dorey, G., FRACTURE BEHAVIOR AND RESIDUAL STRENGTH OF CARBON FIBER COMPOSITES SUBJECTED TO IMPACT LOADS, Paper B3, presented at the NATO AGARD Meeting, Munich, Germany, October 7-9, 1974.

²²Moon, F. C., THEORETICAL ANALYSIS OF IMPACT IN COMPOSITE PLATES, National Aeronautics and Space Administration Report NASA CR-121110, 1972.

²³Moon, F. C., A CRITICAL SURVEY OF WAVE PROPAGATION AND IMPACT IN COMPOSITE MATERIALS, National Aeronautics and Space Administration Report NASA CR-121226, May 1973.

Studies of Hertzian impact in anisotropic bodies have been made by Chen²⁴ and by Willis²⁵. Willis shows that the area of contact in anisotropic materials is elliptic, in contrast to its being a circle in isotropic materials. Earlier work (1964) by Svelko²⁶ considered the Hertzian contact problem in transversely isotropic materials. The solutions to the contact problem can also be obtained from the general theories presented by Lekhnitskii²⁷ and by Green and Zerna²⁸. It is noted here that by combining the solution for the contact problem with the solution for impact between two bodies, the solution for stresses in a target subjected to impact loading can be obtained¹⁰.

Other papers dealing with behavior of composites subjected to impact loading are given as References 24-51, and will be cited where discussed in this report.

FAILURE CRITERIA FOR BRITTLE, ORTHOTROPIC, ANISOTROPIC, AND COMPOSITE MATERIALS

To understand the brittle failure of graphite-epoxy composites requires an understanding of how such materials fail under multiaxial and combined loading. The failure criterion used in predicting impact-induced failures is therefore one of the key factors in understanding the material response. For this reason, and as a part of the literature survey, a bibliography has been compiled on the failure theories for brittle, orthotropic, anisotropic, and composite materials. The various publications dealing with failure of such materials are given in alphabetical order. Most of the papers are on failure of anisotropic and composite materials. Several pertinent references are also included on the failure of brittle, isotropic materials under static and impact loading.

Papers by Franklin, Kaminski and Lantz, Sandhu, and Sendekyj contain reviews and evaluations of a number of failure theories that are given in the literature. Many of the failure theories given in the bibliography are reviewed in a paper by Sandhu. Of the various failure

²⁴Chen, W. T., STRESSES IN SOME ANISOTROPIC MATERIALS DUE TO INDENTATION AND SLIDING, International Journal of Solids and Structures, Vol. 5, 1969, p. 191.

²⁵Willis, J. R., HERTZIAN CONTACT OF ANISOTROPIC BODIES, 1. Mechanics and Physics of Solids, Vol. 14, 1966, pp. 163-176.

²⁶Svelko, V. A., BOUSSINESQ-TYPE PROBLEM FOR ANISOTROPIC SEMISPACE, Prikladnaia Matematika i Mekhanika, Vol. 28, 1964, pp. 908-913.

²⁷Lekhnitskii, S. G., THEORY OF ELASTICITY OF AN ANISOTROPIC ELASTIC BODY, Holden-Day Inc., San Francisco, 1963.

²⁸Green, A. E., and Zerna, W., THEORETICAL ELASTICITY, Oxford at the Clarendon Press, 1954.

theories that exist, no one theory has been shown as THE theory for predicting the strength and failure modes of composites subjected to multiaxial and combined loading.

Stress-Wave Effects in Composite Materials

For certain impact problems involving composites, stress-wave effects have to be considered in studies of impact response. This is particularly true for high impact velocities ($v > 1000$ ft/sec). Although no studies of stress-wave effects were conducted in the program, nevertheless a brief survey was made of the problem.

A thorough review of studies on stress-wave propagation in composite materials is given by Moon²³. The review covers the period up to December 1972. The major properties of waves in composites are discussed, and the major experimental results in this field are summarized. Various theoretical models for analyzing wave propagation in laminated, fiber- and particle-reinforced composites are surveyed. The anisotropic, dispersive, and dissipative properties of stress pulses and shock waves in such materials are reviewed. A brief review of the behavior of composites under impact loading is presented together with the application of wave propagation concepts to the determination of impact stresses in composite plates. An extensive bibliography containing 211 entries is given in the report.

SECTION II

THEORY DEVELOPMENT FOR PREDICTING THE RESPONSE OF COMPOSITES TO IMPACT LOADING

The approach used in studying the response of composite targets to impact by foreign objects was similar to the approach described in References 10 and 46. Whereas the latter references dealt primarily with the response of isotropic and planar isotropic materials subjected to impact by spherical impactors, the results presented here apply to generally orthotropic targets (which can be solids of revolution) impacted by an isotropic or composite impactor in the form of a body of revolution. The approach that was employed is shown in schematic form in Figure 1, and consists of three main steps: (1) determination of time-dependent surface pressure distribution under an impacting particle, (2) determination of internal stresses in a generally orthotropic target caused by the surface pressure, and (3) determination of failure modes in the target caused by the internal stresses.

The pressure distribution under an impacting particle was obtained by analytically combining the dynamic solution to the problem of impact of bodies with the static solution for the pressure between two bodies in contact. Having the time-dependent surface pressure, the time-dependent triaxial stresses in targets made of composite materials were determined using finite-element computer solution. Knowing the internal triaxial stresses, the failure modes and failure envelopes were determined by applying failure criteria for generally orthotropic solids to the stress state in the target. The assumptions made in the theory development were as follows: (1) both the target and projectile are linear elastic, (2) impact duration is long compared to time intervals in stress-wave response, and (3) the projectile impact is normal to the target surface. Assumption (2) was made only in studies of impact response of flat composite plates. However, the studies on the impact response of composite cylinders did consider stress-wave effects.

-
46. Greszczuk, L. B., MECHANICS OF PARTICLE IMPACT, McDonnell Douglas Astronautics Company Report, MDC G2612, March 1973.

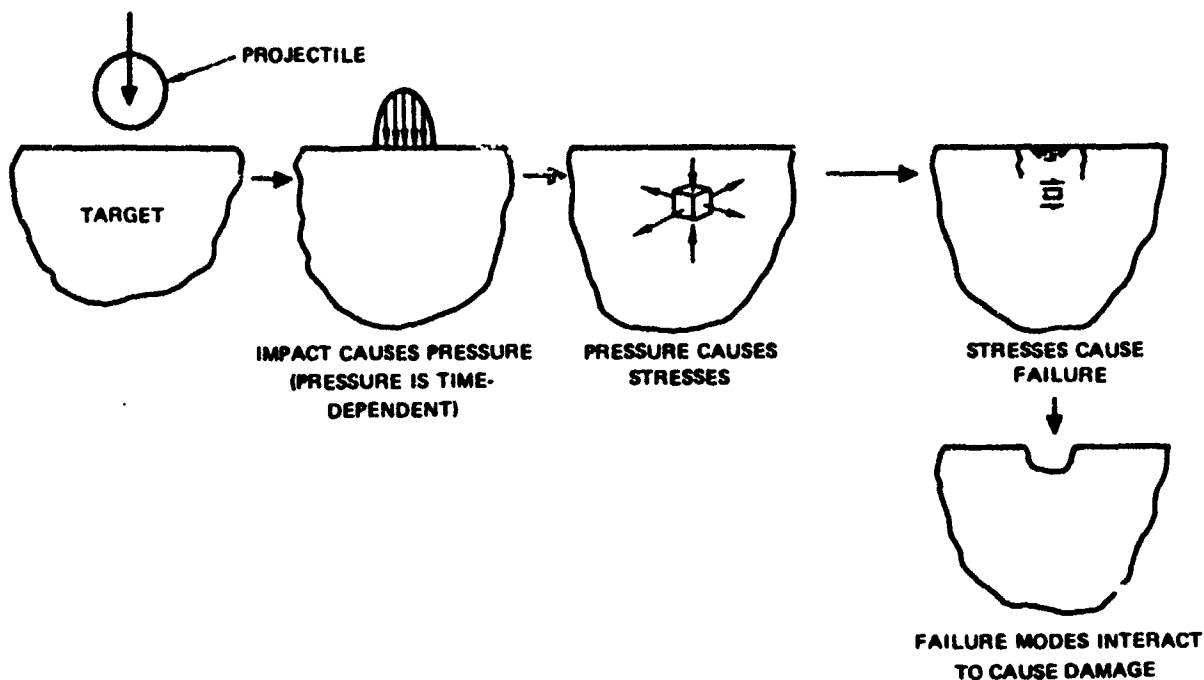


Figure 1. Essential Features of the Approach.

IMPACT BETWEEN TWO ORTHOTROPIC BODIES OF REVOLUTION

To enable determination of stresses and failure modes resulting from an impact of an arbitrary body of revolution into a flat or curved target made of composite materials, a generalized solution has been obtained for the area of contact, maximum surface pressure, pressure distribution, and impact duration for two arbitrary bodies of revolution. The results are readily applicable to special cases such as impact of a sphere or cylinder into flat, curved, and doubly curved semi-infinite targets. The solutions to the above-noted problems were obtained by analytically coupling the dynamic (non-stress-wave) solution for the problem of impact of bodies with the static solution for the pressure between two bodies in contact.^{10, 46, 52, 53}

52. Timoshenko, S., *THEORY OF ELASTICITY*, McGraw Hill Book Company, New York, 1934.
53. Belajef, W. M., *MEMOIRS ON THEORY OF STRUCTURES*, Izdatelstvo Puti (St. Petersburg), 1924. See also Belajef, *STRENGTH OF MATERIALS*, Gosudarstvennoje Izdatelstvo Tekh. - Teor. 1945 (In Russian).

Area of Contact Between Two Impacting Bodies

If a solid (or impactor designated by Subscript 1) having the maximum and minimum radii of curvature of R_{1m} and R_{1M} is pressed by a force P into a target (designated by Subscript 2) having the maximum and minimum radii of curvature R_{2m} and R_{2M} , the area of contact will be elliptical, with major and minor axes of ellipse being

$$a = m \left[\frac{3\pi}{2} P(k_1 + k_2) C_R \right]^{1/3} \quad (1)$$

$$b = n \left[\frac{3\pi}{2} P(k_1 + k_2) C_R \right]^{1/3} \quad (2)$$

where C_R is a term that takes into account the curvature effect

$$C_R^{-1} = \frac{1}{R_{1m}} + \frac{1}{R_{2m}} + \frac{1}{R_{1M}} + \frac{1}{R_{2M}} \quad (3)$$

k_1 and k_2 are the parameters that take into account the properties of the impactor and the targets and are defined later; m and n are parameters that are a function of R_{1m} , R_{1M} , R_{2m} and R_{2M} ⁵². The numerical values for m , n , and s (which is used later) are shown in Figure 2. These are plotted as a function of θ where

$$\theta = \arccos \left\{ C_R \left[\left(\frac{1}{R_{1m}} - \frac{1}{R_{1M}} \right)^2 + \left(\frac{1}{R_{2m}} - \frac{1}{R_{2M}} \right)^2 + 2 \left(\frac{1}{R_{1m}} - \frac{1}{R_{1M}} \right) \left(\frac{1}{R_{2m}} - \frac{1}{R_{2M}} \right) \cos 2\phi \right]^{1/2} \right\} \quad (4)$$

and ϕ is the angle between planes containing R_{1m} and R_{2m} .

If the two bodies are pressed together by a force P , the combined deformation of both bodies can be expressed in terms of similar parameters. The maximum deformation, α_1 , is

$$\alpha_1 = S \left[\frac{9\pi^2 P^2 (k_1 + k_2)^2}{256 C_R} \right]^{1/3} \quad (5)$$

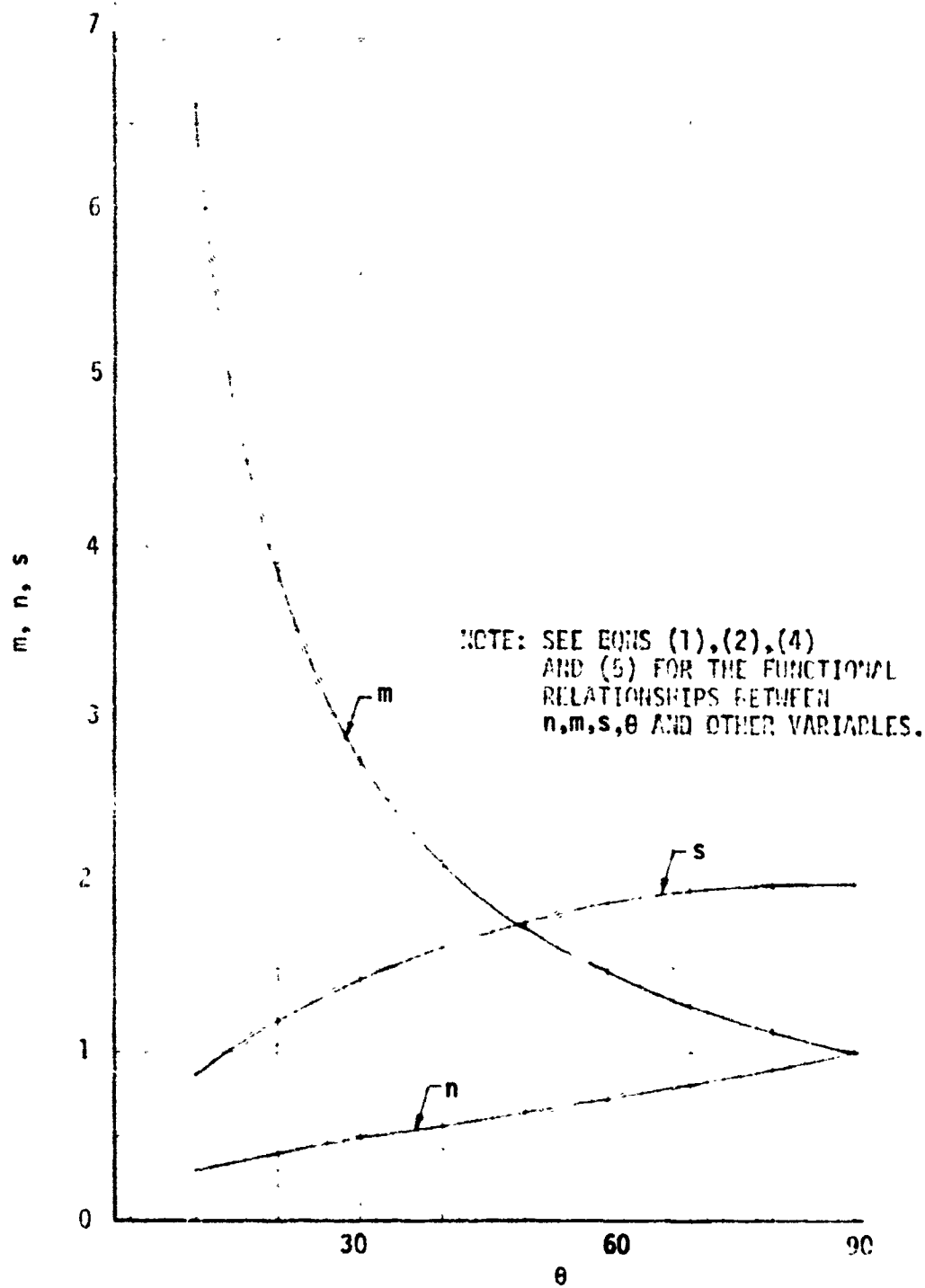


Figure 2. Values of Parameters m , n , and s .

The total force P resulting from impact can be related to the approach velocity v of the two bodies

$$v = v_1 + v_2 \quad (6)$$

using an approach similar to that presented in References 52 and 46

$$P = N^{2/5} \left[\frac{5v^2}{4N_1} \right]^{3/5} \quad (7)$$

where

$$N = \left[\frac{256 C_R}{9S^3 \pi^2 (k_1 + k_2)^2} \right]^{1/2} \quad (8)$$

$$N_1 = \frac{1}{m_1} + \frac{1}{m_2} \quad (9)$$

and m_1 and m_2 are the masses of the impactor and the target.

The major and minor axes of the elliptical area of contact and the maximum deformation, α_1 , can now be expressed in terms of impact velocity, properties of target, and the impactor and their geometries by substituting Equation (7) into Equations (1), (2), and (5):

$$a = m \left[\frac{3\pi}{2} (k_1 + k_2) C_R N^{2/5} \left(\frac{5v^2}{4N_1} \right)^{3/5} \right]^{1/3} \quad (10)$$

$$b = n \left[\frac{3\pi}{2} (k_1 + k_2) C_R N^{2/5} \left(\frac{5v^2}{4N_1} \right)^{3/5} \right]^{1/3} \quad (11)$$

$$\alpha_1 = S \left\{ \left[\frac{9\pi^2 (k_1 + k_2)^2}{256 C_R} \right] \left[N^{4/5} \right] \left[\frac{5v^2}{4N_1} \right]^{6/5} \right\}^{1/3} \quad (12)$$

Surface Pressure and Its Distribution

For the static contact problem, the relationship between the maximum surface pressure acting at the center of the area of contact and the force P is given as ⁵².

$$q_o = \frac{3P}{2\pi ab} \quad (13)$$

In the case of impact problem the maximum surface pressure q_o can be obtained by combining Equations (7), (10), and (11):

$$q_o = \frac{1}{\pi^{4/3}} \left\{ \frac{\left(\frac{3}{2\pi}\right)^{1/3} N^{2/15} \left(\frac{5v^2}{4N_1}\right)^{1/5}}{mn [(k_1 + k_2) C_R]^{2/3}} \right\} \quad (14)$$

whereas the pressure distribution is given by ⁵³

$$q = q_o \left\{ 1 - \left(\frac{x}{a}\right)^2 - \left(\frac{y}{b}\right)^2 \right\}^{1/2} \quad (15)$$

where x and y are the coordinate axes in the directions of the axes of ellipse a and b , respectively.

Equations (14) and (15) are the final equations for the maximum surface pressure and its distribution over the area of contact resulting from an impact of isotropic or composite impactor, in a form of body of revolution, into an isotropic or composite target, also being a body of revolution. The terms entering these equations take into account

1. Shape or curvature effects (through C_R).
2. Properties of impactor and the target (through k_1 and k_2).
3. Impact or approach velocity (through $v = v_1 + v_2$).
4. Masses of the impactor and the target (through N_1).

Equations (10) and (11) give the axes of the ellipse over which the pressure acts, while Equation (12) gives the deformation at the center of the area of contact resulting from impact between two bodies.

Relationship Between k_1 and k_2 and Elastic Properties

The terms k_1 and k_2 appearing in various equations of the previous subsections take into account the mechanical properties of the impactor and the target. For the case of the planar isotropic composite target (see Figure 4), k_2 can be obtained from Reference 54* and is

$$k_2 = \frac{\sqrt{A_{22}} \left\{ (\sqrt{A_{11} A_{22}} + G_2)^2 - (A_{12} + G_2)^2 \right\}^{1/2}}{2\pi \sqrt{G_2} (A_{11} A_{22} - A_{12}^2)} \quad (16)$$

where

$$\left. \begin{aligned} A_{11} &= E_2 (1 - \nu_1) \beta \\ A_{22} &= E_1 \beta \left(\frac{1 - \nu_{12}^2 \delta}{1 + \nu_1} \right) \\ A_{12} &= E_1 \nu_{12} \beta \\ \beta &= \frac{1}{1 - \nu_1 - 2\nu_{12}^2 \delta} \\ \delta &= E_1 / E_2 \end{aligned} \right\} \quad (17)$$

and E , G , and ν are the Young's modulus, shear modulus, and Poisson's ratio of the target, while Subscripts 1 and 2 denote the radial and thickness directions, respectively, 2 being in the direction of impact. For a planar isotropic material the properties in the 1 plane are independent of the orientation. It can be readily shown that for isotropic materials Equation (16) reduces to the well-known equation 52.

$$k = \frac{1 - \nu^2}{\pi E} \quad (18)$$

*The equations given in Reference 54 have several errors, which were corrected to arrive at Equation (16).

54. Conway, H. D., THE PRESSURE DISTRIBUTION BETWEEN TWO ELASTIC BODIES IN CONTACT, Zeitschrift fuer Angewandte Mathematik und Physik, Vol. VII, 1956, pp. 460-465.

If the impactor is also made of material that is planar isotropic, then k_1 will be defined similar to k_2 , except that k_1 will be a function of the elastic properties of the impactor.

As is readily apparent from Equations (10), (11), (12), and (14), the parameters k_1 and k_2 influence the shape of the area of contact as well as the magnitude of the surface pressure. Although no expression has been found for k_2 for generally orthotropic solids and its derivation appears to be extremely complex, it has been noted²³ (based primarily on experimental results) that when an isotropic spherical body is pressed into a unidirectional orthotropic target, the area of contact is slight elliptical, which indicates the dependence of k_2 on inplane fiber orientation. An approximate expression for k_2 for a generally orthotropic material can be obtained from Equations (16) and (17) by making the following substitutions:

$$E_1^{-1} = \frac{\cos^4 \psi}{E_L} + \frac{\sin^4 \psi}{E_T} + \frac{1}{4} \left(\frac{1}{G_{LT}} - \frac{2\nu_{LT}}{E_L} \right) \sin^2 2\psi \quad (19)$$

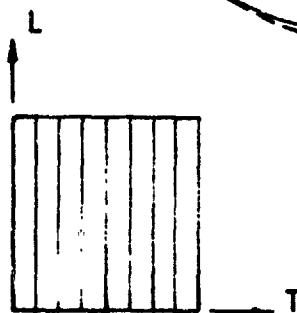
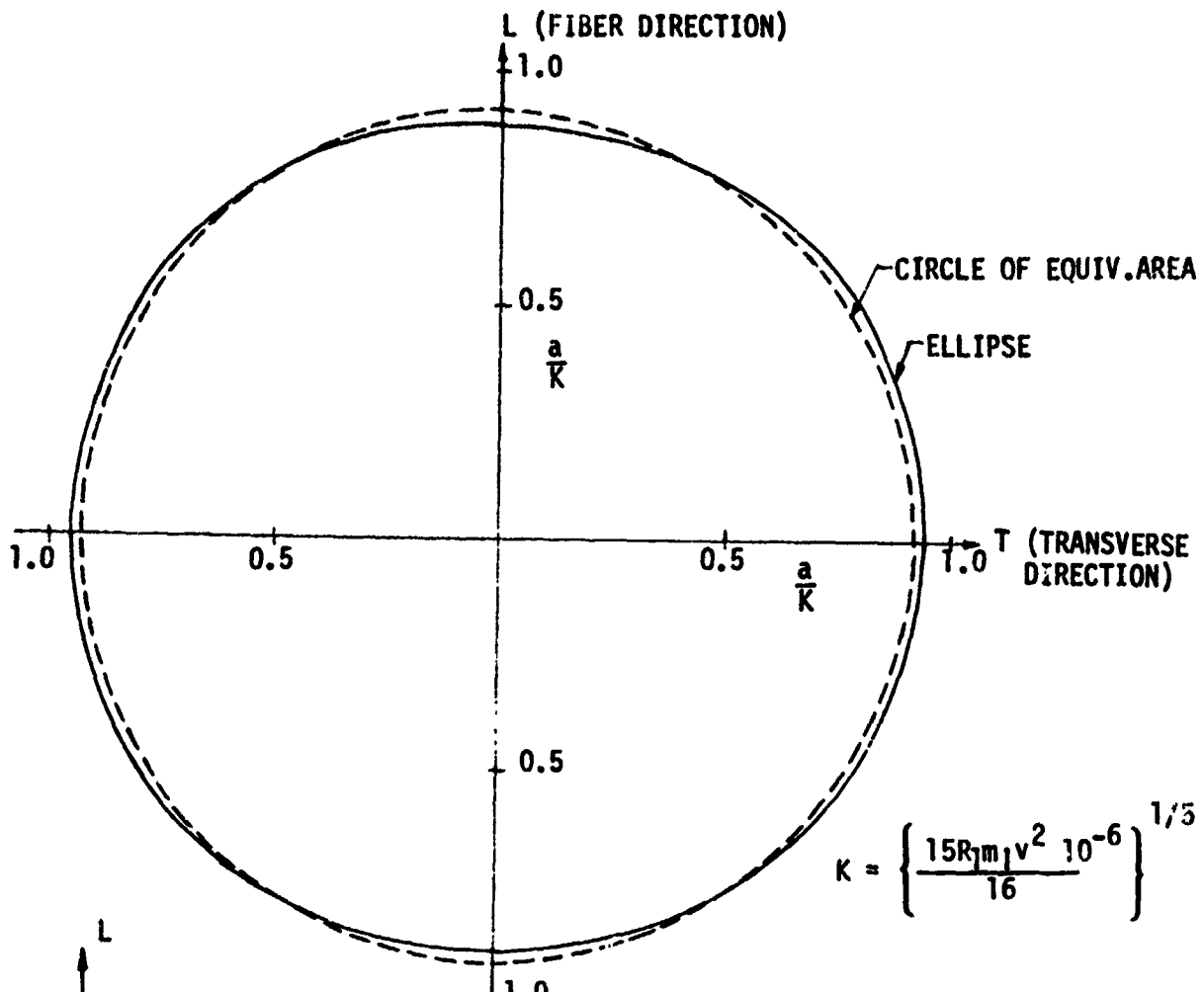
$$\nu_1 = \frac{E_1}{E_L} \left[\nu_{LT} - \frac{1}{4} \left(1 + 2\nu_{LT} + \frac{E_L}{E_T} - \frac{E_L}{G_{LT}} \right) \sin^2 2\psi \right] \quad (20)$$

where for a fiber-reinforced composite, E_L is the inplane Young's modulus in the fiber direction, E_T is the inplane Young's modulus in the transverse direction, G_{LT} is the inplane shear modulus, ν_{LT} is the major inplane Poisson's ratio, and ψ is the angle between the fiber direction and any given inplane direction. Figure 3 shows the nondimensionalized shape of the area of contact in a generally orthotropic solid as well as a circle of equivalent area. Shown there also are the material properties on which the results were based. These material properties are for a unidirectional composite consisting of Courtaulds HTS graphite fibers and an epoxy resin. The important thing to note from Figure 3 is that for even a high degree of inplane orthotropy the area of contact deviates only slightly from circular shape. As noted¹⁰, properties that have the greatest influence on k_2 are the properties associated with the thickness direction, that is, the direction of impact.

Duration of Impact

The maximum pressure q_0 occurs at a time $1/2 t_0$, where t_0 is the impact duration. The latter can be obtained using an approach similar to that presented in Reference 52. From the problem of impact of two bodies

$$\frac{1}{2} (\dot{\alpha}^2 - v^2) = - \frac{2}{5} N N_1 \alpha^{2/5} \quad (21)$$



$$E_L = 21.5 \times 10^6 \text{ psi}$$

$$E_T = E_Z = 1.5 \times 10^6 \text{ psi}$$

$$G_Z = G_{LT} = 0.7 \times 10^6 \text{ psi}$$

$$\nu_{LT} = 0.25$$

$$\nu_Z = \nu_{TL} = 0.017$$

R_1 = RADIUS OF THE SPHERICAL IMPACTOR

E_1 = YOUNG'S MODULUS OF IMPACTOR

m_1 = MASS OF THE IMPACTOR

m_2 = MASS OF THE PLATE

v = IMPACT VELOCITY

$$m_2 \gg m_1$$

$$E_1 \gg E_L, E_T$$

NOTE: IMPACT DIRECTION IS NORMAL TO PLANE LT. PROPERTIES IN THE IMPACT DIRECTION (Z-DIRECTION) ASSUMED THE SAME AS IN T-DIRECTION

Figure 3. Actual and Approximate Shape of the Area of Contact Resulting from an Indentation or Impact of a Rigid Spherical Body Into Generally Orthotropic Composite Material.

and

$$\dot{\alpha} = \left(v^2 - \frac{4}{5} N N_1 \alpha^{5/2} \right)^{1/2} \quad (22)$$

Substituting in the above equations

$$\dot{\alpha} = \frac{dx}{dt} \quad (23)$$

and solving for dt

$$dt = \frac{d\alpha}{\left(v^2 - \frac{4}{5} N N_1 \alpha^{5/2} \right)^{1/2}} \quad (24)$$

Combining Equation (24) with (12) and integrating gives

$$t = \frac{2\alpha_1}{v} \int_0^x \frac{dx}{\sqrt{1 - (x)^{5/2}}} \quad (25)$$

where

$$x = \left(\frac{\alpha}{\alpha_1} \right) \quad (26)$$

The total impact duration t_o is obtained by integrating between the limits $x = 0$ and $x = 1$ and substituting Equation (12) into the resultant equation

$$t_o = \frac{2.94S}{v} \left\{ \left[\frac{9\pi^2 (k_1 + k_2)^2}{256 C_r} \right] \left[N^{4/5} \right] \left[\frac{5v^2}{4N_1} \right]^{6/5} \right\}^{1/3} \quad (27)$$

where the various terms have been defined previously. The value 2.94 comes from the evaluation of the integral appearing in Equation (25).

The pressure q_i and the approach velocity v_i at any given time t_i can be obtained by numerically integrating Equation (25). Knowing the relationship between v_i , v , t_i , and t_o , the pressure q_i and the principal axes of the area of contact a_i and b_i at any given time t_i can be obtained from Equations (10), (11), and (14) by replacing v with v_i .

INTERNAL STRESSES IN FLAT MULTILAYER COMPOSITE PLATES CAUSED BY SURFACE PRESSURE q RESULTING FROM FOREIGN OBJECT IMPACT

Knowing the time-dependent surface pressure, its distribution, the area over which it acts, and the variation of pressure and area of contact as a function of time, it is now possible to determine the internal stresses in composite targets as a function of the variable noted above. The internal

stresses in planar isotropic targets were determined using the SAAS III finite-element computer code ⁵⁵, whereas in generally orthotropic solids the internal stresses were determined using the ASAAS finite-element computer code ⁵⁶ which was modified, as described later on, to handle the problem of generally orthotropic solids.

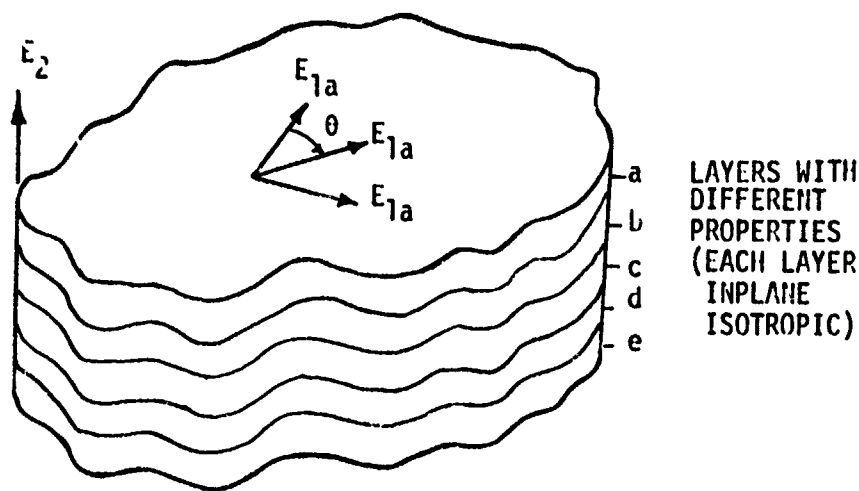
Internal Stresses in Planar Isotropic Targets

The internal stresses in planar isotropic targets subjected to impact-induced surface pressure were determined using the SAAS III finite-element computer code, which was available at McDonnell Douglas Astronautics Company (MDAC) and operational prior to initiation of this program. An example of a planar isotropic material that could be analyzed using SAAS III is a multilayer composite plate in which the inplane properties of any given layer (Young's modulus, Poisson's ratio, and shear modulus) are different from the corresponding properties in the thickness direction of the plate. However, the inplane properties of the plate, although not direction dependent, can be different for various layers, as shown in Figure 4. Figures 5 and 6 show some typical results on the internal stresses in planar isotropic targets subjected to surface pressure q resulting from foreign object impact. The stresses shown there were normalized with respect to q_0 , whereas the distribution of stresses in the target was normalized with respect to a , the radius of the area of contact. Although only the results for normal and radial stresses are shown in Figures 5 and 6, similar results have been obtained for the circumferential and shear stresses.

Internal Stresses in Generally Orthotropic Targets

Although SAAS III can handle special cases of multilayer materials (see Figure 4) subjected to impact-induced pressure, it cannot handle the case of a generally orthotropic multilayer solid such as shown in Figure 7. The three-dimensional stress state in the latter type of material was determined by modifying the ASAAS finite-element computer code, which is the most recent version of SAAS III and is applicable to materials with polar orthotropy. To become applicable to the multilayer generally orthotropic solids having orthogonal orthotropy, the code was modified as described below.

55. Crose, J. G., and Jones, R. M., SAAS III, FINITE ELEMENT STRESS ANALYSIS OF AXISYMMETRIC AND PLANE SOLIDS WITH DIFFERENT ORTHOTROPIC, TEMPERATURE-DEPENDENT MATERIAL PROPERTIES IN TENSION AND COMPRESSION, TR-0059 (S6816-53) - The Aerospace Corporation, San Bernadino, California, June 1971.
56. Crose, J. G., ASAAS - ASYMMETRIC STRESS ANALYSIS OF AXISYMMETRIC SOLIDS WITH ORTHOTROPIC, TEMPERATURE-DEPENDENT MATERIAL PROPERTIES THAT CAN VARY CIRCUMFERENTIALLY, The Aerospace Corporation Report TR-0172(S2816-15)- 1, December 1971.



$$G_1 \neq G_2$$

$$E_1 \neq E_2; \nu_1 \neq \nu_2$$

$$E_{1a} \neq E_{1b} \neq E_{1c} \neq \dots E_{1n}$$

$$\nu_{1a} \neq \nu_{1b} \neq \nu_{1c} \neq \dots \nu_{1n}$$

Figure 4. Planar or Transversely Isotropic Multilayer Material.

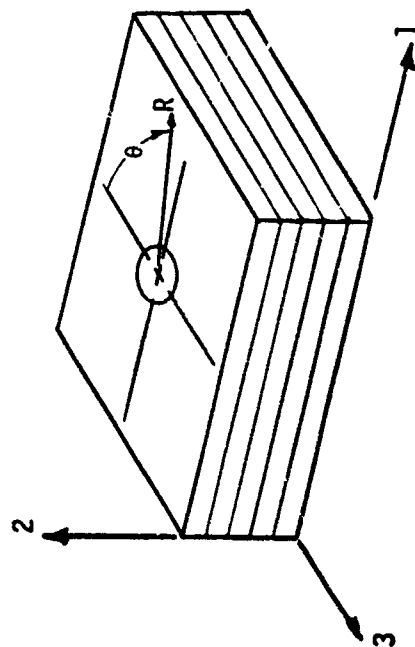
The system of equations solved by SAAS or the more recent version, ASAAS, is of the form

$$\sum_{n=1}^N \left[\int_{\text{vol}} (a^n)^T (C^n) (a^n) dv \right] \{u\} = \sum_{n=1}^N \left[\int_{\text{vol}} (a^n)^T \{\tau^n\} dv \right] + \sum_{n=1}^N \left[\int_{\text{area}} (d^n)^T \{P^n\} dA \right] \quad (28)$$

where

(a^n) = matrix expressing the relation between the strain matrix (ϵ^n) of any element n and the nodal displacement matrix (u)

$(a^n)^T$ = transpose of (a^n)



PLANAR ISOTROPIC MATERIAL

$$E_1 = E_3 \neq f(\theta)$$

$$E_1 = 2.9 \times 10^6 \text{ psi}$$

$$E_2 = 3.3 \times 10^6 \text{ psi}$$

$$\nu_1 = .144$$

$$\nu_{21} = .260$$

$$G_{12} = 0.86 \times 10^6 \text{ psi}$$

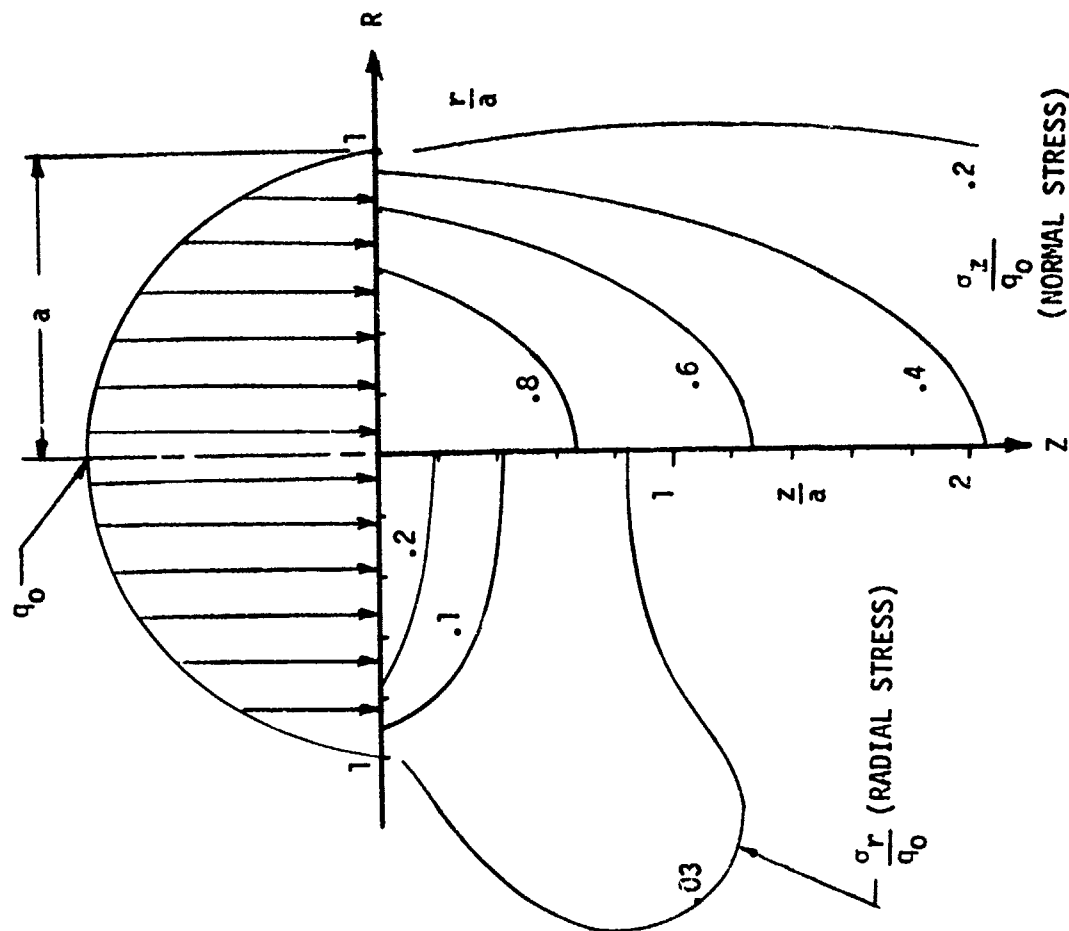


Figure 5. Internal Stress Distribution in Semi-Infinite Multilayer Planar Isotropic Material Resulting from Surface Pressure Caused by Foreign Object Impact ($E_1/E_2 = 0.35$).

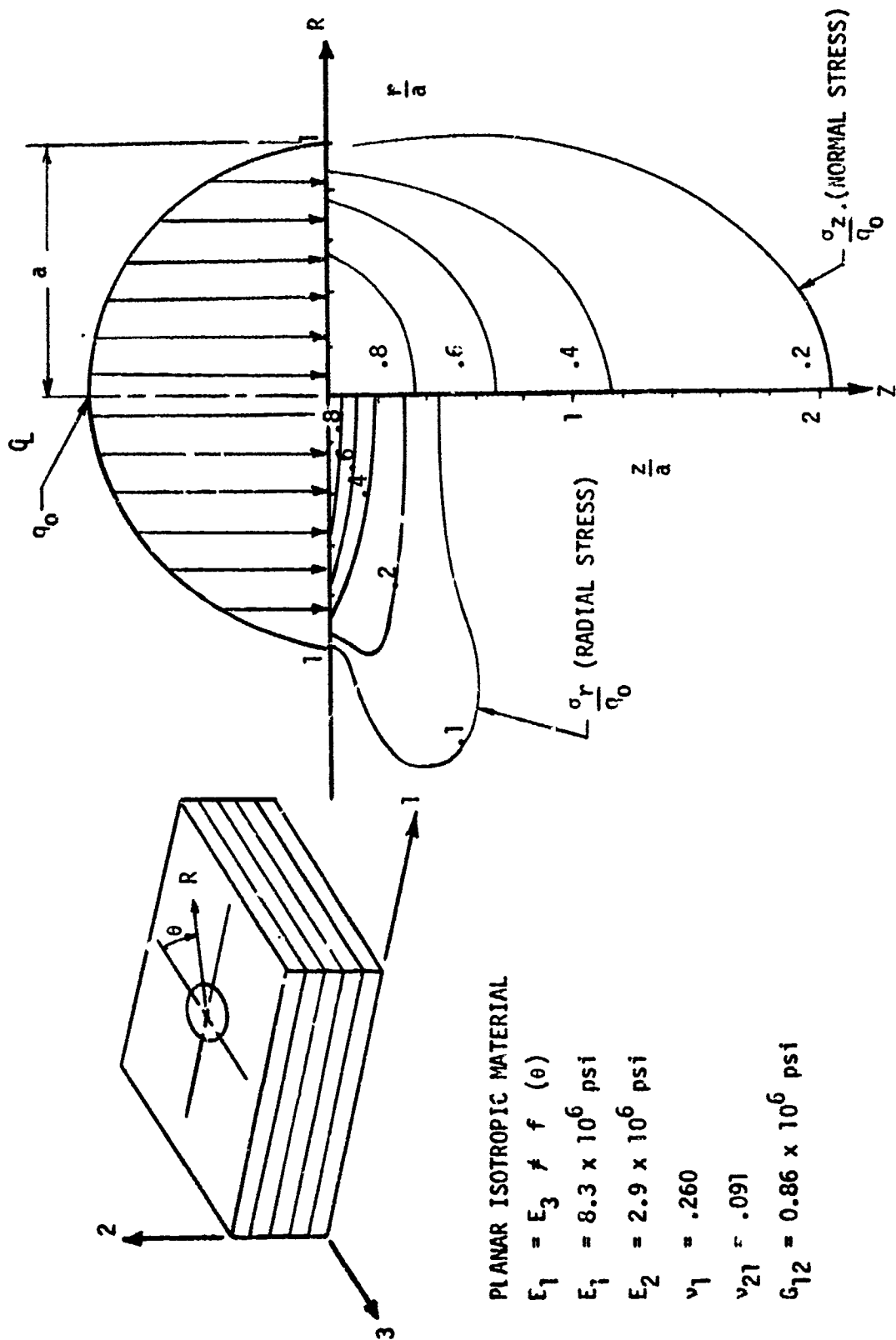


Figure 6. Internal Stress Distribution in Semi-Infinite Multilayer Planar Isotropic Material Resulting from Surface Pressure Caused by Foreign Object Impact ($E_1/E_2 = 2.86$).

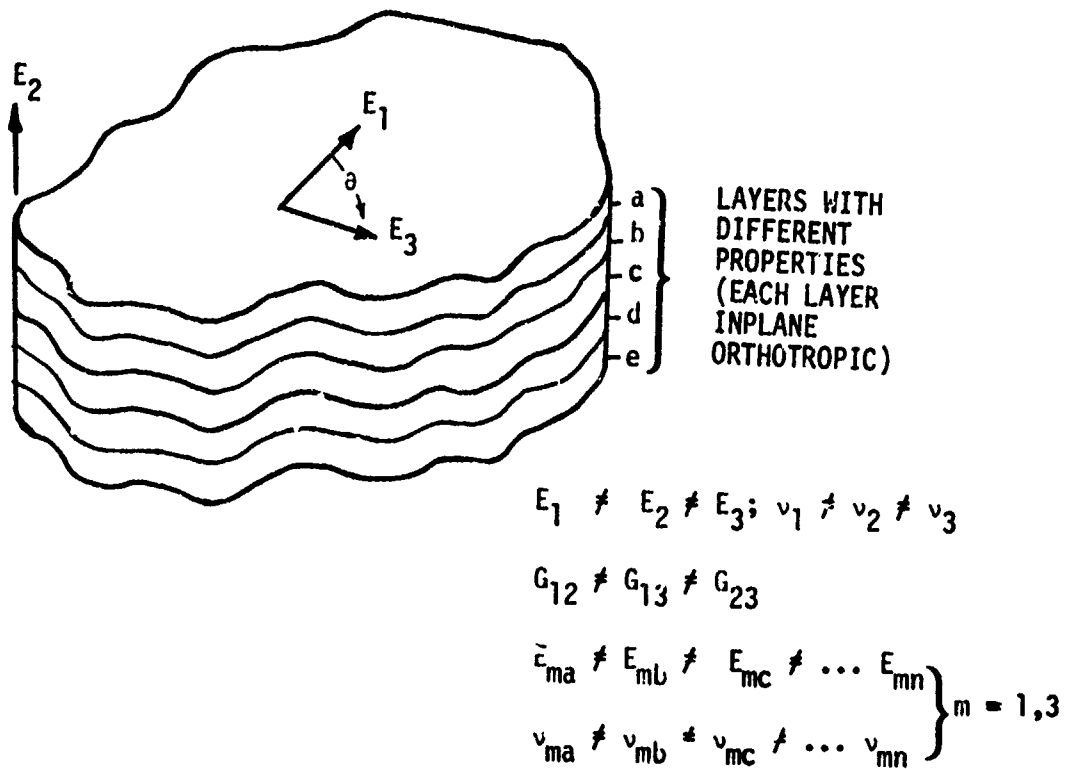


Figure 7. Generally Orthotropic Multilayer Material.

(d^n) = matrix that relates the displacement of any location to the nodal displacement

$(d^n)^T$ = transpose of (d^n)

(C^n) = matrix for the material properties (constitutive relations)

(τ^n) = thermal load matrix

(P^n) = surface traction matrix

The expressions on the right side of Equation (28) represent the thermal loads (first term) and surface tractions (second term). The coefficient of (U) on the left side of Equation (28) is the stiffness matrix. The

matrix (C^n) giving the constitutive relations for the material is the inversion of (A), which is defined as

$$(A) = \begin{Bmatrix} a_{11} & a_{12} & a_{13} & 0 & 0 & 0 \\ a_{21} & a_{22} & a_{23} & 0 & 0 & 0 \\ a_{31} & a_{32} & a_{33} & 0 & 0 & 0 \\ 0 & 0 & 0 & a_{44} & 0 & 0 \\ 0 & 0 & 0 & 0 & a_{55} & 0 \\ 0 & 0 & 0 & 0 & 0 & a_{66} \end{Bmatrix} \quad (29)$$

where, for material such as shown in Figure 4 (transversely isotropic),

$$a_{11} = a_{33} = \frac{1}{E_1}$$

$$a_{22} = \frac{1}{E_2}$$

$$a_{12} = a_{21} = a_{23} = a_{32} = \frac{\nu_{12}}{E_1}$$

$$a_{13} = a_{31} = \frac{\nu_1}{E_1}$$

$$a_{44} = a_{66} = \frac{1}{G_2}$$

$$a_{55} = \frac{1}{G_1}$$

E_1 = inplane Young's modulus

E_2 = Young's modulus associated with thickness direction

ν_1 = inplane Poisson's ratio

ν_{12} = Poisson's ratio associated with Direction 1-2 or 3-2.

G_1 = inplane shear modulus

G_2 = shear modulus associated with Direction 1-2 or 3-2.

In the existing version of the finite-element computer code, the material properties are independent of the θ -coordinate in the plane of the laminae. Therefore, although the existing code could handle some special cases of multilayer composite plates, it was inadequate in handling the influence of fiber orientation or of stacking sequences. The code was modified to enable it to handle the latter types of problems. Instead of using the constitutive relationship given by (29), the following was used in the governing equation (Equation (28)):

$$(A) = \begin{Bmatrix} \bar{a}_{11} & \bar{a}_{12} & \bar{a}_{13} & 0 & \bar{a}_{15} & 0 \\ \bar{a}_{21} & \bar{a}_{22} & \bar{a}_{23} & 0 & \bar{a}_{25} & 0 \\ \bar{a}_{31} & \bar{a}_{32} & \bar{a}_{33} & 0 & \bar{a}_{35} & 0 \\ 0 & 0 & 0 & \bar{a}_{44} & 0 & \bar{a}_{46} \\ \bar{a}_{15} & \bar{a}_{25} & \bar{a}_{35} & 0 & \bar{a}_{55} & 0 \\ 0 & 0 & 0 & \bar{a}_{64} & 0 & \bar{a}_{66} \end{Bmatrix} \quad (30)$$

where

$$\begin{aligned} \bar{a}_{11} = & 1/8 [a_{55} + 2a_{13} + 3(a_{11} + a_{33})] + 1/2 (a_{11} - a_{33}) \cos 2\theta \\ & + 1/8 (a_{11} + a_{33} - a_{55} - 2a_{13}) \cos 4\theta \end{aligned}$$

$$\bar{a}_{12} = 1/2 (a_{12} + a_{23}) + 1/2 (a_{12} - a_{23}) \cos 2\theta$$

$$\begin{aligned} \bar{a}_{13} = & [a_{13} + 1/8 (a_{11} + a_{33} - 2a_{13} - a_{55})] \\ & - 1/8 (a_{11} + a_{33} - 2a_{13} - a_{55}) \cos 4\theta \end{aligned}$$

$$\bar{a}_{15} = 1/2 (a_{33} - a_{11}) \sin 2\theta - 1/4 (a_{11} + a_{33} - a_{55} - 2a_{13}) \sin 4\theta$$

$$\bar{a}_{22} = a_{22}$$

$$\bar{a}_{23} = 1/2 (a_{12} + a_{23}) + 1/2 (a_{23} - a_{12}) \cos 2\theta$$

$$\bar{a}_{25} = (a_{23} - a_{12}) \sin 2\theta$$

$$\begin{aligned} \bar{a}_{33} = & 1/8 [a_{55} + 2a_{13} + 3(a_{11} + a_{33})] + 1/2 (a_{33} - a_{11}) \cos 2\theta \\ & + 1/8 (a_{11} + a_{33} - a_{55} - 2a_{13}) \cos 4\theta \end{aligned}$$

$$\bar{a}_{35} = 1/2 (a_{33} - a_{11}) \sin 2\theta + 1/4 (a_{11} + a_{33} - a_{55} - 2a_{13}) \sin 4\theta$$

$$\bar{a}_{44} = 1/2 (a_{44} + a_{66}) + 1/2 (a_{44} - a_{66}) \cos 2\theta$$

$$\bar{a}_{46} = 1/2 (a_{66} - a_{44}) \sin 2\theta$$

$$\begin{aligned} \bar{a}_{55} = & [a_{55} + 1/2 (a_{11} + a_{13} - 2a_{13} - a_{55})] \\ & - 1/2 (a_{11} + a_{33} - 2a_{13} - a_{55}) \cos 4\theta \end{aligned}$$

$$\bar{a}_{66} = 1/2 (a_{44} + a_{66}) + 1/2 (a_{66} - a_{44}) \cos 2\theta$$

and the terms a_{11} , a_{12} , a_{13} , --, a_{21} , a_{22} , a_{23} , --, a_{31} , a_{32} , a_{33} , --- are related to the engineering elastic constants of a material in the three orthogonal directions. For example, for material such as shown in Figure 7, the various terms now become

$$a_{11} = \frac{1}{E_1}, a_{22} = \frac{1}{E_2}, a_{33} = \frac{1}{E_3} \dots$$

where E_1 , E_2 , and E_3 are the Young's moduli of the material in the three orthogonal directions, each of them being different; that is,

$$E_1 \neq E_2 \neq E_3$$

The above-described modification of ASAAS enabled the following types of problems to be analyzed:

1. Local and overall (plate bending) multiaxial stresses resulting from impact in multilayer generally orthotropic plates (or solids) made of layers having different elastic properties.
2. Multiaxial stresses in multilayer composite plates (or solids), with layers having different fiber orientations (fibers in any given layer have orientation $\pm \theta$ where $0^\circ \leq \theta \leq 90^\circ$).
3. Variations in local and overall multiaxial stresses due to stacking sequence.

The modified version of ASAAS gives a three-dimensional solution for the internal stresses in generally orthotropic solids having orthogonal orthotropy. Inasmuch as closed-form rigorous elasticity solutions could not be found for this type of problem, the modified ASAAS computer code was checked out by applying it to several simple problems involving isotropic and orthotropic materials. The problems involved determination of stresses and deflections in isotropic and orthotropic circular plates fixed along the outer boundary and subjected to uniform

surface pressure. The latter problems have been selected for checkout, because closed-form solutions are available for them. Figure 8 shows a comparison of solutions for deflections in an isotropic circular plate subjected to uniform surface loading. Presented therein are the results from a closed-form solution as well as from SAAS III and ASAAS computer solutions in which two different grid sizes were employed. The closed-form solution for the problem is given in Reference 57. For a given grid size, both the ASAAS and SAAS III computer codes give identical results for the deflection. Inasmuch as SAAS III has been checked out previously¹⁰, this gives a good indication of the accuracy of ASAAS. By decreasing the size of the grid elements, the ASAAS solution is shown to approach the closed-form solution. Further decrease in the grid elements did not influence the results significantly, as discussed later in this section. The slight discrepancy ($\approx 5\%$) between the closed-form and ASAAS solution using Model B grid is not so much an indication of the error in computer solution as an indication of error in the closed-form solution. The computer solution solves the three-dimensional elasticity problem, whereas the closed-form solution was obtained for a two-dimensional plate problem⁵⁷, and its accuracy is governed by the assumptions made in the plate theory.

The next checkout problem considered involved determination of deflections and stresses in an orthotropic circular plate fixed along the boundary and subjected to a uniform surface loading. An approximate closed-form solution (based on plate theory formulation) for this problem is given in Reference 58. For this sample problem the material properties associated with the axes of symmetry of material ($\beta=0$ and $\beta=90^\circ$) were taken as

$$E_L = E_T = E_Z = 1.32 \times 10^6 \text{ psi}$$

$$G_{LT} = G_{LZ} = G_{TZ} = 0.2 \times 10^6 \text{ psi}$$

$$\nu_{LT} = \nu_{TL} = \nu_{LZ} = 0.10$$

The variation of the Young's moduli, shear modulus, and Poisson's ratio as a function of orientation (Angle β) is shown in Figures 9 and 10. Figure 11 shows a comparison of deflections obtained from the closed-form solution⁵⁸ and ASAAS computer solutions using different-sized grid elements. As is readily seen, going from Model B grid to Model C

57. Timoshenko, S. P., THEORY OF PLATES AND SHELLS, McGraw-Hill Book Company, New York, 1940, p. 60.

58. Hearmon, R. F. S., APPLIED ANISOTROPIC ELASTICITY, Oxford University Press, Oxford, 1961, p 126.

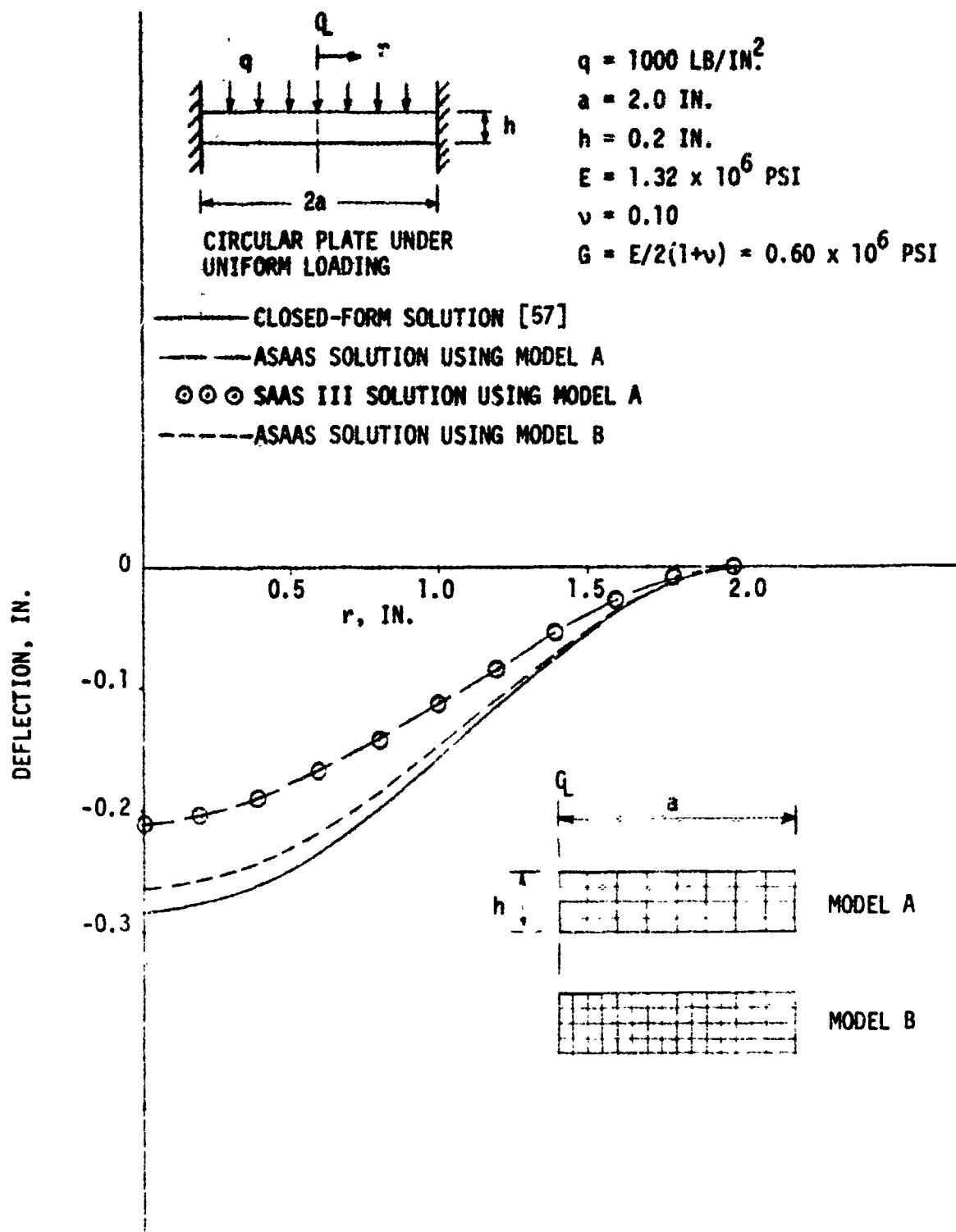


Figure 8. Comparison of Solutions for Deflections in a Circular Isotropic Plate Subjected to Uniform Surface Pressure.

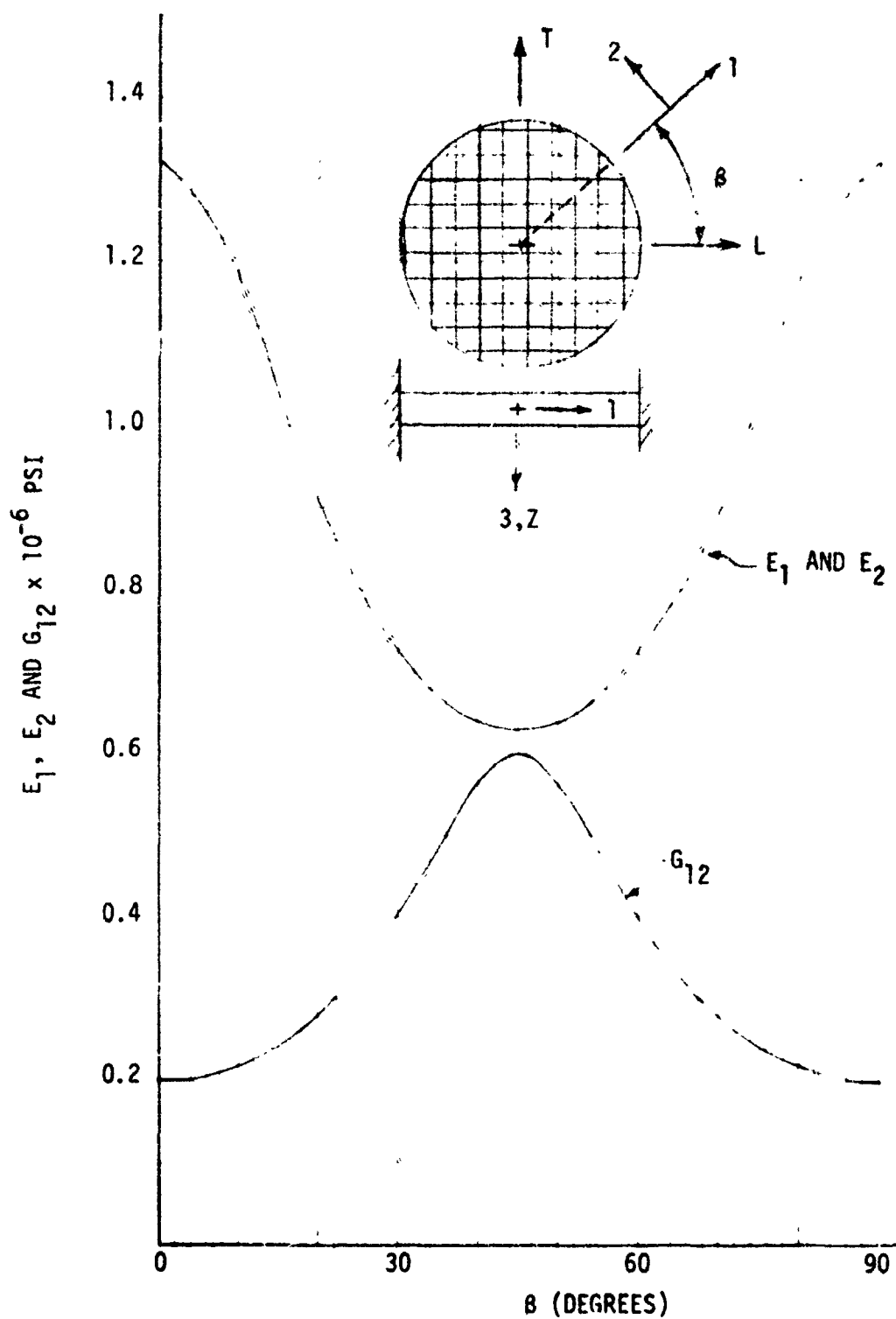


Figure 9. Variation of Young's Moduli and Shear Modulus as a Function of β .

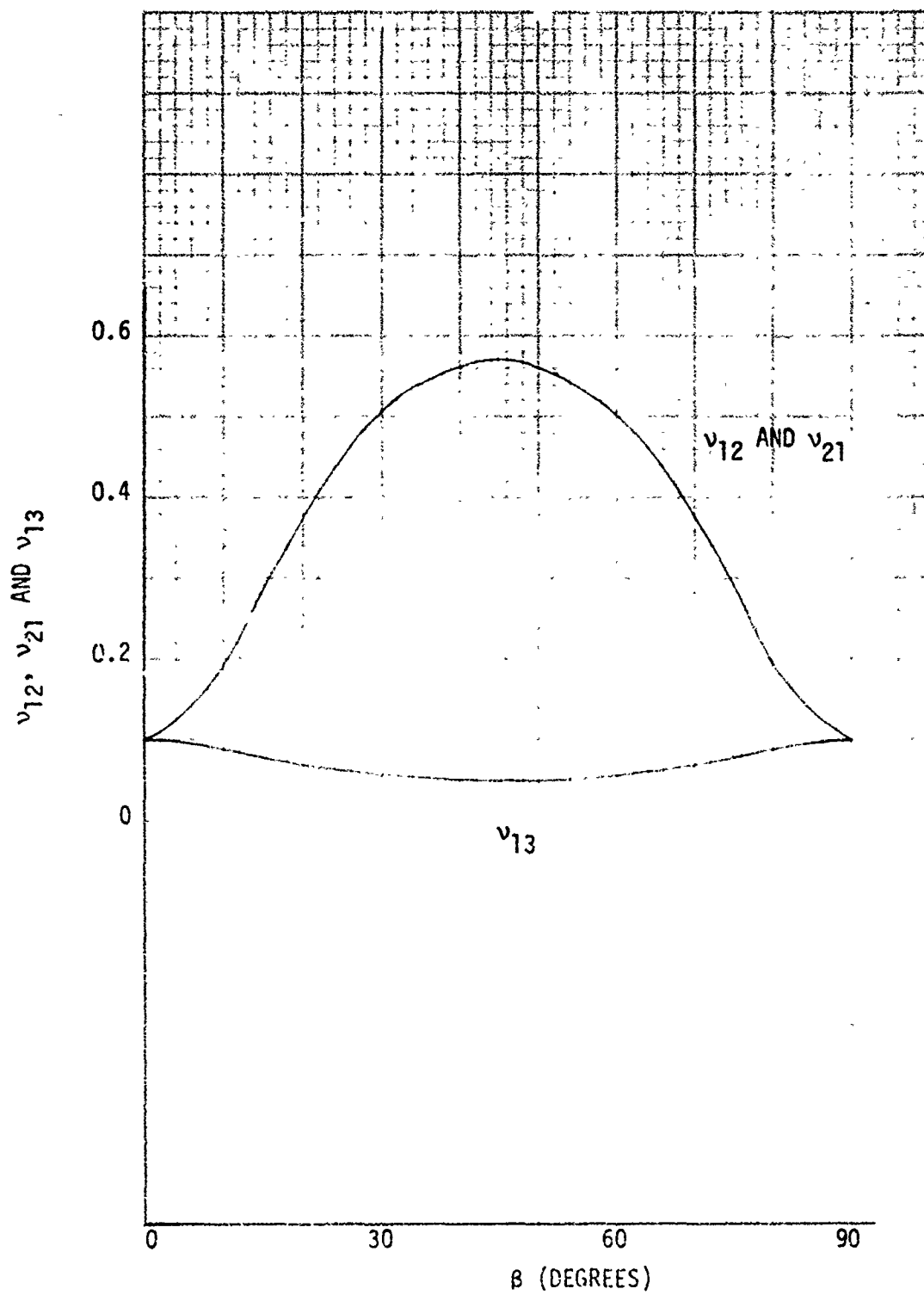


Figure 10. Variation of Poisson's Ratios as a Function of β .

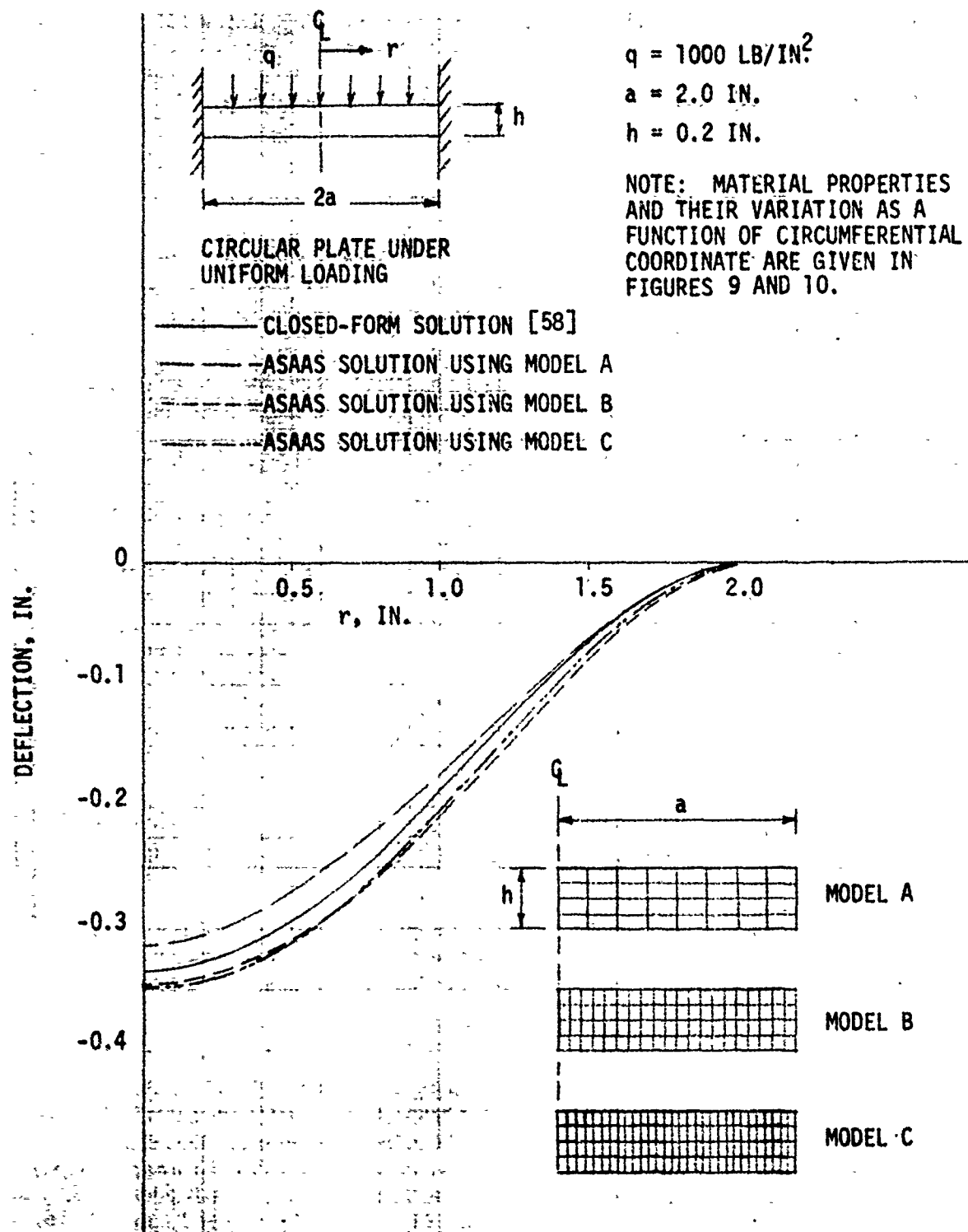


Figure 11. Comparison of Solutions for Deflections in a Circular Orthotropic Plate Subjected to Uniform Surface Pressure.

grid does not influence the results significantly. Consequently, Model B grid was selected for use in the application phase of the program described in Section III. The ASAAS computer running times for the various grid models were as follows:

Model A: 0.034 Machine Units

Model B: 0.065 Machine Units

Model C: 0.095 Machine Units

The fact that the deflections obtained from ASAAS are higher than the closed-form solution (the opposite was true in the case of isotropic plate) is attributed to the influence of low shear moduli that were assumed for the sample problem.

The radial and circumferential stresses obtained from the closed-form solution and ASAAS computer solutions using different grid models are compared in Figure 12. As was the case with deflections, going from grid Model B to grid Model C does not significantly influence the results.

The modified and checked-out code was used in determining internal triaxial stresses in several sample problems involving generally orthotropic solids, prior to applying the code to the problems of interest. Tables I and II show some typical results for the normal (σ_z) and radial (σ_r) stresses in a sample problem shown in Figure 13. Although only σ_z and σ_r are shown in Tables I and II, similar results have also been obtained for the circumferential (σ_θ) and shear stresses (σ_{rz} and $\sigma_{\theta z}$) at various points within the target. The results shown in Tables I and II are for HTS graphite-epoxy composites having properties as shown in Figure 3.

INTERNAL STRESSES IN MULTILAYER ORTHOTROPIC CYLINDERS CAUSED BY SURFACE PRESSURE q RESULTING FROM FOREIGN- OBJECT IMPACT

The impact-induced stresses in multilayer orthotropic cylinders were determined using the CYLINDER computer code⁵⁹. This code uses Sander's shell equations⁶⁰ and an explicit finite-difference integration

-
59. Chane, H. L., ELASTIC PLASTIC ASYMMETRIC TRANSIENT RESPONSE OF ORTHOTROPIC CYLINDRICAL SHELLS SUBJECTED TO MECHANICAL AND THERMAL LOADS, McDonnell Douglas Astronautics Company/Western Division MDC G 3750 (in preparation).
60. Sanders, Jr., J. L., NONLINEAR THEORIES FOR THIN SHELLS, Quarterly Applied Mathematics, Vol. 21, No. 1, April 1963, pp. 21-36.

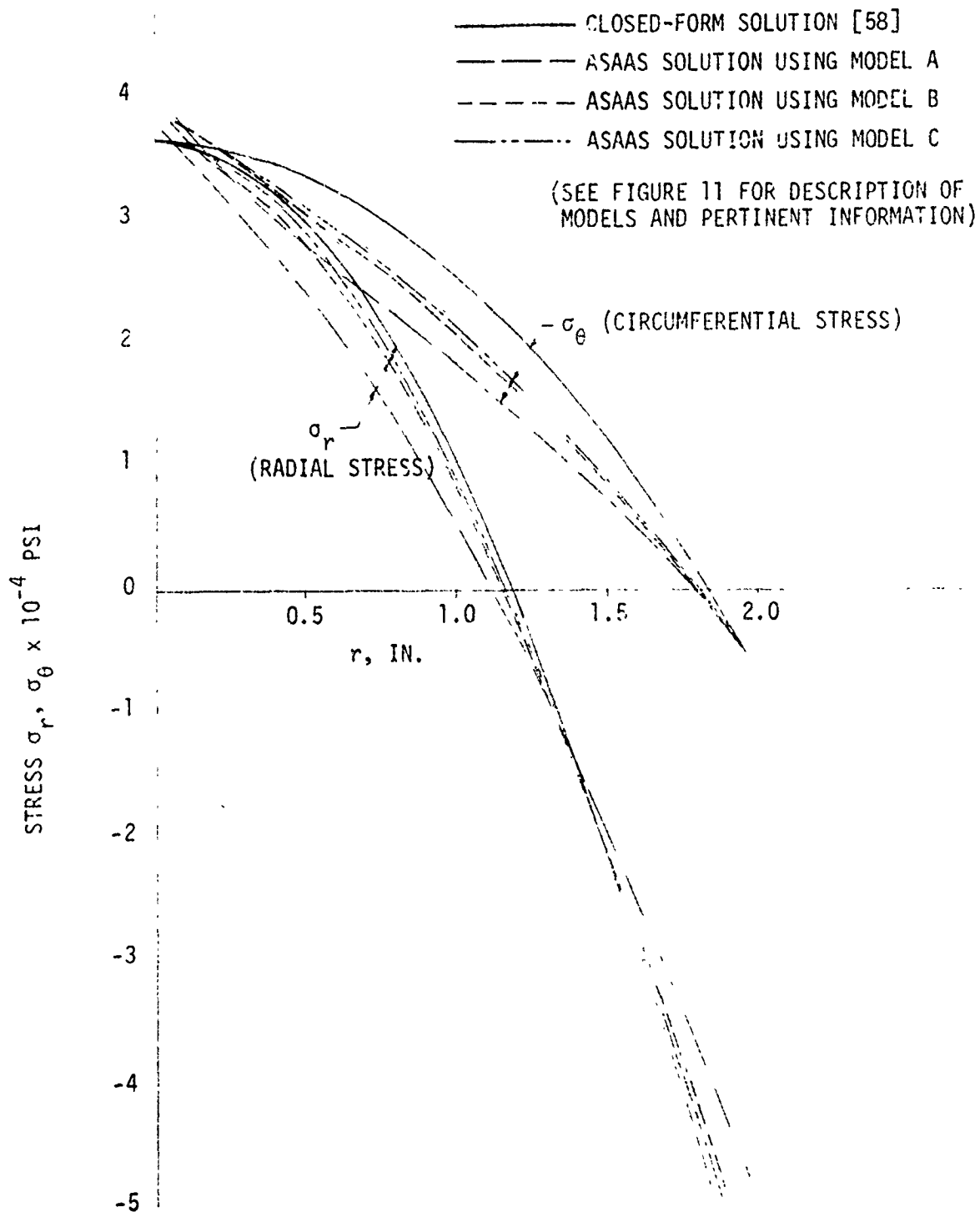


Figure 12. Comparison of Solutions for Stresses in a Circular Orthotropic Plate Subjected to Uniform Surface Pressure.

Table I
NORMAL STRESSES IN ORTHOTROPIC SOLID

| ELEM | $\sigma_z(R=0.1)$ | | | ELEM | $\sigma_z(R=0.3)$ | | | ELEM | $\sigma_z(R=0.7)$ | | |
|------|--------------------|----------|----------|------|--------------------|----------|----------|------|--------------------|----------|----------|
| | 0° | 30° | 60° | | 0° | 30° | 60° | | 0° | 30° | 60° |
| 1 | -7887(5) | -7244(5) | -8590(5) | 13 | -7513(5) | -7092(5) | -7832(5) | 37 | -4850(5) | -4622(5) | -4933(5) |
| 2 | -5110(5) | -5078(5) | -5279(5) | 14 | -4582(5) | -4549(5) | -4832(5) | 38 | -2937(5) | -2921(5) | -3196(5) |
| 3 | -3081(5) | -3204(5) | -2956(5) | 15 | -2820(5) | -2906(5) | -2824(5) | 39 | -2034(5) | -2080(5) | -2159(5) |
| 4 | -1956(5) | -2125(5) | -1739(5) | 16 | -1867(5) | -1981(5) | -1761(5) | 40 | -1489(5) | -1558(5) | -1515(5) |
| 5 | -1111(5) | -1333(5) | -8132(4) | 17 | -1115(5) | -1264(5) | -9379(4) | 41 | -9844(4) | -1068(5) | -9241(4) |
| 6 | -5987(4) | -8781(4) | -2178(4) | 18 | -6458(4) | -8334(4) | -4076(4) | 42 | -6208(4) | -7241(4) | -5072(4) |
| 7 | -3507(4) | -6736(4) | -9138(3) | 19 | -4183(4) | -6350(4) | -1377(4) | 43 | -4299(4) | -5485(4) | -2852(4) |
| 8 | -2125(4) | -5676(4) | -2745(4) | 20 | -2919(4) | -5301(4) | -1902(3) | 44 | -3208(4) | -4507(4) | -1553(4) |
| 9 | -1289(4) | -5067(4) | -3896(4) | 21 | -2158(4) | -4691(4) | -1162(4) | 45 | -2543(4) | -3922(4) | -7462(4) |
| 10 | -7718(3) | -4698(4) | -4620(4) | 22 | -1690(4) | -4321(4) | -1771(4) | 46 | -2132(4) | -3561(4) | -2399(3) |
| 11 | -4674(3) | -4481(4) | -5048(4) | 23 | -1414(4) | -4103(4) | -2131(4) | 47 | -1890(4) | -3349(4) | -6013(2) |
| 12 | -3257(3) | -4381(4) | -5247(4) | 24 | -1286(4) | -4001(4) | -2298(4) | 48 | -1777(4) | -3249(4) | -2003(3) |
| | | | | | | | | | | | |
| ELEM | $\sigma_z(R=0.90)$ | | | ELEM | $\sigma_z(R=2.35)$ | | | ELEM | $\sigma_z(R=5.05)$ | | |
| | 0° | 30° | 60° | | 0° | 30° | 60° | | 0° | 30° | 60° |
| 49 | -2506(5) | -2378(5) | -2667(5) | 73 | -3454(3) | -3296(3) | -5664(3) | 109 | -3654(1) | -3362(2) | -1213(3) |
| 50 | -2024(5) | -2018(5) | -2254(5) | 74 | -4638(3) | -8413(3) | -1938(4) | 110 | -4689(2) | -4090(1) | -1653(3) |
| 51 | -1610(5) | -1647(5) | -1754(5) | 75 | -1684(4) | -2058(4) | -2978(4) | 111 | -5384(2) | -8277(2) | -2167(3) |
| 52 | -1265(5) | -1324(5) | -1322(5) | 76 | -2455(4) | -2820(4) | -3416(4) | 112 | -3303(1) | -1915(3) | -4059(3) |
| 53 | -8908(4) | -9613(4) | -8631(4) | 77 | -2604(4) | -3267(4) | -3396(4) | 113 | -1538(3) | -3900(3) | -5711(3) |
| 54 | -5863(4) | -6726(4) | -5055(4) | 78 | -2809(4) | -3245(4) | -2930(4) | 114 | -3666(3) | -6387(3) | -7234(3) |
| 55 | -4161(4) | -5148(4) | -3053(4) | 79 | -2903(4) | -2989(4) | -2376(4) | 115 | -5348(3) | -8343(3) | -8002(3) |
| 56 | -3160(4) | -4238(4) | -1858(4) | 80 | -2197(4) | -2723(4) | -1976(4) | 116 | -6434(3) | -9672(3) | -8225(3) |
| 57 | -2543(4) | -3685(4) | -1109(4) | 81 | -1952(4) | -2505(4) | -1547(4) | 117 | -7057(3) | -1049(4) | -8136(3) |
| 58 | -2158(4) | -3340(4) | -6361(3) | 82 | -1777(4) | -2345(4) | -1291(4) | 118 | -7386(3) | -1096(4) | -7923(3) |
| 59 | -1930(4) | -3136(4) | -3547(3) | 83 | -1665(4) | -2242(4) | -1128(4) | 119 | -7546(3) | -1121(4) | -7717(3) |
| 60 | -1824(4) | -3040(4) | -2229(3) | 84 | -1610(4) | -2191(4) | -1049(4) | 120 | -7610(3) | -1132(4) | -7597(3) |

NOTE: Number such as 0.7887(5) denotes 0.7887×10^5 ; R denotes radial distance in inches

Table II
RADIAL STRESSES IN ORTHOTROPIC SOLID

| ELEM | $\sigma_R (R=0.1)$ | | | ELEM | $\sigma_R (R=0.3)$ | | | ELEM | $\sigma_R (R=0.7)$ | | |
|------|---------------------|-----------|-----------|------|---------------------|-----------|-----------|------|---------------------|-----------|-----------|
| | 0° | 30° | 60° | | 0° | 30° | 60° | | 0° | 30° | 60° |
| 1 | -.2960(5) | .3135(5) | -.3990(5) | 13 | -.2211(5) | .1337(5) | -.2512(6) | 37 | -.1357(5) | .7561(3) | -.1178(6) |
| 2 | -.6384(4) | .2544(3) | -.3884(5) | 14 | -.4055(4) | .4125(4) | -.2587(5) | 38 | -.3821(4) | .4120(4) | -.2186(5) |
| 3 | .4392(2) | -.1287(5) | .6130(5) | 15 | -.4843(3) | -.7691(4) | .3000(5) | 39 | -.1238(4) | -.3016(4) | .1210(5) |
| 4 | .2595(4) | -.1469(5) | .1006(6) | 16 | -.8407(3) | -.1014(5) | .6033(5) | 40 | .4747(0) | -.5028(4) | .2739(5) |
| 5 | .4917(4) | -.1747(5) | .1397(6) | 17 | .1954(4) | -.1275(5) | .8691(5) | 41 | .7179(3) | -.6933(4) | .4327(5) |
| 6 | .7072(4) | -.2080(5) | .1808(6) | 18 | .2884(4) | -.1551(5) | .1146(6) | 42 | .1214(4) | -.8835(4) | .5945(5) |
| 7 | .8567(4) | -.2347(5) | .2108(6) | 19 | .3678(4) | -.1762(5) | .1344(6) | 43 | .1482(4) | -.1023(5) | .7082(5) |
| 8 | .9626(4) | -.2551(5) | .2327(6) | 20 | .4182(4) | -.1916(5) | .1488(6) | 44 | .1681(4) | -.1121(5) | .7895(5) |
| 9 | .1036(5) | -.2696(5) | .2479(6) | 21 | .4532(4) | -.2026(5) | .1588(6) | 45 | .1825(4) | -.1188(5) | .8454(5) |
| 10 | .1083(5) | -.2792(5) | .2579(6) | 22 | .4761(4) | -.2098(5) | .1653(6) | 46 | .1923(4) | -.1232(5) | .8817(5) |
| 11 | .1111(5) | -.2849(5) | .2639(6) | 23 | .4898(4) | -.2140(5) | .1692(6) | 47 | .1983(4) | -.1257(5) | .9032(5) |
| 12 | .1125(5) | -.2876(5) | .2666(6) | 24 | .4961(4) | -.2160(5) | .1710(6) | 48 | .2011(4) | -.1269(5) | .9131(5) |
| ELEM | $\sigma_R (R=0.90)$ | | | ELEM | $\sigma_R (R=2.35)$ | | | ELEM | $\sigma_R (R=5.05)$ | | |
| | 0° | 30° | 60° | | 0° | 30° | 60° | | 0° | 30° | 60° |
| 49 | -.6668(4) | -.3967(4) | -.8845(5) | 73 | .1870(4) | .3374(4) | -.1912(5) | 109 | .8948(3) | .1052(4) | -.5061(4) |
| 50 | -.6637(4) | .1181(3) | -.2052(5) | 74 | .1224(4) | .6114(3) | -.1277(5) | 110 | .4037(3) | .5255(3) | -.3889(4) |
| 51 | -.1824(4) | -.2368(4) | .8174(4) | 75 | -.1777(4) | -.1093(4) | -.1101(4) | 111 | .6198(1) | -.6503(2) | -.1035(4) |
| 52 | -.3290(3) | -.3980(4) | .2073(5) | 76 | -.1368(4) | .1943(4) | .6312(4) | 112 | -.2606(3) | -.6399(3) | .2093(4) |
| 53 | .4647(3) | -.5568(4) | .3431(5) | 77 | -.7328(3) | -.2663(4) | .1338(5) | 113 | .4205(3) | -.1338(4) | .6027(4) |
| 54 | .9357(3) | -.7217(4) | .4800(5) | 78 | -.1700(3) | .3419(4) | .2032(5) | 114 | -.4563(3) | -.2046(4) | .1013(5) |
| 55 | .1158(4) | -.8427(4) | .5758(5) | 79 | .1250(3) | -.4036(4) | .2519(5) | 115 | -.3934(3) | -.2518(4) | .1297(5) |
| 56 | .1308(4) | -.9278(4) | .6439(5) | 80 | .2732(3) | -.4446(4) | .2858(5) | 116 | -.3175(3) | -.2833(4) | .1489(5) |
| 57 | .1418(4) | -.2858(4) | .6906(5) | 81 | .3540(3) | -.4761(4) | .3088(5) | 117 | -.2563(3) | -.3042(4) | .1616(5) |
| 58 | .1493(4) | -.1023(5) | .7209(5) | 82 | .4006(3) | -.4968(4) | .3236(5) | 118 | -.2137(3) | -.3177(4) | .1697(5) |
| 59 | .1539(4) | -.1045(5) | .7388(5) | 83 | .4268(3) | -.5091(4) | .3323(5) | 119 | -.1876(3) | -.3258(4) | .1744(5) |
| 60 | .1561(4) | -.1055(5) | .7471(5) | 84 | .4387(3) | -.5148(4) | .3363(5) | 120 | -.1752(3) | -.3295(4) | .1765(5) |

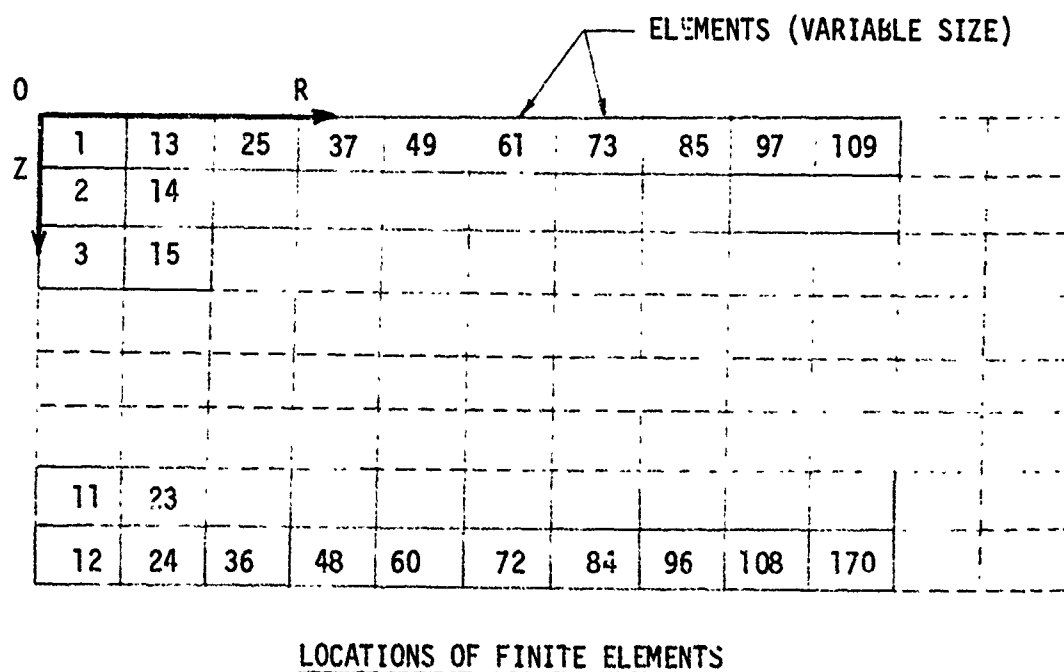
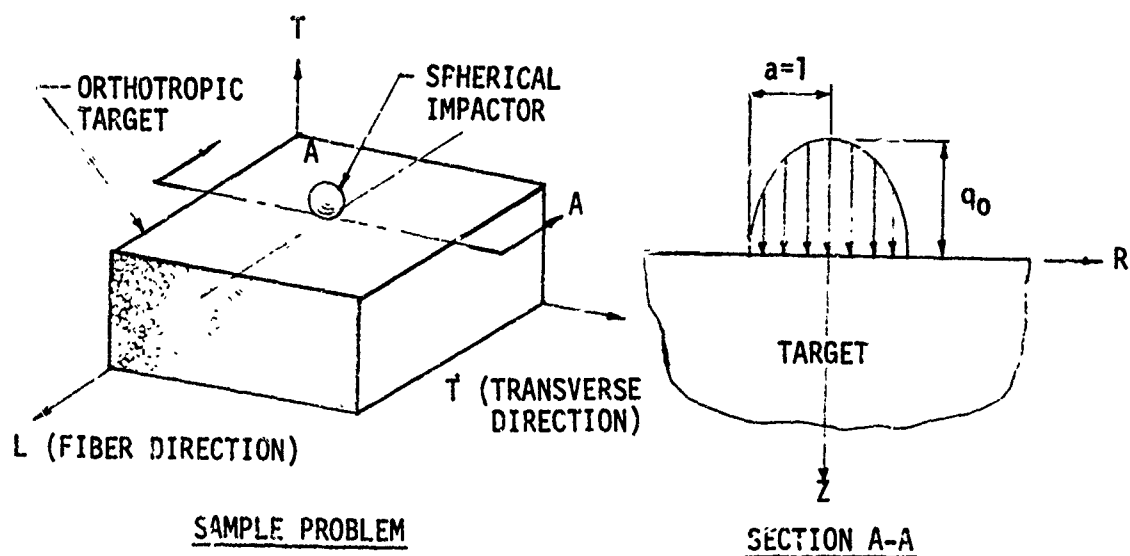


Figure 13. Sample Problem Used in Modified ASAAS Code.

scheme. It accounts for orthotropic elastic perfectly plastic material behavior by using a modified Hill-von Mises yield condition and flow rule, and for isotropic elastic strain-hardening material behavior by using a mechanical sublayer model ⁶¹ as well as von Mises yield condition and flow rule. The calculation proceeds in incremental time steps using an explicit integration scheme. The shell thickness is modeled as equal area and equally spaced layers connected by infinitely thin bond layers of infinite transverse shear rigidity. Strain increments are calculated using Kirchhoff's assumptions for deformations. The finite-difference mesh used represents one fourth of the shell, employing symmetry conditions on a half circle and symmetry conditions on a half length.

The CYLINDER code was originally developed by the Kaman Sciences Corporation ^{62, 63}. The code in operation at MDAC ⁵⁹ was modified to eliminate various problems that were encountered in implementing the code and to improve its analysis capabilities for vulnerability and hardness analyses. Modifications or improvements included:

- Nonconvergence in the iterative plasticity calculations due to a poor initial guess of the plasticity proportionality factor used for determining the plastic strain increments was eliminated by incorporating a quadratic function to determine a much more accurate initial value of the proportionality factor.
- A set of consistent nonlinear equilibrium equations was added to replace linear equilibrium equations that produced inaccurate results when deflections became moderately large. These equations were taken from the aforementioned Sander's formulation.
- Strain-displacement relations were modified to include the effect of inplane displacements on shell surface tangent rotations removing the Donnell-Mushtari-Vlasov approximation originally in the code, and the effect of rotations about the shell surface normal was also included.
- For isotropic materials, kinematic hardening (Bauschinger effect) and isotropic hardening materials models were incorporated.

-
61. Leech, J. W., PETROS 1: FINITE-DIFFERENCE CALCULATION METHOD FOR LARGE ELASTIC-PLASTIC DYNAMICALLY INDUCED DEFORMATIONS OF GENERAL THIN SHELLS, M.T, AFFDL-TR-66-171, December 1966.
 62. Franke, R. H., CYLINDER: A COMPUTER PROGRAM FOR THE INELASTIC DYNAMIC RESPONSE OF ORTHOTROPIC CYLINDRICAL SHELLS, Kaman Nuclear, KN-67-533(R), September 1967.
 63. Hubka, W. F., FURTHER RESULTS IN THE INELASTIC DYNAMIC ANALYSIS OF CYLINDRICAL SHELLS, Kaman Nuclear, KN-67-452(R), September 1967.

- Viscous damping behavior was added.

During this program, additional modifications and improvements were made in the CYLINDER computer code, including addition of an option to input different orthotropic properties for different layers, increasing of mesh size from 15 x 15 to 16 x 50 segments, and addition of new pressure input option to facilitate the input of arbitrary distributed spot loads resulting from impact. In contrast to the plate solution described previously, the solution obtained from the CYLINDER code is the two-dimensional stress solution. Moreover, the CYLINDER code gives the dynamic stresses caused by impact, including stress-wave effects, whereas in the flat-plate analysis only the quasi-dynamic stresses can be calculated.

The input and output of the modified CYLINDER code used in this program are listed on Page 55. The model and the grid used in the code are shown in Figure 14. The cylinder wall can consist of a maximum of eight layers made of orthotropic materials. Each layer can have a different set of elastic properties. The grid contains 50 elements (51 nodes) in the circumferential direction (half the circumference) and 16 elements (17 nodes) in the axial direction (half the cylinder length). By using this type of grid, approximately 80% of the available CDC 6600 computer core storage is utilized (250 Kg of the 320 Kg storage locations are used). Use of finer grid, although feasible, is not practical from the standpoint of computer running time. Figure 15 shows the idealized and actual area of contact resulting from impact by a spherical impactor. Shown also in Figure 15 is the idealized and actual load/pressure distribution at the centerline of the area of contact. Figure 16 shows the computer idealization and actual pressure-time relationship.

The sample problem used for code checkout is shown in Figure 17. The problem involved determination of stresses in a multilayer cylinder subjected to time-dependent surface pressure caused by a 100-ft/sec impact by a spherical impactor. All the pertinent information for the sample problem is shown in Figure 17. The cylinder consisted of eight layers. The fibers in the three layers on the outer surface and the three layers on the inner surface were oriented in the circumferential direction, while the fibers in the center two layers were oriented in the axial direction. The results shown in Figure 17 are for a cylinder made of HTS graphite fibers and epoxy matrix. For such a composite, the mechanical properties associated with the principal directions are:

Young's modulus in the fiber direction, $E_L = 21.5 \times 10^6$ psi

Young's modulus in the transverse direction, $E_T = 1.5 \times 10^6$ psi

Inplane shear modulus, $G_{LT} = 0.7 \times 10^6$ psi

Principal Poisson's ratio, $\nu_{LT} = 0.25$

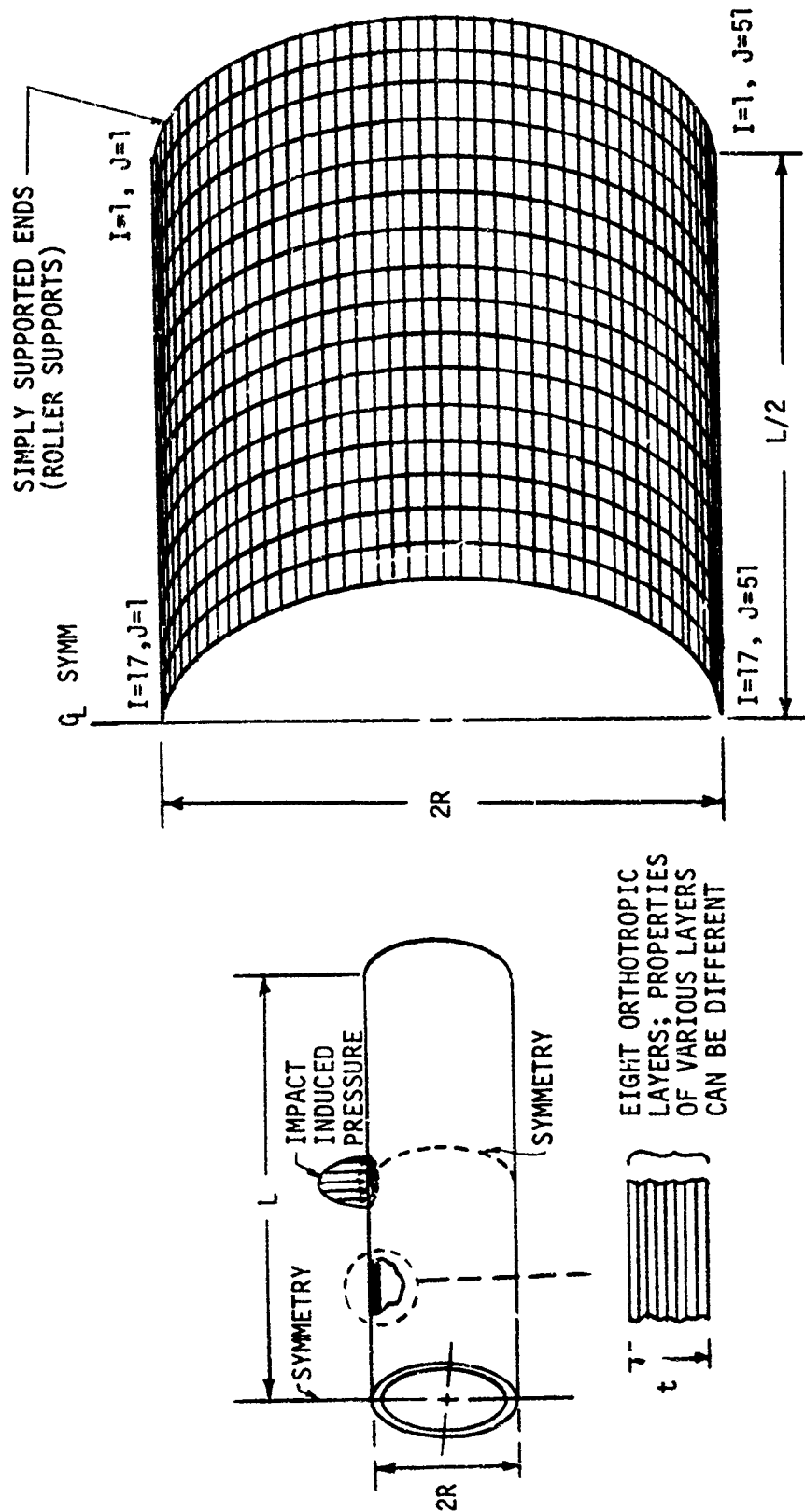
LISTING OF INPUT AND OUTPUT FOR THE CYLINDER COMPUTER PROGRAM

INPUTS TO THE COMPUTER PROGRAM

1. Cylinder Length L
2. Cylinder Radius R
3. Cylinder Thickness t
 - a. Thicknesses of layers within the wall thickness (maximum of 8 layers).
 - b. Orthotropic elastic properties of layers; two Young's moduli (E_x , E_θ), Poisson's ratio ($\nu_{x\theta}$) and shear modulus ($G_{x\theta}$). The properties of each layer can be different.
 - c. Density of each layer
4. Pressure-time History
5. Time steps for which calculations are to be made.
6. Total response time and edit time at which printout is obtained.

OUTPUT OF THE CYLINDER CODE AS A FUNCTION OF TIME AND LOCATION

1. Axial, circumferential and shear stresses in each layer (σ_x , σ_θ and $\sigma_{x\theta}$)
2. Axial, circumferential and shear strains in each layer (ϵ_x , ϵ_θ and $\epsilon_{x\theta}$)
3. Axial, circumferential and shear forces acting on the cylinder wall (N_x , N_θ and $N_{x\theta}$)
4. Axial, circumferential and torsional moments acting on the cylinder wall (M_x , M_θ and $M_{x\theta}$)
5. Axial, circumferential and radial displacements U , V and W , respectively.
6. Axial (U) and Radial (W) deflections and their variation at the crown of the cylinder ($\theta = 0$) as a function of axial coordinate ($J = 1, 2, \dots, 17$)
7. Circumferential (V) and Radial (W) deflections and their variation at centerline of cylinder ($X = L/2$) and their variation as a function of circumferential coordinate, s ($I = 1, 2, \dots, 51$).



GRID USED IN THE CYLINDER CODE
 (50 ELEMENTS IN CIRCUMFERENTIAL DIRECTION)
 (16 ELEMENTS IN AXIAL DIRECTION)

CYLINDER SUBJECTED TO
 TIME-DEPENDENT LOADING
 RESULTING FROM IMPACT

Figure 14. Model Used in the Cylinder Code.

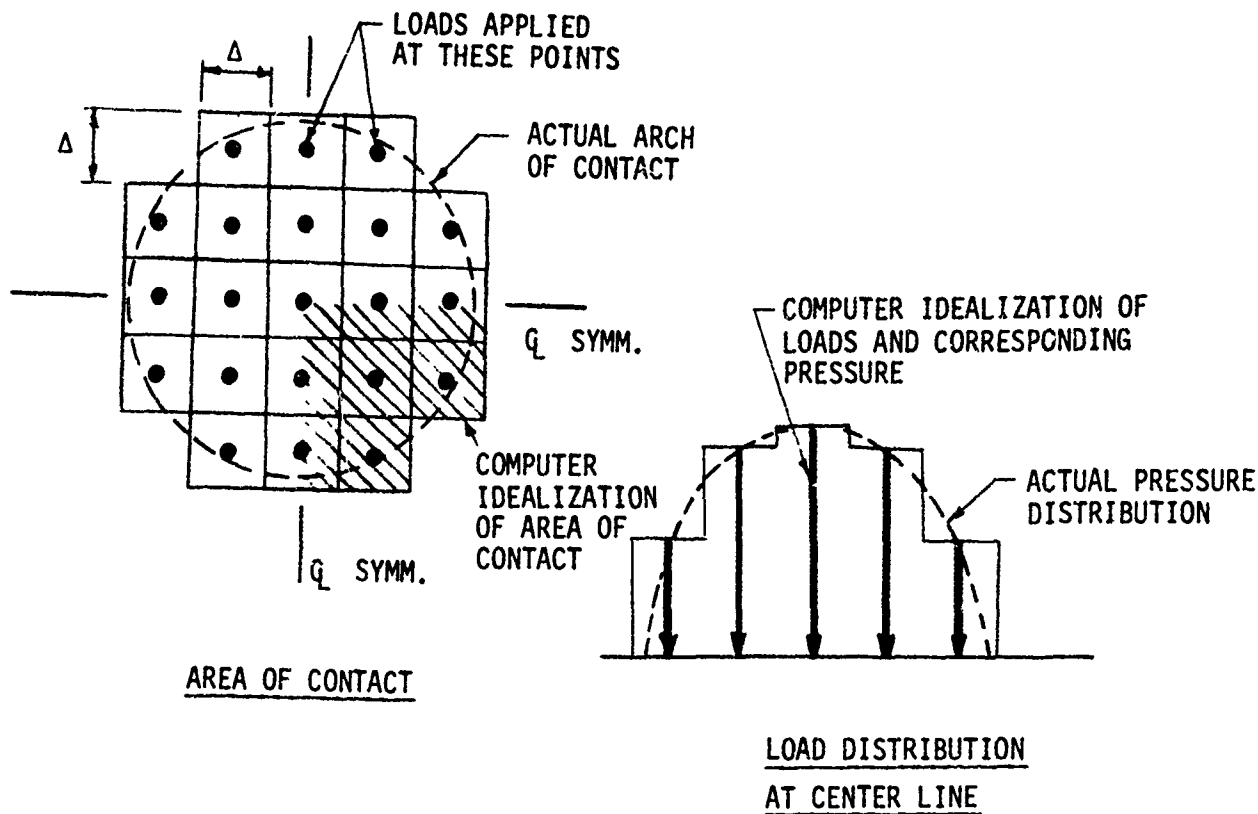


Figure 15. Area of Contact and Pressure/Load Distribution.

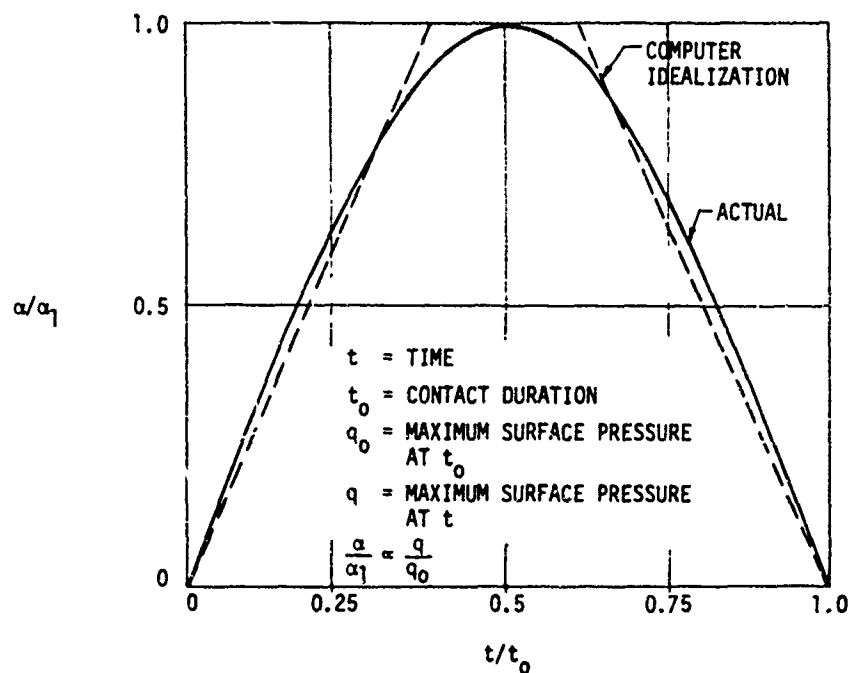


Figure 16. Actual and Computer Idealization of Pressure-Time Distribution.

IMPACT VELOCITY, $V = 100$ FT/SEC
 IMPACTOR DIAMETER, $D = 1.5$ IN.
 IMPACTOR DENSITY, $\rho_1 = 0.288$ LB/IN³
 MAX. IMPACT PRESSURE, $q_0 = 309$ KSI (AT t_0)
 CONTACT DURATION, $t_0 = 72$ μ SEC
 AREA OF CONTACT, $A = 0.165$ IN²
 MAX. LOAD FROM IMPACT, $P = 34,000$ LBS

$R = 1.59$ IN.
 $L = 3.18$ IN.
 $t = 0.252$ IN.
 $t_H = 0.028$ IN.
 $t_L = 0.042$ IN.
 $\rho = 0.054$ LB/IN³
 (COMPOSITE DENSITY)

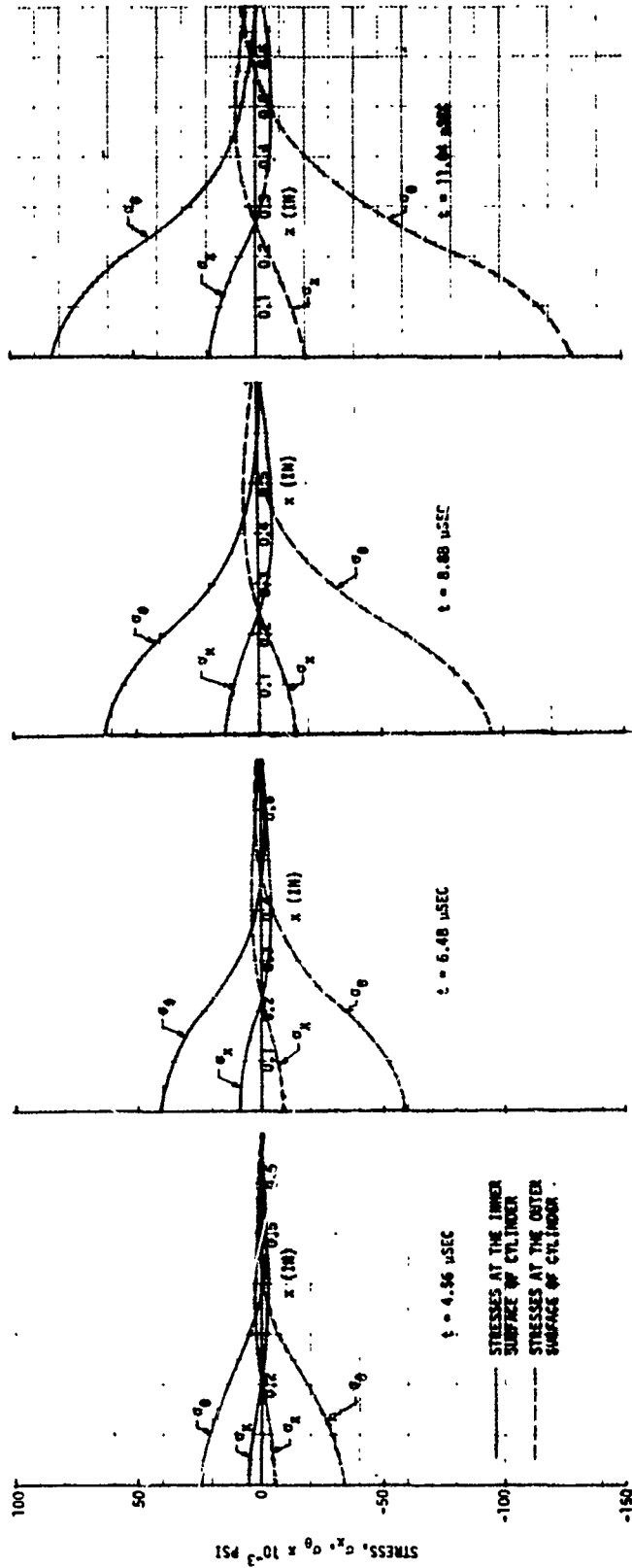
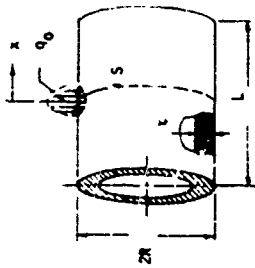


Figure 17. Variation of Impact-Induced Stresses (at $s = 0$) as a Function of Time and Axial Coordinate, x .

Tensile strength in the fiber direction, $\sigma_{Lt} = 204 \times 10^3$ psi

Tensile strength in the transverse direction, $\sigma_{Tt} = 11.8 \times 10^3$ psi

Compressive strength in the fiber direction, $\sigma_{Lc} = 201 \times 10^3$ psi

Compressive strength in the transverse direction, $\sigma_{Tc} = 34.4 \times 10^3$ psi

Shear strength (interlaminar), $\tau = 14 \times 10^3$ psi

Figure 17 shows the circumferential and axial stresses at the inner and outer surfaces of the cylinder as a function of axial (x) coordinate and a function of time, t. The variation of stresses as a function of time and circumferential coordinate is shown in Figure 18. The maximum stresses at $x = s = 0$ (center of contact) as a function of time are shown in Figure 19. Figures 20 and 21 show some results, based on maximum stress criteria, on the initiation and progression of failure as a function of time. For the problem considered, the total contact duration was calculated to be $t_0 = 172 \mu\text{sec}$. As shown in Figure 20, failure of material initiates in the transverse direction in the innermost layer of the cylinder at $t = 7.92 \mu\text{sec}$. The failure region increases with increasing t until at $t = 9.84 \mu\text{sec}$, failure initiates in another layer (No. 7).

As time increases beyond $t = 11.04 \mu\text{sec}$, the damage zone grows and failure progresses to other layers. At $t = 15.4 \mu\text{sec}$, critical damage takes place in the layer on the outer surface of the cylinder, as shown in Figure 21. At that time increment, compression failure takes place in the direction of the fibers. The damage in other layers at the critical time increment ($t = 15.4 \mu\text{sec}$) is also shown in Figure 21.

The results for stresses and deformation were obtained at 0.06- μsec time intervals. Although the total response time of interest is 172 μsec (total contact duration), only the early-time response ($t = 11.28 \mu\text{sec}$) was obtained in the printout, primarily to minimize the computer running time in the checkout problem. The computer running time (total machine units) for the early-time response ($t = 11.28 \mu\text{sec}$) was ~15 minutes. The computer performed approximately 190 time-step calculations within that time.

COUPLING BETWEEN IMPACT PARAMETERS, TARGET PROPERTIES, AND FAILURE MODES

The final step in the theory development was to establish failure modes resulting from internal triaxial stresses caused by impact-induced surface pressure, as well as the time sequence for occurrence of the various failure modes. This was done by applying the failure criterion for generally orthotropic solids to the impact-induced triaxial stress

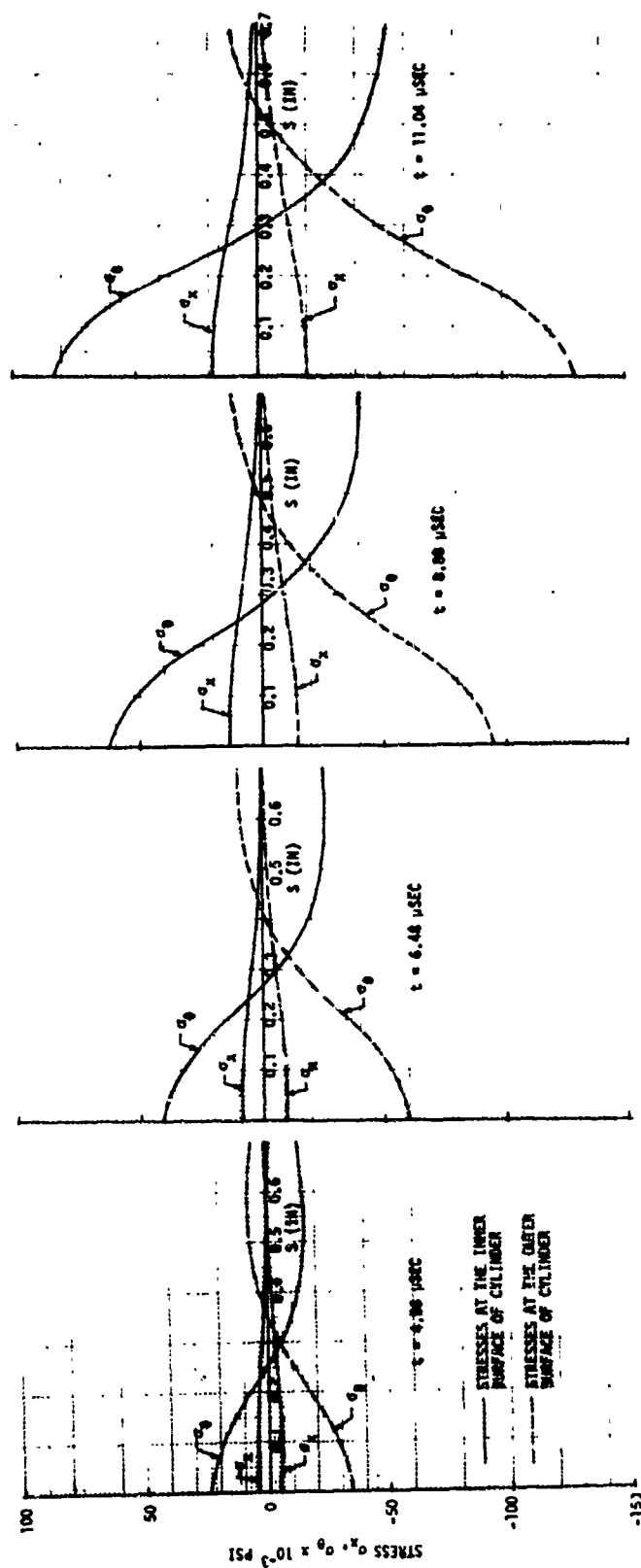


Figure 18. Variation of Impact-Induced Stresses (at $x = 0$) as a Function of Time and Circumferential Coordinate, (s).

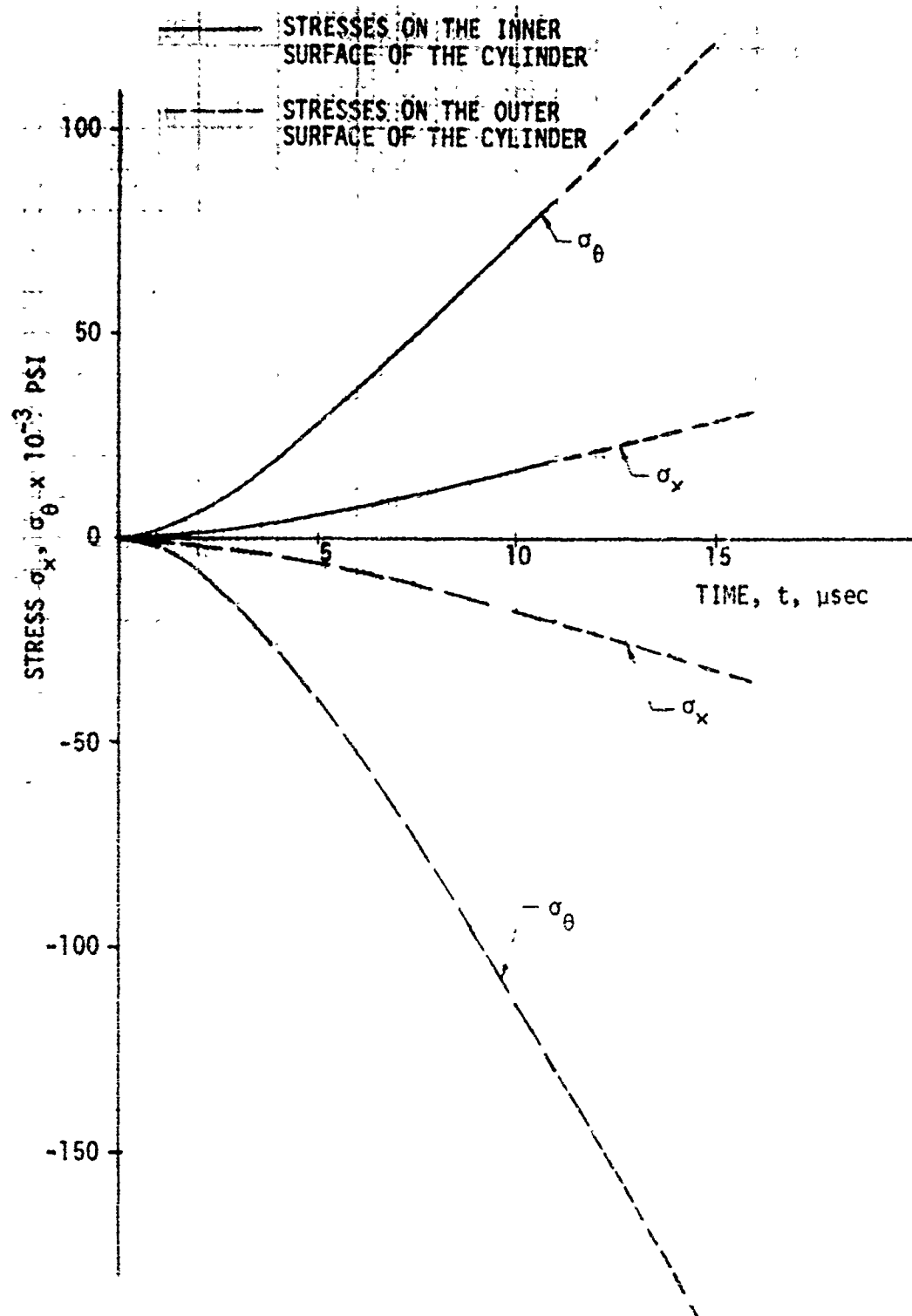


Figure 19. Variation of Stresses at $x = 0$, $s = 0$ as a Function of Time.

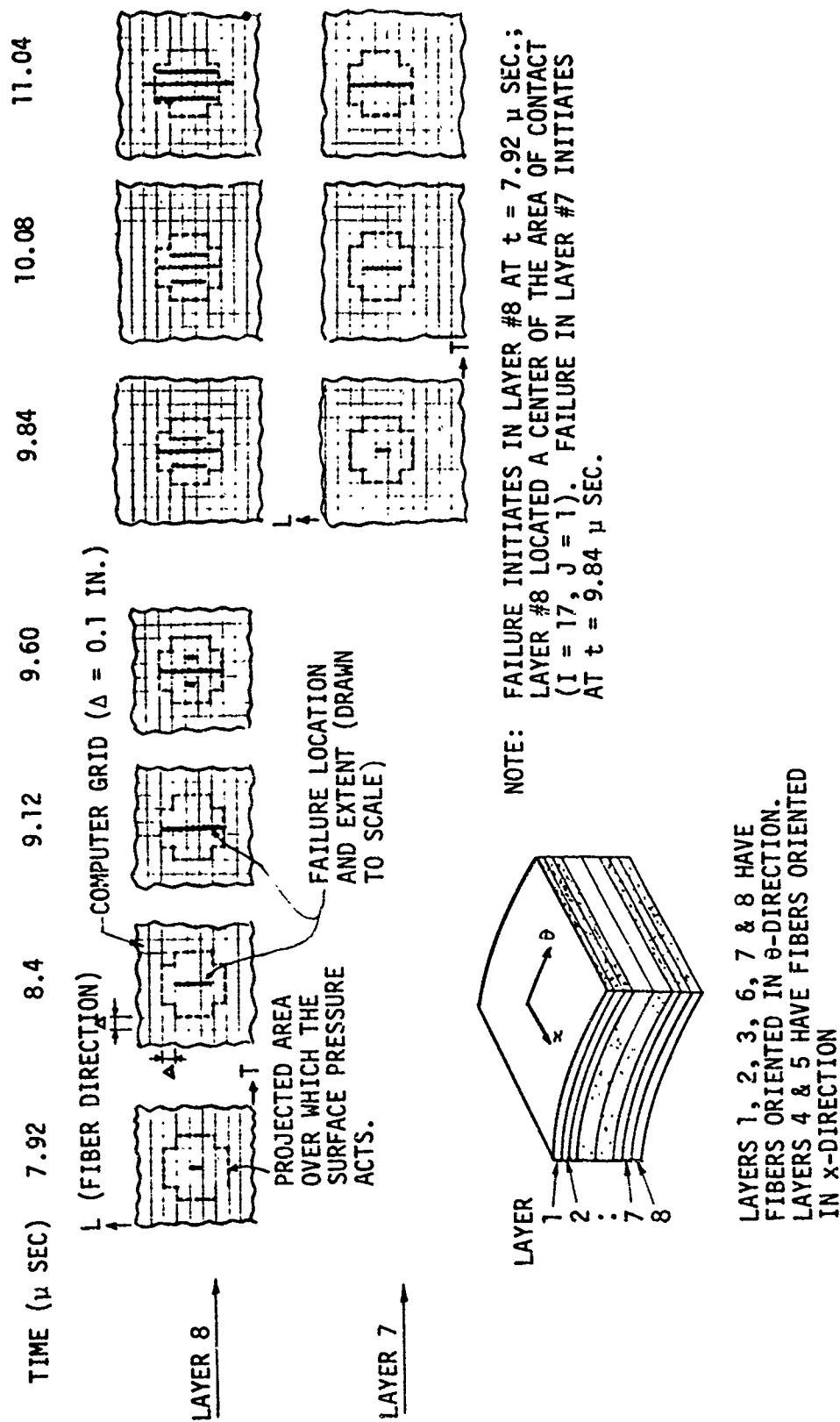


Figure 20. Initiation and Growth of Failure in a Multilayer Composite Cylinder Subjected to Impact.

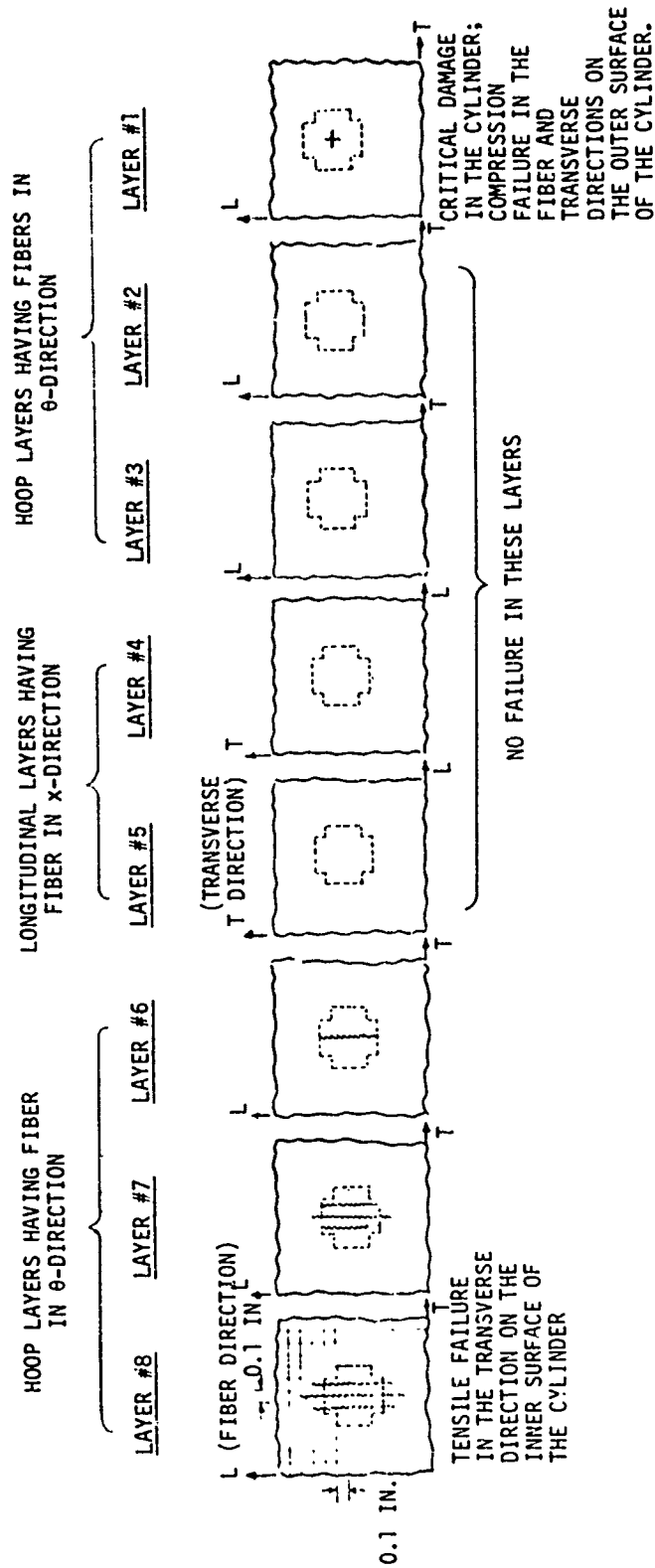


Figure 21. Failure in Various Layers at $t = 15.4 \mu\text{sec}$ When Critical Damage Occurs (Failure of Layer Number 1 in the Fiber Direction).

state in the target. The following failure criterion, based on distortion-energy theory ⁶⁴, was used to predict failure and failure envelopes:

$$\begin{aligned}
 1 = & \frac{\sigma_{11}^2}{F_{11}^2} + \frac{\sigma_{22}^2}{F_{22}^2} + \frac{\sigma_{33}^2}{F_{33}^2} + \frac{\sigma_{12}^2}{F_{12}^2} + \frac{\sigma_{13}^2}{F_{13}^2} + \frac{\sigma_{23}^2}{F_{23}^2} \\
 & - \left(\frac{\sigma_{11}}{F_{11}} \right) \left(\frac{\sigma_{22}}{F_{22}} \right) \left[\frac{(1 + 2\nu_{21} - \nu_{23})E_1 + (1 + 2\nu_{12} - \nu_{13})E_2}{[(2 + \nu_{12} + \nu_{13})(2 + \nu_{21} + \nu_{23})E_1E_2]^{1/2}} \right] \\
 & - \left(\frac{\sigma_{11}}{F_{11}} \right) \left(\frac{\sigma_{33}}{F_{33}} \right) \left[\frac{(1 + 2\nu_{31} - \nu_{32})E_1 + (1 + 2\nu_{13} - \nu_{12})E_3}{[(2 + \nu_{12} + \nu_{13})(2 + \nu_{31} + \nu_{32})E_1E_2]^{1/2}} \right] \\
 & - \left(\frac{\sigma_{22}}{F_{22}} \right) \left(\frac{\sigma_{33}}{F_{33}} \right) \left[\frac{(1 + 2\nu_{23} - \nu_{21})E_3 + (1 + 2\nu_{32} - \nu_{31})E_2}{[(2 + \nu_{21} + \nu_{23})(2 + \nu_{31} + \nu_{32})E_2E_3]^{1/2}} \right]
 \end{aligned} \quad (31)$$

where σ 's are the impact-induced direct and shear stresses, F 's are the allowable strength properties of material associated with the three orthogonal directions, and E 's and ν 's are the Young's moduli and Poisson's ratios associated with Directions 1, 2, and 3. The failure criterion was incorporated into the SAAS III and ASAAS as a subroutine. To take into account differences in tensile and compressive strength in any given direction, an allowance was made in the computer subroutine that allowable compressive strength, F_c , is used if the corresponding σ is negative, and allowable tensile strength, F_t , is used if σ is positive.

64. Greszczuk, L. B., FAILURE CRITERIA FOR THREE-DIMENSIONAL ORTHOTROPIC SOLIDS, Douglas Aircraft Company Report DAC 60869, October 1967.

SECTION III

THEORY APPLICATION

The analysis methods that were developed as described in Section II were applied to study the impact response and failure modes of graphite-epoxy composites as influenced by fiber and matrix properties, fiber orientation, stacking sequence, plate thickness, curvature effects, and material combinations (hybrid composites and interleaved materials). In conjunction with this work, data reported in the literature was compiled on properties of various fibers and composites, and candidate composites were selected for detailed analytical studies to establish how the variables noted above affect the impact response.

CANDIDATE REINFORCEMENT, MATRIX AND COMPOSITE MATERIALS AND THEIR PROPERTIES

There exist numerous types of graphite fibers and other kinds of reinforcement materials for use in composites and structural components made of composites. The various reinforcing fibers, including the numerous graphite and carbon fibers as well as their properties and other pertinent data, are listed in Table III. Table IV shows the properties of composites made with various types of fibers. Finally, Table V shows the properties of composites made with Thornel 300 graphite fibers and different resins. The properties shown in Tables III and IV were obtained from various references given in the literature and data provided by the fiber and composite manufacturers as well as from MDC in-house programs on composites.

Candidate Fibers and Composites for Analytical Studies

Because of the profusion of graphite fibers and even more so of composites, it was found necessary to concentrate on the following three main groups of composites:

1. Composites having ultra-high Young's modulus (such as Thornel 75-epoxy and Celion GY70-epoxy).
2. Composites having high modulus and moderate strength (such as HMS graphite-epoxy and Thornel 50s-epoxy).
3. Composites having high strength and moderate modulus (such as HTS graphite-epoxy and Thornel 300-epoxy).

Table VI gives the unidirectional properties of two graphite-epoxy composites belonging to each group. For later use, properties of

Table III

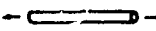


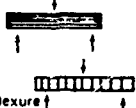
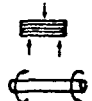


[illegible]

... THE AVERAGE ANGLE THAT THE LAMAL PLANE WITHIN THE CRYSTALLITES MAKE WITH THE FIBER AXIS

Table IV





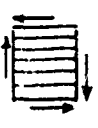
[illegible]

Table V
PROPERTIES OF THORNEIL 300 GRAPHITE-FIBER COMPOSITES

| | Property | Units | Composite (Fiber/Resin) | | | | | | | | | | AVERAGE |
|---|---|--|-------------------------|--------------------|---------------|---------------|----------------------|----------------------|---------------|---------------|------------------|------------------------------|---------|
| | | | T300/934 (1) | | T300/2544 (1) | | T300/5208 (2) | | T300/1004 (1) | | T300/ 3MPR266 | | |
| | | | SB(4) | C (4) | SB | C | SB | C | SB | C | SB | | |
|  Fiber | σ_f E_f e_f d | 10^3 psi 10^6 psi lbs/in ³ 10^{-3} in. | | | | | | | | | | 325 34 0.0614 0.304 | |
| Volumes of Constituents | k_f k_v | % % | ~73 — | | 67 — | | 65-68 — | | 67 — | | | ~68 — | |
| Composite Density | ρ_{co} | lbs/in ³ | | | | | | | | | | ~0.056 | |
|  Axial | σ_{iL} E_{iL} e_{iL} | 10^3 psi 10^6 psi % | 241.1 24.8 | 215.4 23.2 | 229.6 23.3 | 173.5 21.6 | 247.1 25.7 1.0 | 215.0 20.5 1.0 | 221.6 21.8 | 208.1 21.8 | 258.0 25.8 | 223.2 24.2 1.0 | |
| | σ_{cL} E_{cL} e_{cL} ν_{LT} | 10^3 psi 10^6 psi % — | 238.5 21.5 | 173.0 | 231.8 20.1 | 172.3 | 255.8 22.3 1.5 | 198.0 20.0 | 220.7 20.6 | 192.3 | 265.0 18.9 | 216.4 20.6 1.5 | |
|  Transverse | σ_{iT} E_{iT} e_{iT} | 10^3 psi 10^6 psi % | | | | | 10.7 2.4 0.48 | 6.8 1.5 0.47 | | | | 8.7 1.9 0.48 | |
| | σ_{cT} E_{cT} e_{cT} ν_{TL} | 10^3 psi 10^6 psi % % | | | | | | 33.0 | | | | 33.0 | |
|  Flexure | σ_{fL} E_{fL} | 10^3 psi 10^6 psi | | 263.7 20.8 | | 253.8 19.8 | | 280.5 21.0 | | 231.4 19.0 | | 257.3 20.2 | |
| | σ_{iT} E_{iT} | 10^3 psi 10^6 psi | | | | | | 11.5 1.6 | | | | 11.5 1.6 | |
|  Shear | τ_{LT} G_{LT} | 10^3 psi 10^6 psi | | 17.4 | | 15.8 | | 17.6 | | 15.9 | 15.3 | 16.4 | |
|  45° | σ_t E_t | 10^3 psi 10^6 psi | | | | 21.6 3.5 | | | | 13.7 2.4 | | 17.6 2.9 | |
|  Pseudo Isotropic | σ_t E_t e_t | 10^3 psi 10^6 psi % | | 62.4 7.6 0.8 | | | | | | | | 68.0 (3) 8.3 (3) 0.8 | |

- (1) Inhouse test results;
- (2) Test data from inhouse programs and from Narmco
- (3) Normalized to fiber content of $k = 68\%$
- (4) SB denotes sandwich beam test; C denotes coupon test

Table VI
PROPERTIES OF THE CANDIDATE GROUPS OF COMPOSITES

| | PROPERTY | UNITS | ULTRA HIGH E | | HIGH E | | HIGH σ | | S-GLASS/ EPOXY |
|---|-----------------|--------------------|--------------|-------------|-----------|-----------|---------------|-----------|-------------------|
| | | | T75s/4617 | GY70/R-350A | HMS/BP907 | T50s/4617 | HTS/BP907 | T300/5208 | |
|   AXIAL PROPERTIES | k_f | % | 57 | 58 | 58 | 60 | 59 | 66 | 67 |
| | σ_{tL} | 10^3 psi | 214 | 90 | 135 | 143 | 204 | 215 | 289 |
| | E_{tL} | 10^6 psi | 44 | 42 | 30.1 | 33 | 21.5 | 20.5 | 8.3 |
| | ϵ_{tL} | % | 0.46 | 0.21 | 0.43 | 0.48 | 0.92 | 1.0 | 3.5 |
| | σ_{cL} | 10^3 psi | 97 | 90 | 128 | 100 | 201 | 198 | 170 |
| | E_{cL} | 10^6 psi | 44 | 42 | 30 | 33 | 21 | 20 | 8.3 |
| | ϵ_{cL} | % | 0.26 | (0.2) | 0.53 | 0.35 | 1.22 | (0.99) | (2.05) |
| | ν_{LT} | --- | 0.32 | 0.25 | 0.28 | 0.30 | 0.25 | (0.25) | 0.26 |
|   TRANSVERSE PROPERTIES | σ_{tT} | 10^3 psi | 4.6 | 3.0 | 7.6 | 4.5 | 11.8 | 6.8 | 11.0 |
| | E_{tT} | 10^6 psi | 0.9 | 0.86 | 1.0 | 1.0 | 1.44 | 1.5 | 2.9 |
| | ϵ_{tT} | % | 0.5 | (0.35) | 0.77 | 0.46 | 0.88 | 0.47 | 0.4 |
| | σ_{cT} | 10^3 psi | 27 | (1.01) | 32.6 | 29.0 | 34.4 | 33.0 | 29.0 |
| | E_{cT} | 10^6 psi | 1.0 | (1.01) | 1.4 | 1.1 | 1.6 | (1.77) | 2.9 |
| | ϵ_{cT} | % | 2.1 | (0.005) | 4.1 | 3.0 | 3.44 | (1.86) | (1.0) |
| | ν_{TL} | --- | 0.007 | (0.005) | (0.009) | (0.0095) | (0.018) | (0.0202) | 0.091 |
| | | | | | | | | | |
|  SHEAR PROPERTIES | τ_{ts} | 10^3 psi | 6.0 | 8.6 | 13.7 | 8.0 | 14.0 | 17.6 | 9.0 |
| | τ_{LT} | 10^3 psi | (6.0)* | (8.6)* | 10.4 | (8.0)* | 10.6 | (13.3) | --- |
| | γ_{LT} | % | (0.86) | (1.43) | (1.22) | (1.10) | (1.25) | (1.57) | (1.05) |
| | G_{LT} | 10^6 psi | (0.70) | 0.60 | 0.85 | (0.73) | 0.85 | (0.85) | 0.86 |

() Calculated or estimated from data for other composites for which results are shown in the table.

()* τ_{LT} assumed the same as τ_{ts}

unidirectional glass-epoxy composites are also given therein. The results presented in Table VI are experimental values, except as noted therein. Using the properties shown in Table VI, calculations were made for the properties of pseudo-isotropic laminates for use in the SAAS computer code. Table VII shows the final results, while Figure 22 shows a comparison of predicted tensile strength and Young's modulus of pseudo-isotropic composites with limited data found in the literature.

Inasmuch as the properties of the two composites within any of the three groups are approximately the same* the seven candidate materials were narrowed down to three graphite-epoxy composites and glass-epoxy. The properties required for use with SAAS III of the four final materials are given in Table VIII. The properties used in ASAAS were those shown in Table VI.

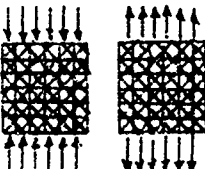
Candidate Resin Materials

Most of the data given in the literature is for composites made with epoxy resins having Young's modulus of between 0.5×10^6 to 0.6×10^6 psi. No data were found for composites made with low-modulus ($E_r \sim 0.10 \times 10^6$ psi) or high-modulus ($E_r \sim 1 \times 10^6$ psi) resins. Consequently, to establish how properties of resin affect impact behavior of composites, it was found necessary to make estimates for the various properties of low- and high-modulus resins. This was done by compiling test data for various epoxy resins, plotting tensile strength of resin versus its modulus in tension, compressive strength of resin versus its compressive modulus, and compressive modulus versus tensile modulus, and extrapolating the curves to estimate the various properties of the resins with high and low Young's modulus. Figure 23 shows a plot of the compressive strength of various resins versus Young's modulus in compression. The estimated properties of the high-, low-, and ultra-low-modulus resins are given in Table IX, together with data for a typical epoxy resin (Mid E) used in composites for which data are given in the literature and shown in Tables VI, VII, and VIII. Except for the resin designated as ULE, the strength properties of the remaining resins were estimated as described above. The strength of the ULE matrix was arbitrarily assumed to be high. Using the properties given in Table IX, calculations were made for the properties of composites made with Thornel 300-graphite fibers and the various matrix materials. Table X shows the final results. The properties of the Thornel 300 fibers used in these calculations were as follows:

Young's modulus of the fiber in the fiber direction,
 $E_{fL} = 34 \times 10^6$ psi

*Except for the difference in tensile strength between Thornel 75s-epoxy and Celion GY70-epoxy.

Table VII
PROPERTIES OF PSEUDO-ISOTROPIC LAMINATES (CALCULATED)

| | PROPERTY | UNITS | ULTRA HIGH E | | HIGH E | | HIGH σ | | S-GLASS/ EPOXY |
|---|-------------|--------------------|--------------|-------------|-----------|-----------|---------------|-----------|-------------------|
| | | | T75/4617 | GY70/R-350A | HMS/BP907 | T50s/4617 | HTS/BP907 | T300/5208 | |
| | | | | | | | | | |
|  | k | % | 57 | 58 | 58 | 60 | 59 | 66 | 67 |
| | σ_t | 10^3 psi | 69.6 | 33.4 | 49.7 | 53.5 | 72.6 | 76.2 | 91.5 |
| | σ_c | 10^3 psi | 33.4 | 33.4 | 47.4 | 36.2 | 79.1 | 79.1 | 75.7 |
| | τ_{ts} | 10^3 psi | 6.0 | 8.6 | 13.7 | 8.0 | 14.0 | 17.6 | 9.0 |
| | τ_{tn} | 10^3 psi | | | | | | | |
| | E | 10^6 psi | 15.6 | 14.8 | 11.10 | 11.92 | 8.26 | 8.00 | 4.42 |
| | G | 10^6 psi | 5.9 | 5.61 | 4.24 | 4.54 | 3.18 | 3.08 | 1.67 |
| | ν | --- | 0.318 | 0.318 | 0.305 | 0.312 | 0.30 | 0.30 | 0.32 |
| | DESIGNATION | | 1 | 2 | 3 | 4 | 5 | 6 | 7 |

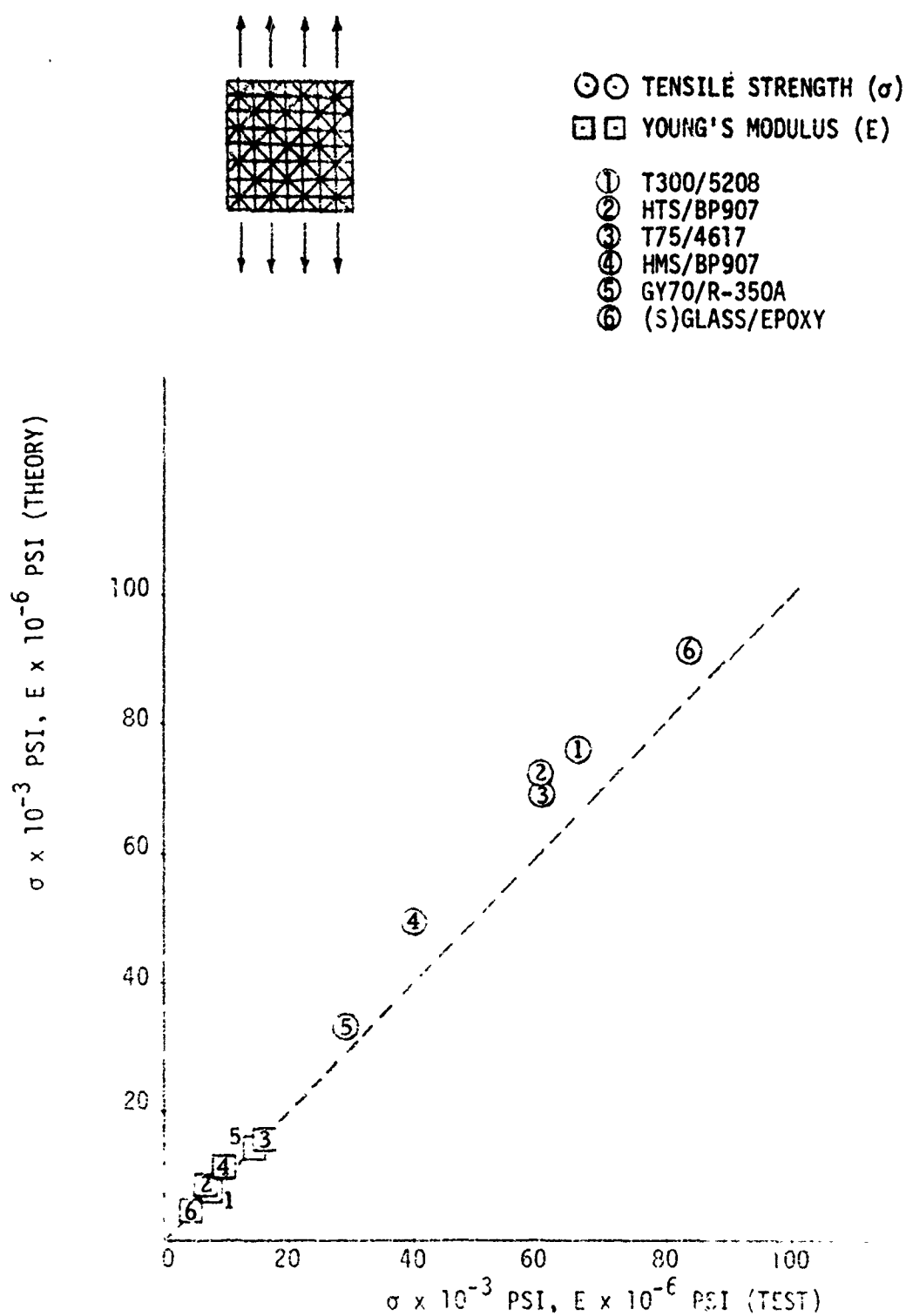


Figure 22. Test-Theory Comparison of Tensile Strength and Young's Modulus of Pseudo-Isotropic Composites Made of Various Fiber-Matrix Combinations.

Table VIII
PROPERTIES OF THE CANDIDATE COMPOSITE MATERIALS

| PROPERTY | UNITS | MATERIAL | | | | |
|-------------------------------------|------------|----------|-------|--------|-------|--|
| | | GY70/E | HMS/E | T300/E | GL/E | |
| YOUNG'S MODULUS, E_r | 10^6 psi | 14.8 | 11.10 | 8.0 | 4.42 | |
| YOUNG'S MODULUS, E_z | 10^6 psi | 1.01 | 1.4 | 1.77 | 2.9 | |
| SHEAR MODULUS, G_z | 10^6 psi | 0.60 | 0.85 | 0.85 | 0.86 | |
| POISSON'S RATIO, ν_r | --- | 0.318 | 0.305 | 0.30 | 0.32 | |
| POISSON'S RATIO, ν_z | --- | 0.005 | 0.009 | 0.0202 | 0.091 | |
| TENSILE STRENGTH, σ_{rt} | 10^3 psi | 33.4 | 49.7 | 76.2 | 91.5 | |
| TENSILE STRENGTH, σ_{zt} | 10^3 psi | 4.0 | 7.6 | 6.8 | 11.0 | |
| COMPRESSIVE STRENGTH, σ_{rc} | 10^3 psi | 33.4 | 47.4 | 79.1 | 75.7 | |
| COMPRESSIVE STRENGTH, σ_{zc} | 10^3 psi | 27.0 | 32.6 | 33.0 | 29.0 | |
| SHEAR STRENGTH, σ_{zr} | 10^3 psi | 8.6 | 13.7 | 17.6 | 9.0 | |
| DESIGNATION | | 2 | 3 | 6 | 7 | |

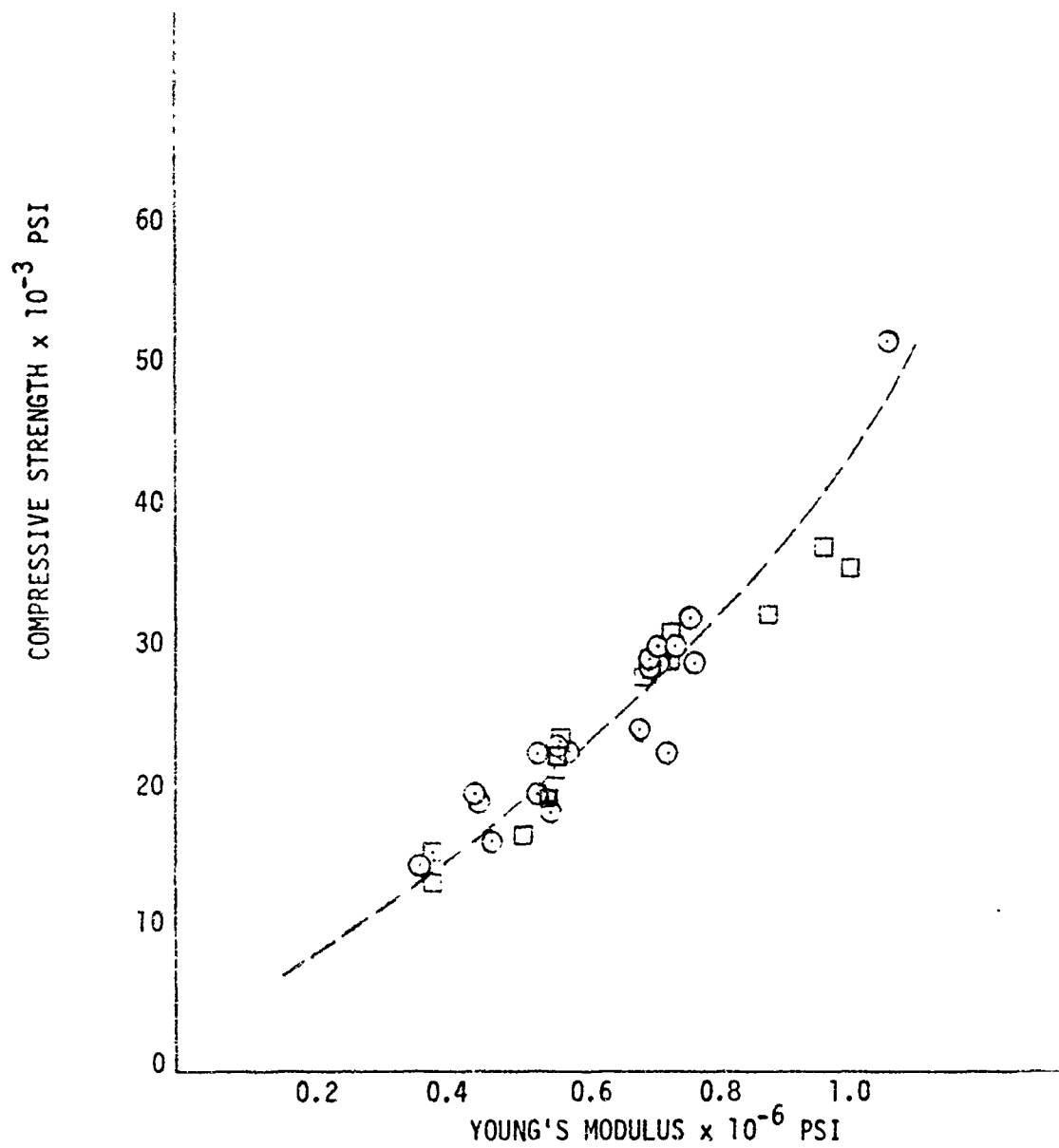


Figure 23. Correlation Between Compressive Strength and Compressive Modulus of Epoxy Resins.

Table IX
PROPERTIES OF CANDIDATE RESINS (ESTIMATED)

| TYPE | DESIGNATION | YOUNG'S MODULUS X 10 ⁻⁶ PSI | | STRENGTH X 10 ⁻³ PSI | | SHEAR MODULUS* X 10 ⁻⁶ PSI | POISSONS RATIO |
|-------------|-------------|--|-------------|---------------------------------|-------------|--|-------------------|
| | | TENSION | COMPRESSION | TENSION | COMPRESSION | | |
| ULTRA LOW E | ULE | 0.10 | 0.10 | 13.5 | - | 0.035 | 0.43 |
| LOW E | LE | 0.25 | 0.22 | 5.5 | 9.0 | 0.084 | 0.40 |
| MID E | ME | 0.50 | 0.55 | 13.5 | 21.0 | 0.193 | 0.36 |
| HIGH E | HE | 1.00 | 0.86 | 13.2 | 45.0 | 0.363 | 0.28 |

*CALCULATED FROM $G = E_{AVE}/2(1+\nu)$

Table X
PROPERTIES OF UNIDIRECTIONAL COMPOSITES (CALCULATED)

| COMPOSITE* (FIBER/RESIN) | ELASTIC CONSTANTS | | | | STRENGTH X 10 ⁻³ PSI | | | | |
|-----------------------------|------------------------------|------------------------------|---------------------------------|------------|---------------------------------|---------------|---------------|---------------|----------------------|
| | E_L X 10 ⁻⁶ PSI | E_T X 10 ⁻⁶ PSI | G_{LT} X 10 ⁻⁶ PSI | ν_{LT} | TENSION | | COMPRESSIVE | | SHEAR τ_{LT} |
| | | | | | σ_{Lt} | σ_{Tt} | σ_{LC} | σ_{TC} | |
| T300/ULE | 22.48 | 0.60 | 0.37 | 0.278 | 214.5 | 6.0 | 214.5 | 19.2 | 11.8 |
| T300/LE | 22.53 | 0.95 | 0.51 | 0.268 | 215.5 | 2.2 | 215.5 | 26.3 | 4.3 |
| T300/ME | 22.63 | 1.42 | 0.71 | 0.254 | 216.3 | 9.3 | 216.3 | 32.6 | 18.4 |
| T300/HE | 22.77 | 1.80 | 0.82 | 0.278 | 217.7 | 9.9 | 217.7 | 36.3 | 19.6 |

*FIBER VOLUME FRACTION OF ALL COMPOSITES WAS TAKEN AS $k_f = 0.66$.

Young's modulus of the fiber in the transverse direction,
 $E_{fT} = 3.1 \times 10^6$ psi

Shear modulus of the fiber, $G_f = 1.5 \times 10^6$ psi

Poisson's ratio of the fiber, $\nu_f = 0.2$

Tensile strength of the fiber, $\sigma_{ft} = 325 \times 10^3$ psi

Compressive strength of the fiber, $\sigma_{fc} = 325 \times 10^3$ psi

The elastic properties of unidirectional composites (E_L , E_T , G_{LT} , and ν_{LT}) were calculated using equations given in Reference 65. The tensile and compressive strengths of the composites in the fiber direction were calculated from the law of mixtures. Transverse tensile strength of the composites, σ_{Tt} , was calculated from equations given in Reference 66. In calculating σ_{Tt} , it was assumed that the volume fraction of voids within the composites was $k_v = 2\%$. The compressive strength of the composites in the transverse direction was estimated from the results shown in Figure 24, which shows an empirical relationship between the compressive Young's modulus in the transverse direction and the transverse compressive strength of the composite. The results shown in Figure 24 are similar to the strength-modulus relationship for the resins, which is shown in Figure 23. Finally the interlaminar shear strength, τ_{LT} , was estimated from the results given in Reference 67, where it is shown that a relationship exists between σ_{Tt} and τ_{LT} .

Using the properties of unidirectional composites given in Table X, the various properties of pseudo-isotropic laminates were then calculated. The final results are shown in Table XI. These results are analogous to the results given in Table VIII except that the variable here is the matrix material, whereas in Table VIII the variable was the fiber material.

INFLUENCE OF MATERIAL PROPERTIES ON IMPACT PARAMETERS (SURFACE PRESSURE, AREA OF CONTACT, AND IMPACT DURATION VERSUS IMPACT VELOCITY)

The analyses described in Section II were applied to predict the influence of impact velocity on the surface pressure, area of contact, and impact

65. Greszczuk, L. B., THEORETICAL AND EXPERIMENTAL STUDIES ON PROPERTIES AND BEHAVIOR OF FILAMENTARY COMPOSITES, Proceedings of the 21st Annual Technical Conference of the Society of Plastics Industries, Chicago, Illinois, February 1966.
66. Greszczuk, L. B., MICROMECHANICS FAILURE CRITERIA FOR COMPOSITES, Final Summary Report prepared under Naval Air Systems Command Contract No. N00019-72-0221, May 1973.
67. Greszczuk, L. B., MECHANICS OF FAILURE OF COMPOSITES, Final Summary Report prepared under Naval Air Systems Command Contract No. N00019-73-0405, May 1974.

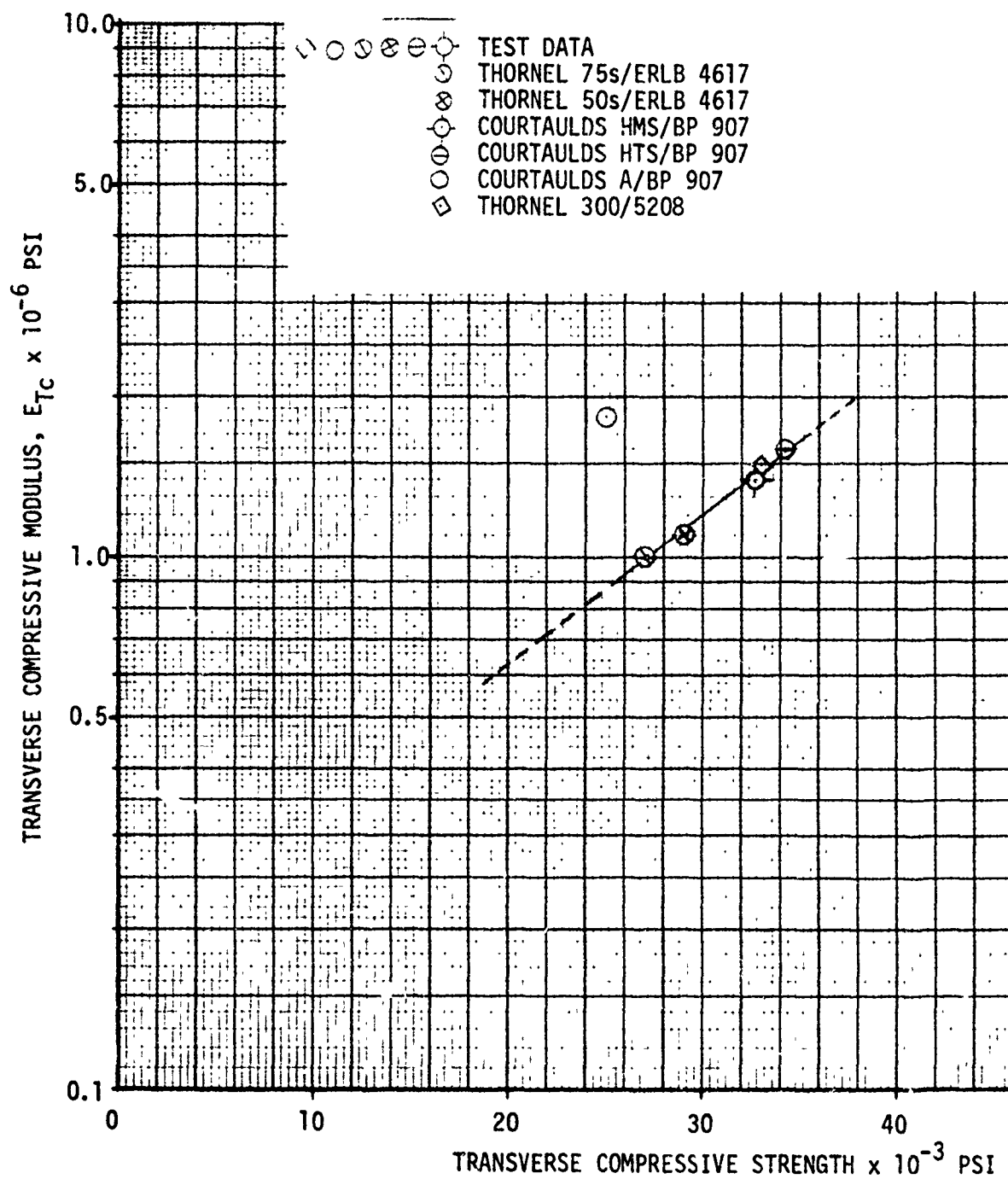


Figure 24. Correlation Between Transverse Young's Modulus and Transverse Compressive Strength of Graphite-Epoxy Composites.

Table XI

PROPERTIES OF TRANSVERSELY ISOTROPIC* COMPOSITE MATERIALS MADE WITH
RESINS HAVING DIFFERENT MODULI

| PROPERTY | UNITS | MATERIAL | | | |
|-------------------------------------|------------|----------|---------|---------|---------|
| | | T300/ULE | T300/LE | T300/ME | T300/HE |
| YOUNG'S MODULUS, E_r | 10^6 PSI | 8.00 | 8.30 | 8.60 | 8.85 |
| YOUNG'S MODULUS, E_z | 10^6 PSI | 0.60 | 0.95 | 1.42 | 1.80 |
| SHEAR MODULUS, G_z | 10^6 PSI | 0.37 | 0.51 | 0.71 | 0.82 |
| POISSON'S RATIO, ν_r | -- | 0.3175 | 0.3145 | 0.3088 | 0.3052 |
| POISSON'S RATIO, ν_z | -- | 0.0074 | 0.0112 | 0.0159 | 0.0180 |
| TENSILE STRENGTH, σ_{rt} | 10^3 PSI | 76.3 | 79.3 | 82.1 | 84.6 |
| TENSILE STRENGTH, σ_{zt} | 10^3 PSI | 6.0 | 2.2 | 9.3 | 9.9 |
| COMPRESSIVE STRENGTH, σ_{rc} | 10^3 PSI | 76.3 | 79.3 | 82.1 | 84.6 |
| COMPRESSIVE STRENGTH, σ_{zc} | 10^3 PSI | 19.2 | 26.3 | 32.6 | 36.3 |
| SHEAR STRENGTH, σ_{zr} | 10^3 PSI | 11.8 | 4.3 | 18.4 | 19.6 |

*MATERIAL ASSUMED TO HAVE PSEUDO-ISOTROPIC LAYUP IN THE PLANE OF THE TARGET. IN-PLANE TARGET PROPERTIES DESIGNATED BY r; PROPERTIES OF THE TARGET IN THE THICKNESS DIRECTION DESIGNATED BY z. IMPACT DIRECTION COINCIDES WITH z-DIRECTION.

duration for the four materials described in Table VIII. In calculating the required relationships, the target thickness in the impact direction was assumed to be large compared to the impactor dimensions; fiber layup in all four composites was assumed to be pseudo-isotropic, and the impactor was assumed to be a steel sphere. The properties of the impactor were taken as (see Section II for definition of terms):

$$\begin{aligned} m &= 1 ; & E_1 &= 30 \times 10^6 \text{ psi} \\ n &= 1 ; & \nu_1 &= 0.33 \\ s &= 2 ; & \rho_1 &= 0.288 \text{ lb/in.}^3 \\ R_{1m} = R_{1M} &= 0.75 \text{ in.} \end{aligned}$$

The target was assumed to be flat so that $R_{2m} = R_{2M} = \infty$, and its mass was assumed to be large compared to impactor mass. Using the equations given in Section 2 and the properties given above and in Table VIII, calculations were made of k_2 's for the various materials. These in turn were used to calculate the surface pressure, area of contact, and impact duration as a function of impact velocity for the four materials of interest. The values of k_2 's (for the targets) are shown in Table XII. The latter also shows values of k_1 for the impactor and $k_1 + k_2$ values. The variation of the maximum surface pressure, q_0 , radius of the area of contact, a , and duration of contact, t_0 , as a function of impact velocity is shown in Figures 25, 26, and 27, respectively. Both the radius of the area of contact, a , and the impact duration, t_0 , have been normalized with respect to R , the radius of the spherical impactor. Thus the results

Table XII
VALUES OF k_2 FOR DIFFERENT COMPOSITES
(BASED ON PROPERTIES DATA SHOWN IN TABLE VIII)

| MATERIAL | MATERIAL DESIGNATION | TARGET $k_2 \times 10^7$ (in. ² /lb) | IMPACTOR $k_1 \times 10^7$ (in. ² /lb) | $(k_1 + k_2) \times 10^7$ (in. ² /lb) |
|--------------------|----------------------|---|---|---|
| CELION GY-70-EPOXY | 2 | 2.324 | 0.095 | 2.419 |
| HMS-EPOXY | 3 | 1.726 | 0.095 | 1.821 |
| THORNEL 300-EPOXY | 6 | 1.541 | 0.095 | 1.636 |
| S-GLASS-EPOXY | 7 | 1.177 | 0.095 | 1.272 |

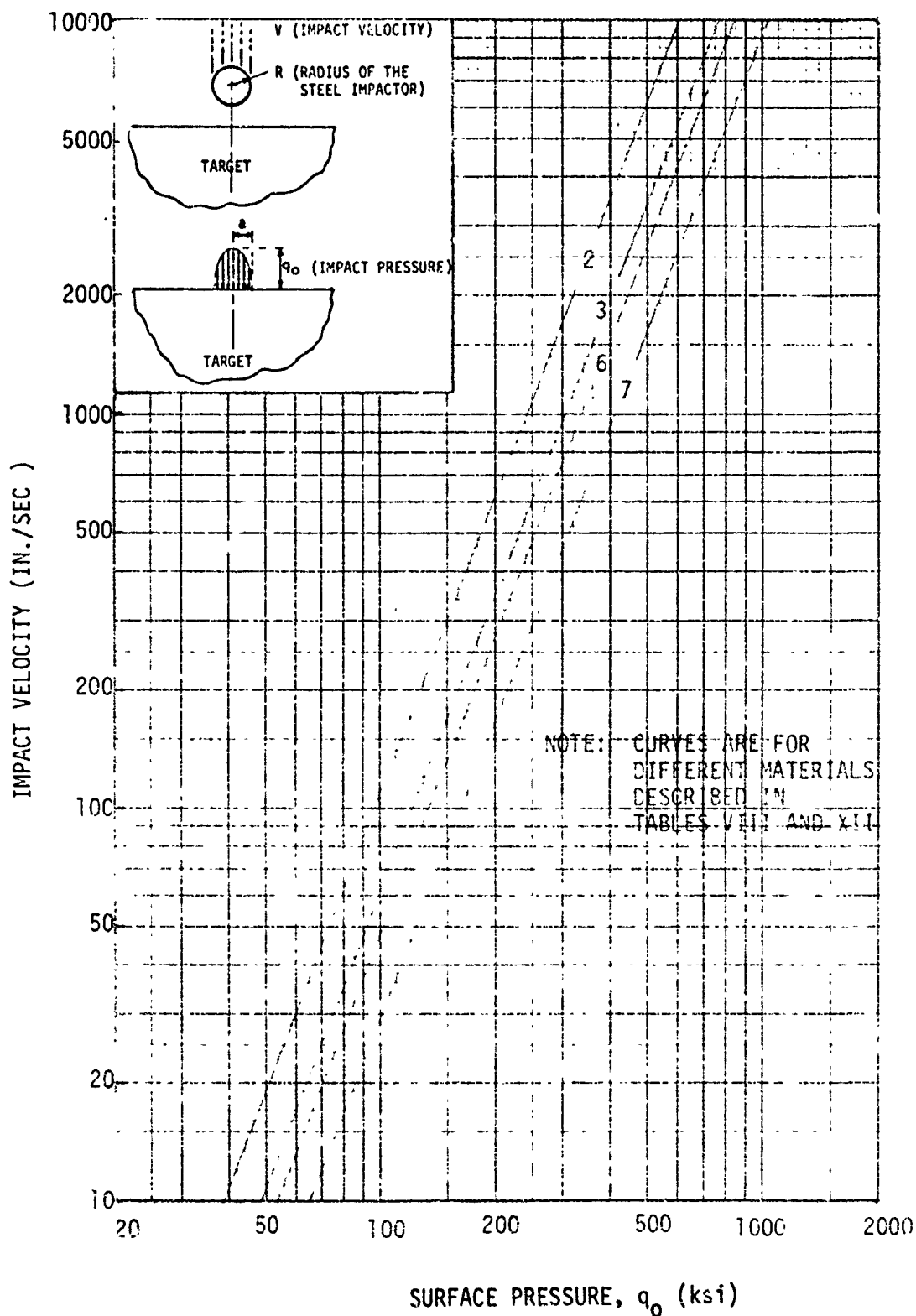


Figure 25. Maximum Surface Pressure Versus Impact Velocity.

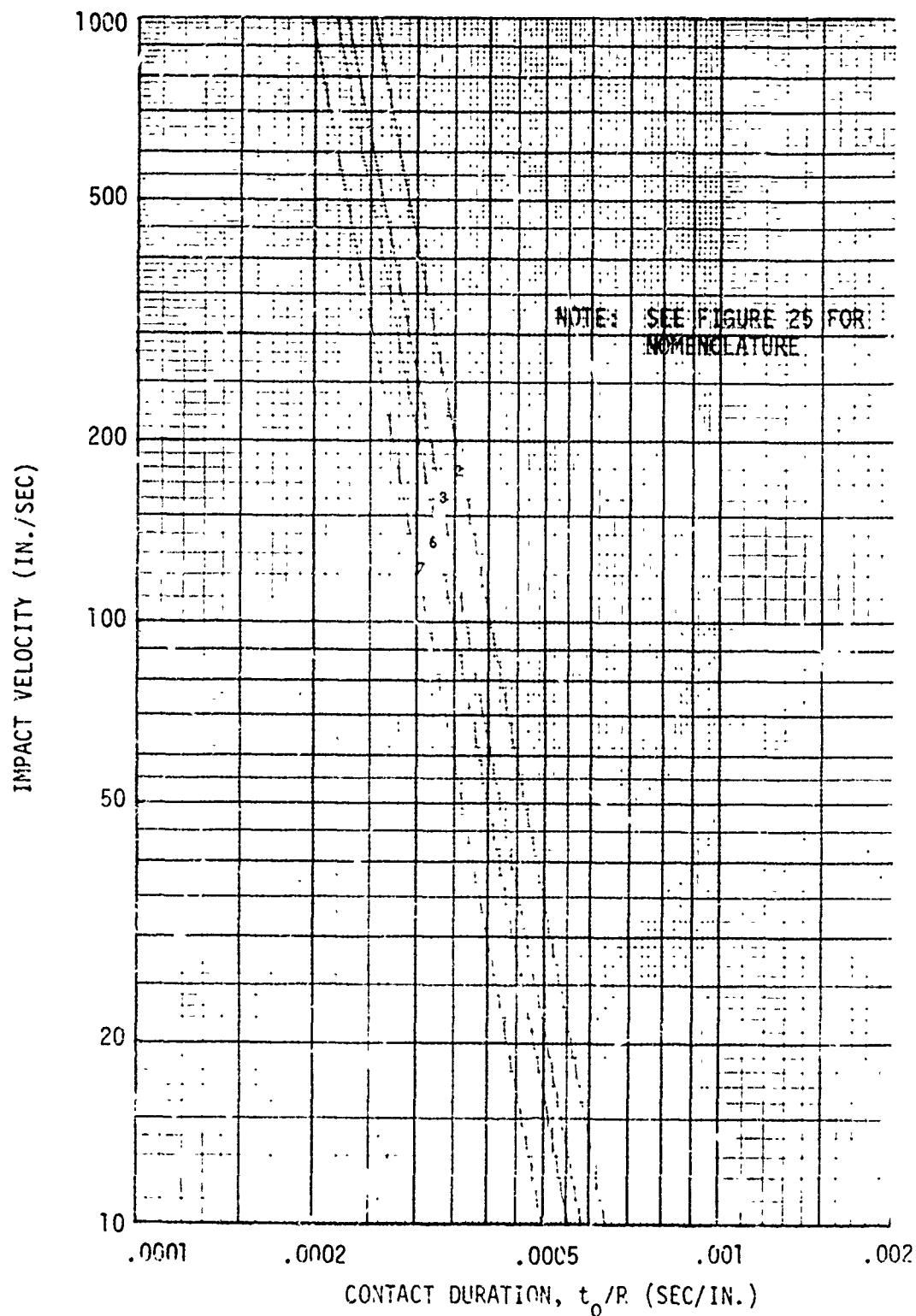


Figure 26. Contact Duration Between Target and Impactor Versus Impact Velocity.

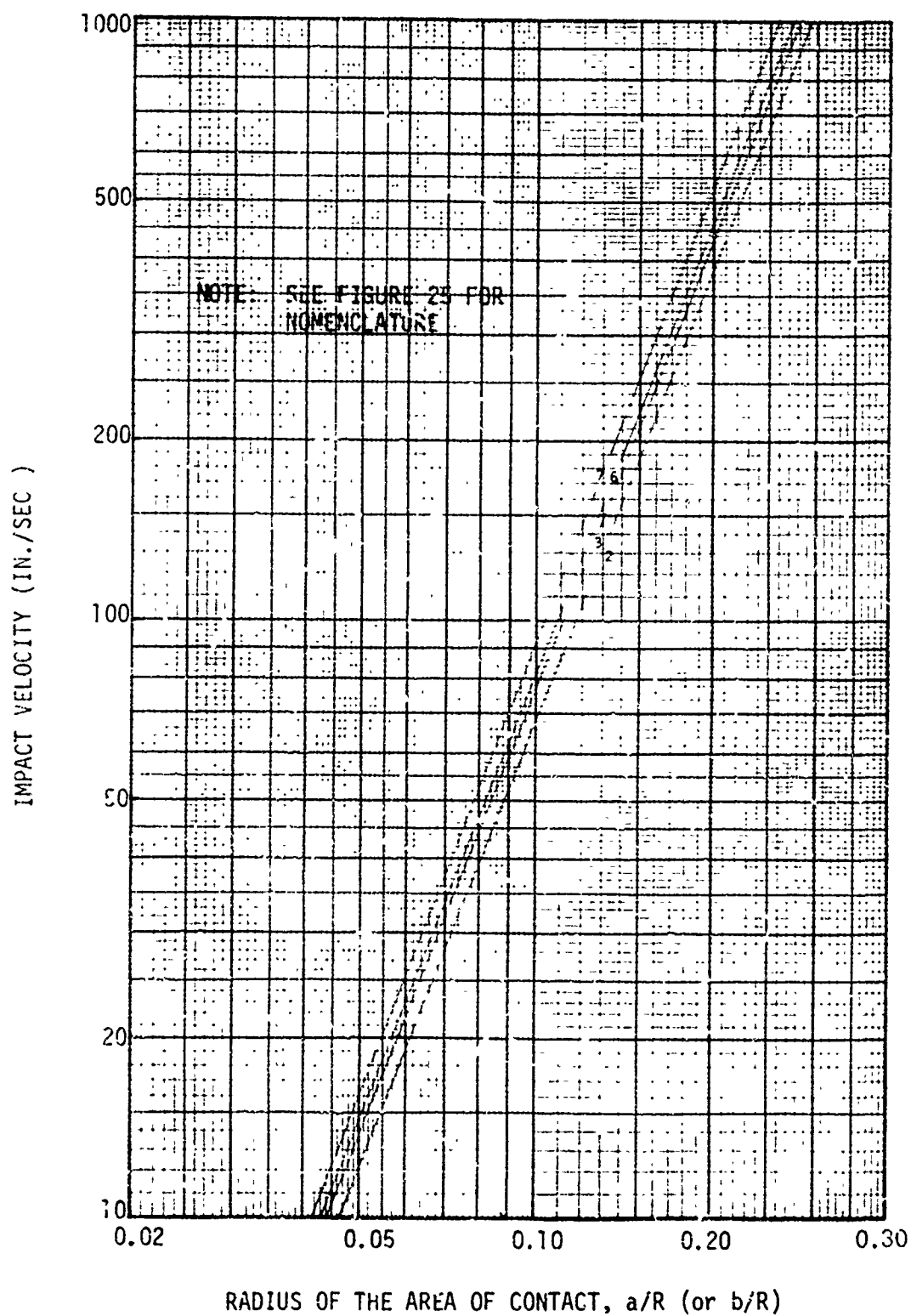


Figure 27. Nondimensional Contact Radius as a Function of Impact Velocity.

presented in Figures 25, 26, and 27 apply to steel spherical impactors of arbitrary radii. Moreover, as can readily be shown from equations given in Section II, for a spherical impactor impacting a flat target, $q_0 \neq f(R_1)$, so that the curves shown in Figure 25 also apply to spherical impactors of arbitrary radii, provided the latter are made of steel.

INFLUENCE OF FIBER PROPERTIES ON IMPACT RESPONSE

With the relationship between q_0 , a , and v known, a nondimensional solution was obtained (using SAAS III computer program described in Section II and the grid model shown in Figure 28) for the internal stresses in targets made of various composite materials described in Table VIII. To determine which composite is most resistant to impact and to minimize the number of variables, the layup in all composite materials was assumed to be pseudo-isotropic. Moreover, the thickness of the target in the direction of impact was assumed to be large compared to the radius of the impactor, so that only local stresses and deformations (in the region of impact) had to be considered. For a given q_0 and a , the computer output consisted of radial, circumferential, normal, and shear stresses at various points within the target; deformations at various points within the targets; principal stresses at various points within the targets; and equivalent stress contours as obtained by applying the failure criterion at various points within the target. For a given q_0 and a , the failure envelope was also determined. Figures 29 and 30 show the computer printout of the equivalent stress, σ_e , contours for Materials 2 and 6. Those were used to define the failure zone for any given impact condition. Failure occurs at points where $\sigma_e \geq 1$.

The pertinent results for the impact response of the three graphite-epoxy composites are presented in Tables XIII and XIV. Table XIII shows the pertinent data for the case when q_0 is kept constant, the latter being equal to the maximum surface pressure resulting from an impact of a 0.75-in. -radius steel spherical impactor. Table XIV shows the results for a constant impact velocity. Of the three materials for which results are presented, Material 6 (Thornel 300-epoxy) has minimum \bar{Y} . Examination of results obtained to date shows that q_0 is extremely sensitive to E_z , the Young's modulus in the direction of impact. By decreasing E_z , q_0 and \bar{Y} will also decrease. Moreover, since material exhibits yield behavior in compression it appears desirable to take this into account in future work (through reduced E_z) when calculating q_0 and a . However, to establish the relative rating of different composites, the assumption of elastic behavior appears sufficient at this time. On the basis of results presented in Tables XIII and XIV, the ranking of the three materials for response to impact damage is (starting with the best material)

1. Thornel 300-Epoxy
2. HMS-Epoxy
3. GY70-Epoxy

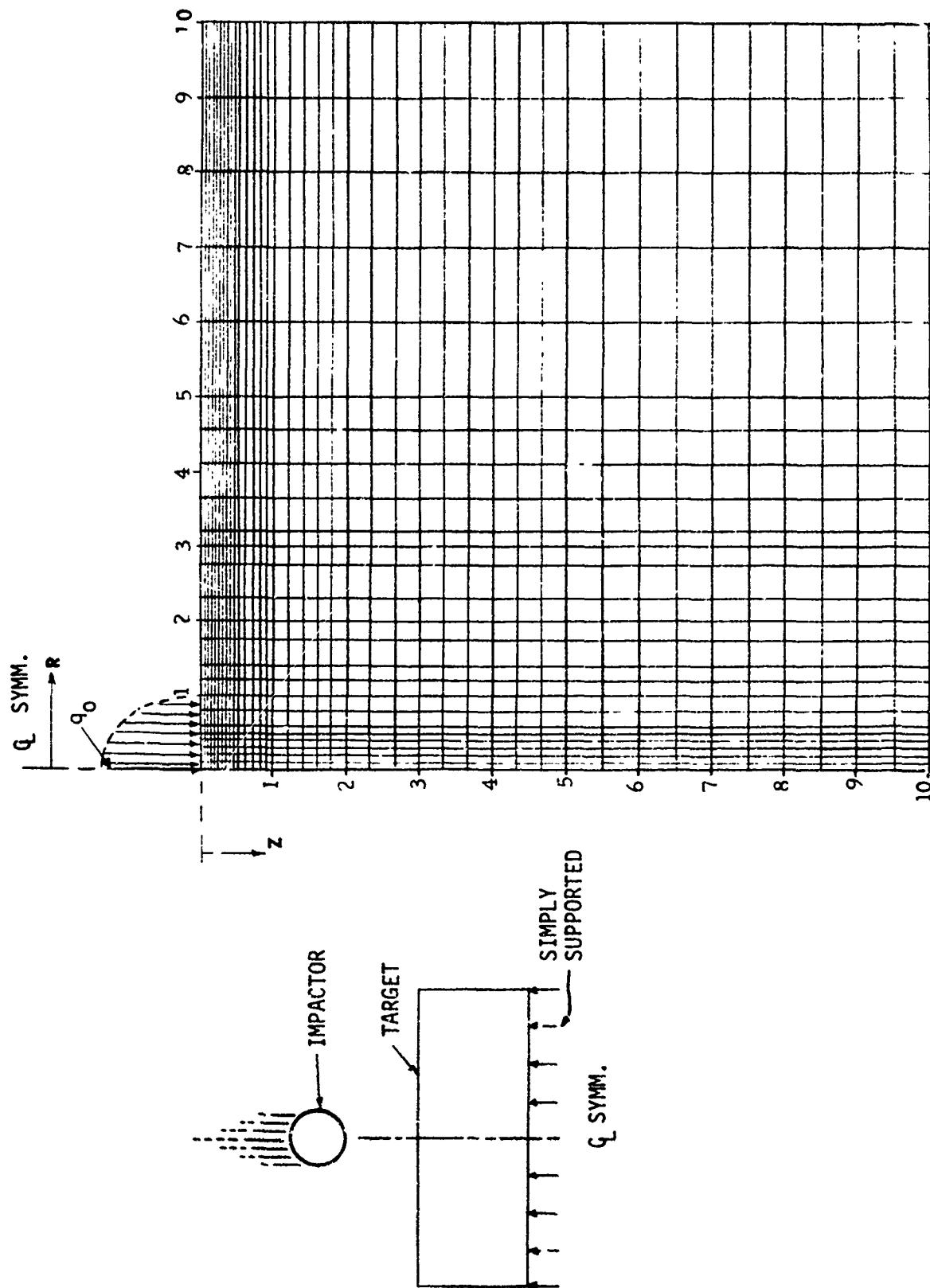


Figure 28. Grid Used in the Computer Solution.

ORTHO($E_R=14.8, E_Z=1.4, G_Z=0.6, V=.318, V_Z=.005$) $q_0 = 100 \text{ KSI, J}$

NORM EQUIV STRESS
CONTOURS PLOTTED

• 2.500E-01
◻ 5.000E-01
+ 7.500E-01
• 1.000E+00
• 1.500E+00
◻ 2.000E+00
• 3.000E+00
• 5.000E+00

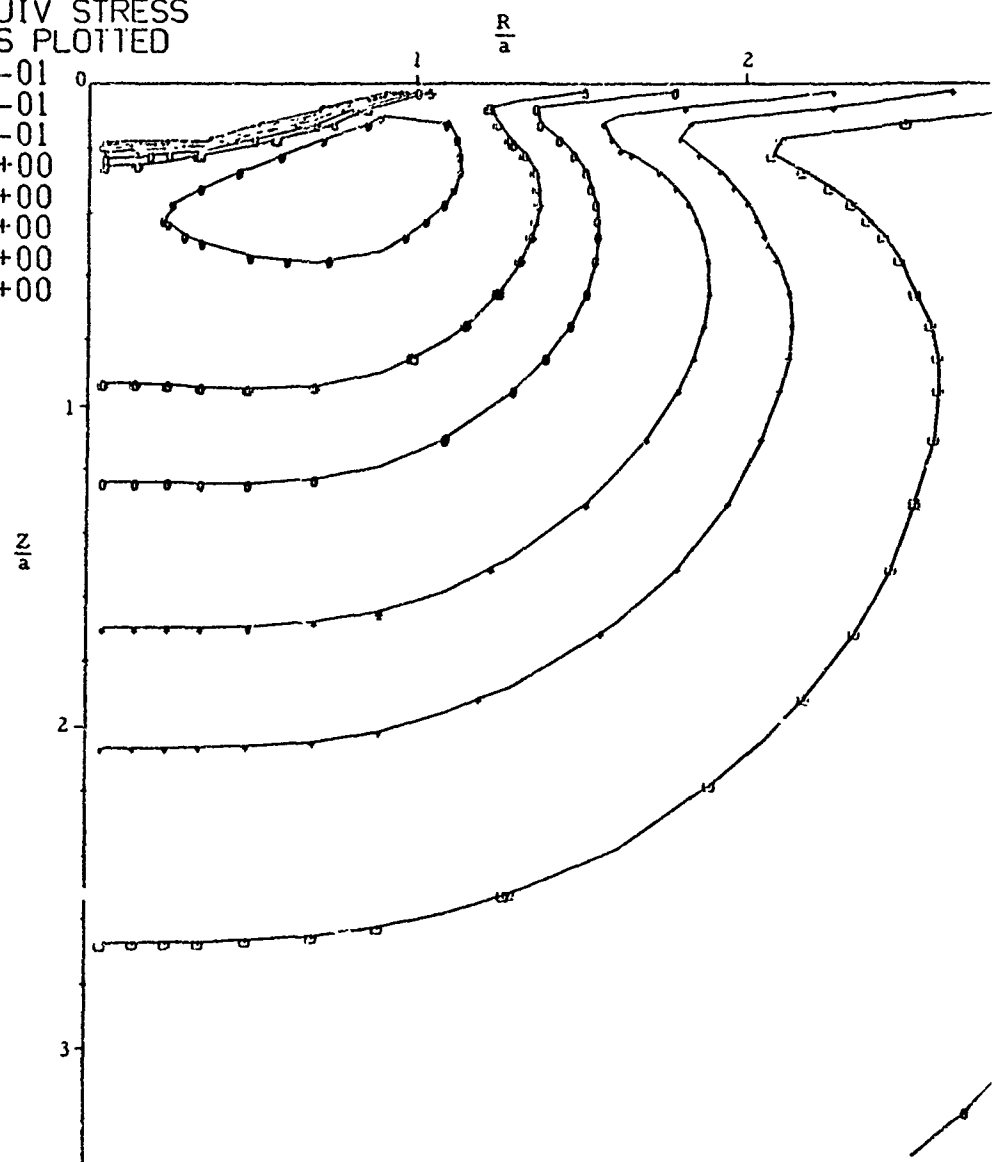


Figure 29. Equivalent Stress Coutours for Celion GY70-Epoxy
(Material No. 2) Subjected to $q_0 = 100 \text{ ksi}$.

ORTHOC(ER=8.0,EZ=1.77,GZ=.85,V=.30,VZ=.0202) q_0 =100KSI,J=40

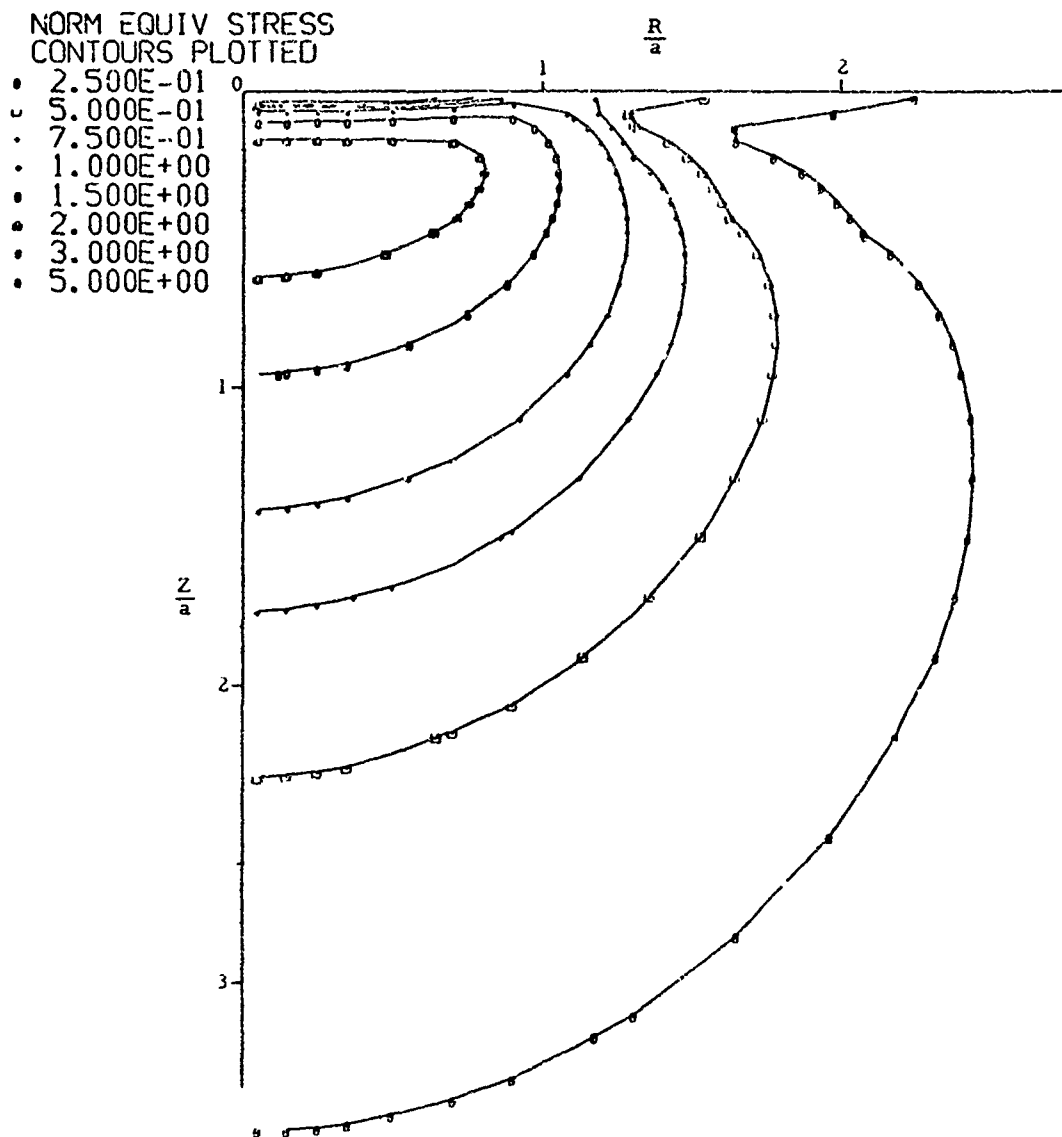


Figure 30. Equivalent Stress Contours for Thornel 300-Epoxy (Material No. 6) Subjected to $q_0 = 100$ ksi.

Table XIII
DAMAGE ZONE FOR A CONSTANT SURFACE PRESSURE
($q_o = 100$ KSI)

| MATERIAL | $k_1 + k_2 \times 10^7$ (IN. ² /LB) | CONTACT RADIUS, a (IN.) | IMPACT VELOCITY v (IN./SEC) | $\frac{Y_Z}{a}$ | $\frac{Y_R}{a}$ | \bar{Y} (IN.) |
|------------|---|---------------------------------|--|-----------------|-----------------|-----------------|
| 2 (GY70-E) | 2.42 | 0.089 | 105 | 1.70 | 1.87 | 0.158 |
| 3 (HMS-E) | 1.82 | 0.067 | 59 | 1.40 | 1.48 | 0.096 |
| 6 (T300-E) | 1.63 | 0.061 | 48 | 1.26 | 1.26 | 0.081 |

Y_Z = Depth of damage zone

Y_R = Half the width of the damage zone.

$\bar{Y} = \sqrt{Y_Z Y_R}$ = Equivalent radius of the damage zone.

Table XIV
DAMAGE ZONE FOR A CONSTANT IMPACT VELOCITY
($v = 100$ IN./SEC)

| MATERIAL | $q_o \times 10^{-3}$ PSI | a (IN.) | $\frac{Y_Z}{a}$ | $\frac{Y_R}{a}$ | \bar{Y} (IN.) |
|------------|-----------------------------|--------------|-----------------|-----------------|--------------------|
| 2 (GY70-E) | 98 | 0.088 | 2.11 | 2.21 | 0.190 |
| 3 (HMS-E) | 124 | 0.083 | 2.06 | 1.94 | 0.166 |
| 6 (T300-E) | 134 | 0.081 | 2.22 | 1.74 | 0.158 |

In addition to the above, studies were also conducted on local failures resulting from impact. This included determination of relative velocities to cause subsurface shear failure and its location, and determination of the velocity to cause tensile failure at the edge of the area of contact where the tensile stresses are maximum. The results for the local failures are shown in Tables XV and XVI, and demonstrate that Thornel 300-epoxy is the best material. Moreover, they show that the failure is initiated by subsurface shear.

INFLUENCE OF MATRIX PROPERTIES ON IMPACT RESPONSE OF COMPOSITES REINFORCED WITH THORNEL 300 GRAPHITE FIBERS

To establish if the response to impact loading of composites made with Thornel 300 could be further improved by changing the matrix properties, studies similar to those described in the previous section were conducted on composites made with resins described in Table IX. The properties of the latter composites, calculated as described in Section 3, are given in Tables X and XI.

The damage zones in composites made with different resins and subjected to a 100-in./sec impact by a 1.5-in. -diameter steel sphere are shown in Figure 31. The results shown there are for a semi-infinite target. The cross-sectional areas of the damage zones in the various materials are given in Table XVII.

Thus, of the first four materials listed in Table XVII, the damage zone in material T300/ME appears to be the lowest, although the damage zones in materials T300/ULE and T300/HE do not differ significantly from the lowest value. Material T300/LE has the largest damage zone. Its shape indicates that the low shear strength of T300/LE is the parameter that governs the size and shape of the damage zone (see Table XI). The fact that the damage zone in T300/ULE is approximately the same as in T300/HF indicates that the resin strength has a larger influence than the resin modulus. To verify this conclusion, the impact response of one more material was investigated: a material with elastic properties corresponding to those of T300/ULE and strength properties corresponding to those of T300/ME. The damage zone in the latter material, designated in Table XVII as conceptual material T300/ULE - T300/ME, was significantly lower than that of the other materials shown therein. This result further confirms the conclusion that resin strength rather than modulus has the dominating influence on the size of damage zone.

INFLUENCE OF TARGET THICKNESS ON IMPACT RESPONSE OF COMPOSITES

The composite material selected for establishing how impact response and failure modes are influenced by thickness of the composite target was Thornel 300-epoxy. The properties of this composite are given in Table VIII, wherein the material is designated as Material 6. Inasmuch as target thickness was the only variable of interest, the composite was assumed to have a pseudo-isotropic layup in the plane of the target.

Table XV
RELATIVE IMPACT VELOCITIES TO INITIATE SHEAR FAILURE
AT A POINT WITHIN THE TARGET

| MATERIAL | MAXIMUM SHEAR STRESS τ_{RZ}/q_o | LOCATION OF MAXIMUM τ_{RZ} | | RELATIVE IMPACT VELOCITY TO INITIATE FAILURE* |
|------------|--|------------------------------------|---------------|--|
| | | $\frac{R}{a}$ | $\frac{Z}{a}$ | |
| 2 (GY70-E) | 0.354 | 0.90 | 0.175 | 1 |
| 3 (HMS-E) | 0.326 | 0.90 | 0.175 | 2.2 |
| 6 (T300-E) | 0.288 | 0.90 | 0.225 | 4.5 |

*Normalized with respect to v_{2S} , the velocity to cause shear failure in material #2.

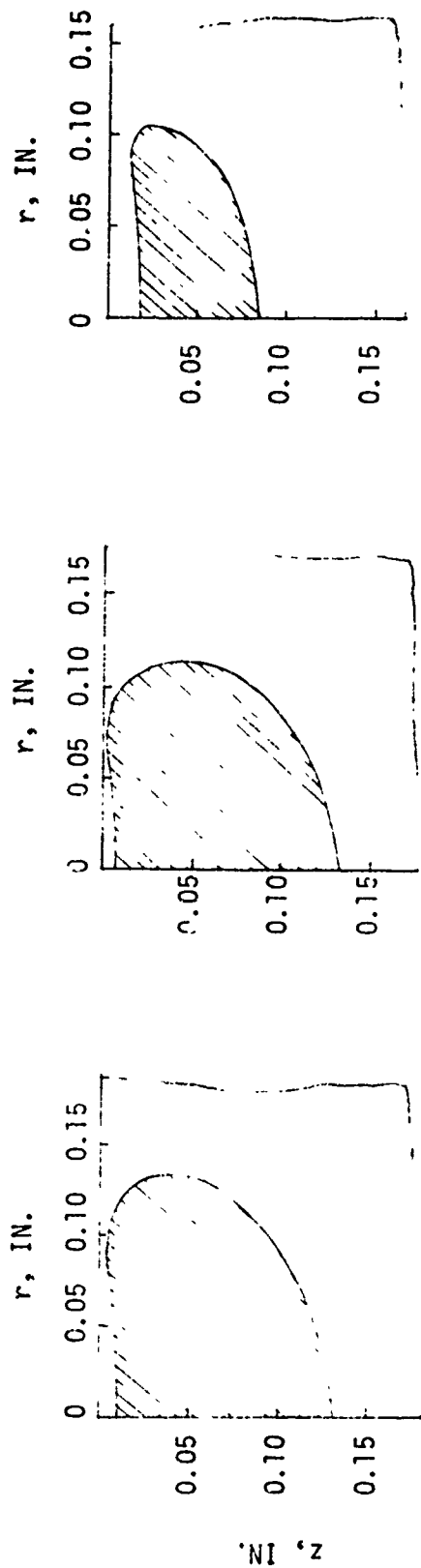
Table XVI
RELATIVE IMPACT VELOCITY TO INITIATE TENSILE FAILURES
(at $\frac{r}{a} = 1$)

| MATERIAL | MAXIMUM TENSILE STRESS, $\frac{\sigma_r}{q_o}$ | RELATIVE IMPACT VELOCITY TO INITIATE FAILURE* |
|------------|---|---|
| 2 (GY70-E) | 0.86 | 3.2 |
| 3 (HMS-E) | 0.63 | 10.7 |
| 6 (T300-E) | 0.45 | 59.0 |

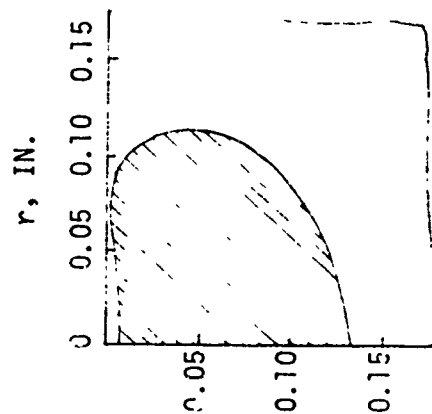
*Normalized with respect to v_{2S} .

Table XVII
INFLUENCE OF RESIN ON SIZE OF DAMAGE ZONE
IN COMPOSITES MADE WITH THORNEL 300 FIBERS

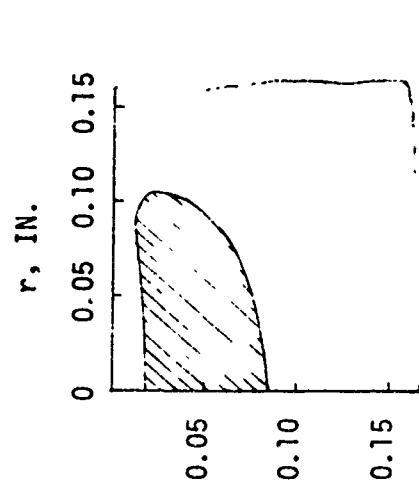
| MATERIAL | CROSS-SECTIONAL AREA OF DAMAGE ZONE (IN. ²) |
|---|---|
| T300/ULE | 0.0133 |
| T300/LE | 0.0325 |
| T300/ME | 0.0119 |
| T300/HE | 0.0122 |
| Conceptual Material T300/ULE - T300/ME | 0.0057 |



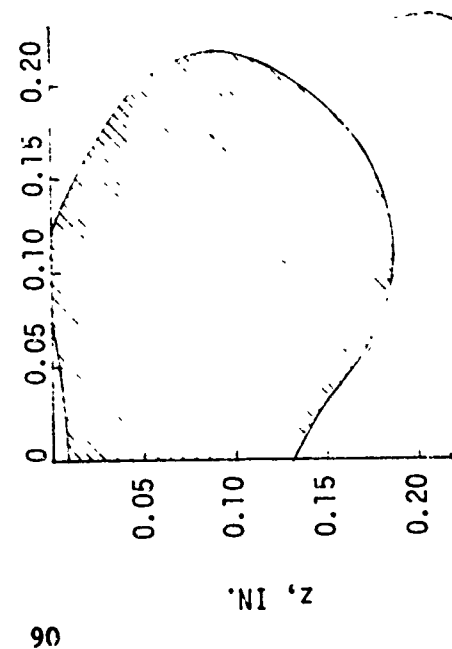
(a) T300/ULE



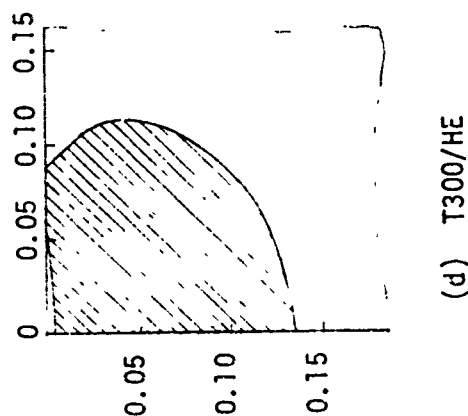
(c) T300/ME



(e) T300/ULE - T300/ME



(b) T300/LE



(d) T300/HE

Figure 31. Damage Resulting From a 100-In./Sec Impact of a 1.5-In.-Diameter Steel Sphere Into Semi-Infinite Composite Targets Made of Thornel 300 Fibers and Different Resins.

The influence of target mass on surface pressure resulting from foreign object impact was determined from Equation (14). If, for a given set of impact conditions, q_f is the maximum surface pressure in a target of finite thickness and q_∞ is the maximum surface pressure in a semi-infinite target, then it follows from Equation (14) that the relationship between q_f , q_∞ , and masses of the target and the impactor is

$$\frac{q_f}{q_\infty} = \left(\frac{\lambda}{1+\lambda} \right)^{1/5} \quad (32)$$

where

$$\lambda = \frac{m_2}{m_1}$$

m_2 is the effective mass of the target and m_1 is the mass of the impactor. The effective mass of the target, m_2 , will, in general, be greater than m_1 ; therefore, $\lambda \geq 1$. For the extreme case of $\lambda = 1$, evaluation of Equation (32) gives

$$\frac{q_f}{q_\infty} = 0.87$$

As λ increases, the ratio $q_f/q_\infty \rightarrow 1$. The above results show that use of Equation (14) to predict surface pressure in targets of finite thickness gives conservative results. Consequently, when studying the influence of target thickness on impact response, Equation (14) was used to calculate the maximum surface pressure.

In obtaining the numerical results on the plate thickness effects, it was assumed that the plates were circular in shape and were clamped along the outer boundary. Moreover, the impactor was assumed to be spherical in shape and its properties were assumed to be the same as those used in the numerical examples given previously (Section III):

$$m = 1 ; \quad E_1 = 30 \times 10^6 \text{ psi}$$

$$n = 1 ; \quad \nu_1 = 0.33$$

$$s = 2 ; \quad \rho_1 = 0.288 \text{ lb/in.}^3$$

$$R_{1m} = R_{1M} = 0.75 \text{ in.}$$

Some typical results on the influence of plate thickness and dimensions on the impact-induced radial stresses are shown in Figures 32 and 33. The results presented therein give the distribution of radial stresses through the thickness of the plate along the line passing through the

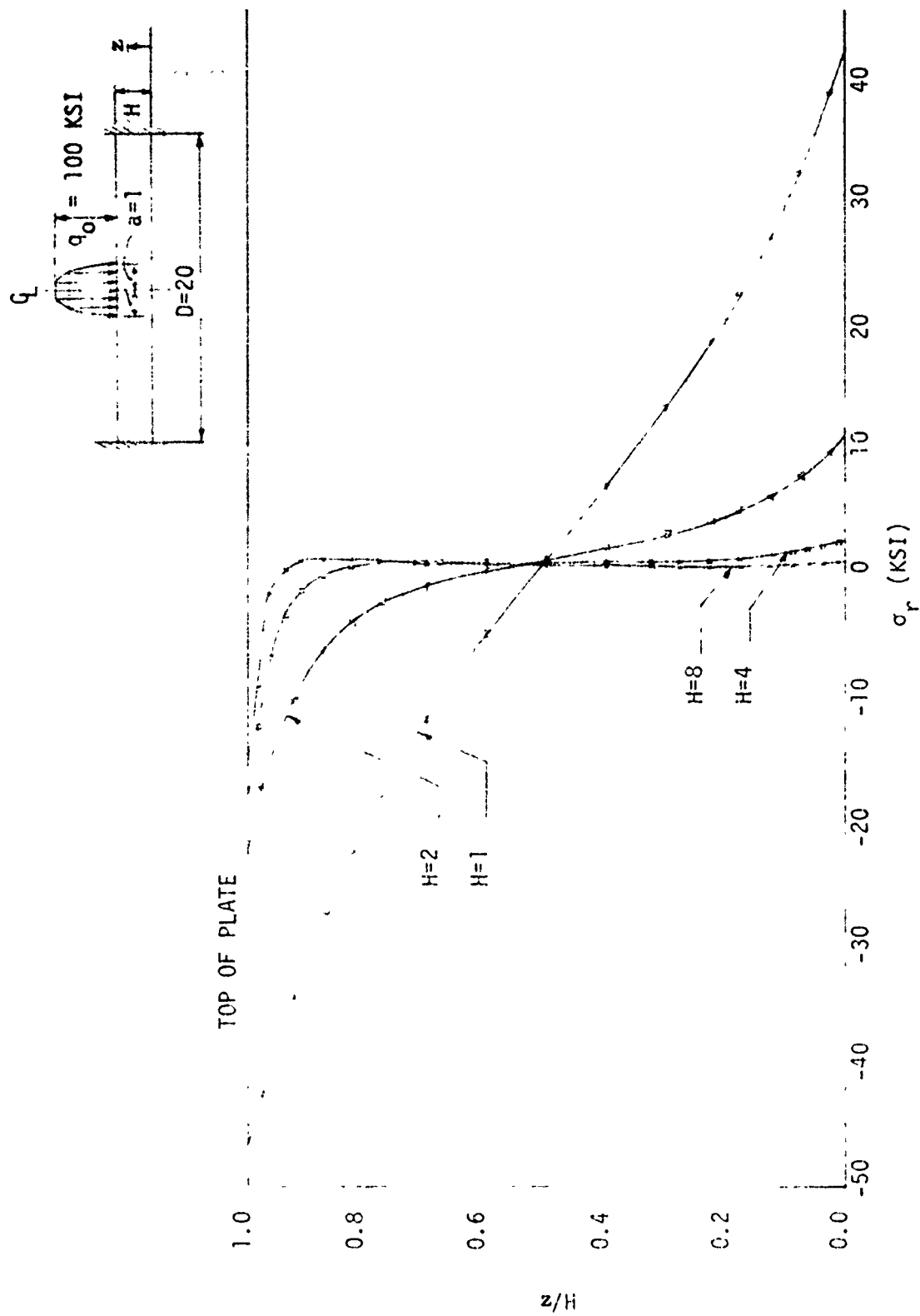


Figure 32. Radial Stress at Center of Circular Plate ($D = \text{Constant}$).

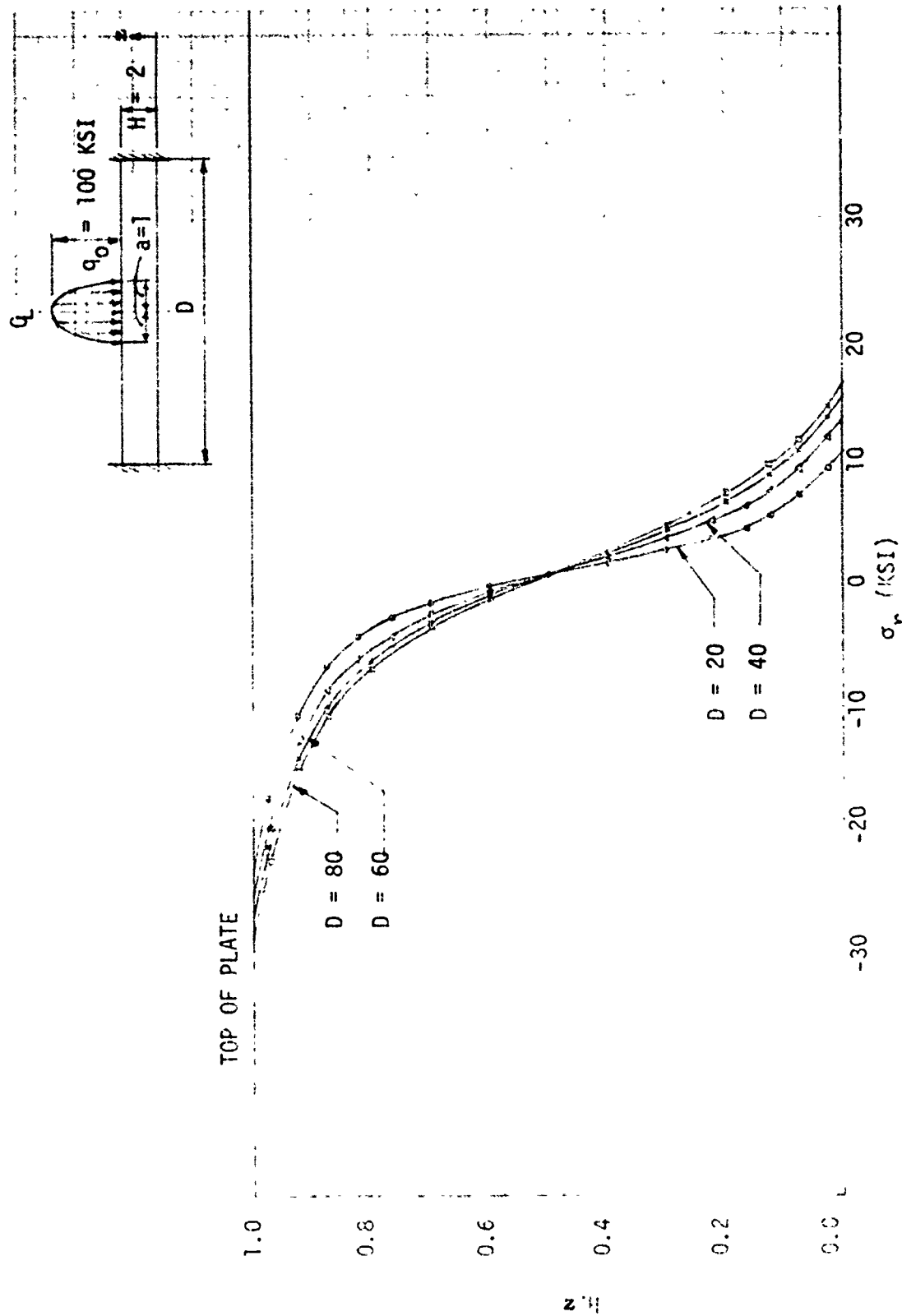


Figure 33. Radial Stress at Center of Plate ($H = \text{Constant}$).

center of the area of contact. To make the results of practical interest, both the plate thickness and its diameter were nondimensionalized with respect to the radius of the area of contact, a . Thus, H and D appearing in Figures 32 and 33 represent the nondimensionalized thickness and diameter, respectively. Figure 32 shows the influence of plate thickness on the distribution of radial stresses for a plate with a given D , whereas the results shown in Figure 33 are for a plate with constant H and varying D . For the numerical example given in Figure 32, plate thickness effect is seen to be significant when the radius of the area of contact is equal to the plate thickness, that is, when $H = 1$. If $H > 1$, the radial stresses appear to be governed by local deformation of the plate, whereas if $H < 1$, the radial stresses appear to be governed by plate bending deformations.

The influence of local deformations and plate bending deformations is further illustrated in Figures 34a and 35. The deformations at the edge of the area of contact have been normalized with respect to the maximum deformation at the center of the area of contact. Moreover, as before, both the plate radius, R , and the plate thickness, H , have been nondimensionalized with respect to the radius of the area of contact, a .

As is readily apparent from the results presented in Figures 32-35, the dimensions of the impacted plate (thickness and radius) have a significant influence on the stress state within the plate and on the plate deformation resulting from a foreign object impact. To establish how the impact-induced failure modes are influenced by the dimensions of the composite target, SAAS III finite-element computer code was used. The pertinent results for the influence of plate thickness and plate radius on the failure modes are shown in Figures 36 and 37. Figure 36 shows the maximum critical surface pressure, q_0^* , at which failure initiates at a point in the plate. The results plotted there are for a constant R and varying H , the nondimensional plate radius and plate thickness, respectively. The results presented in Figure 36 show that for $H \lesssim 1.5$, the failure is governed by bending stresses and initiates on the bottom surface of the plate. For $H \gtrsim 1.5$, the failure is governed by local contact stresses and occurs on the top surface of the plate. As H increases, q_0^* approaches a constant value, indicating that the failure consists of local damage. Figure 37 shows results similar to those presented in Figure 36 except that the variable is the nondimensionalized plate radius R .

As was discussed in Section II, for a given set of impact parameters, both the surface pressure and the area of contact over which it acts are time dependent. For the case of a semi-infinite composite target, the variation of the maximum surface pressure with time is shown in Figure 38. The extent of damage in such a target at pressure or time intervals denoted in Figure 38 as a, b, c, \dots, f , is shown in Figure 39. The points in Figure 38 denoted by a, b, c, \dots, f , correspond to Sections (a), (b), (c) \dots (f) of Figure 39. All the results shown in Figure 39 are drawn to scale. This includes relative magnitude of the

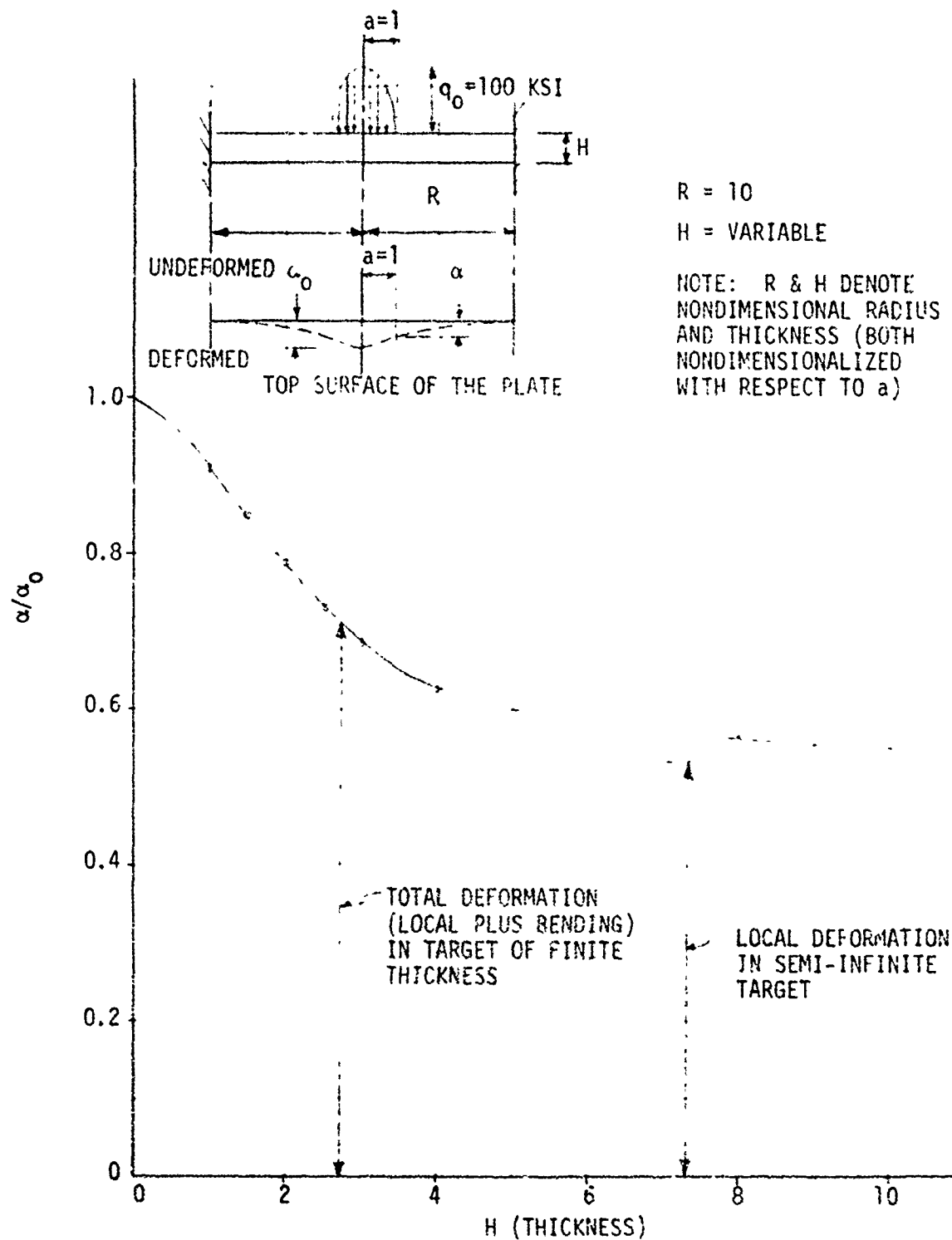


Figure 34. Influence of Plate Thickness on Local and Plate Bending Deformations at the Edge of the Area of Contact

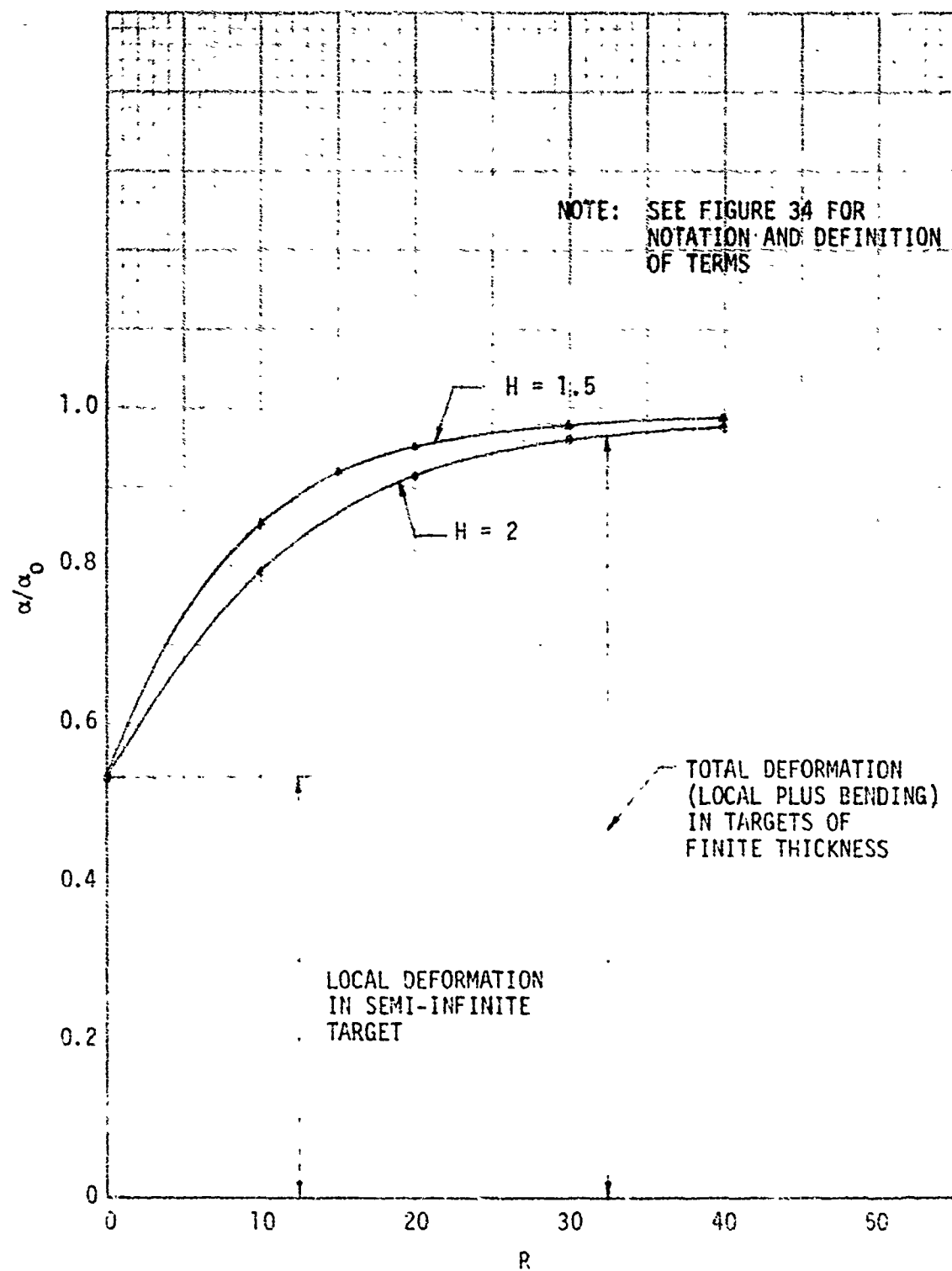


Figure 35. Influence of Plate Radius on Local and Plate Bending Deformations at the Edge of the Area of Contact.

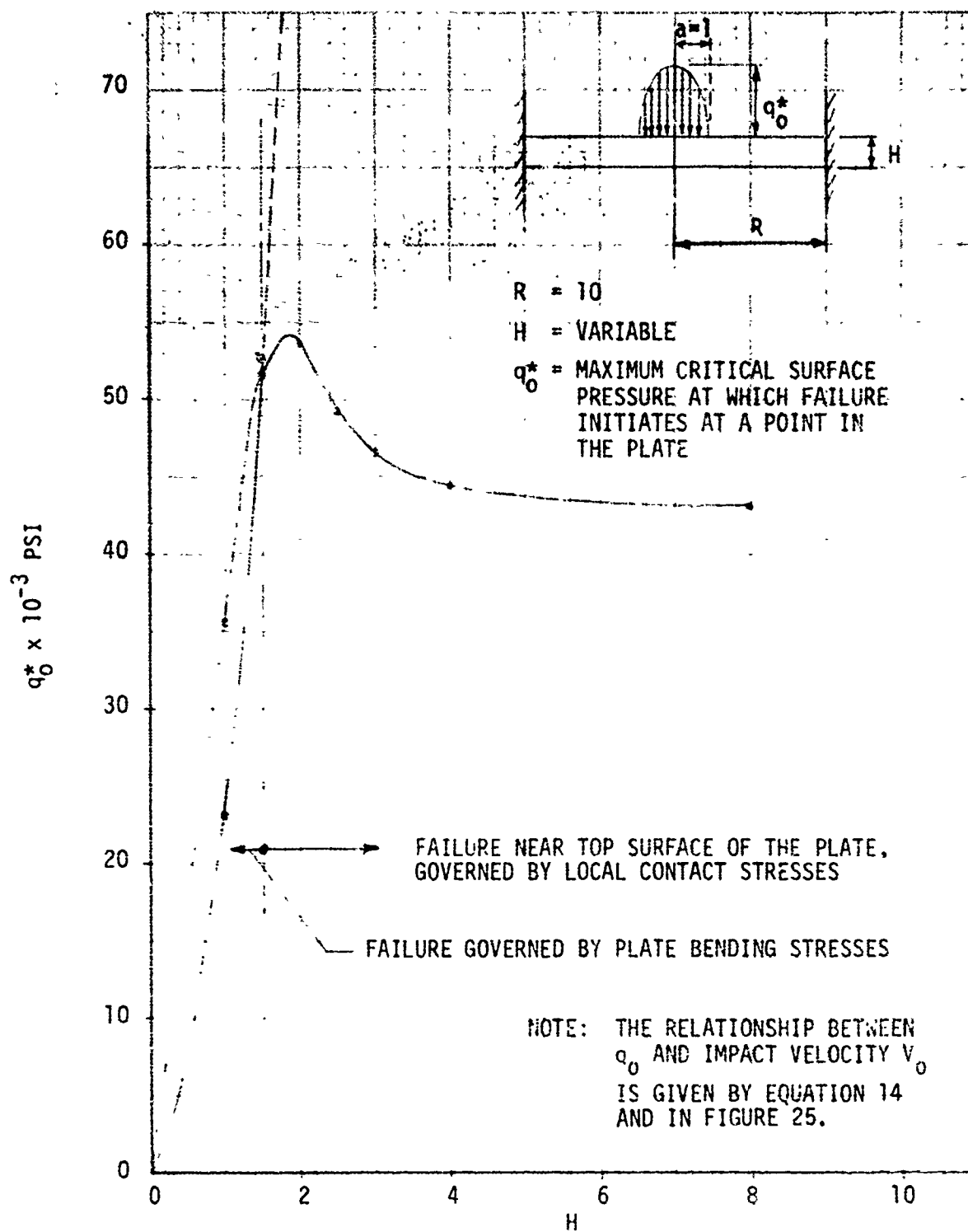


Figure 36. Influence of Plate Thickness on Maximum Surface Pressure at Which Failure Initiates at a Point in a Plate.

F_L = FAILURE ON TOP SURFACE OF THE PLATE,
GOVERNED BY LOCAL CONTACT STRESSES

F_B = FAILURE GOVERNED BY PLATE BENDING
STRESSES

q_o^* = MAXIMUM CRITICAL SURFACE PRESSURE AT
WHICH FAILURE INITIATES AT A POINT
IN THE PLATE

NOTE: SEE FIGURE 36 FOR DEFINITION OF TERMS

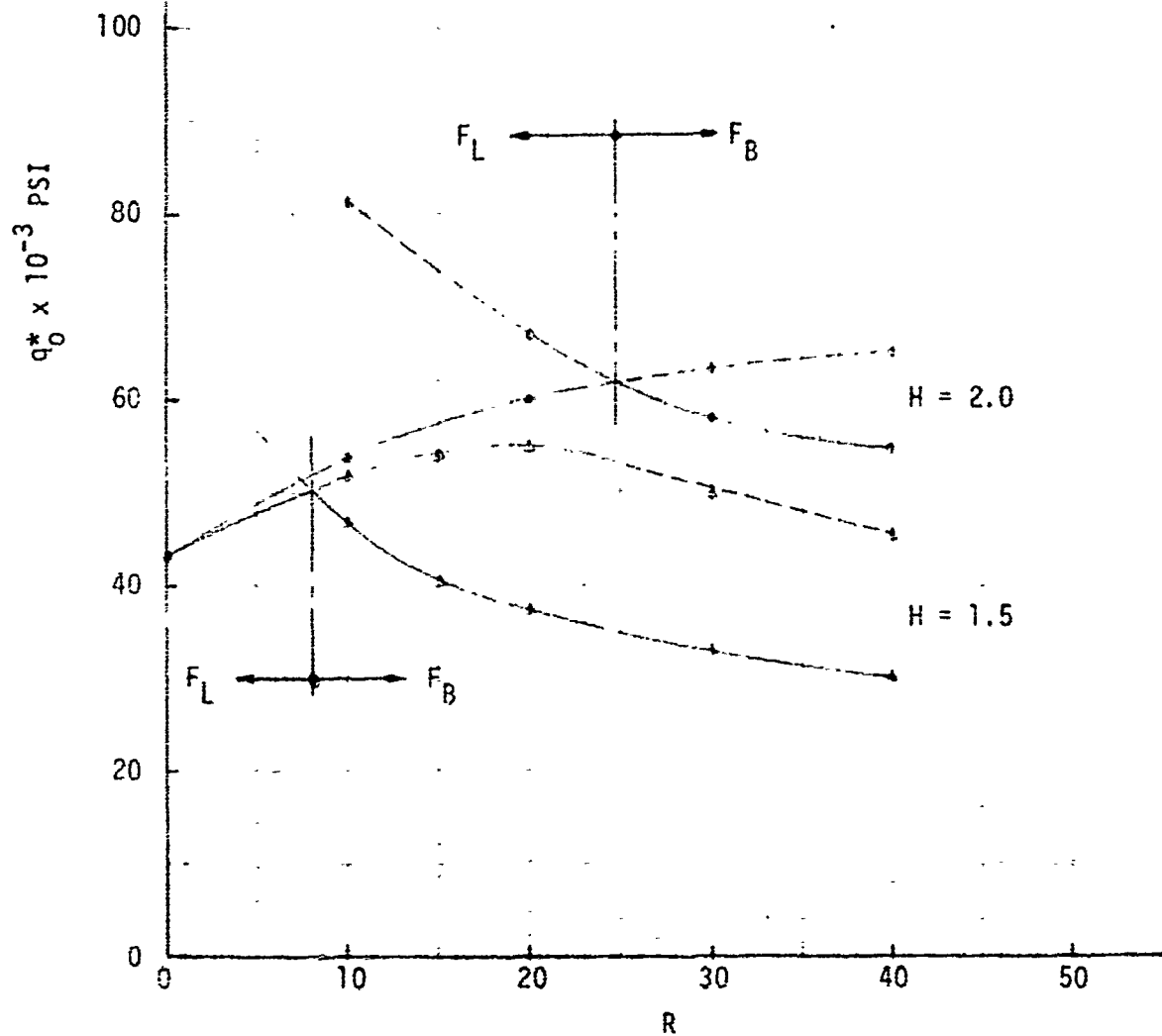


Figure 37. Influence of Plate Radius on Maximum Surface Pressure at Which Failure Initiates at a Point in a Plate.

PERTINENT DATA USED IN OBTAINING THE RESULTS SHOWN
HERE ARE:

IMPACTOR RADIUS, $R_{1m} = R_{1hi} = 0.75$ IN.

IMPACTOR MATERIAL: STEEL ($E_1 = 30 \times 10^6$ PSI, $\nu_1 = 0.33$, $w_1 = 0.509$ LB.
 $\rho_1 = 0.288$ LB/IN.³, $m_1 = 1.31 \times 10^{-3}$ LB-SEC²/IN.)

TARGET MATERIAL: THORNEL 300/EPOXY

TARGET MASS: SEMI-INFINITE ($m_2 \gg m_1$)

IMPACT VELOCITY, $V_0 = 1500$ IN./SEC

IMPACT DURATION, $t_0 = 152 \mu$ SEC

MAXIMUM AREA OF CONTACT, $a_0 = 0.242$ IN. (AT $t = 0.5 t_0$)

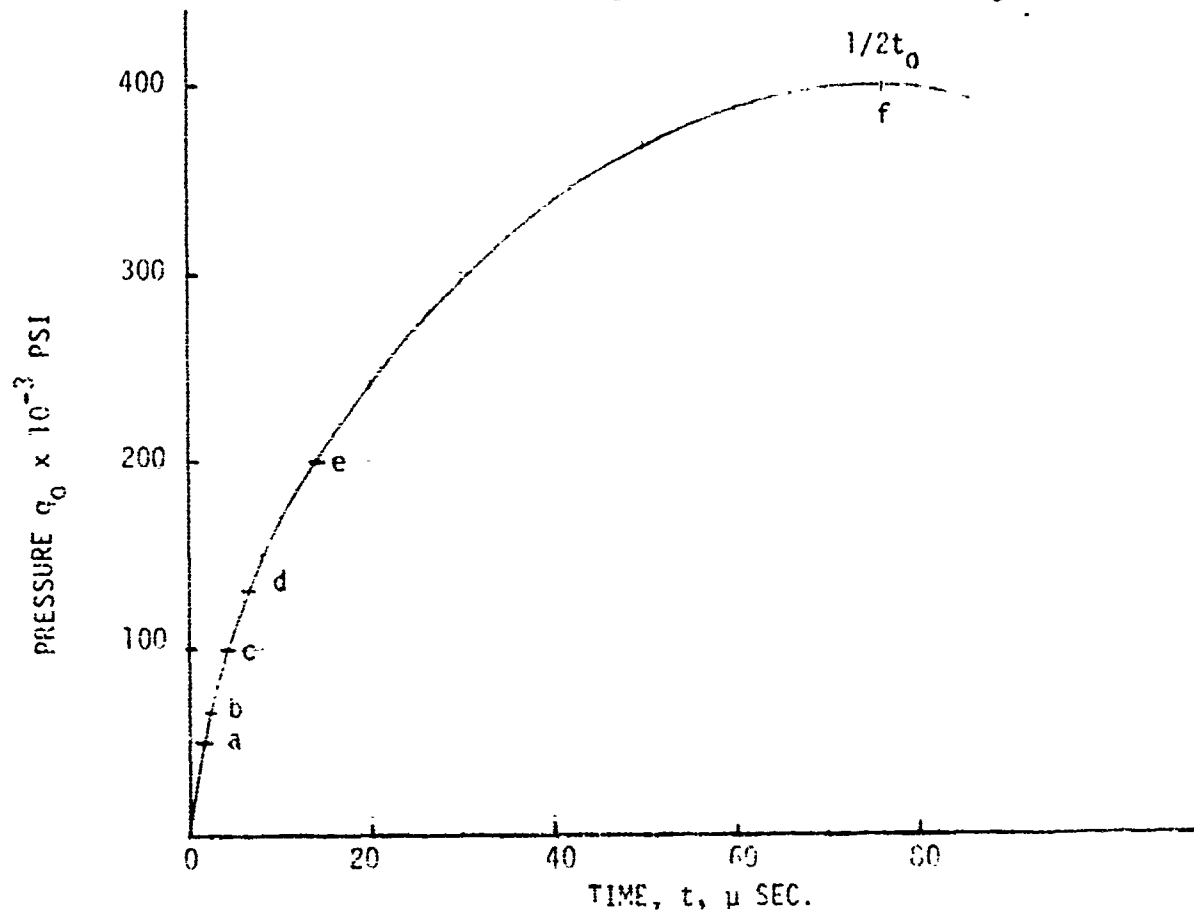


Figure 38. Increase of Maximum Surface Pressure With Time.

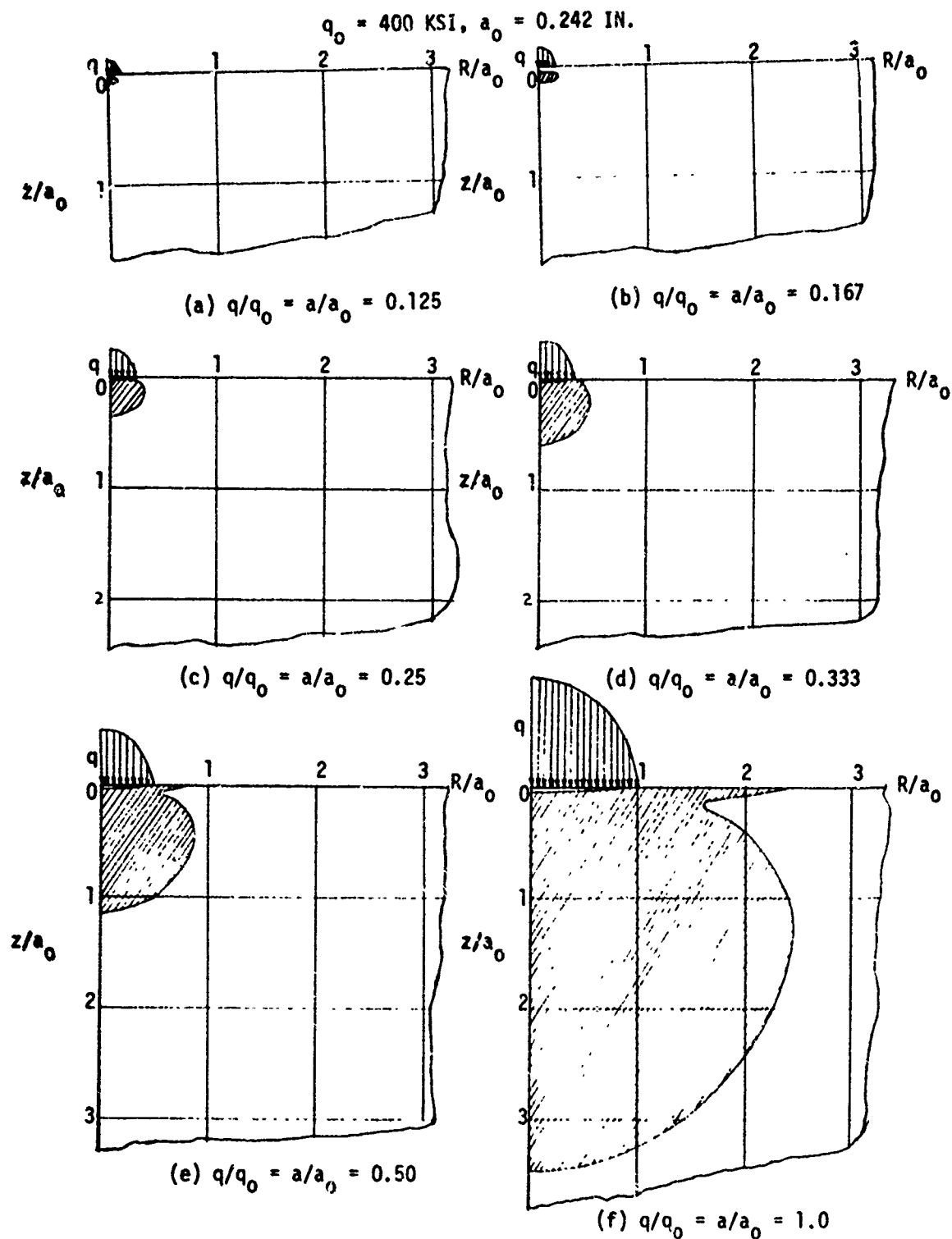


Figure 39. Increase in Damage Zone (Shaded Area) With Increasing Surface Pressure or Time (See Figure 38) in a Semi-Infinite Target.

surface pressure, areas over which it acts, and the size of the failure zone. The results shown in Figure 39 can also be used for determining the damage zone if $v_0 < 1500$ in./sec. For example, if the impact velocity is $v_0 = 270$ in./sec, then from the curves given in Figure 25, $q_0 = 200$ ksi. The failure or damage zone for this impact condition is given in Figure 39(e).

The increase in the damage zone in plates of finite thickness as a function of increasing surface pressure (or correspondingly increasing impact velocity) is shown in Figures 40 and 41. Figure 40 shows the growth of the damage zone for the case when the thickness and radius of the plate are kept constant and the impact velocity is increased. Figure 41 shows the growth of the damage zone (shaded area) for the case where R , H , and q vary, but R/H remains constant.

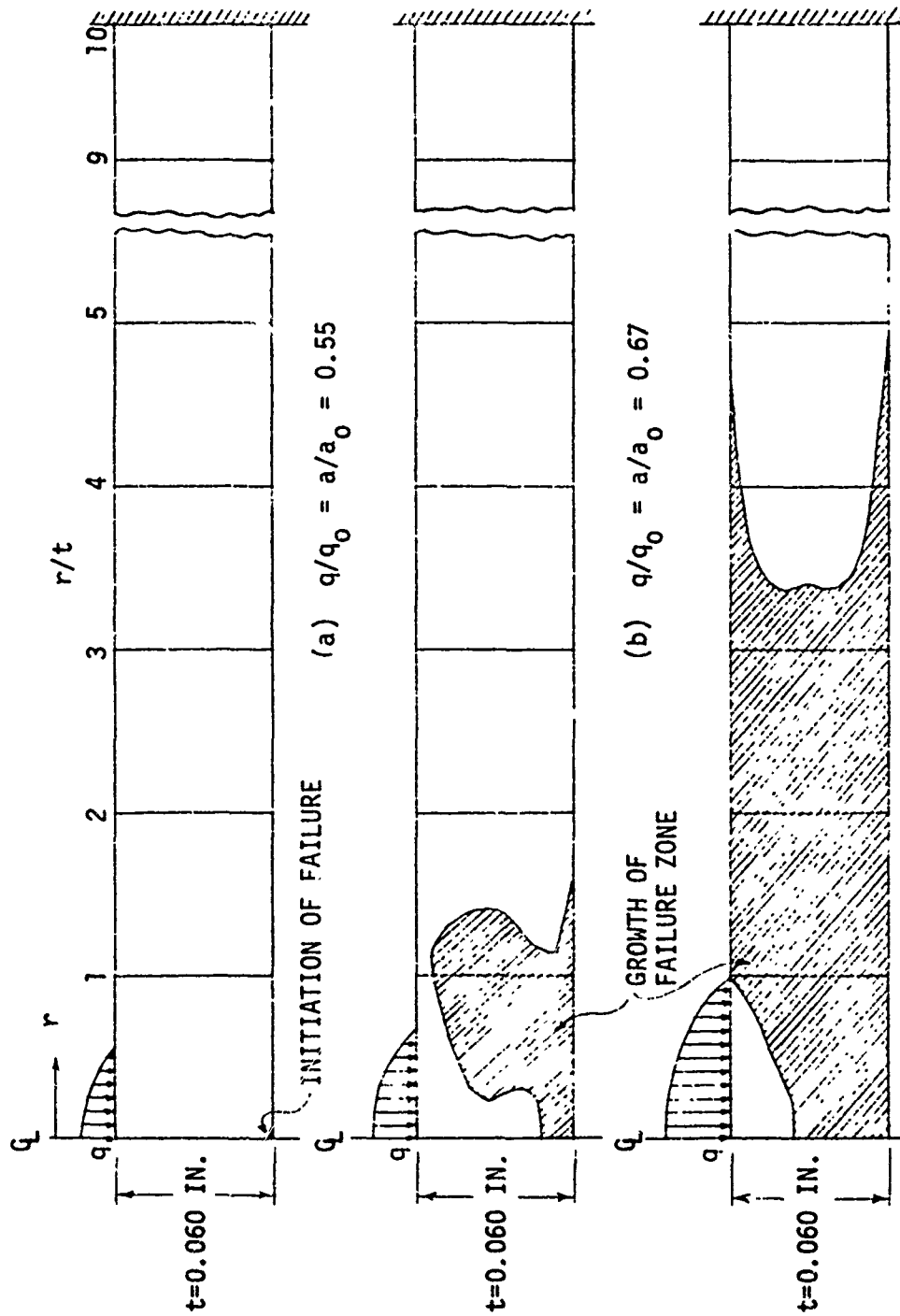
The results presented in Figures 39, 40, and 41 further illustrate how thickness of the target and its dimensions influence the damage induced by foreign objects impacting targets made of composite materials.

INFLUENCE OF PLATE BOUNDARY CONDITIONS ON IMPACT RESPONSE

The results obtained in Section III were for circular composite plates clamped along the outer periphery. Two other cases of plate support were investigated: (1) plates with roller supports along the outer boundary and (2) plates with hinge supports along the outer boundary.

In all cases, the plate material (Thornel 300-epoxy), fiber layup (inplane pseudo-isotropic), and plate dimensions (1.5-in. radius; 0.125-in. thickness) were kept constant. Impactor was assumed to be a 1.5-in. -diameter steel sphere, whereas the impact velocities investigated were $v = 30$ in./sec and $v = 50$ in./sec. At an impact velocity of 30 in./sec, the damage zone was localized near the impact surface. The width, w , and the depth, d , of the damage zone for plates with various edge supports are shown in Table XVIII. The results on the dimensions of damage zones resulting from 50-in./sec impact are presented in Table XIX. In the latter case, the damage zone extended through the thickness of the plate for all three types of plate boundary supports. Figure 42 shows the dimensions of the damage zones (resulting from a 50-in./sec impact by a 1.5-in. -diameter steel sphere) in composite plates with three types of boundary conditions.

From the results presented above it is seen that for impact velocities which cause local damage, the end fixity of the plate has a negligible influence on the size of the damage zone. On the other hand, as the impact velocity is increased so that damage occurs on top and bottom surfaces of the plate, the plate edge fixity has a significant influence on the width of the damage zone. For an impact velocity of 50 in./sec, the width of damage zone was smallest in plates with clamped edges and largest in plates with roller-supported edges.



$$q_0 = 100 \text{ KSI}$$

$$v_0 = 47.0 \text{ IN./SEC.}$$

$$H = t/a_0 = 1$$

$$a_0 = 0.060 \text{ IN.}$$

$$\text{NOTE: FOR THIS CASE } R = r_{\text{max}}/a_0 = 10$$

Figure 40. Initiation and Growth of Failure Zone with Increasing Surface Pressure (or Increasing Impact Velocity).

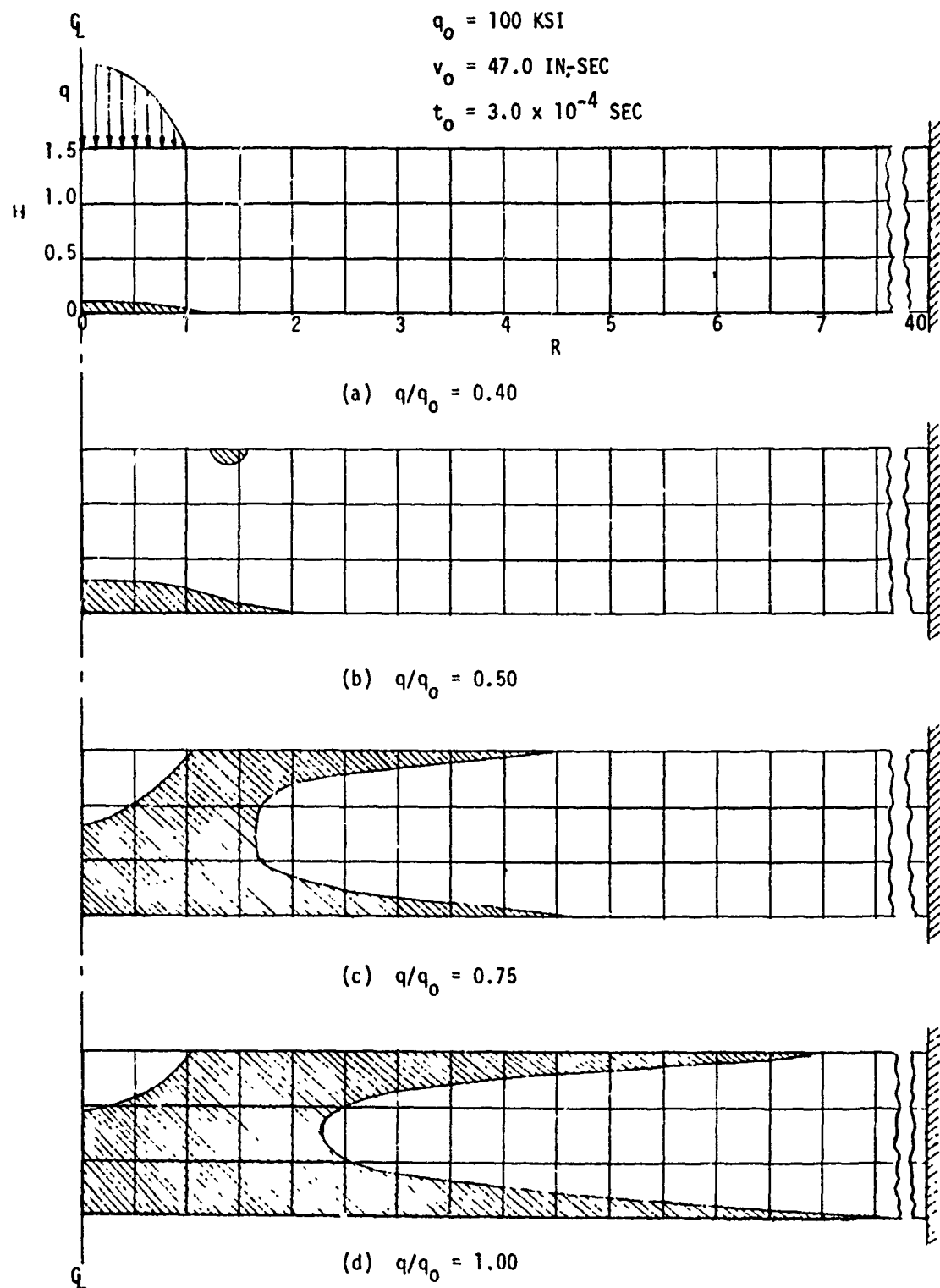


Figure 41. Increase in Damage Zone as a Function of Increasing Surface Pressure and/or Increasing Impact Velocity ($R/H = \text{Constant}$).

Table XVIII
INFLUENCE OF PLATE BOUNDARY CONDITIONS ON DIMENSIONS
OF DAMAGE ZONE CAUSED BY 30 IN./SEC IMPACT
BY A 1.5-IN.-DIAMETER STEEL SPHERE

| EDGE SUPPORT OF THE PLATE | w(in.) | d(in.) |
|---------------------------|--------|--------|
| CLAMPED EDGES | 0.120 | 0.050 |
| ROLLER SUPPORTED EDGES | 0.119 | 0.044 |
| HINGE SUPPORTED EDGES | 0.119 | 0.045 |

Table XIX
INFLUENCE OF PLATE BOUNDARY CONDITIONS ON DIMENSIONS
OF DAMAGE ZONE CAUSED BY 50 IN./SEC IMPACT
BY A 1.5-IN.-DIAMETER STEEL IMPACTOR

| EDGE SUPPORT OF THE PLATE | WIDTH OF DAMAGE ZONE (IN.) | |
|---------------------------|----------------------------|----------------|
| | TOP SURFACE* | BOTTOM SURFACE |
| CLAMPED EDGES | 0.217 | 0.231 |
| ROLLER SUPPORTED EDGES | 0.422 | 0.460 |
| HINGE SUPPORTED EDGES | 0.305 | 0.354 |

*Impacted surface

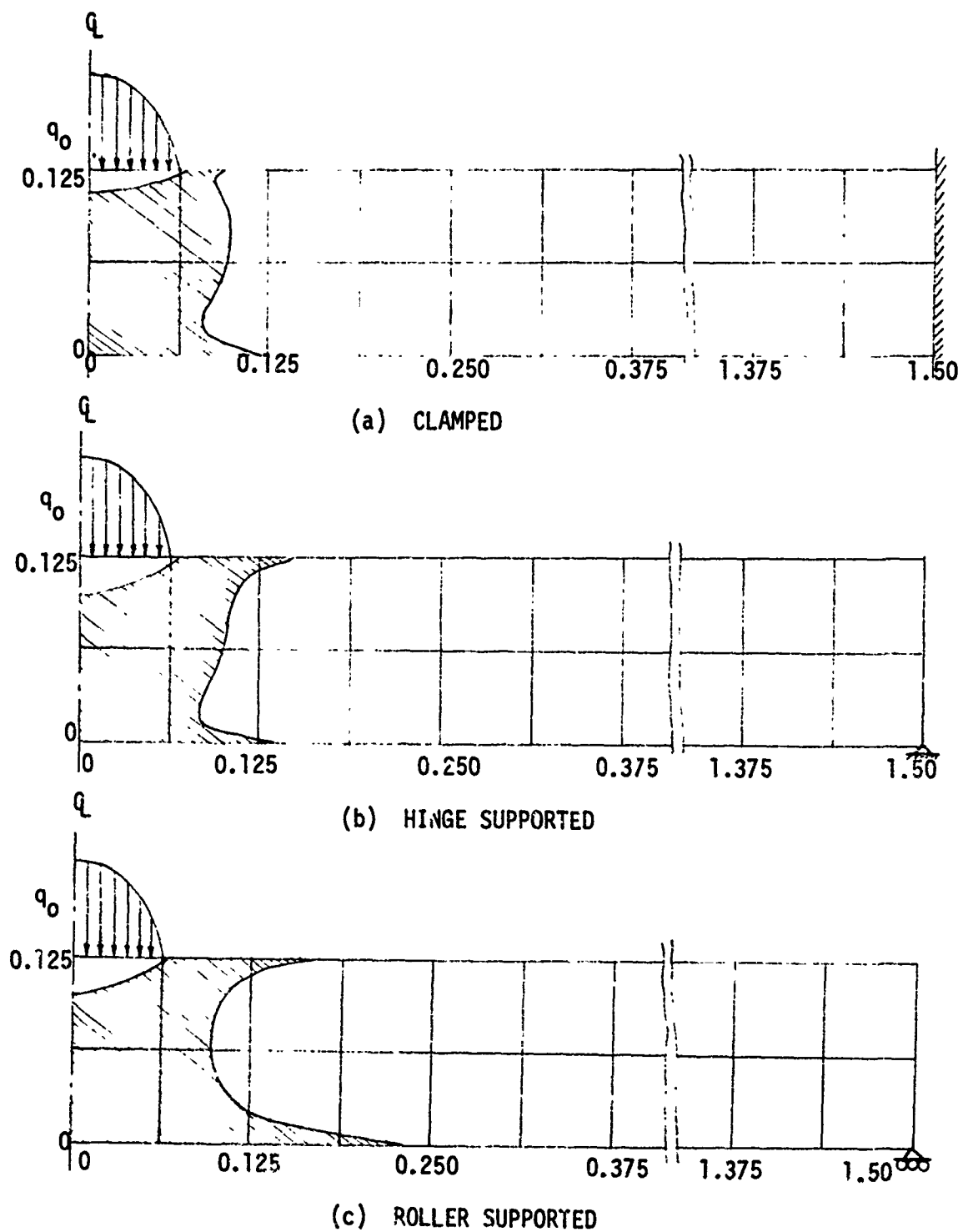


Figure 42. Influence of Plate Boundary Conditions on Impact Response ($v = 50$ In./Sec, $q_0 = 102$ ksi).

INFLUENCE OF FIBER ORIENTATION AND LAMINATE STACKING SEQUENCE ON IMPACT RESPONSE

The material properties used in studying the influence of fiber orientation and laminate stacking sequence were taken to be those corresponding to Thornel 300-epoxy, which is designated as Material 6 in Table VIII. The fiber orientations investigated included unidirectional composites, bidirectional composites having $0^\circ/90^\circ$ or $\pm 45^\circ$ dispersed fiber layup, and tridirectional composites having $0^\circ/\pm 60^\circ$ fiber layup (inplane pseudo-isotropic). In all cases the target was assumed to be a circular plate, 0.125 in. thick and having a 3-in. diameter. The plate was assumed to be fixed along its periphery. As before, the impactor was a 1.5-in. diameter steel sphere. Because of the shape of the plate and the fact that impact was assumed to occur at the center of the plate, a material with $\pm 45^\circ$ fiber layup is indistinguishable from a material with $0^\circ/90^\circ$ fiber layup. The pertinent results for the influence of fiber orientation on the impact response are presented in Figures 43 through 46. In obtaining the results shown therein the plate geometry and the impactor material size and shape were kept constant. The results shown in Figures 43, 44, and 45 were calculated for an impact velocity of 30 in./sec. Thus, the only variable in Figures 43 to 45 was the fiber orientation. The cross-hatched area in each of the figures gives the damage zone in the material resulting from a 30-in./sec impact by a 1.5-in. diameter steel sphere. Figure 46 shows the damage zone in one of the materials corresponding to a 50-in./sec impact. From the results presented in Figures 45 and 46, it is readily seen that if a plate is subjected to 30-in./sec impact, all the damage is within the plate, whereas a 50-in./sec impact causes the damage to extend to the outer surfaces of the plates.

Of the three fiber layups investigated, plates having only unidirectional fibers show the largest damage zone, whereas the smallest damage zone was found to exist in plates with bidirectional fiber layup. The damage zone in plates with tridirectional fiber layup is somewhat larger than it is in plates having bidirectional fibers.

To establish how stacking sequence influences the impact response, the following problems have been investigated:

1. Bidirectional composite with layers dispersed through the thickness so that the bidirectional composite could be considered as an equivalent homogeneous orthotropic material.
2. Bidirectional composite consisting of nine discrete layers having fiber orientations of 0° and 90° . Any one given layer was considered as homogeneous orthotropic, whereas the composite is treated as multilayer heterogeneous orthotropic.

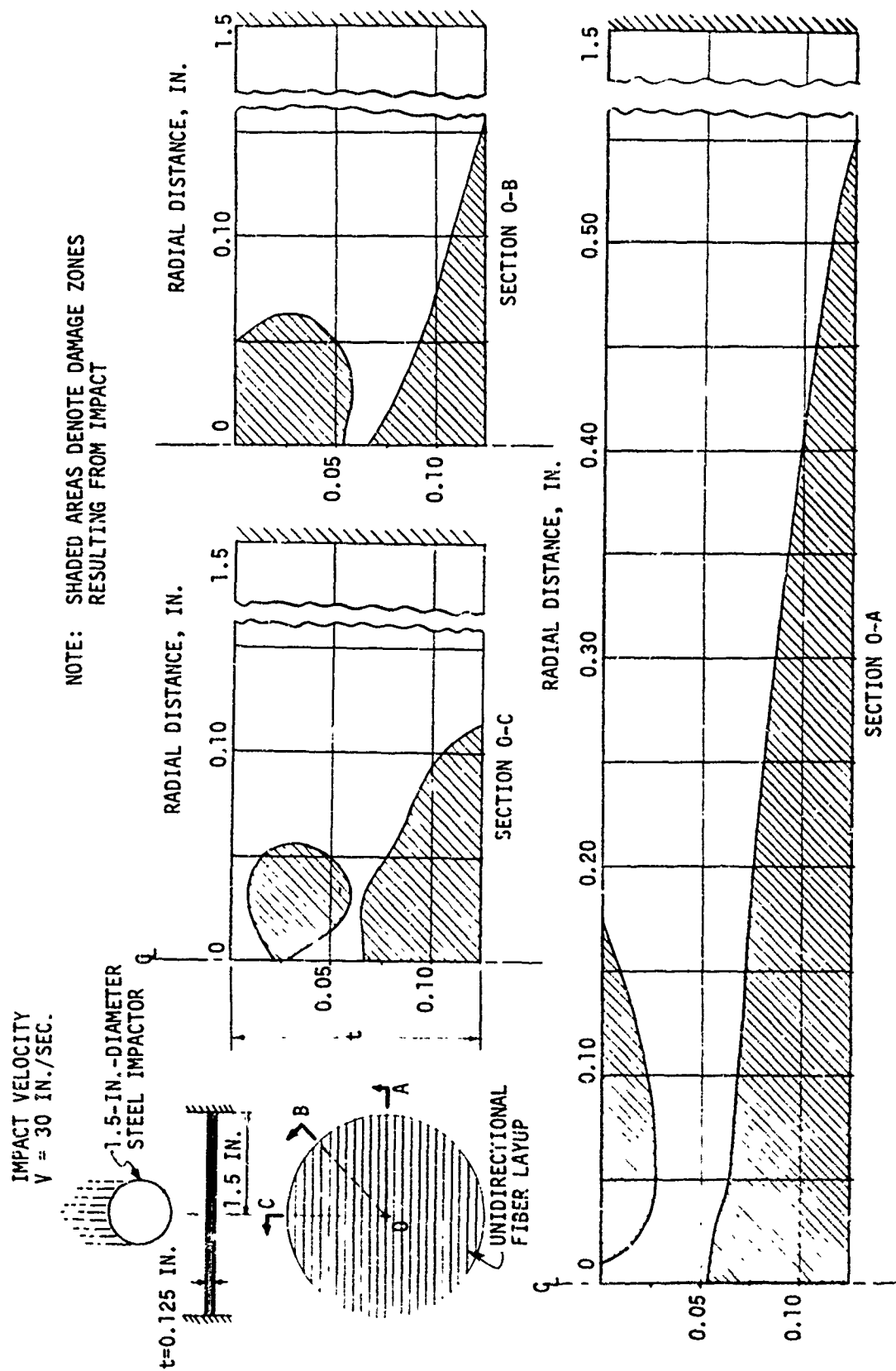


Figure 43. Foreign Object Impact-Induced Damage in Unidirectional Thornel 300-Epoxy Composite.

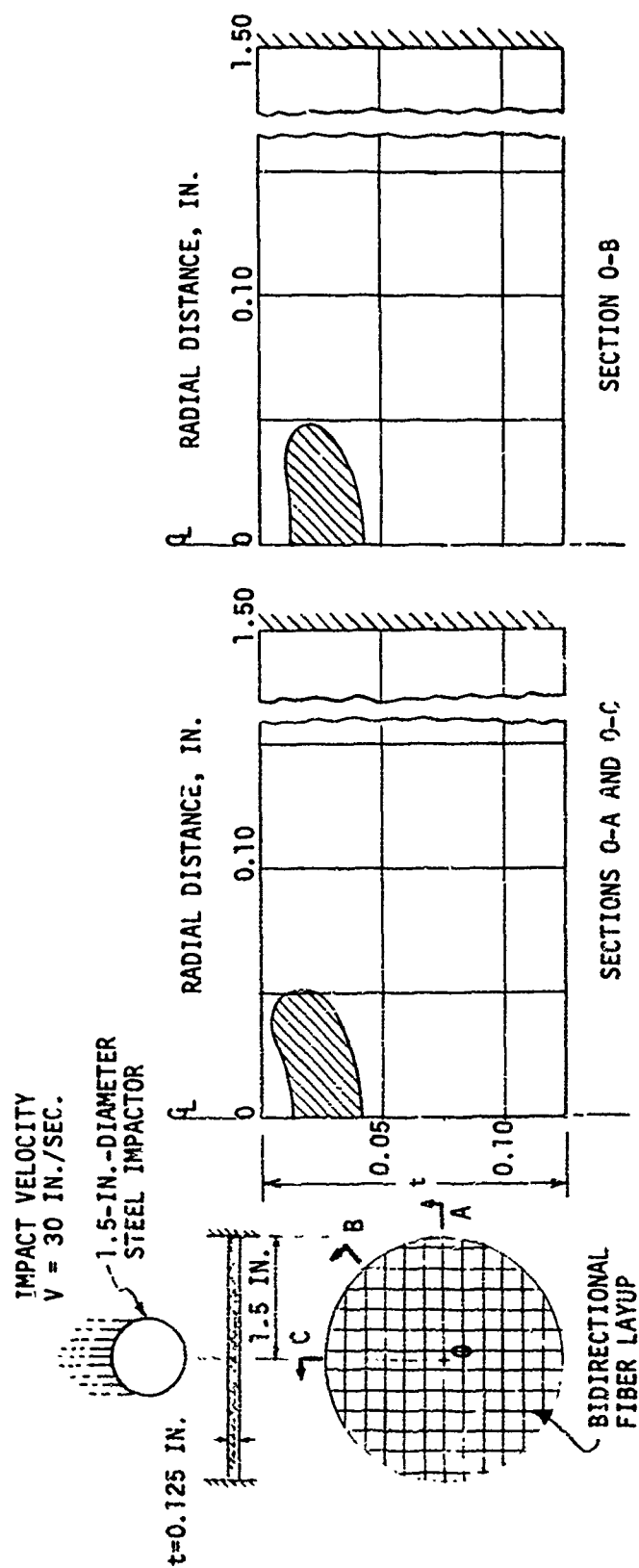


Figure 44. Foreign Object Impact-Induced Damage in 1:1 Bidirectional Thornel 300-Epoxy Composite.

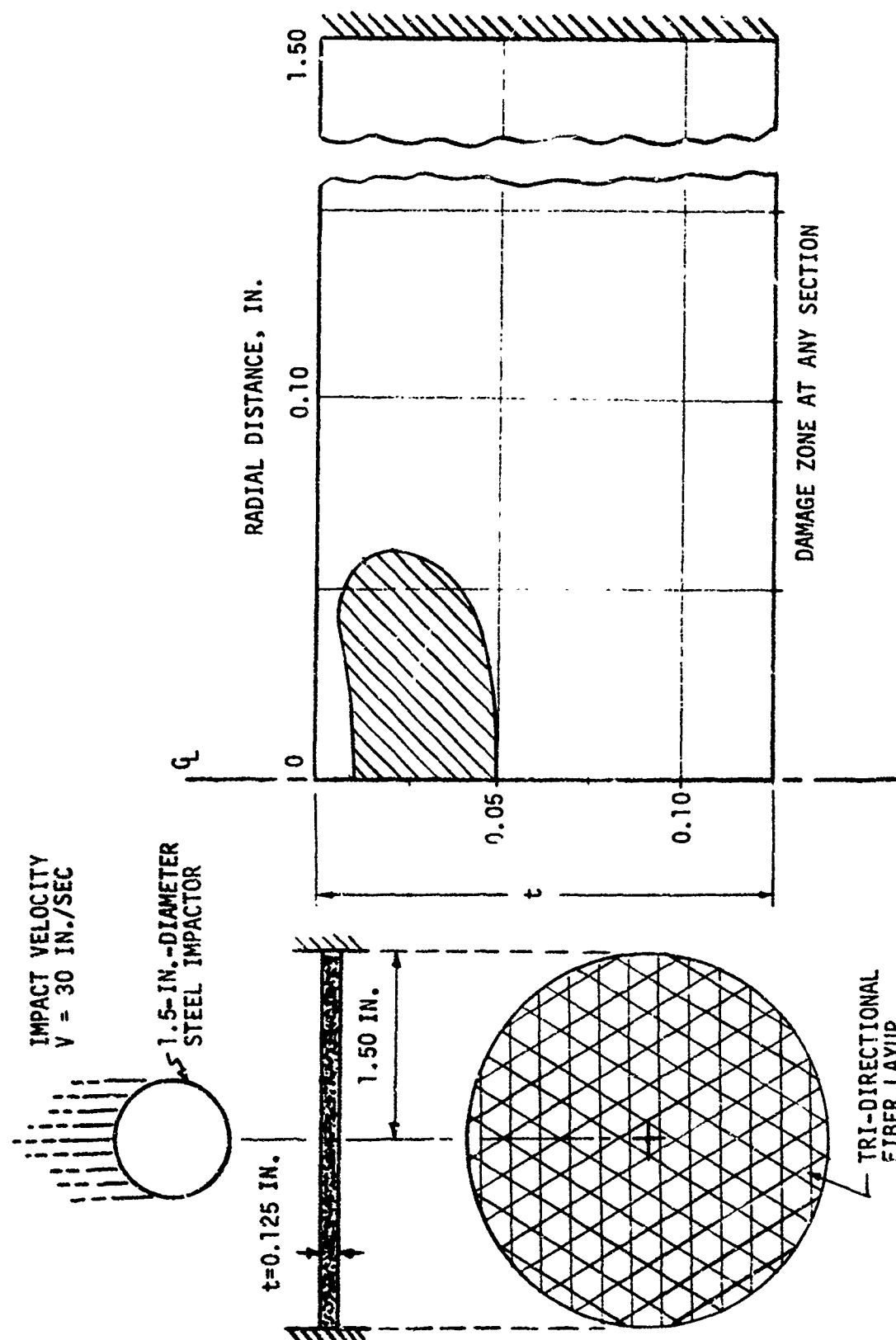
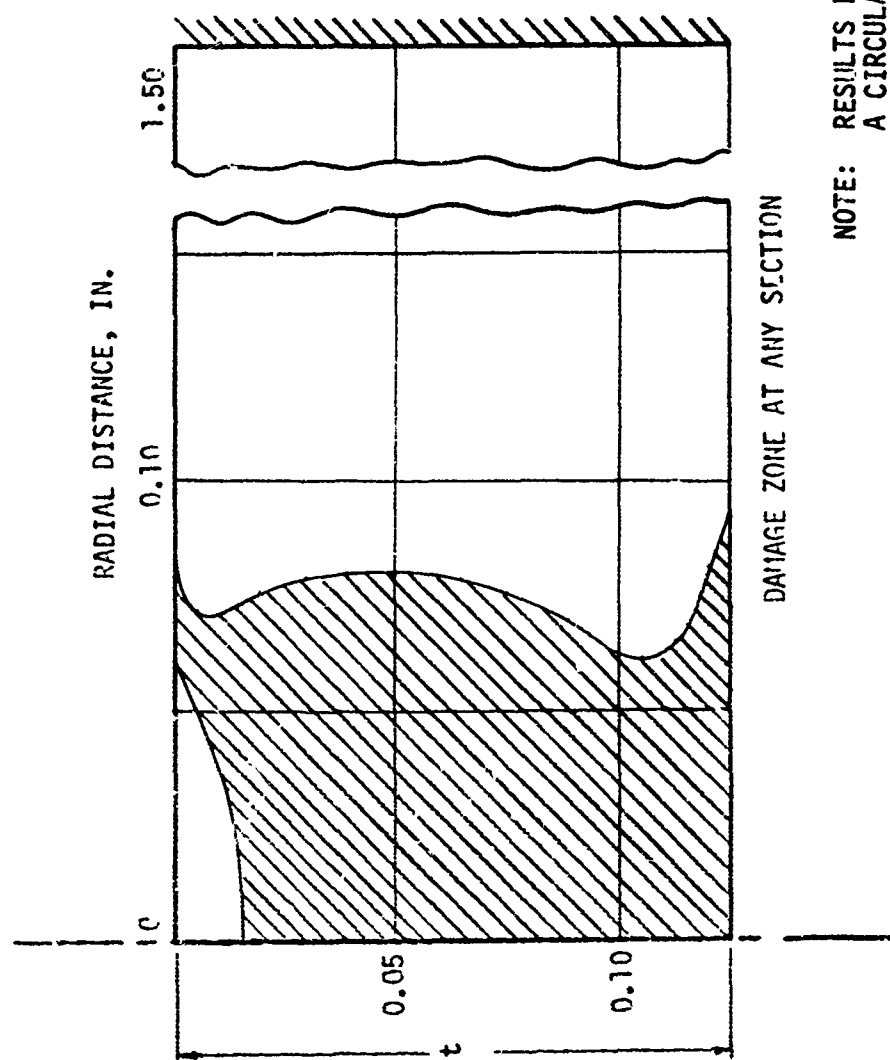


Figure 45. Foreign Object Impact-Induced Damage in Tri-directional Thornel 300-Epoxy Composite (Material In-Plane Pseudo-Isotropic).



NOTE: RESULTS PRESENTED HERE ARE FOR
A CIRCULAR COMPOSITE PLATE
HAVING TRI-DIRECTIONAL FIBER
LAYUP (SEE FIG. 44). PLATE
SUBJECTED TO A 50 IN./SEC.
IMPACT BY A 1.5-IN.-DIAMETER
STEEL IMPACTOR

Figure 46. Foreign Object Impact Damage in a Tridirectional Thornel
300-Epoxy Composite Subjected to 50-In./Sec Impact by a
1.5-In.-Diameter Steel Sphere.

3. Bidirectional composite consisting of three discrete homogeneous orthotropic layers, two of these having fibers oriented in the 0° direction and one layer having fibers oriented at 90° direction.

The results on the size of the damage zone in Problem 1 are shown in Figure 44. Figures 47 and 48 show the results for Problems 2 and 3. Comparison of results shown in Figures 44 and 47 shows that treating the bidirectional composite as an equivalent homogeneous orthotropic material does not allow for the complete determination of the damage zone. Similar results would be expected if the composite plate for which the results are presented in Figure 48 were treated as an equivalent orthotropic material. Considering the plates as multilayer heterogeneous orthotropic, however, allows for a more accurate determination of the damage zone. The influence of the stacking sequence can be seen by comparing the results shown in Figures 47 and 48. From the results shown therein it is seen that the damage zone is reduced if the layers are dispersed through the thickness.

INFLUENCE OF HYBRIDIZATION (COMBINING DIFFERENT COMPOSITES) ON IMPACT RESPONSE

To establish if impact response of composites could be improved through hybridization, analytical studies were conducted on material combinations and constructions shown in Figure 51. Combinations of materials considered included: bidirectional fiberglass-epoxy layers combined with bidirectional Thornel 300-epoxy layers; and bidirectional PRD 49-epoxy layers combined with bidirectional Thornel 300-epoxy layers. In all cases it was assumed that the total plate thickness remained 0.125 inch. As before, the plates were assumed to have 1.5-in. radii to be clamped along the outer boundary, and to be subjected to impact by a 1.5-in. -diameter steel impactor. The final results for the damage zones in fiberglass-epoxy/Thornel 300-epoxy and PRD 49-epoxy/Thornel 300-epoxy hybrid composite plates subjected to 30-in./sec and 50-in./sec impact are shown in Figures 52, 53, 54, and 55. For comparison purposes, Figures 52 and 53 show also the damage zones in Thornel 300-epoxy plates. Results from studies on fiberglass-epoxy/Thornel 300-epoxy hybrid composites showed the material Configurations (a) and (b) to be superior to material Configuration (c) (see Figures 52 and 53); consequently only the former material configurations were considered in investigating the impact response of hybrid composites consisting of PRD 49-epoxy and Thornel 300-epoxy. All the results given in Figures 52 through 55 were calculated using the material properties given in Tables IV and VI. The pertinent information on the maximum width and depth of the damage

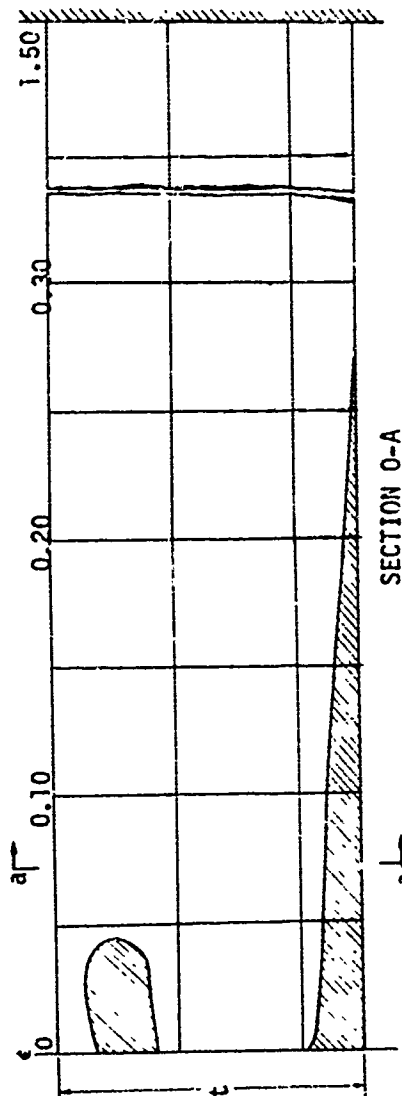
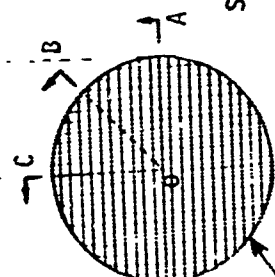
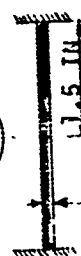
NOTE: SHADED AREAS DENOTE DAMAGE ZONES RESULTING FROM IMPACT

IMPACT VELOCITY

$V = 30 \text{ IN./SEC}$

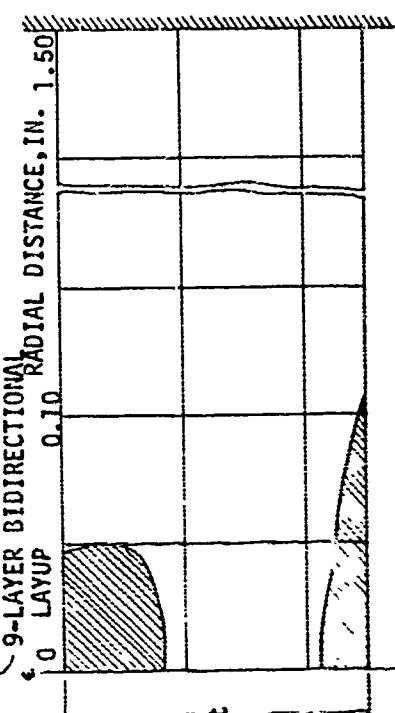
1.5-IN.-DIAMETER
STEEL IMPACTOR

$t = 0.125 \text{ IN.}$

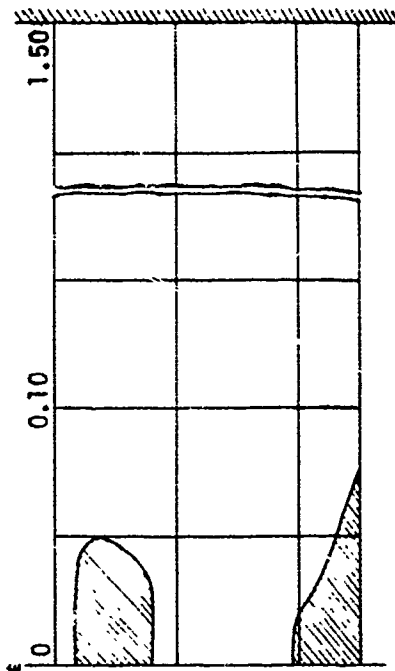


SECTION O-A

RADIAL DISTANCE, IN.

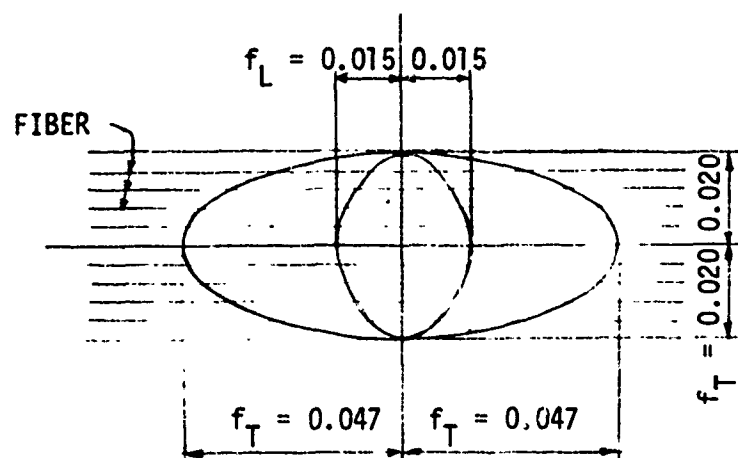


SECTION O-B



SECTION O-C

Figure 47. Foreign Object Impact-Induced Damage in a Bidirectional Thornel 300-Epoxy Plate Having a Nine-Layer Dispersed Construction.

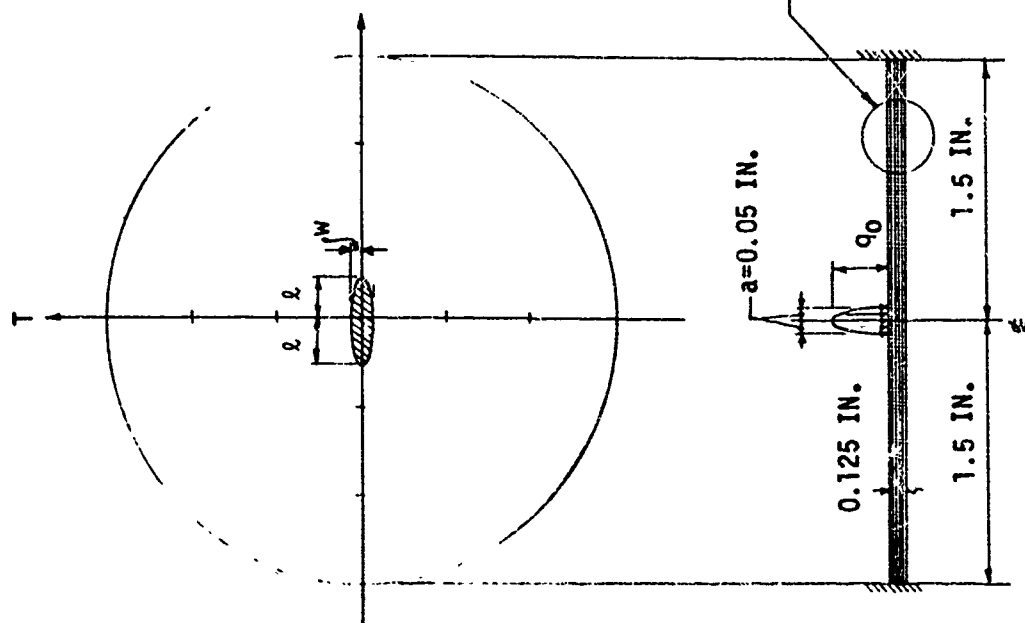


f_L = FAILURE IN FIBER DIRECTION

f_T = FAILURE IN TRANSVERSE DIRECTION

NOTE: ALL DIMENSIONS ARE IN INCHES

Figure 49. Impact Damage on the Top Surface (Impacted Surface) of a Nine-Layer Bidirectional Thornel 300-Epoxy Plate.



| | | LOCAL FAILURE (TOP) | | | TENSILE FAILURE (BOTTOM) | | | | |
|-------------|--|---------------------|--------|-------|--------------------------|--------|--------|-------|--------|
| | | UNIDIRECTIONAL | | TRAN. | UNIDIRECTIONAL | | | TRAN. | |
| | | 1 LAY. 3 LAY. | 9 LAY. | ISO. | 1 LAY. | 3 LAY. | 9 LAY. | ISO. | ISO. |
| q_0 (KSI) | | 87 | 84 | 84 | 83 | 87 | 84 | 84 | 83 |
| f_L | | 0.029 | 0.020 | 0.015 | -- | 0.022 | 0.020 | 0.012 | -- |
| f_T | | 0.160 | 0.102 | 0.047 | -- | 0.500 | 0.430 | 0.206 | 0.155 |
| f_L | | -- | -- | -- | -- | -- | -- | -- | -- |
| f_T | | 0.035 | 0.033 | 0.020 | -- | 0.120 | 0.107 | 0.072 | 0.0155 |

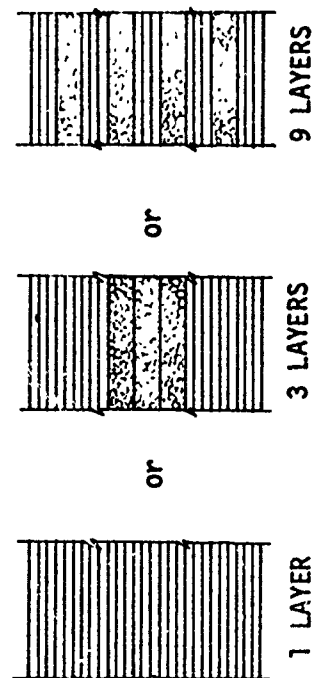


Figure 50. Surface Damage Caused by Impact of a 1.5-In. -Diameter Steel Ball.

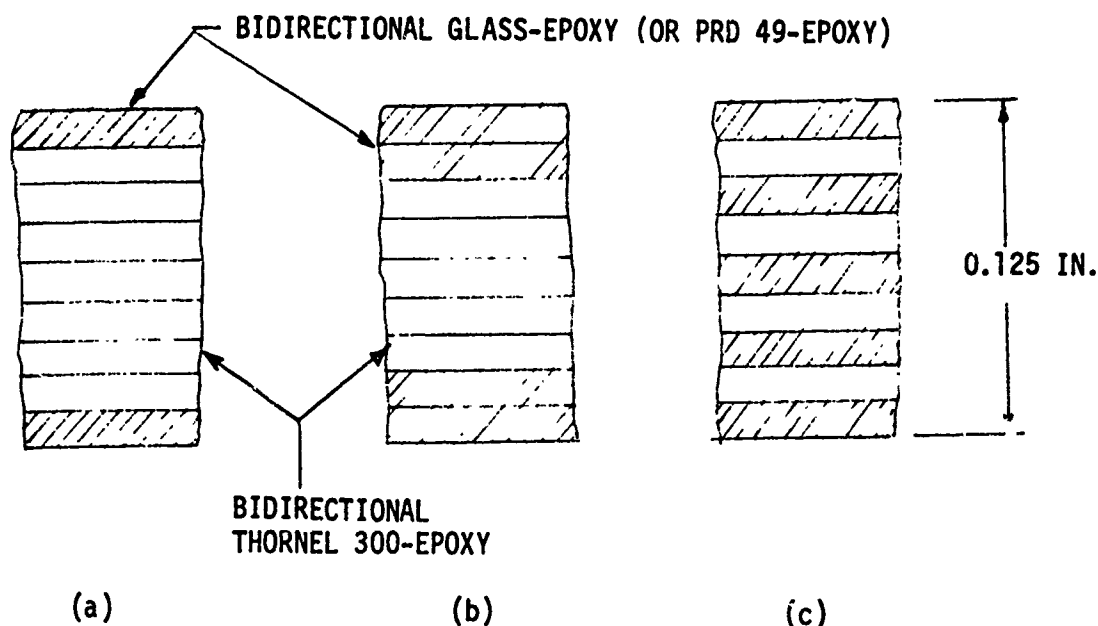


Figure 51. Material Configurations for Studying the Influence of Hybridization on Impact Response.

zones in various hybrid composite plates subjected to impact velocities at 30 in./sec and 50 in./sec is summarized in Table XX and XXI, respectively.

Because the damage zone has a highly irregular shape, no well-defined trends could be established for the influence of hybridization on impact response. However, from the results presented in Figures 52 through 55 and in Tables XX and XXI it is readily seen that concentrating fiberglass epoxy at the outer plate surfaces makes the composite more resistant to impact damage than if the fiberglass is dispersed through the thickness. If the fiberglass outer layers are replaced with PRD 49-epoxy, the damage zone grows in radius but decreases in depth. For material Configurations (a) and (b), the increase in impact velocity causes a greater increase in the depth of the damage zone than in its radius.

INFLUENCE OF CURVATURE ON IMPACT RESPONSE

In studying the influence of target curvature on impact response, it was assumed that the targets are cylindrical and are made of Thornel 300-epoxy, with 67% of the fibers (five layers) oriented in the circumferential direction and 33% of the fibers (four layers) oriented in the axial direction. The cross section of cylinder wall, showing the distribution of material and thicknesses of the nine layers, is shown in Figure 56. Radii of the cylinders were taken as 1.5 in. and 3.0 in., whereas their thicknesses were taken as $t = 0.125$ in. As before, the impactor

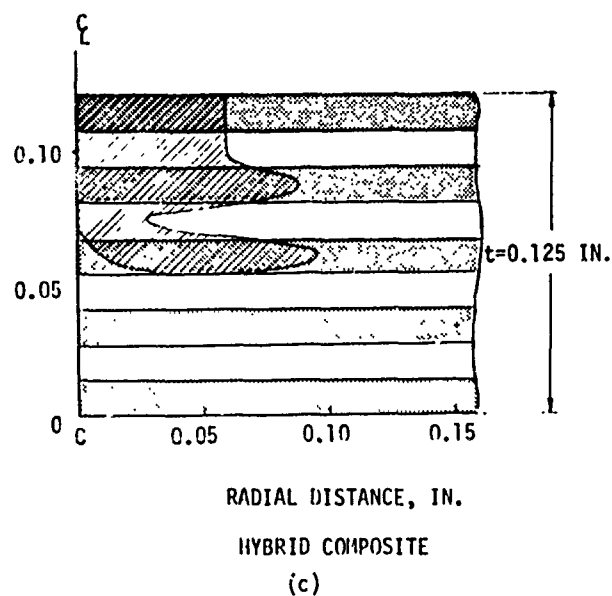
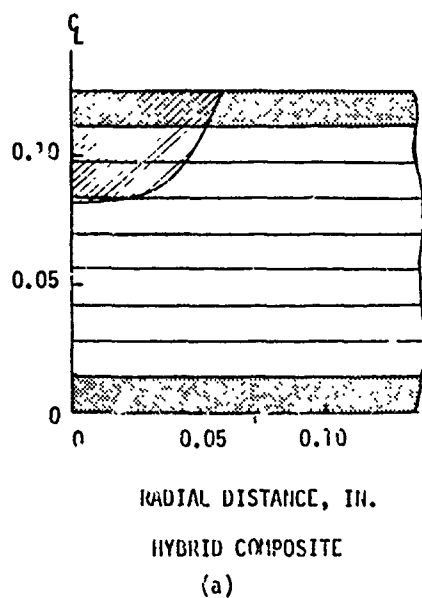
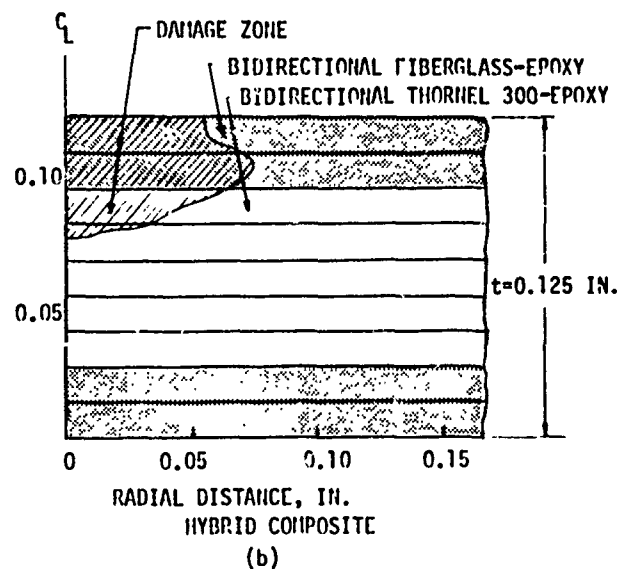
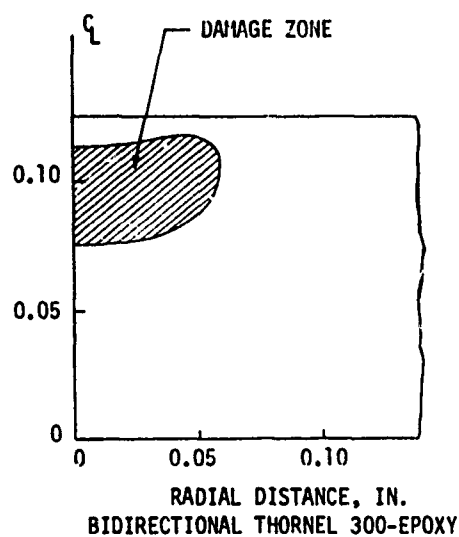


Figure 52. Damage Zone in 3-In. -Diameter Glass-Epoxy/Thornel 300-Epoxy Hybrid Composite Plates Subjected to 30-In. / Sec Impact by a 1.5-In. -Diameter Steel Impactor.

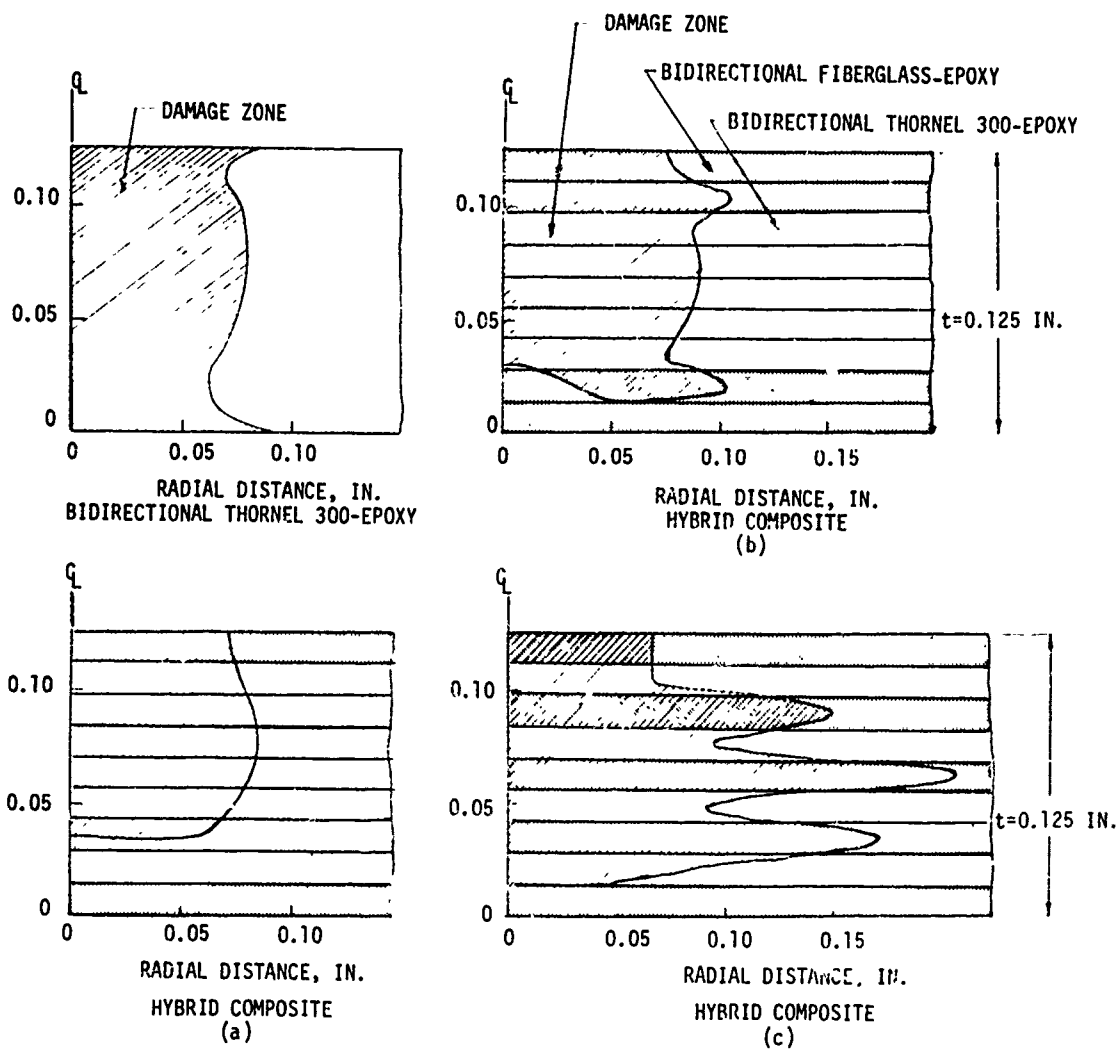


Figure 53. Damage Zone in 3-In. -Diameter Hybrid Composite Plates Subjected to 50-In./Sec Impact by a 1.5-In. -Diameter Steel Impactor.

Table XX

INFLUENCE OF COMBINING MATERIALS ON THE SIZE OF DAMAGE ZONE RESULTING
FROM A 30-IN./SEC IMPACT BY A 1.5-IN.-DIAMETER STEEL SPHERE

| MATERIAL CONFIGURATION† | FIBERGLASS-EPOXY COMBINED WITH THORNEL 300-EPOXY | | PRD 49-EPOXY COMBINED WITH THORNEL 30C-EPOXY | |
|----------------------------|---|--------|---|-------|
| | w(in)* | d(in)* | w(in) | d(in) |
| a | 0.124 | 0.043 | 0.316 | 0.040 |
| b | 0.150 | 0.048 | 0.300 | 0.023 |
| c | 0.194 | 0.070 | --- | --- |

* w = maximum width of the damage zone in the radial direction
d = maximum depth of the damage zone in the thickness direction

† see Figure 51

Table XXI

INFLUENCE OF COMBINING MATERIALS ON THE SIZE OF DAMAGE ZONE RESULTING
FROM A 50-IN./SEC IMPACT BY A 1.5-IN.-DIAMETER STEEL SPHERE

| MATERIAL CONFIGURATION [†] | FIBERGLASS-EPOXY COMBINED WITH THORNEL 300-EPOXY | | PRD 49-EPOXY COMBINED WITH THORNEL 300-EPOXY | |
|--|---|--------|---|-------|
| | w(in)* | d(in)* | w(in) | d(in) |
| a | 0.173 | 0.090 | 0.688 | 0.078 |
| b | 0.210 | 0.110 | 0.670 | 0.092 |
| c | 0.415 | 0.111 | --- | --- |

[†]* see Table XX for definition of terms

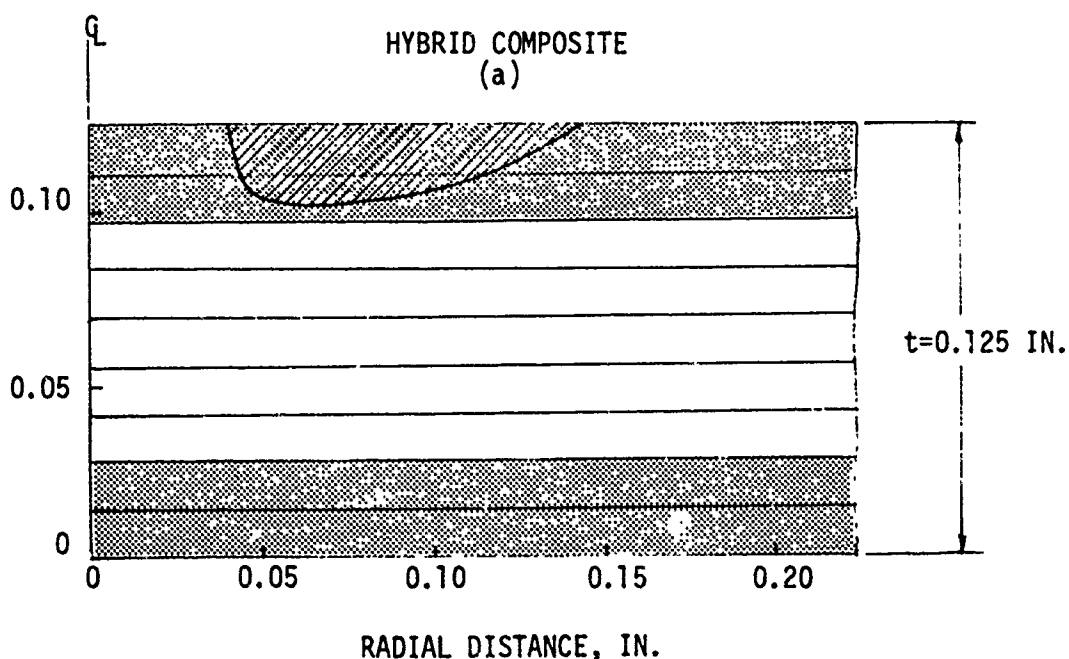
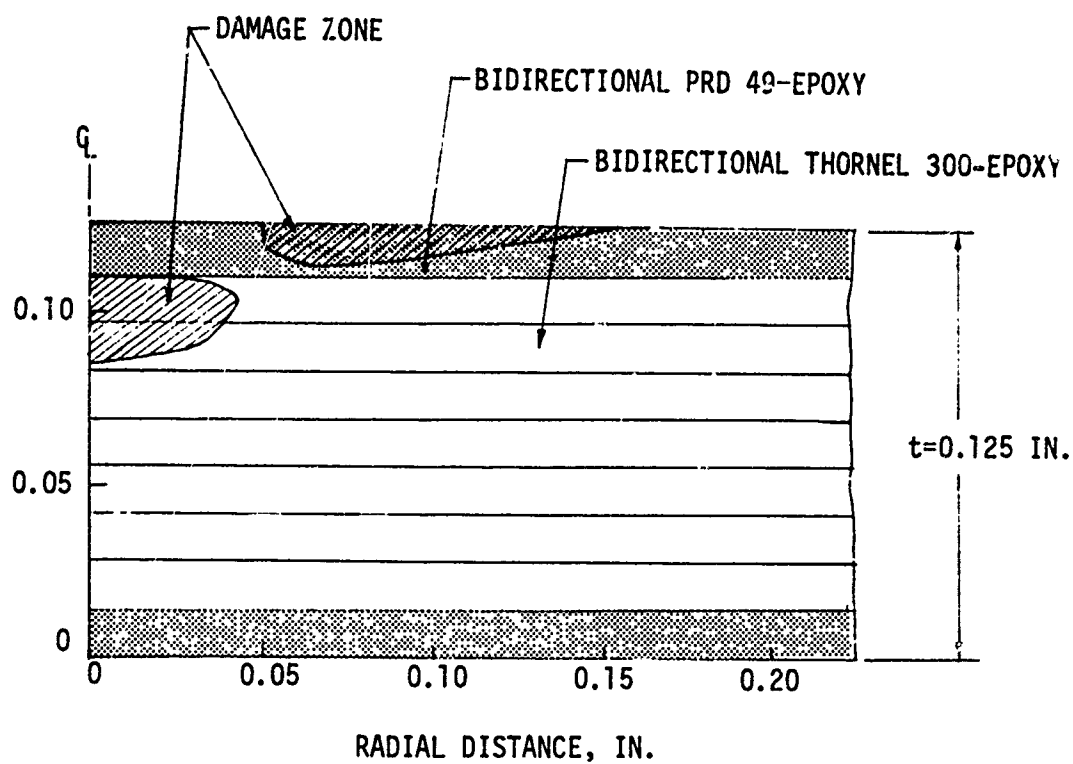


Figure 54. Damage Zone in 3-In. -Diameter PRD 49-Epoxy/Thornel 300-Epoxy Hybrid Composite Plates Subjected to 30-In. / Sec Impact by a 1.5-In. -Diameter Steel Impact:

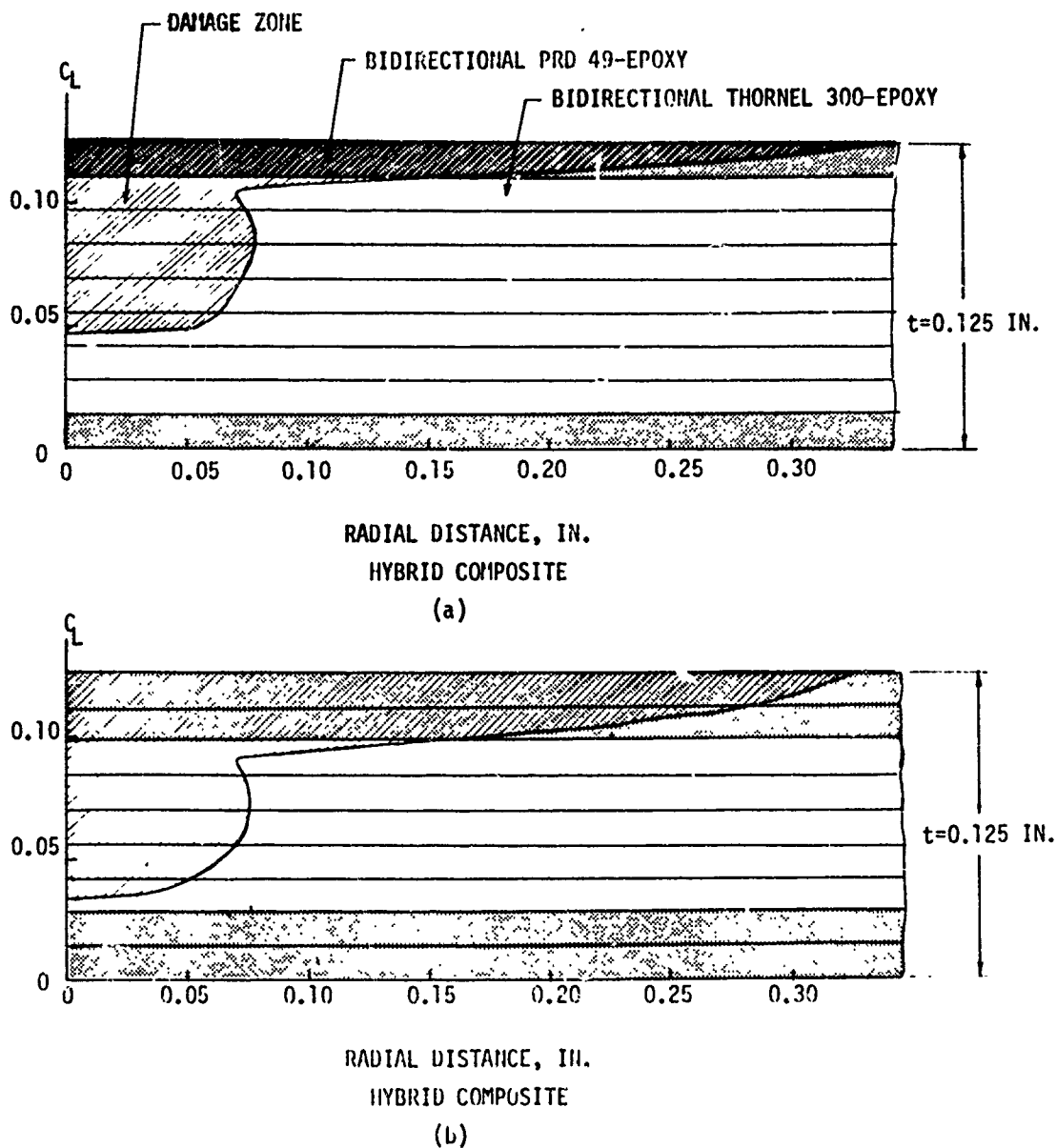


Figure 55. Damage Zone in 3-In. -Diameter PRD 49-Epoxy/Thornel 300-Epoxy Hybrid Composite Plates Subjected to 50-In. / Sec Impact by a 1.5-In. -Diameter Steel Impactor.

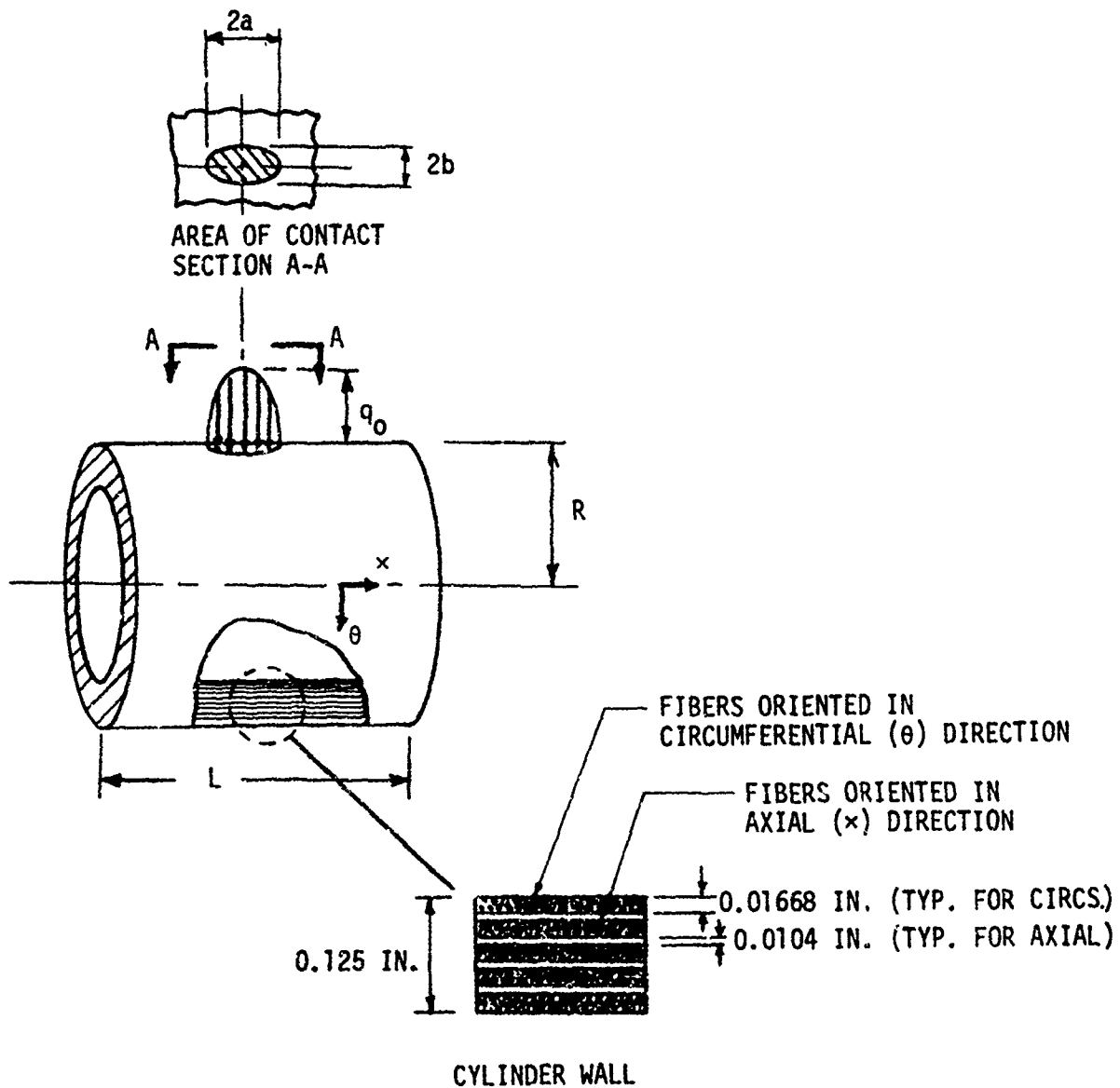


Figure 56. Cylinder Geometry and Material Distribution Through the Wall Thickness of the Cylinder.

was assumed to be a 1.5-in. -diameter steel sphere. Target curvature was found to influence the shape and size of the area of contact, maximum pressure, total load, and contact duration. The pertinent results for the influence of target curvature on the impact parameters are presented in Table XXII.

Using data shown in Table XXII as an input to the previously described CYLINDER code, calculations were made for the dynamic stresses in the cylindrical target, which was assumed to have simply supported ends. Because the low impact velocity resulted in a small area of contact, it was not possible to represent the surface load and the area of contact as described in Section II without further extensive modifications of the computer code. The best that could be done for the problem considered here (without exceeding computer storage capacity or exceeding 25 minutes of computer time) was to assume the load to be concentrated on one rectangular element, the area of which was the same as the area of the ellipse. The input to the code and its output were the same as described on Page 55 of Section II. The calculated stresses were used to determine the failure location, failure mode, and failure sequence using maximum stress criteria. Final results of these calculations are presented in Table XXIII. From the results presented in Tables XXII and XXIII, the following conclusions can be made on the influence of curvature on impact response (assuming impact velocity, target properties, and impactor mass, shape, and size remain constant):

1. In the case of a cylinder impacted by a sphere, the area of contact is elliptical and approaches a circle as the radius of the cylinder increases (approaches flat surface).
2. Area of contact decreases with decreasing cylinder radius.
3. Maximum load, resulting from impact, decreases with decreasing cylinder radius.
4. Maximum surface pressure increases with decreasing cylinder radius.
5. Contact duration increases with decreasing cylinder radius.
6. Time required to cause various failure modes decreases with decreasing cylinder radius.
7. Time sequence in which different failure modes take place changes as the cylinder radius changes.

Table XXII
INFLUENCE OF TARGET CURVATURE ON IMPACT PARAMETERS

| | | | |
|---|-----------------------|-----------------------|-----------------------|
| CLYINDER RADIUS, R, IN. | 1.5 | 3.0 | ∞ |
| CYLINDER LENGTH, L, IN. | 3.0 | 6.0 | - |
| CYLINDER THICKNESS, IN. | 0.125 | 0.125 | 0.125 |
| IMPACT VELOCITY, IN/SEC | 100 | 100 | 100 |
| SHAPE OF THE AREA OF CONTACT | ELLIPSE | ELLIPSE | CIRCLE |
| MINOR RADIUS, b, IN. | 6.52×10^{-2} | 7.16×10^{-2} | 8.09×10^{-2} |
| MAJOR RADIUS, a, IN. | 8.53×10^{-2} | 8.34×10^{-2} | 8.09×10^{-2} |
| AREA OF CONTACT, A = πab , IN ² | 0.0175 | 0.0188 | 0.0206 |
| MAXIMUM LOAD, P, LB. | 1806 | 1830 | 1876 |
| MAXIMUM SURFACE PRESSURE, q_0 , KSI | 155 | 146 | 137 |
| CONTACT DUKATION, $\delta \times 10^{-4}$ SEC | 2.67 | 2.62 | 2.57 |

Table XXIII
FAILURE MODE, LOCATION AND SEQUENCE
IN 3-INCH- AND 6-INCH-DIAMETER CYLINDERS

| FAILURE MODE | TIME AT WHICH FAILURE TAKES PLACE (μ sec) | |
|---|---|-----------------------------|
| | 3-INCH-DIAMETER CYLINDER | 6-INCH-DIAMETER CYLINDER |
| Transverse Tensile Failure on the Inner Surface | 14.3 | 23.0 |
| Compression Failure in the Fiber Direction on the Outer Surface | 61.1 | 64.7 |
| Compression Failure in Transverse Direction on the Outer Surface | 78.0 | 89.0 |
| Tensile Failure in Fiber Direction on the Inner Surface | 79.7 | 85.4 |

SECTION IV
DESCRIPTION OF MATERIAL AND SPECIMENS USED
IN THE TEST PROGRAM

Following the theory application phase of the program, a test plan for determining the threshold energy levels that cause fracture in graphite-epoxy composites subjected to impact was prepared and submitted for approval to the Project Officer. Following its approval, the test plan was implemented. Appropriate graphite-epoxy specimens were then fabricated and tested to experimentally establish the influence of the following variables on impact response: fiber and matrix properties; fiber orientation, layup, and stacking sequence; laminate thickness; curvature effects; and hybridization. Two types of specimens were employed: flat plates and cylinders. The basic material (Thornel 300 epoxy) used in the majority of test specimens was characterized for its mechanical properties. Moreover, appropriate quality assurance tests were also performed on all materials used in the test program.

DESCRIPTION OF MATERIALS USED IN TEST PROGRAM

Five different reinforcing fibers and three different resins were used in the various tasks of the test program. These materials and their properties are described in Table XXIV. The properties data shown therein were obtained from various vendors and from literature.

QUALITY ASSURANCE TESTS ON INCOMING MATERIALS AND SPECIMEN FABRICATION

Quality assurance tests were conducted on the various prepreg materials to ensure that the material was of acceptable quality and to verify and/or establish the processing parameters. The quality control (QC) tests included flexure tests and short-beam shear tests. Table XXV shows the results from the QC tests, as well as other pertinent information. The final cure cycles that were used in various composites incorporating different resin systems were as follows:

1. Composites made with 5208 epoxy
 - a. Enter cold autoclave under vacuum.
 - b. Hold vacuum and raise temperature to 275°F at 5-9°F/min.

Table XXIV
REINFORCEMENT AND MATRIX MATERIALS

| | Type | Specific Gravity | Average Mechanical Properties | |
|-----------------------|--------------------------------|------------------|---|--|
| | | | Young's Modulus x 10 ⁻⁶ psi | Tensile Strength x 10 ⁻³ psi |
| REINFORCING FIBERS | THORNEL 300 | 1.76 | 34 | 325 |
| | CELION GY-70 | 1.96 | 75 | 310 |
| | MODMOR II | 1.71 | 35 | 350 |
| | E-GLASS | 2.48 | 10.5 | 400 |
| | PRD-49 (or KEVLAR 49) | 1.45 | 19 | 400 |
| MATRIX MATERIALS | NARMCO 5208 EPOXY | 1.265 | -- | -- |
| | U.C.C. ERLA 4617 EPOXY | 1.267 | 0.70 | 9.0 |
| | U.S. POLYMETRIC POLYSULFONE | 1.24 | 0.36 | 10.2 |

Table XXV
MECHANICAL PROPERTIES DATA FROM QC TESTS

| Material | Fiber Pattern | Thickness Per Ply (in.) | Flexure Strength $\times 10^{-3}$ psi | Flexure Modulus $\times 10^{-6}$ psi | Interlaminar Shear Strength $\times 10^{-3}$ psi |
|-------------------------|---------------|-------------------------|---------------------------------------|--------------------------------------|--|
| CELION GY-70/5208 | 0° | 0.00542 | 131.18 | 52.07 | 11.68 |
| MODMOR II/5208 | 0° | 0.00672 | 241.46 | 23.61 | 15.07 |
| THORNEL 300/POLYSULFONE | 0° | 0.00742 | 48.37 | 7.81 | N.F.(1) |
| KEVLAR 49/5208 | 0° | 0.00667 | 114.26 | 11.18 | 11.23 |
| THORNEL 300/4617 | 0° | --- | 345.06 | 20.75 | 16.05 |
| THORNEL 300/5208 (2) | 0° | 0.00521 | 290.5 | 20.20 | 19.33 |
| THORNEL 300/5208 (3) | 0° | 0.00504 | 334.0 | 25.0 | 19.13 |

(1) Denotes no failure because of excessive deformation

(2) Material Batch 312

(3) Material Batch 324

- c. Hold at 275°F under vacuum for 45 minutes.
 - d. Raise temperature to 350°F at 5-9°F/min and pressure to 100 psi.
 - e. When pressure reaches 20 psi., vent bag to atmosphere.
 - f. Hold at 350°F and 100 psi for 2 hours.
 - g. Cool under pressure to below 150°F and remove.
2. Composites made with ERLA 4617 epoxy
- a. Enter cold autoclave under vacuum.
 - b. Hold vacuum throughout cure.
 - c. Raise temperature to 175°F at 5-9°F/min.
 - d. Hold at 175°F for 3 hours.
 - e. Raise temperature to 200°F at 5-9°F/min.
 - f. Hold at 200°F for 1 hour.
 - g. Raise temperature to 250°F at 5-9°F/min and pressure to 80 psi.
 - h. Hold at 250°F and 80 psi for 2 hours.
 - i. Raise temperature to 300°F at 5-9°F/min.
 - j. Hold at 300°F and 80 psi for 2 hours.
3. Composites made with Polysulfone matrix.
- a. Enter hot press at 450°F.
 - b. Apply contact pressure for 10-15 min.
 - c. Relieve pressure to allow volatiles to escape.
 - d. Apply 100 psi for 30 min.
 - e. Remove from press and cool under deadweight pressure of approximately 2-5 psi.

MECHANICAL PROPERTIES OF UNIDIRECTIONAL THORNEL 300/ 5208 COMPOSITES

Because most of the test specimens were to be fabricated from Thornel 300/5208, appropriate tests were conducted on the material to obtain the mechanical properties data. Figure 57 shows the geometry of the various test specimens, whereas the typical failed specimens and the final test data are presented in Figure 58 and Table XXVI, respectively. As noted in Table XXVI, most of the test values are an average from three tests. The test data shown in Table XXVI show good correlation with test data given in the literature and shown earlier in Table V of Section III.

DESCRIPTION OF TEST SPECIMENS

The various specimens that were used in the experimental phase of the program are described in Table XXVII. The latter gives the panel or cylinder designation (for later reference), fiber, and matrix material from which a given panel or cylinder was made, and the fiber layup. Table XXVIII relates the panels and cylinders to the experimental variables that were investigated. A further description of the various specimens that were fabricated is given in Table XXIX. The latter gives the specimen's weight, its dimensions, density of composite, fiber and void content, and the thickness per ply. The densities that are given were calculated by gravimetric technique and also from the weights and dimensions of the specimens. The fiber contents in the various specimens were determined by (1) a nitric acid digestion in the case of graphite-fiber-reinforced composites, (2) nitric acid digestion followed by burnout in the case of Thornel-epoxy/glass-epoxy hybrid composites, and (3) nitric acid digestion followed by sulphuric acid digestion in the case of Thornel 300-epoxy/Kevlar 49-epoxy hybrid composites.

One problem encountered in fabricating plates was that the plate thicknesses could not be kept exactly at 0.125 in. because different prepregs and fiber layups give different thicknesses per ply of cured prepreg tape. Moreover, to prevent warping, the fiber layup had to be kept symmetrical with respect to the midplane of the plate. Consequently, only the total number of plies of prepreg in each plate was kept constant, except for the plates in which the plate thickness was a variable.

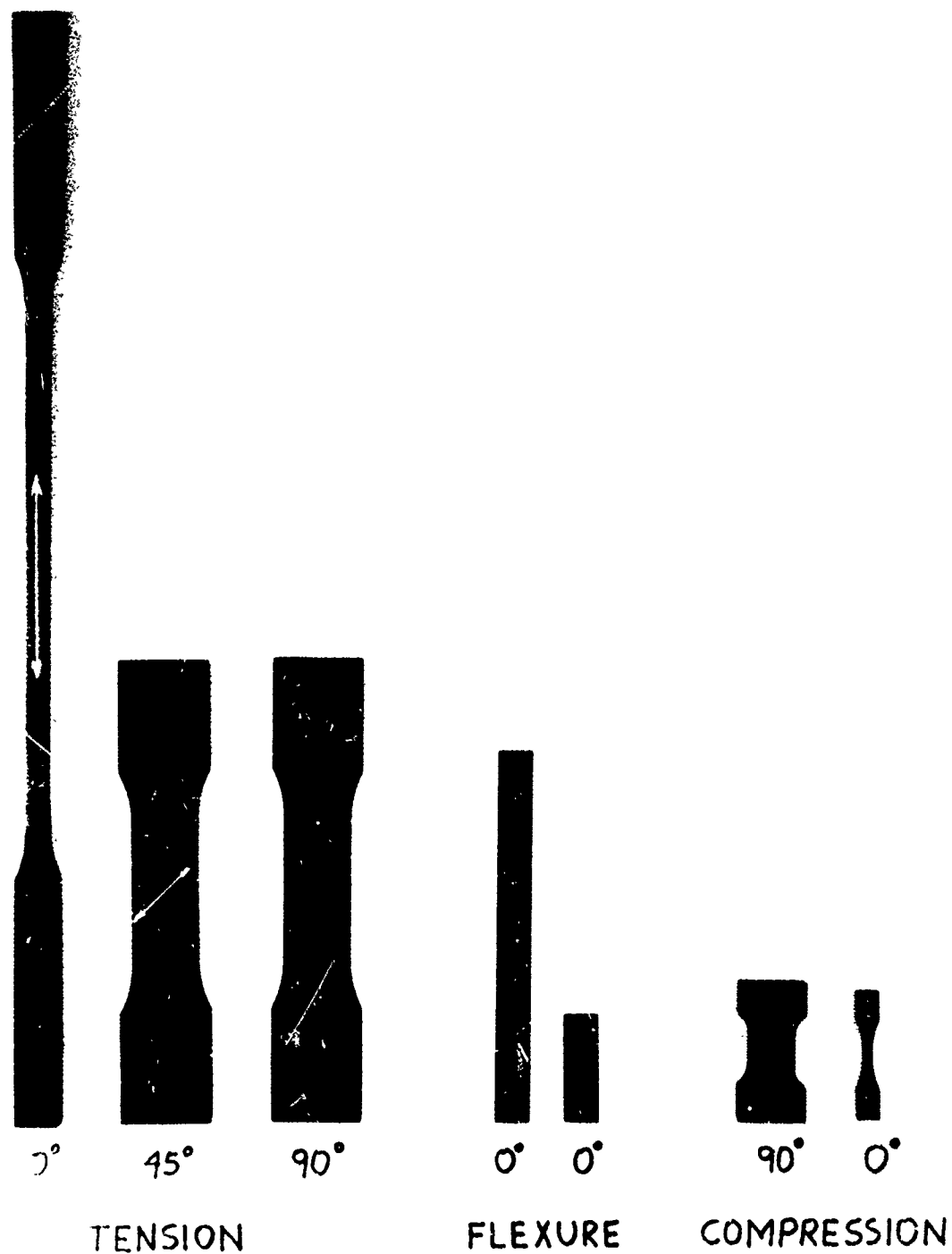


Figure 57. Test Specimens for Measuring the Mechanical Properties of Thornel 300-5208 Unidirectional Composite.

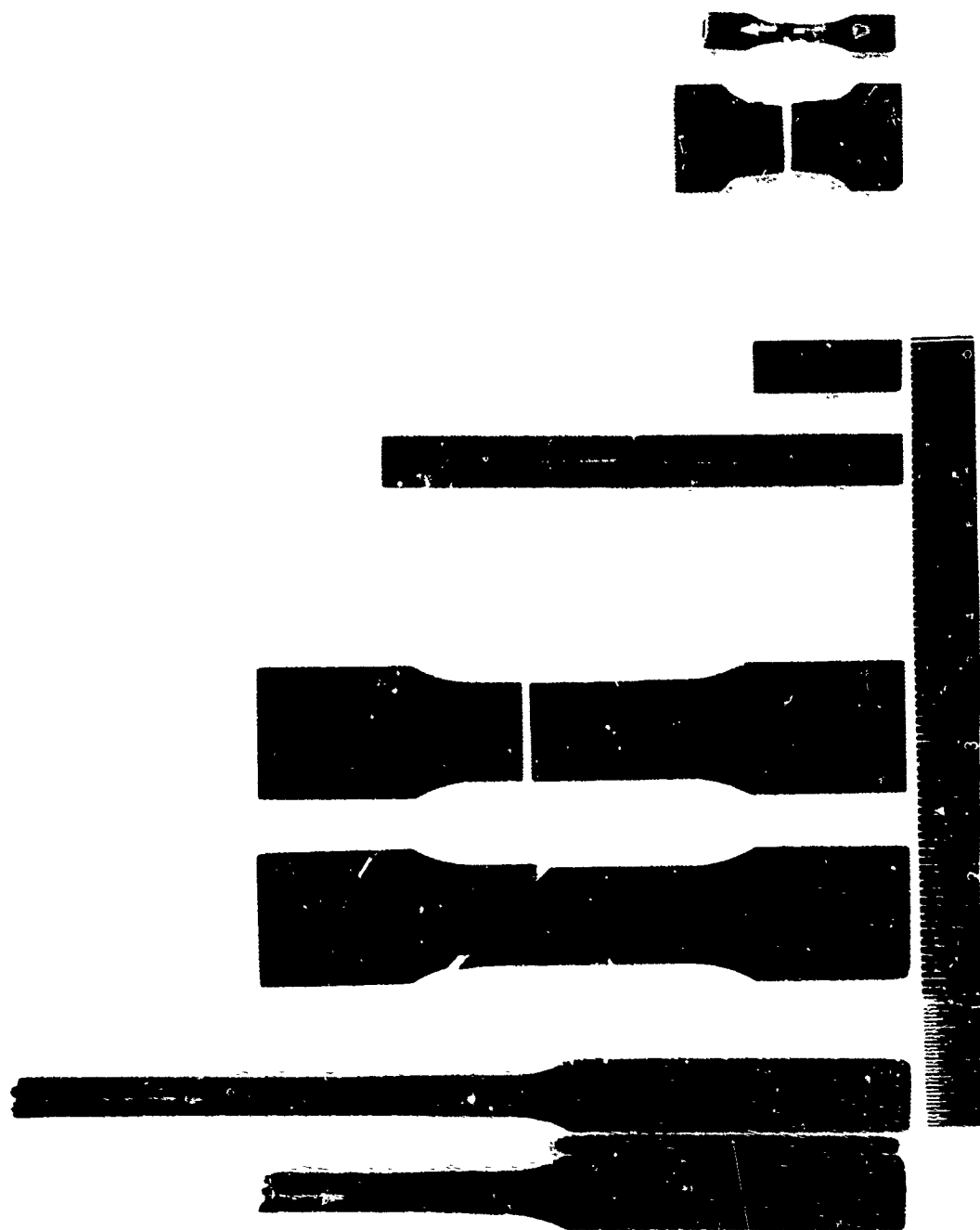


Figure 58. Failed Specimens (Typical Results).

Table XXVI
AVERAGE MECHANICAL PROPERTIES FOR THORNEL 300-5208
UNIDIRECTIONAL COMPOSITES (MEASURED DATA)

| DIRECTION | PROPERTY | VALUE |
|--|--|--|
| | Fiber Content by Volume (3)** | $k = 58.5\%$ |
| | Void Content (3) | $k_v = 0.85\%$ |
| | Composite Density | $\rho = 0.0557 \text{ LB/IN.}^3$ |
| | Thickness per ply | $t = 0.00578 \text{ IN.}$ |
| AXIAL | Tensile Strength (3) | $\sigma_{Lt} = 196.7 \times 10^3 \text{ PSI}$ |
| | Tensile Modulus (4) | $E_{Lt} = 19.4 \times 10^6 \text{ PSI}$ |
| | Tensile Strain at Failure (3) | $\epsilon_{Lt} = 1.01\%$ |
| | Compressive Strength (6), | $\sigma_{Lc} = 203 \times 10^3 \text{ PSI}$ |
| | Flexure Strength (3), Flexure Modulus (2), | $\sigma_{Lf} = 210.5 \times 10^3 \text{ PSI}$ $E_{Lf} = 20.8 \times 10^6 \text{ PSI}$ |
| | Interlaminar Shear Strength (3), | $\tau = 15.89 \times 10^3 \text{ PSI}$ |
| TRANSVERSE | Tensile Strength (3), | $\sigma_{Tt} = 6.29 \times 10^3 \text{ PSI}$ |
| | Tensile Modulus (3), | $E_{Tt} = 1.31 \times 10^6 \text{ PSI}$ |
| | Tensile Strain at Failure (2), | $\epsilon_{Tt} = 0.50\%$ |
| | Minor Poisson's Ratio (3), | $\nu_{TL} = 0.0136$ |
| | Compressive Strength (3), | $\sigma_{Tc} = 34.03 \times 10^3 \text{ PSI}$ |
| | Compressive Modulus (2), Compressive Strain at Failure (2), | $E_{Tc} = 1.45 \times 10^6 \text{ PSI}$ $\epsilon_{Tc} = 2.67\%$ |
| 45° (WITH RESPECT TO FIBER DIRECTION) | Tensile Strength (3), | $\sigma_{45t} = 11.94 \times 10^3 \text{ PSI}$ |
| | Tensile Modulus (3), | $E_{45t} = 1.90 \times 10^6 \text{ PSI}$ |
| | Poisson's Ratio (3), | $\nu_{45} = 0.263$ |
| | Tensile Strain at Failure (2), | $\epsilon_{45} = 0.70\%$ |
| * | Inplane Shear Strength (3), | $\tau_{LT} = 16.87 \times 10^3 \text{ PSI}$ |
| | Inplane Shear Modulus (3), | $G_{LT} = 0.754 \times 10^6 \text{ PSI}$ |

* Calculated from data on tensile specimens with 45° fiber orientation.

** Denotes number of tests on which average is based.

Table XXVII
DESCRIPTION OF FIBER AND RESIN MATERIALS AND
FIBER PATTERNS IN VARIOUS PANELS AND CYLINDERS

| Panel or Cylinder Designation | Fiber Material | Resin Material | Fiber Layup | Remarks |
|-------------------------------------|------------------------|---------------------|--|---|
| 1.1a* | CELION GY-70 | 5208 | $[(0, -60, 60)(0, 60, -60)]_3$ S | PSEUDO-ISOTROPIC* |
| 1.1b | THORNEL 300 | 5208 | $[(0, -60, 60)]_4$ S | PSEUDO-ISOTROPIC |
| 1.1c | MODMOR II | 5208 | $[(0, -60, 60)]_4$ S | PSEUDO-ISOTROPIC |
| 1.2a | THORNEL 300 | ERLA 4617 | $[(0, 60, -60)]_3$ S | PSEUDO-ISOTROPIC |
| 1.2b | THORNEL 300 | Polysulfone | $[(0, 60, -60)]_3$ S | PSEUDO-ISOTROPIC |
| 1.3a | THORNEL 300 | 5208 | $(0)_{24}$ | UNIDIRECTIONAL |
| 1.3b | THORNEL 300 | 5208 | $[(0, 90)]_6$ S | 1:1 BIDIRECTIONAL |
| 1.3c | THORNEL 300 | 5208 | $[(0, 0, 90)]_4$ S | 2:1 BIDIRECTIONAL |
| 1.4a | THORNEL 300 | 5208 | $[(60, -60)]_4 (0)_4$ S | |
| 1.4b | THORNEL 300 | 5208 | $[(0)_4, (60, -60)]_4$ S | |
| 1.5a** | THORNEL 300/FIBERGLASS | 5208 | $[(0, 90)_F(0, 90, 0, 90)_G(0, 90)_F(0, 90)_G(0, 90)_F]$ S | HYBRID COMPOSITE |
| 1.5b** | THORNEL 300/FIBERGLASS | 5208 | $\{[(0, 90)_F]_3 [(0, 30)_G]_3\}$ S | HYBRID COMPOSITE |
| 1.5c** | THORNEL 300/KEVLAR 49 | 5208 | $[(0, 90)_K(0, 90, 0, 90)_K(0, 90)_K(0, 90)_G(0, 90)_K]$ S | HYBRID COMPOSITE |
| 1.5d** | THORNEL 300/KEVLAR 49 | 5208 | $\{[(0, 90)_K]_3 [(0, 90)_G]_3\}$ S | HYBRID COMPOSITE |
| 2.1a | THORNEL 300 | 5208 | $[(0, 60, -60)]_2$ S | PSEUDO-ISOTROPIC |
| 2.1b | THORNEL 300 | 5208 | $[(0, 60, -60)]_8$ S | PSEUDO-ISOTROPIC |
| AP-1 | THORNEL 300 | APCO 2450/APCO 2342 | $[(90, 45, -45)]_2$ S | |
| AP-2 | THORNEL 300 | APCO 2450/APCO 2342 | $[(90, 45, -45)]_5$ S | |
| 2.2a | THORNEL 300 | 5208 | $(0, 0, 90)_8$ | 2:1 BIDIRECTIONAL WITH 0° MATERIAL ORIENTED IN HOOP DIRECTION |
| 2.2b | THORNEL 300 | 5208 | $[(0, 0, 90)]_4$ S | |

* One of the panels had 18 plies with layup $[(0, 60, -60)]_3$ S

** G denotes graphite; F denotes fiberglass (E-Glass); K denotes Kevlar 49.

Table XXVIII
SPECIMENS FOR INVESTIGATING THE TEST VARIABLES

| VARIABLE | TEST SPECIMENS FOR INVESTIGATING THE VARIABLE |
|-------------------|---|
| FIBER PROPERTIES | 1.1a, 1.1b, 1.1c |
| MATRIX PROPERTIES | 1.2a, 1.2b, 1.1b |
| FIBER LAYUP | 1.3a, 1.3b, 1.3c, 1.1b |
| STACKING SEQUENCE | 1.4a, 1.4b, 1.1b |
| THICKNESS | 2.1a, 1.1b, 2.1c |
| HYBRIDIZATION | 1.5a, 1.5b, 1.5c, 1.5d |
| CURVATURE | 2.2a, 2.2b, 1.1b |

Table XXIX
DESCRIPTION OF COMPOSITE TEST SPECIMENS

| PLATE | PLATE SIZE (WIDTH X LENGTH X THICKNESS) (IN.) | PLATE WEIGHT (LB.) | DENSITY OF MATERIAL | | FIBER CONTENT BY VOLUME (%) (2) | VOID CONTENT (%) (2) | AVERAGE THICKNESS PER PLY (IN.) |
|----------|--|-----------------------|-----------------------------|-----------------------------|--|----------------------------|--|
| | | | LB./IN. ³ (1) | LB./IN. ³ (2) | | | |
| 1.1(a) 1 | 10.016 x 10.017 x 0.1324 | 0.809 | 0.0608 | | | | |
| 1.1(a) 2 | 9.985 x 9.989 x 0.1317 | 0.804 | 0.0611 | 0.0611 | 61.7 | 0.12 | 0.00548 |
| 1.1(a) 3 | 9.986 x 10.024 x 0.0981 | 0.601 | 0.0611 | | | | |
| 1.1(b) 1 | 10.000 x 10.000 x 0.1391 | 0.772 | 0.0555 | | | | |
| 1.1(b) 2 | 10.000 x 10.010 x 0.1395 | 0.772 | 0.0552 | 0.0556 | 58.0 | 0.93 | 0.00580 |
| 1.1(b) 3 | 10.015 x 10.015 x 0.1391 | 0.772 | 0.0553 | | | | |
| 1.1(c) 1 | 10.008 x 10.014 x 0.1632 | 0.895 | 0.0546 | | | | |
| 1.1(c) 2 | 10.014 x 10.007 x 0.1684 | 0.898 | 0.0531 | 0.0544 | 55.9 | 0.81 | 0.00695 |
| 1.1(c) 3 | 10.004 x 11.010 x 0.1690 | 0.896 | 0.0529 | | | | |
| 1.2(a) 1 | 10.011 x 10.024 x 0.1041 | 0.610 | 0.0582 | | | | |
| 1.2(a) 2 | 10.016 x 10.021 x 0.1130 | 0.616 | 0.0568 | 0.0551 | 54.1 | 0.61 | 0.00608 |
| 1.2(a) 3 | 10.015 x 10.020 x 0.1116 | 0.628 | 0.0559 | | | | |
| 1.2(b) 1 | 10.072 x 9.972 x 0.1229 | 0.623 | 0.0505 | | | | |
| 1.2(b) 2 | 10.018 x 9.989 x 0.1211 | 0.618 | 0.0511 | 0.0510 | 50.7 | 8.50 | 0.00677 |
| 1.2(b) 3 | 10.022 x 9.981 x 0.1228 | 0.622 | 0.0507 | | | | |
| 1.3(a) 1 | 12.017 x 12.012 x 0.1366 | 1.100 | 0.0557 | | | | |
| 1.3(a) 2 | 12.014 x 12.014 x 0.1397 | 1.120 | 0.0555 | 0.0557 | 58.5 | 0.85 | 0.00578 |
| 1.3(a) 3 | 12.036 x 12.033 x 0.1403 | 1.120 | 0.0551 | | | | |
| 1.3(b) 1 | 10.015 x 10.008 x 0.1410 | 0.775 | 0.0548 | | | | |
| 1.3(b) 2 | 10.012 x 10.012 x 0.1444 | 0.794 | 0.0547 | 0.0552 | 50.2 | 0.92 | 0.00595 |
| 1.3(b) 3 | 10.016 x 10.016 x 0.1430 | 0.790 | 0.0550 | | | | |
| 1.3(c) 1 | 9.996 x 10.010 x 0.1370 | 0.765 | 0.0542 | | | | |
| 1.3(c) 2 | 10.005 x 10.002 x 0.1427 | 0.790 | 0.0554 | 0.0558 | 58.1 | 0.70 | 0.00586 |
| 1.3(c) 3 | 10.017 x 10.012 x 0.1419 | 0.786 | 0.0552 | | | | |
| 1.4(a) 1 | 10.007 x 10.018 x 0.1324 | 0.737 | 0.0555 | | | | |
| 1.4(a) 2 | 10.015 x 10.016 x 0.1332 | 0.739 | 0.0553 | 0.0561 | 60.6 | 0.84 | 0.00553 |
| 1.4(a) 3 | 10.020 x 10.007 x 0.1322 | 0.737 | 0.0555 | | | | |
| 1.4(b) 1 | 10.013 x 10.015 x 0.1348 | 0.751 | 0.0555 | | | | |
| 1.4(b) 2 | 10.015 x 10.012 x 0.1352 | 0.752 | 0.0554 | 0.0559 | 59.1 | 0.85 | 0.00563 |
| 1.4(b) 3 | 10.004 x 10.015 x 0.1351 | 0.751 | 0.0555 | | | | |
| 1.5(a) 1 | 9.993 x 9.962 x 0.1400 | 0.885 | 0.0634 | | | | |
| 1.5(a) 2 | 10.058 x 10.020 x 0.1391 | 0.900 | 0.0641 | 0.0641 | 27.4/32.4 (3) | 1.20 | --- |
| 1.5(a) 3 | 10.032 x 10.202 x 0.1352 | 0.910 | 0.0668 | | | | |
| 1.5(b) 1 | 9.995 x 10.003 x 0.1389 | 0.892 | 0.0642 | | | | |
| 1.5(b) 2 | 9.964 x 10.002 x 0.1410 | 0.890 | 0.0642 | 0.0640 | 28.0/31.7 (3) | 1.25 | --- |
| 1.5(b) 3 | 9.996 x 9.998 x 0.1391 | 0.890 | 0.0639 | | | | |
| 1.5(c) 1 | 10.002 x 10.012 x 0.1510 | 0.789 | 0.0521 | | | | |
| 1.5(c) 2 | 10.000 x 10.000 x 0.1541 | 0.791 | 0.0513 | 0.0522 | 31.0/30.7 (3) | 1.96 | --- |
| 1.5(c) 3 | 10.030 x 10.009 x 0.1560 | 0.790 | 0.0504 | | | | |
| 1.5(d) 1 | 9.995 x 10.005 x 0.1529 | 0.793 | 0.0519 | | | | |
| 1.5(d) 2 | 10.005 x 10.027 x 0.1510 | 0.795 | 0.0525 | 0.0524 | 28.3/35.0 (3) | 0.90 | --- |
| 1.5(d) 3 | 10.008 x 10.017 x 0.1531 | 0.799 | 0.0520 | | | | |
| 2.1(a) 1 | 10.820 x 10.256 x 0.0664 | 0.401 | 0.0544 | | | | |
| 2.1(a) 2 | 10.028 x 10.012 x 0.0662 | 0.369 | 0.0554 | 0.0564 | 63.5 | 1.03 | 0.00550 |
| 2.1(a) 3 | 10.012 x 10.012 x 0.0654 | 0.363 | 0.0554 | | | | |
| 2.1(c) 1 | 10.000 x 10.015 x 0.2675 | 1.521 | 0.0567 | | | | |
| 2.1(c) 2 | 10.001 x 10.012 x 0.2707 | 1.527 | 0.0562 | 0.0557 | 58.5 | 1.07 | 0.00561 |
| 2.1(c) 3 | 10.016 x 10.013 x 0.2685 | 1.524 | 0.0565 | | | | |
| AP-1 | 9.964 x 10.185 x 0.1268 | 0.673 | 0.0524 | --- | | | |
| AP-2 | 10.075 x 10.200 x 0.2592 | 1.397 | 0.0525 | --- | | | |
| 2.2(a) 1 | 3.076" O.D. x 3.985 x 0.138 | 0.283 | 0.0557 | --- | | | |
| 2.2(a) 2 | 3.072" O.D. x 4.007 x 0.143 | 0.277 | 0.0526 | --- | | | 0.00582 |
| 2.2(a) 3 | 3.076" O.D. x 4.000 x 0.138 | 0.280 | 0.0550 | --- | | | |
| 2.2(b) 1 | { Specimens contained surface irregularities and were not tested | | | | | | |
| 2.2(b) 2 | | | | | | | |
| 2.2(b) 3 | | | | | | | |

(1) From weights and dimensions of plates or cylinders.

(2) From gravimetric test and acid digestion.

(3) First and second numbers denote percentages of graphite and E-Glass or Kevlar-49 fibers respectively.

SECTION V

EXPERIMENTAL STUDIES ON IMPACT RESPONSE OF COMPOSITES

To establish threshold energy levels required to cause brittle fracture in graphite-epoxy composites and to establish the influence of variables discussed previously on the impact response, ball-drop impact tests were conducted on the various composite panels and cylinders. Specimens were instrumented with strain gages and manganin gages to enable the impact-induced strains and surface pressure to be experimentally determined. A number of techniques were employed to detect damage in composite plates, including visual observations, dye penetrants, X-rays, through-transmission, and coating of specimens with powder prior to impact. Use of surface coatings and dye penetrants to detect surface damage was fairly successful. Internal damage within composite specimens could not be detected by conventional techniques.

TEST TECHNIQUE AND SPECIMEN INSTRUMENTATION

Because of the low predicted velocities required to initiate damage ($v = 30\text{-}50$ in./sec), the impact tests were conducted using ball-drop tests (employing a 1.5-in.-diameter steel sphere) rather than low-pressure gas-gun tests as planned initially. The test setup is shown schematically in Figure 59, whereas Figure 60 shows the actual test setup. Such test setups have previously been employed at MDAC. Impact velocities ranging up to $v = 300$ in./sec were achieved. Moreover, ball-drop impact tests have also been used by other investigators studying the impact response of graphite-epoxy composites.

The flat plate specimens and the cylindrical specimens were supported as shown in Figure 61. Several plate specimens were also tested using 6-in.-diameter support rings. Two of the completed cylindrical specimens ready for testing are shown in Figure 62.

Two types of instrumentation were employed on several of the plate and cylindrical specimens: (1) strain gages to measure strain versus time and (2) manganin gages to measure pressure versus time. Both types of instrumentation were used on the flat plates and on the cylinders. The instrumentation for a given impact location in plates was as follows:

1. One manganin gage at the impact point ($r = 0$).
2. One biaxial strain gage on the surface opposite the impact surface ($r = 0$).

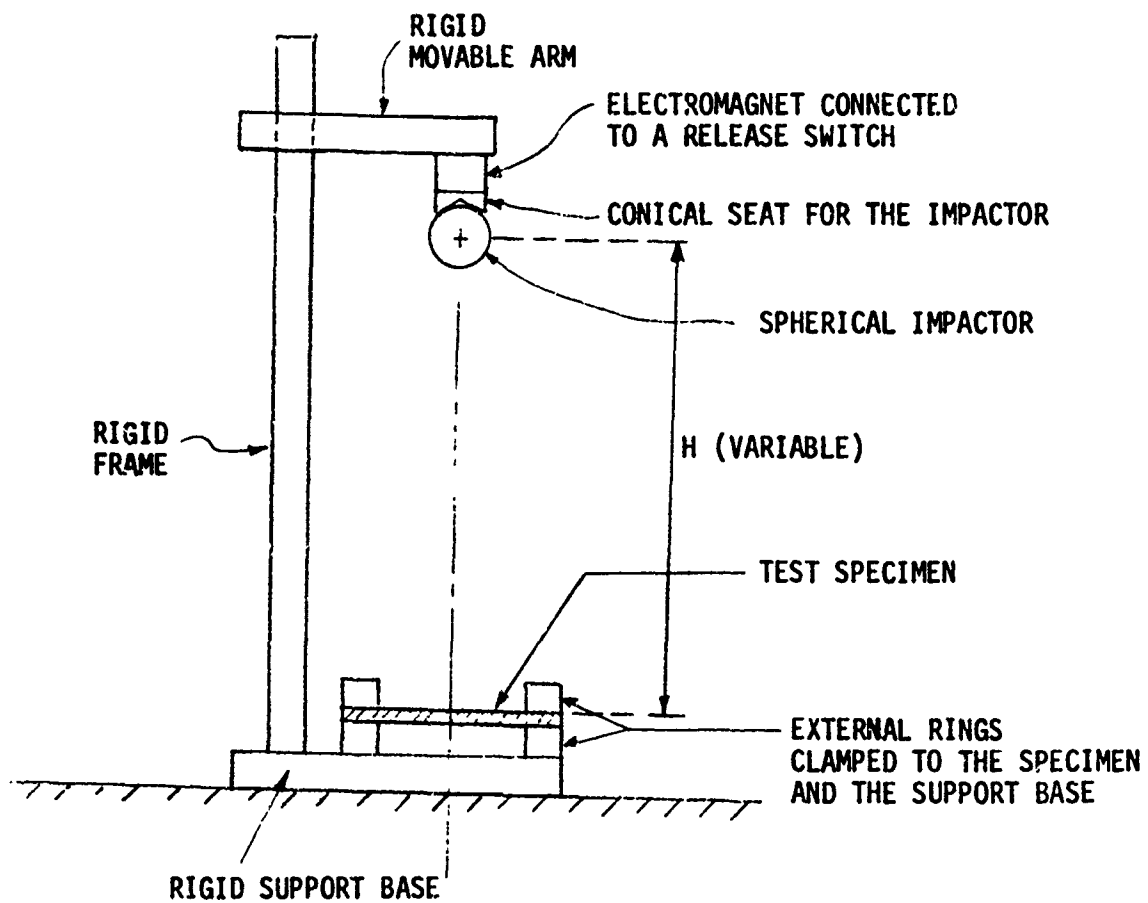


Figure 59. Test Setup for Low-Velocity Impact.

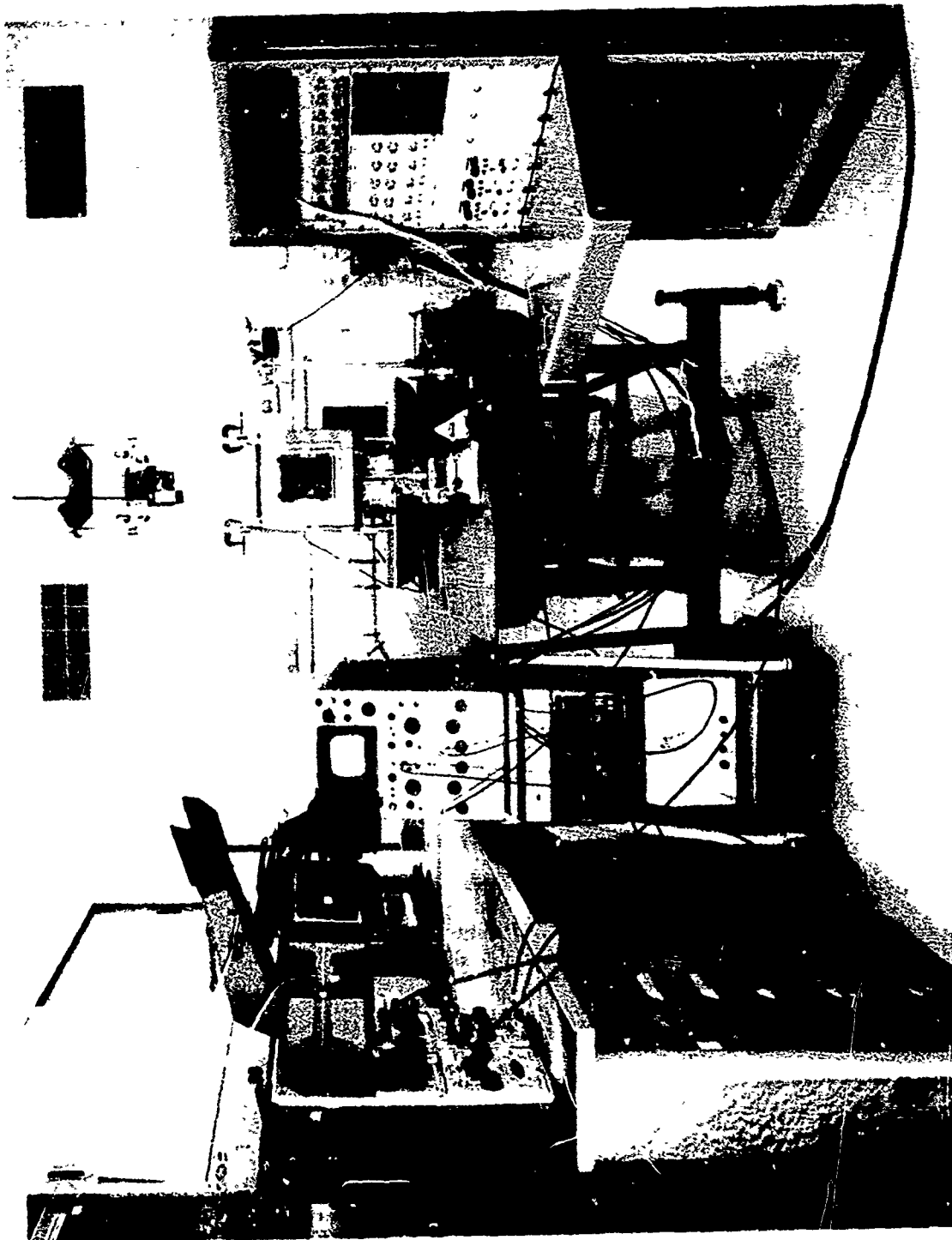
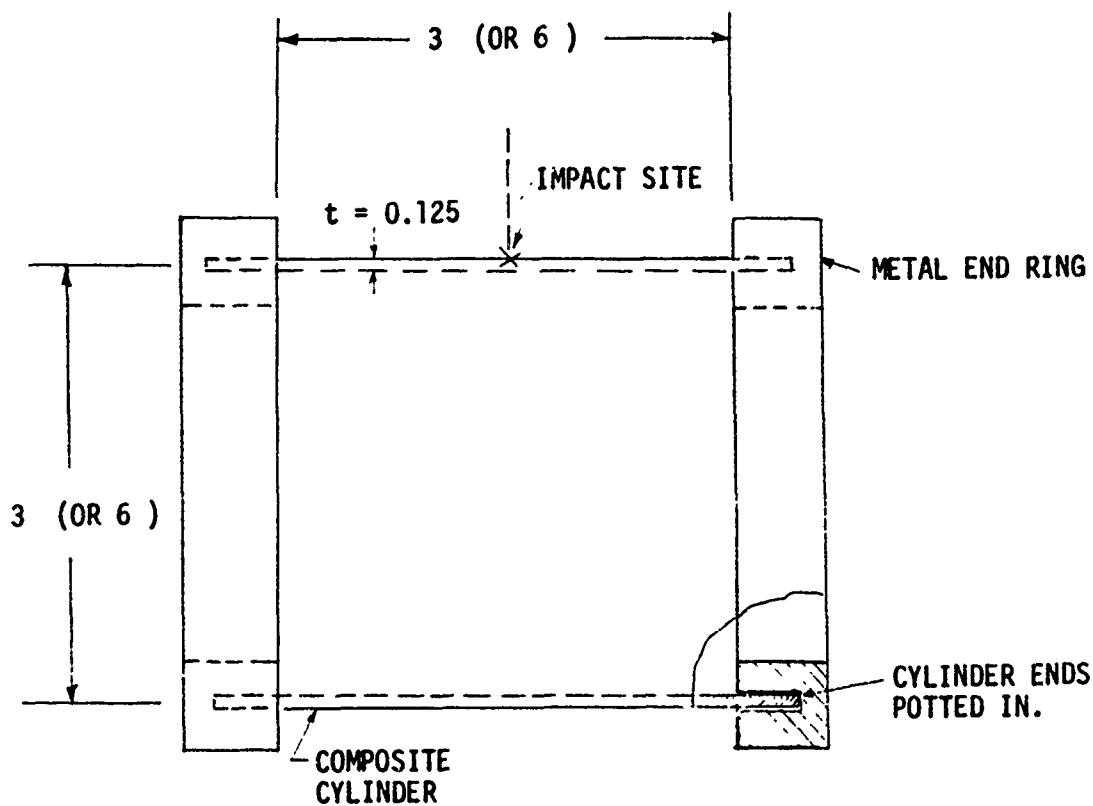
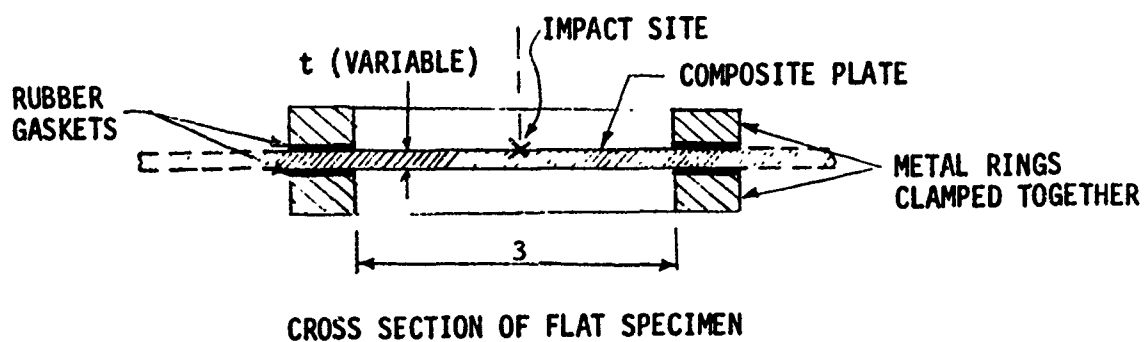


Figure 60. Test Setup and Instrumentation.



NOTE: ALL DIMENSIONS SHOWN ARE IN INCHES.

Figure 61. Test Specimens and Supports.



3-INCH DIAMETER



6-INCH DIAMETER

Figure 62. Cylindrical Test Specimens.

3. One strain gage midway between the impact site and the edge of the support ($r = R/2$).
4. One strain gage at a quarter point from the impact site to the edge of the support ($r = R/4$).

where R is the radius of the support rings ($R = 1.5$ in.). The instrumentation for a given cylinder was as follows:

1. One manganin gage at the impact point.
2. One biaxial gage on the surface opposite the impact surface.
3. One strain gage at 180° from the impact point.

Table XXX describes in detail the instrumentation that was used in the various specimens.

The strain-versus-time traces for a given impact test were obtained using an oscilloscope. The technique for recording the output from the instrumented specimens was verified using a 1/8-in.-thick aluminum plate. The instrumentation on the latter plate was the same as on the all-composite plates. Typical outputs of the various gages are shown in the oscilloscope traces of Figure 63. Figure 63(a) shows two oscilloscope traces. The top trace is for the manganin pressure gage located at $r = 0$; the vertical sensitivity is 1×10^{-4} V/cm. The bottom trace is for element No. 1 of the biaxial strain gage located at $r = 0$. The vertical sensitivity is 1000 μ in./in./cm. Figure 63(b) shows three oscilloscope traces. The top trace is for element No. 2 of the biaxial strain gage located at $r = 0$; the vertical sensitivity is 1000 μ in./in./cm. The middle trace is for the strain gage at $R/4$; the vertical sensitivity is 500 μ in./in./cm. The bottom trace is for the strain gage at $R/2$; the vertical sensitivity is 500 μ in./in./cm. The horizontal sensitivities were 200 μ sec/cm for all traces. As can be seen, for a 1.5-in.-diameter steel sphere impacting at 100 in./sec, the duration of impact was approximately 1 millisecond, with a peak strain reading of approximately 3300 μ in.

Those plates and cylinders which were not instrumented were tested only under impact using 1.5-in.-diameter steel sphere as the impactor. For a given plate the distance between impact sites was ~ 3 inches. The techniques that were employed for detecting impact damage are described later on.

RESULTS FROM NONINSTRUMENTED IMPACT TESTS

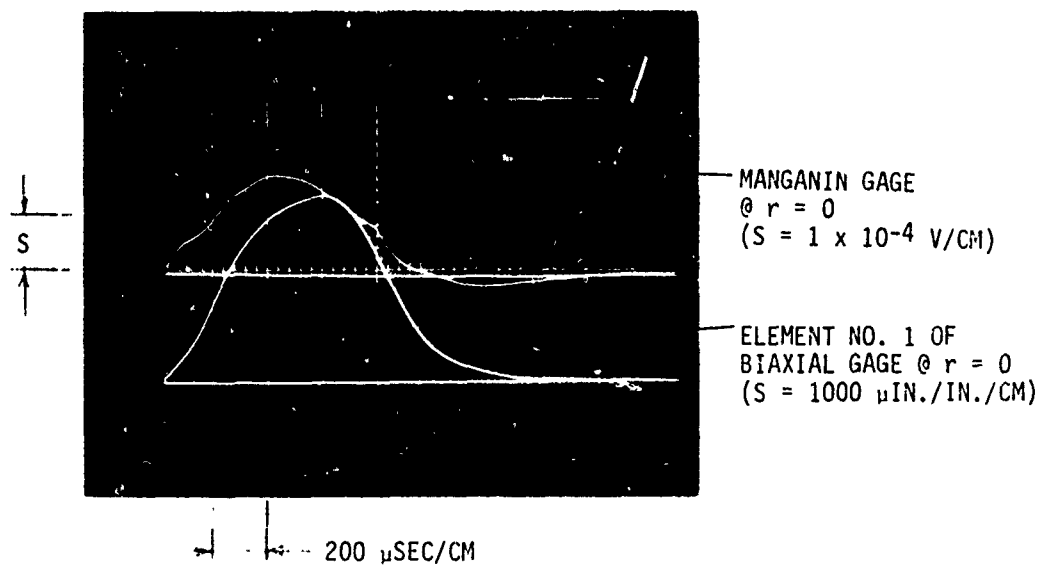
The test setup described in the previous paragraphs was used to study the influence that the variables described in Table XXVIII had on the impact response of composites. The impact velocities selected on the basis of theoretical studies were 30 in./sec, 50 in./sec, and 100 in./sec. Initial impact tests performed on the various specimens at the above velocities did not show any visible damage. Moreover, even at 150-in./sec impacts, no damage could be observed. X-rays were then taken of the various

Table XXX
SPECIMEN INSTRUMENTATION⁽¹⁾

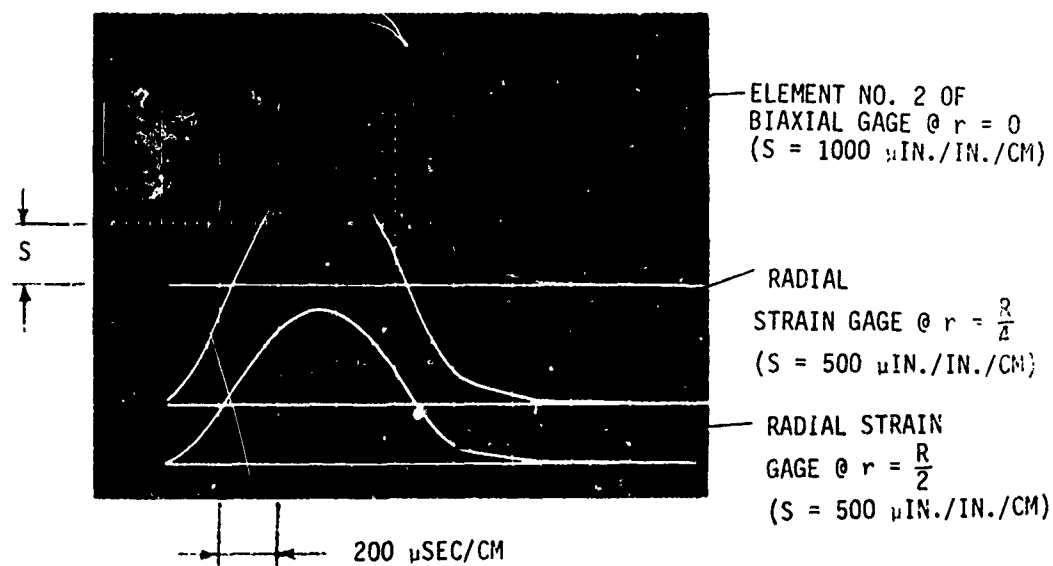
| Plate or Cylinder | Location On Plate Or Cylinder | Front Face (Impacted) | Back Face | | |
|----------------------|-------------------------------------|--------------------------|-----------|----------------------------------|-----------------------------------|
| | | | r=0 | r=R/4 (or $\theta=90^\circ$) | r=R/2 (or $\theta=180^\circ$) |
| 1.1(b)-1 | 1 | MG | BSG | USG | USG |
| | 2 | -- | BSG | USG | USG |
| 1.1(b)-2 | 1 | MG | BSG | USG | USG |
| | 2 | MG | - | - | - |
| | 3 | MG | - | - | - |
| 1.1(c)-1 | 1 | MG | BSG | USG | USG |
| | 2 | - | BSG | USG | USG |
| 1.1(c)-2 | 1 | MG | BSG | USG | USG |
| | 2 | MG | - | - | - |
| | 3 | MG | - | - | - |
| 1.3(c)-1 | 1 | MG | BSG | USG | USG |
| | 2 | MG | - | - | - |
| | 3 | MG | - | - | - |
| 2.2(a) | 1 | MG | BSG | - | BSG |
| 2.2(b) | 1 | MG | BSG | - | BSG ⁽²⁾ |

(1) MG denotes manganin gage
BSG denotes biaxial gage
USG denotes uniaxial gage

(2) Gage was on outer surface of cylinder



(a)



(b)

Figure 63. Oscilloscope Traces From Instrumented Aluminum Plate Impacted at 100 In./Sec With a 1.5-In.-Diameter Steel Sphere.

specimens to see if impact damage, such as cracking or delaminations, could be detected. The latter technique proved unsuccessful. Another technique that was tried in an attempt to establish at what impact velocities damage initiated, consisted of sprinkling white powder on the front-faces (impacted) and backfaces of the specimens before impact. The technique was quite successful. Upon impact, a "footprint" was left on the impacted surface, showing an area proportional and concentric to the area of contact. Moreover, when failure such as transverse cracking took place on the backface of the specimens, this could readily be seen. All subsequent testing of graphite-epoxy specimens involved use of powder coating. The specimens that were tested initially (without any preparations for determining damage) were retested by impacting them at another location on the plate. Failures were observed to occur at impact velocities of 100 in./sec, whereas during the initial testing of unprepared specimens no damage could be detected visually or by using x-rays, even at velocities of 150 in./sec.

Impact tests performed on a number of specimens at velocities of 30 in./sec and 50 in./sec showed no surface damage; consequently, the majority of the specimens were subjected to impact velocities equal to or greater than 100 in./sec. Testing at lower velocities was conducted only in the case of specimens exhibiting significant damage at 100 in./sec. It was found that a number of specimens did indeed fail at impact velocities of 50 in./sec.

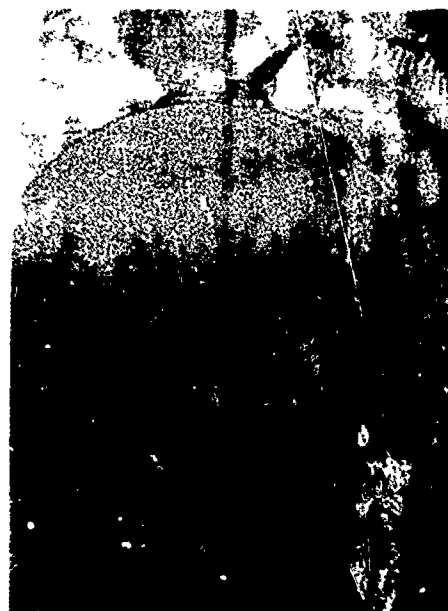
Influence of Fiber Properties on Impact Response

The specimens used in establishing the influence of fiber properties on impact response are designated as 1.1a, 1.1b, and 1.1c. The fiber layup in all three specimens was pseudo-isotropic, whereas the matrix was Na-mco 5208 epoxy. The reinforcing fibers in the three specimens were Celion GY-70 in 1.1a; Thornel 300 in 1.1b, and Modmor II in 1.1c. Results from the impact tests performed at velocities ranging from 50 in./sec to 160 in./sec are presented in Table XXXI. None of the three materials failed at an impact velocity of 50 in./sec. All the impacts at 100 in./sec caused significant damage in Celion GY-70/5208. One of the 1.1b specimens impacted at 100 in./sec also showed cracking in the transverse direction. Only one out of three of the 1.1c specimens failed under 100-in./sec impact. Upon increasing the impact velocity to 128 in./sec, the latter specimen (1.1c) did not show any damage. Further increase in velocity to 160 in./sec caused cracking on the backface of the plate. Figure 64 shows typical failures resulting from impact on the three groups of specimens. In all cases cracking occurred in the transverse direction. In the case of Celion GY-70/5208, the failure was at least three layers deep, as can readily be seen from Figure 64, where the failure pattern shown follows the fiber pattern in adjacent layers.

Of the three materials for which the results are shown in Table XXXI and in Figure 64, the rating of materials with respect to resistance to impact damage is as follows (starting with the best material):



$v = 100 \text{ IN./SEC}$
SPEC. # 1.1a-



$v = 100 \text{ IN./SEC}$
SPEC. # 1.1a-

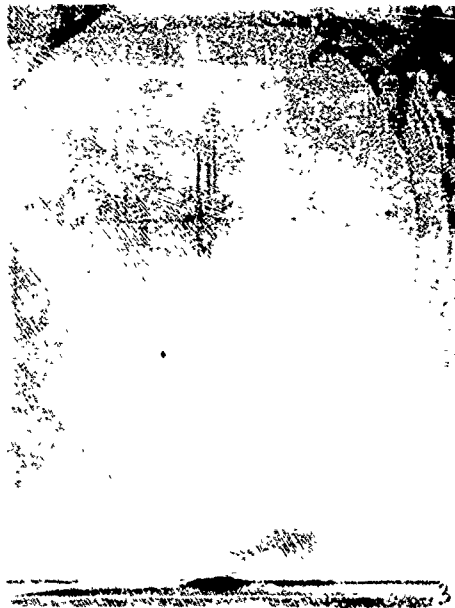


$v = 100 \text{ IN./SEC}$
SPEC. # 1.1c-



$v = 160 \text{ IN./SEC}$
SPEC. # 1.1c-

Figure 64. Back Face Impact Damage in Composite Plates Made With Three Different Reinforcing Fibers.



v = 100 IN./SEC
SPEC. # 1.1b-



v = 100 IN./SEC
SPEC. # 1.1b-

- 1.1a - CELION GY70/5208
- 1.1b - THORNEL 300/5208
- 1.1c - MODMOR II/5208

Figure 64. Continued.

Table XXXI
INFLUENCE OF FIBER PROPERTIES ON EXPERIMENTALLY
OBSERVED IMPACT DAMAGE

| Specimen | Reinforcing Fiber | Impact Velocity, in/sec | (1) Major and Minor Diameters of the Area of Contact, in. (Front Face) | Damage on Back Face (or Front Face) |
|----------|----------------------|-------------------------------|---|--|
| 1.1a | Celion GY 70 | 50 | --- | No visible damage |
| 1.1a | | 50 | --- | No visible damage |
| 1.1a | | 100 | --- | Branching (Y) cracks and broken fibers crack lengths 0.4 in., 0.55 in., 0.7 in. (surface crushing) |
| 1.1a | | 100 | --- | Branching (Y) cracks and broken fibers and surface crushing |
| 1.1a | | 100 | --- | Cracks at $0 \pm 60^\circ$; max length 0.8 in. (surface crushing) |
| 1.1b | Thornel 300 | 100 | --- | No visible damage |
| 1.1b | | 100 | 0.13 x 0.12 | No visible damage |
| 1.1b | | 100 | 0.13 x 0.13 | No visible damage |
| 1.1b | | 100 | 0.11 x 0.12 | 1 crack 0.6 in. long |
| 1.1b | | 128 | 0.12 x 0.12 | 3 cracks 0.6 in. to 0.78 in. long [0.07] (2) |
| 1.1c | Modmor II | 100 | --- | No visible damage |
| 1.1c | | 100 | --- | No visible damage |
| 1.1c | | 100 | 0.13 x 0.13 | 2 cracks, 0.47 in. and 0.6 in. [0.07] |
| 1.1c | | 128 | --- | No visible damage |
| 1.1c | | 160 | --- | 1 crack 1.2 in. long |

(1) If two numbers are the same the area proportional to the area of contact was circular; if two numbers are different the area was elliptical.

(2) Numbers in brackets denote width of damage zone.

1. Modmor II/5208
2. Thornel 300/5208
3. Celion GY-70/5208

The Modmor II/5208 specimens were approximately 30% thicker than the other specimens (see Table XXIX). If all specimens were of the same thickness, more extensive damage would be expected in the Modmor II/5208 specimens than is shown in Table XXXI or in Figure 64.

Influence of Matrix Properties on Impact Response

Specimens 1.2a, 1.2b, 1.1b, and AP of Tables XXVIII and XXIX were used for establishing the influence of matrix properties on impact response. As before, the fiber pattern in Specimens 1.2a, 1.2b, and 1.1b was pseudo-isotropic, and the reinforcing fibers used in these specimens were Thornel 300. Specimens AP were added to the test group at the suggestion of the Project Officer. These specimens were also made with Thornel 300 fibers; however, the layup was not pseudo-isotropic (see Table XXVII). The results from the impact tests are shown in Table XXXII, whereas Figures 65, 66, and 67 show typical failure in the various specimens. Of the four groups of specimens, those made with a polysulfone matrix are unquestionably most resistant to impact damage. The four groups of materials are rated as follows with respect to resistance to impact damage:

1. Thornel 300/polysulfone
2. Thornel 300/5208
3. Thornel 300/4617
4. Thornel 300/APCO

Influence of Fiber Orientation on Impact Response

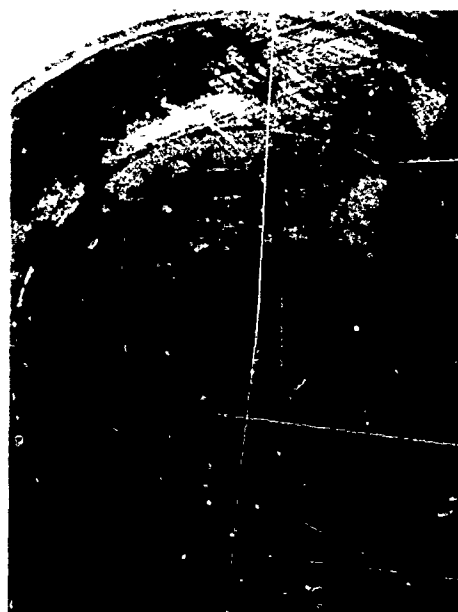
Composite plates (consisting of Thornel 300/5208) with four different fiber orientations were used in experimental investigation of the influence of the latter parameters on impact response. The fiber orientations in the various specimens were as follows:

1. Unidirectional fibers in Specimen 1.3a
2. 1:1 Bidirectional fibers in Specimen 1.3b
3. 2:1 Bidirectional fibers in Specimen 1.3c
4. Unidirectional fibers in Specimen 1.1b

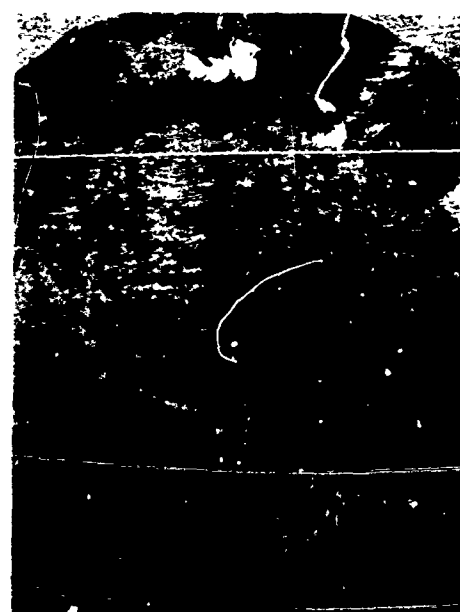
FRONT
FACE



BACK
FACE

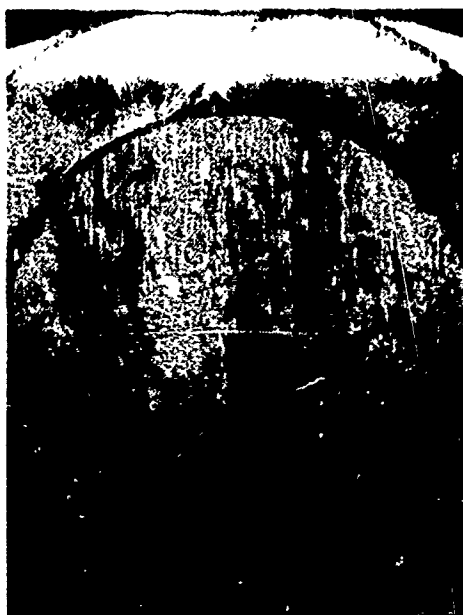


$v = 100 \text{ IN./SEC}$
SPEC # 1.2a -



$v = 100 \text{ IN./SEC}$
SPEC. # APCO -

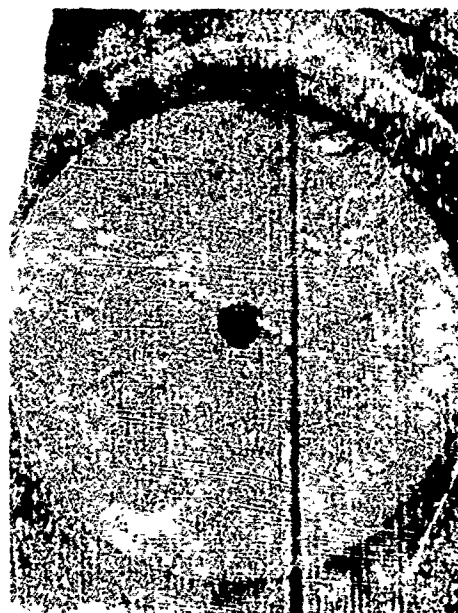
Figure 65. Impact Site and Corresponding Damage on the Back Surface in Composite Plates Made With Thornel 300 Fibers and ERLA 4617 (Specimen 1.2a) or APCO Resin.



$v = 100 \text{ IN./SEC}$
SPEC. # APCO -

Figure 65. Continued.

FRONT
FACE



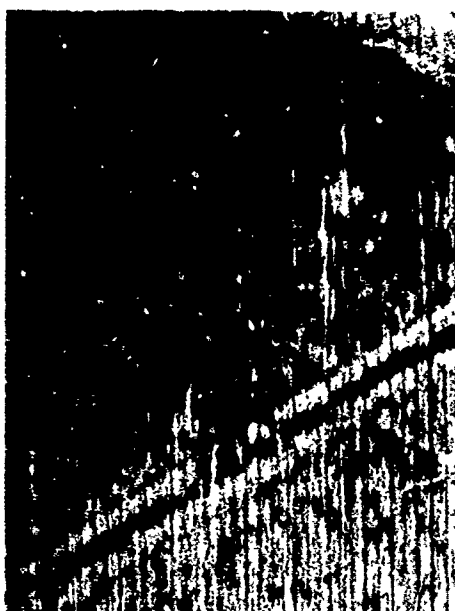
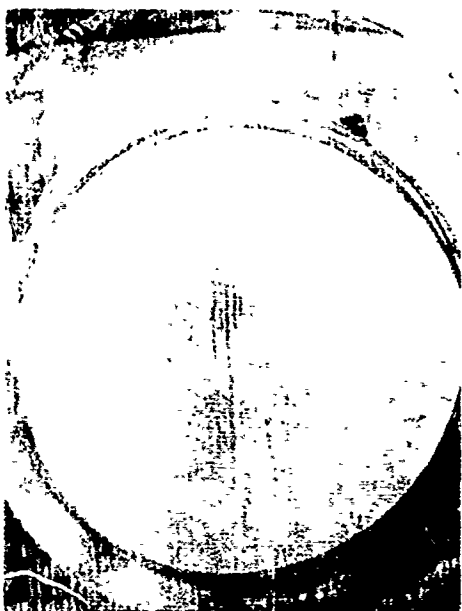
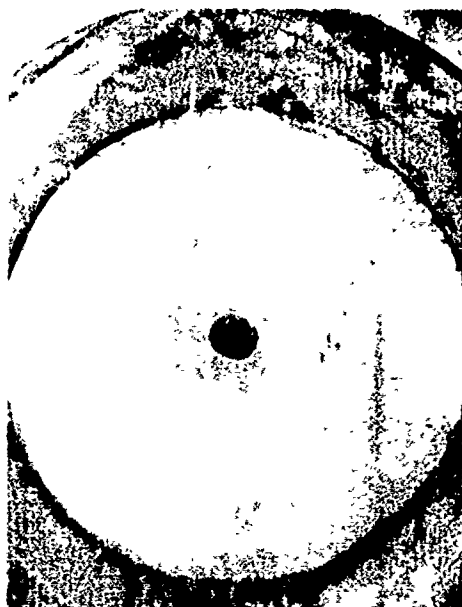
BACK
FACE



$v = 100 \text{ IN./SEC}$
SPEC. # 1.2 b-

$v = 192 \text{ IN./SEC}$
SPEC # 1.2b-

Figure 66. Impact Damage in Thornel 300-Polysulfone as a Function of Impact Velocity.



v = 250 IN./SEC
SPEC. # 1.2b-

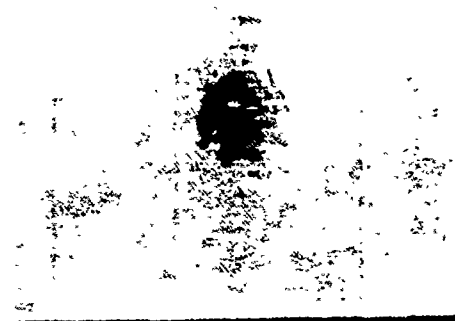
v = 250 IN./SEC
SPEC. # 1.2b-

Figure 66. Continued.



v = 250 IN./SEC
SPEC. # 1.2b-

OVERALL VIEW OF
FRONT FACE



v = 250 IN./SEC
SPEC. # 1.2b-

ENLARGED VIEW
OF IMPACT SITE

NOTE: NO DAMAGE WAS VISIBLE ON THE
BACK FACE OF THE SPECIMEN

Figure 67. Damage on the Top Face in Thornel 300-Polysulfone Composite Plate.

Table XXXII
INFLUENCE OF RESIN PROPERTIES ON EXPERIMENTALLY
OBSERVED IMPACT DAMAGE⁽¹⁾

| Specimen | Matrix Material | Impact Velocity, in/sec | Major and Minor Diameters of the Area of Contact, in. (Front Face) | Damage on Back Face (or Front Face) |
|----------|-------------------------|-------------------------|--|---|
| 1.2a | ERLA 4617 | 100 | 0.09 x 0.09 | No visible damage |
| 1.2a | | 100 | 0.09 x 0.09 | 1 crack, 0.7 in. long |
| 1.2a | | 100 | 0.12 x 0.12 | 1 crack, 0.35 in. long |
| 1.2b | Polysulfone | 100 | 0.2 x 0.2 | No visible damage |
| 1.2b | | 100 | 0.2 x 0.2 | No visible damage |
| 1.2b | | 100 | 0.21 x 0.21 | No visible damage |
| 1.2b | | 128 | 0.20 x 0.26 | No visible damage |
| 1.2b | | 160 | --- | No visible damage |
| 1.2b | | 192 | --- | No visible damage |
| 1.2b | | 250 | 0.27 x 0.30 | No visible damage (some indentation on impacted face) |
| 1.2b | | 250 | 0.30 x 0.30 | No visible damage (some indentation on impacted face) |
| 1.2b | 5208 | 250 | 0.28 x 0.30 | Broken fibers (some indentation on impacted face) [.33] |
| 1.2b | | 250 | 0.30 x 0.30 | Longitudinal cracks from 0.12 in. to 1.0 in. long [.26] |
| 1.1b | | | | See Table XXXI |
| 1.1b | | | | |
| AP-1 | APCO 2450/ APCO 2342 | 50 | --- | No visible damage |
| AP-1 | | 100 | 0.18 x 0.22 | 3 cracks, longest one 0.5 in. [.0.13] |
| AP-1 | | 100 | 0.12 x 0.13 | 2 cracks each ~ 0.55 in. [.0.06] |
| AP-1 | | 100 | 0.12 x 0.12 | 2 cracks each ~ 0.35 in. [.0.04] |

(1) See Footnotes in Table XXXI

The pertinent data on the impact damage in the specimens described above are presented in Table XXXIII. Figure 68 shows some typical failure modes in the various specimens. From the results presented in Table XXXIII and Figure 68, the rating of the four groups of specimens for resistance to impact damage is as follows (starting with the best material):

1. 1:1 Bidirectional Thornel 300/5208
2. Tridirectional Thornel 300/5208
3. 2:1 Bidirectional Thornel 300/5208
4. Unidirectional Thornel 300/5208

As is readily seen from Figure 68, in the case of unidirectional specimens, the crack formed on impact progressed through the width of the specimen, and only the support ring stopped further crack growth. In the case of plates with multidirectional fibers, the reinforcement normal to the crack direction acted as the crack stopper and thus limited crack growth.

Influence of Stacking Sequence on Impact Response

The test results for the influence of the stacking sequence on impact response are presented in Table XXXIV, which also contains a description of the stacking sequences in the various groups of specimens. Typical results for the failure modes within groups of specimens are presented in Figure 69. Based on data presented in Tables XXXI and XXXIV, the rating of specimens with respect to resistance to impact damage is as follows:

1. Specimens 1.1b with stacking sequence $[0, -60, +60]_4]_S$
2. Specimens 1.4a with stacking sequence $[(+60, -60)_4 (0)_4]_S$
3. Specimens 1.4b with stacking sequence $[(0)_4 (+60, -60)_4]_S$

Influence of Plate Thickness on Impact Response

Plates of three different thicknesses were used to experimentally investigate the influence of the latter parameter on impact response. The nominal plate thicknesses were 0.066 in., 0.14 in., and 0.27 in. Most of the specimens were made with Thornel 300/5208, with a pseudo-isotropic fiber layup, $[0, 60, -60]_n]_S$, where n was selected to give the desired thickness. One 0.26-in. plate made with Thornel 300/APCO resin was also tested for impact response in order to compare the impact response data with the corresponding data obtained on a thinner plate described previously (see Table XXXII). The pertinent results from the impact tests are presented in Table XXXV, whereas Figures 70, 71, and 72

Table XXXIII
INFLUENCE OF FIBER ORIENTATION ON EXPERIMENTALLY
OBSERVED IMPACT DAMAGE

| Specimen | Fiber Orientation | Impact Velocity, in./sec | Major and Minor Diameters of the Area of Contact, in. (Front Face) | Damage on Back Face (or Front Face) |
|----------|--------------------|--------------------------|--|---|
| 1.3a | Unidirectional | 50 | --- | No visible damage |
| 1.3a | | 50 | --- | No visible damage |
| 1.3a | | 50 | 0.08 x 0.08 | No visible damage |
| 1.3a | | 100 | --- | 3-in.-long crack |
| 1.3a | | 100 | 0.10 x 0.16 | 3-in.-long crack |
| 1.3a | | 100 | 0.10 x 0.17 | 3-in.-long crack |
| 1.3b | 1:1 Bi-directional | 100 | 0.12 x 0.12 | No visible damage |
| 1.3b | | 100 | 0.12 x 0.12 | No visible damage |
| 1.3b | | 100 | 0.12 x 0.12 | One crack, \approx 0.5 in. long |
| 1.3b | | 100 | 0.12 x 0.12 | One crack, \approx 0.5 in. long |
| 1.3b | | 100 | 0.11 x 0.11 | 2 cracks, 0.4 in. and 0.25 in. long [0.3 in.] |
| 1.3b | | 100 | 0.11 x 0.11 | 2 cracks, 0.4 in. and 0.25 in. long [0.3 in.] |
| 1.3c | 2:1 Bi-directional | 50 | - | No visible damage |
| 1.3c | | 100 | 0.12 x 0.12 | 2 cracks 1.0 in. and 0.9 in. long [0.05 in.] |
| 1.3c | | 100 | 0.10 x 0.10 | One crack, 1.1 in. long |
| 1.1b | Tridirectional | | | See Table XXXI |

(1) See Footnotes in Table XXXI

BACK
FACE



FRONT
FACE



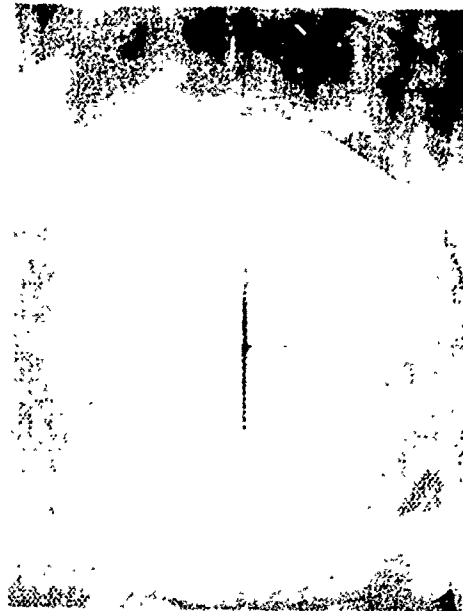
$v = 50 \text{ IN./SEC}$
SPEC. # 1.3a-

$v = 100 \text{ IN./SEC}$
SPEC. # 1.3a-

Figure 63. Impact Damage in Composite Plates Having Different Fiber Orientations.



$v = 100 \text{ IN./SEC}$
SPEC. # 1.3b-



$v = 100 \text{ IN./SEC}$
SPEC. # 1.3c-

- 1.3a - UNIDIRECTIONAL THORNEL 300/5208
- 1.3b - 1:1 BI-DIRECTIONAL THORNEL 300/5208
- 1.3c - 2:1 BI-DIRECTIONAL THORNEL 300/5208

Figure 68. Continued.

Table XXXIV
INFLUENCE OF STACKING SEQUENCE ON EXPERIMENTALLY
OBSERVED IMPACT DAMAGE(1)

| Specimen | Stacking Sequence | Impact Velocity, in/sec | Major and Minor Diameter: of the Area of Contact, in. (Front Face) | Damage on Back Face (or Front Face) |
|----------|-------------------|-------------------------|--|---|
| 1.4a | (2) | 100 | 0.11 x 0.11 | No visible damage One crack, 0.47 in. long Two cracks \approx 0.55 in. long |
| 1.4a | | 100 | 0.11 x 0.11 | |
| 1.4a | | 100 | --- | |
| 1.4b | (3) | 100 | --- | No visible damage One crack, 3 in. long One crack, 2.55 in. long |
| 1.4b | | 100 | 0.08 x 0.10 | |
| 1.4b | | 100 | 0.12 x 0.12 | |
| 1.1b | (4) | | | See Table XXXI |

(1) See Footnotes in Table XXXI

(2) $[(+60, -60)_4 (0)_4]^S$

(3) $[(0)_4 (+60, -60)_4]^S$

(4) $1'0, -60 +60)_4]^S$

Table XXXV
INFLUENCE OF PLATE THICKNESS ON EXPERIMENTALLY
OBSERVED IMPACT DAMAGE(1)

| Specimen | Plate Thickness, in. | Impact Velocity, in/sec | Major and Minor Diameters of the Area of Contact, in. (Front Face) | Damage on Back Face |
|----------|----------------------|-------------------------|--|---|
| 2.1a | 0.066 | 50 | 0.06 x 0.06 | No visible damage |
| 2.1a | | 50 | --- | No visible damage |
| 2.1a | | 50 | --- | No visible damage |
| 2.1a | | 75 | --- | No visible damage |
| 2.1a | | 75 | --- | One crack, 1 in. long |
| 2.1a | | 100 | 0.10 x 0.10 | Two cracks \approx 1.2 in. long |
| 2.1a | | 100 | --- | Three cracks, 0.6 in., 1.1 in. and 1.1 in. long [0.10] |
| 2.1a | | 100 | --- | Three cracks, 0.8 in., 0.9 in. and 1.1 in. long [0.07] |
| 2.1b | 0.139 | | | See Table XXXII |
| 2.1c | 0.269 | 100 | --- | No visible damage |
| 2.1c | | 100 | --- | No visible damage |
| 2.1c | | 192 | --- | No visible damage |
| 2.1c | | 192 | 0.16 x 0.16 | No visible damage |
| 2.1c | | 200 | 0.18 x 0.18 | No visible damage |
| 2.1c | | 200 | 0.16 x 0.16 | No visible damage |
| 2.1c | | 200 | 0.16 x 0.20 | One crack, 0.93 in. long |
| 2.1c | | 250 | 0.20 x 0.20 | Two cracks, 0.65 in. and 0.85 in. long [0.10] |
| 2.1c | | 266 | 0.18 x 0.19 | Three cracks, 0.95 in., 1.2 in. and 1.2 in. long [0.16] Six cracks ranging in length from 0.3 in. to 1.2 in. [0.6] |
| AP-2 | 0.259 | 192 | 0.20 x 0.22 | No visible damage |
| AP-2 | | 200 | | No visible damage |
| AP-2 | | 250 | 0.24 x 0.25 | No visible damage |
| AP-2 | | 250 | --- | Four cracks from 0.2 in. to 0.4 in. long [0.15] |
| AP-2 | | 266 | 0.24 x 0.24 | Three cracks from 0.2 in. to 0.35 in. [0.16] |

(1) See Footnotes in Table XXI



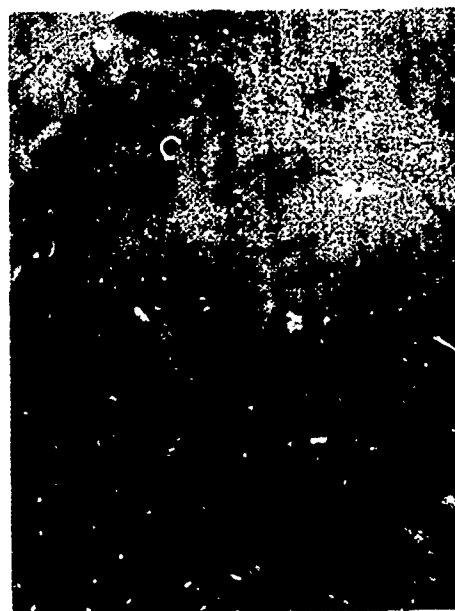
$v = 100 \text{ IN./SEC}$
SPEC. # 1.4a-



$v = 100 \text{ IN./SEC}$
SPEC. # 1.4a-



$v = 100 \text{ IN./SEC}$
SPEC. # 1.4b-



$v = 100 \text{ IN./SEC}$
SPEC. # 1.4b-

Figure 69. Impact Damage in Composite Plates Having Different Fiber Stacking Sequences.



$v = 75 \text{ IN./SEC}$
SPEC. # 2.1a-



$v = 100 \text{ IN./SEC}$
SPEC. # 2.1a-



$v = 100 \text{ IN./SEC}$
SPEC. # 2.1a-

Figure 70. Impact Damage in 0.066-In. - Thick Thornel 300-5208 Composite Plates.



$v = 200 \text{ IN./SEC}$
SPEC. # 2.1c-



$v = 200 \text{ IN./SEC}$
SPEC. # 2.1c-



$v = 250 \text{ IN./SEC}$
SPEC. # 2.1c-



$v = 266 \text{ IN./SEC}$
SPEC. # 2.1c-

Figure 71. Impact Damage in 0.25-In. - Thick Thornel 300-5208 Composite Plates as a Function of Increasing Impact Velocity.



$v = 200 \text{ IN./SEC}$
SPEC. # 2.1c-

Figure 71. Continued.



v = 250 IN./SEC
SPEC. # APCO-

Figure 72. Impact Damage in Thornei 300-APCO Resin Composite Plate (Back Face).

show some typical failure modes in plates of various thicknesses. The results for the 0.14-in. -thick plate were presented in Table XXXI and Figure 64. As one would expect, increasing the thickness of the plates causes increased resistance to impact damage.

To establish if impact-induced damage could be measured independently of visual observations, two types of through-transmission techniques were used on the 0.066-in. -thick plate: (1) ultrasonic attenuation and (2) measurement of longitudinal velocity through the thickness of the plate. The experimental results from these tests are presented in Figures 73 and 74. From the results shown in Figure 73, it is apparent that an impact velocity of ~100 in./sec causes change in the material—probably delamination within the plate—since the transverse cracking was observed to take place at an impact velocity of 75 in./sec (see Table XXXV. The step-type curve for the longitudinal-wave velocity versus impact velocity (Figure 74) is indicative of the different failure modes that take place as the target is impacted at progressively higher velocities. Additional experimental studies are required in order to understand and interpret the results from the two test techniques and to accurately assess their value in the impact problems involving composites.

Influence of Hybridization (Combining Different Materials) on Impact Response

To establish if impact resistance of graphite-epoxy could be improved through hybridization, experimental studies were conducted on the following two different combinations of materials:

1. Bidirectional Thornel 300/5208 combined with bidirectional fiberglass/5208.
2. Bidirectional Thornel 300/5208 combined with bidirectional Kevlar 49/5208.

As described in Table XXVII, for either combination, the materials were either dispersed uniformly through the thickness, or the second-phase material was added on the top and bottom surfaces of graphite-epoxy, giving a three-layer construction. The experimental results for impact response of hybrid composites are presented in Table XXXVI. Figures 75 and 76 show typical failure modes in the Thornel 300-fiberglass-5208 hybrid composite plates. Impact velocities as low as 50 in./sec were sufficient to cause failures in the bottom layer. At an impact velocity of 100 in./sec, failure in at least two adjacent layers was observed to take place as shown by the orthogonal crack pattern corresponding to the fiber directions in the two layers. To enhance the crack visibility and to ensure that no cracks existed before testing, dye penetrants were applied to the surface opposite the impacted surface. White powder coatings employed for graphite-epoxy plate could not be used for hybrid composites because there was insufficient contrast between the white color of the powder, and the yellow color of the fiberglass and Kevlar 49. The use of dye penetrants



$v = 100 \text{ IN./SEC}$
SPEC. # 1.5b-

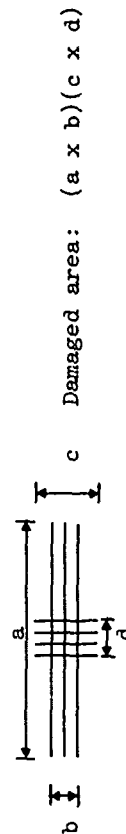
Figure 76. Continued.

Table XXXVI
IMPACT DAMAGE IN HYBRID(1) COMPOSITES

| Specimen | Material Combination | Construction (3) | Impact Velocity, in./sec | Damage on Back Face |
|----------|-----------------------------------|------------------|--------------------------|--|
| 1.5a | Thornel 300-Fiberglass-5208 Epoxy | D | 50 | No visible damage |
| 1.5a | | | 50 | No visible damage |
| 1.5a | | | 50 | Two cracks, 0.3 in. and 0.57 in. long [0.06] |
| 1.5a | | | 100 | Cracks in two layers (1.2 in. x 0.5 in.) (0.3 in. x 0.25 in.) (2) |
| 1.5a | | | 100 | Cracks in two layers (0.9 in. x 0.28 in.) (0.4 in. x 0.25 in.) |
| 1.5b | Thornel 300-Fiberglass-5208 Epoxy | 3L | 50 | No visible damage |
| 1.5b | | | 50 | Two Cracks, 0.3 in. and 0.45 in. long [0.07] |
| 1.5b | | | 50 | One crack, 0.3 in. long |
| 1.5b | | | 100 | Cracks in two layers (1.2 in. x 0.26 in.) (0.6 in. x 0.25 in.) |
| 1.5b | | | 100 | Cracks in two layers (0.8 in. x 0.23 in.) (0.45 in. x 0.23 in.) |
| 1.5c | Thornel 300-Kevlar 49-5208 Epoxy | D | 50 | No visible damage |
| 1.5c | | | 100 | Two cracks, 0.3 in. and 0.25 in. long [0.07] |
| 1.5c | | | 266 | Subsurface delamination within area 0.32 in. x 0.66 in. |
| 1.5d | Thornel 300-Kevlar 49-5208 Epoxy | 3L | 50 | No visible damage |
| 1.5d | | | 100 | Three cracks, 0.38 in., 0.38 in. and 0.6 in. long [0.14] |
| 1.5d | | | 100 | Four cracks ranging in length from 0.4 in. to 0.45 in. long [0.14] |
| 1.5d | | | 100 | Three cracks, 0.36 in., 0.36 in. and 0.6 in. long [0.14] |
| 1.5d | | | 100 | Three cracks 0.35 in., 0.35 in. and 0.5 in. long [0.13] |

(1) See footnotes in Table XXXI

(2) Numbers in parentheses refer to the size and shape of the damage zone as shown below



(3) D denotes layers of bidirectional fiberglass or Kevlar 49 dispersed between layers of bidirectional graphite; 3L denotes three-layer construction with outer two layers being bidirectional fiberglass or Kevlar 49 and center layer being bidirectional graphite.



$v = 50 \text{ IN./SEC}$
SPEC. # 1.5a-



$v = 100 \text{ IN./SEC}$
SPEC. # 1.5a-



$v = 100 \text{ IN./SEC}$
SPEC. # 1.5a-

Figure 75. Impact Damage in Thornel 300-Fiberglass-5208 Epoxy Hybrid Composite Having Dispersed Construction.

was quite successful, as can be seen from Figure 76. In the case of hybrid composite plates made with fiberglass, no cracks were detected in the specimens before impact testing. On the contrary, hybrid composite plates made with Kevlar 49 exhibited extensive cracking, transverse to the fiber direction, before testing. Figure 77 shows the crack pattern in one of the plates. The surface on which these cracks were present was adjacent to the caul plate during specimen fabrication. The cracks on the opposite plate surface, which was adjacent to the bleeder cloth during fabrication, were not as numerous as those shown in Figure 76. Consequently, when testing the plates made with Kevlar 49-Thornel 300, the latter surface was placed opposite the impact surface. Figures 78 and 79 show some typical failure modes in hybrid composites made with Kevlar 49 and Thornel 300. Figure 78a shows the crack pattern in the plate before testing. Although use of dye penetrant enhanced the visibility of the cracks, they could not be photographed readily. Consequently, to permit the initial crack pattern to be photographed, ink traces were then marked on the surface, as shown in Figure 78b.

An approach similar to that described above was used in identifying which cracks formed during impact in the three-layer Thornel 300-Kevlar 49-5208 epoxy composite. Typical results for the failure modes in the latter material are presented in Figure 79.

From the results presented in Table XXXVI and Figures 75 through 79, hybridization does not appear to increase the threshold velocity at which impact induces damage. Part of the reason why impact response of hybrid composites was so poor may be the presence of initial cracks in the as-fabricated specimen. Although use of dye penetrants allowed identification of the cracks open to the plate surfaces, there is also a possibility that the specimens could have contained subsurface cracks into which the dye penetrant could not penetrate. The results presented in Table XXXVI seem to indicate that for resistance to impact damage, dispersed construction is superior to three-layer construction, and hybrid composites consisting of Thornel 300-Kevlar 49-5208 epoxy are somewhat more resistant to impact damage than are those made of Thornel 300-Kevlar 49-5208 epoxy.

Influence of Curvature on Impact Response

Three types of specimens were used in studying the influence of curvature on impact response: 3-in. - and 6-in. -diameter cylinders, and flat plates ($R = \infty$). The fiber layup in the various specimens was 2:1 bidirectional. In the case of cylinders, twice as many fibers were oriented in the hoop direction as in the axial direction. Most of the impact tests were conducted on cylinders whose ends were potted into metal rings, as shown in Figure 61. A 3-in. -diameter cylinder with free ends was also tested to establish how the end fixity influences impact response. The results from impact tests on cylinders are described in Table XXXVII. Impact tests at 100 in./sec on a 3-in. -diameter cylinder with free ends showed no damage on the inner surface of the cylinder. However, when a 3-in. -diameter cylinder with end rings (clamped ends) was subjected to a



$v = 50 \text{ IN./SEC}$
SPEC. # 1.5b-



$v = 50 \text{ IN./SEC}$
SPEC. # 1.5b-

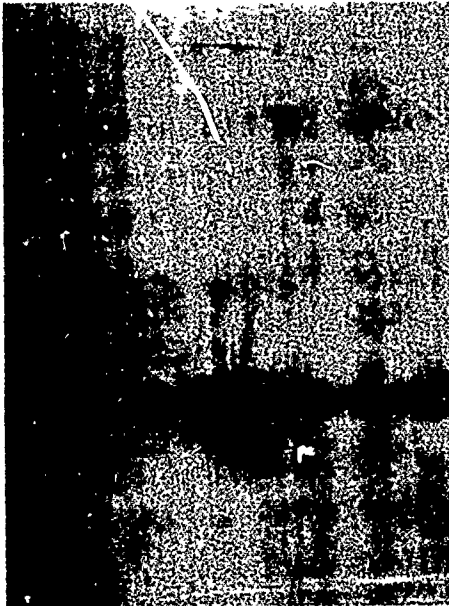


$v = 100 \text{ IN./SEC}$
SPEC. # 1.5b-



$v = 100 \text{ IN./SEC}$
SPEC. # 1.5b-

Figure 76. Impact Damage in Three-Layer Thornel 300-Fiberglass-5208 Epoxy Hybrid Composite Plate.

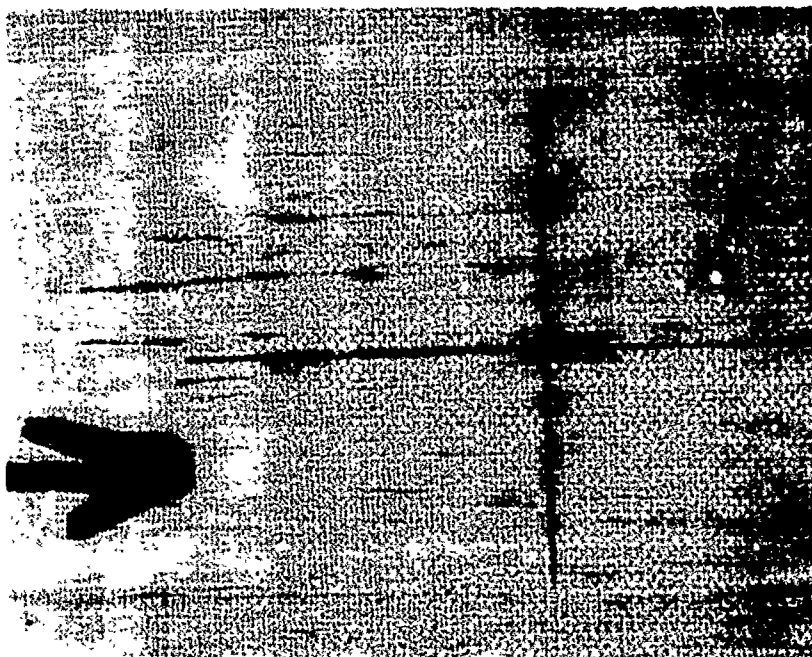


$v = 100 \text{ IN./SEC}$
SPEC. # 1.5b-

Figure 76. Continued.



Figure 77. Resin Surface Cracks in Thornel 300-Kevlar 49 Hybrid Composite Plate Prior to Testing (Cracks are in Kevlar 49).



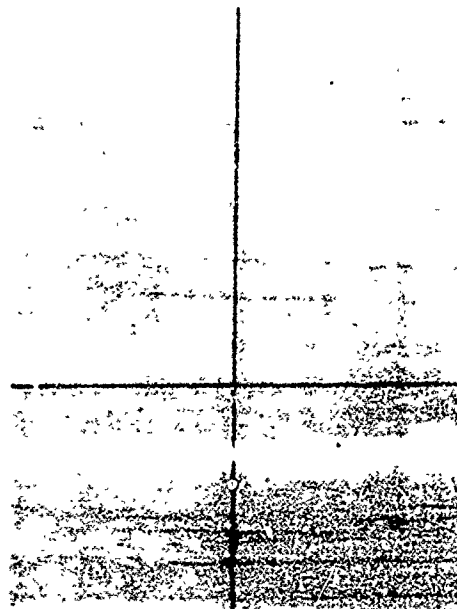
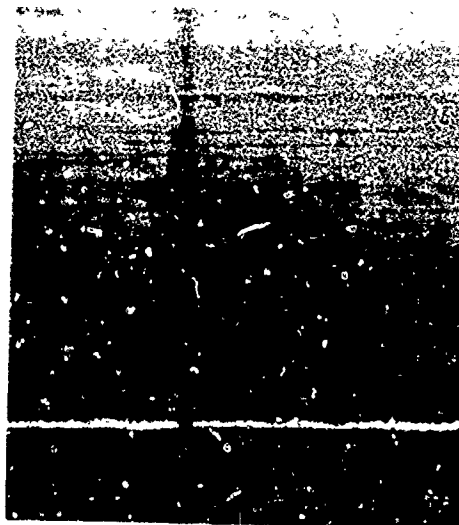
V = 100 IN./SEC
SPEC. # 1.5c-
AFTER TEST



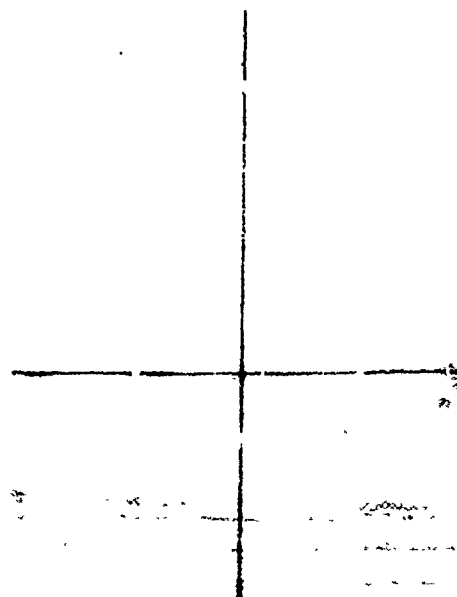
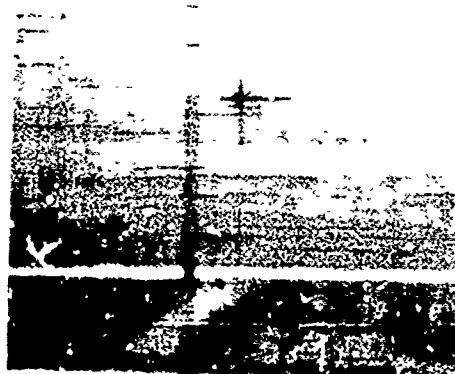
V = 100 IN./SEC
SPEC. # 1.5c-
BEFORE TEST

Figure 78. Impact Damage in Thornel 300-Kevlar 49-5208 Epoxy Hybrid Composite Plate Having Dispersed Construction.

BOTTOM SURFACE OF THE
PLATE BEFORE IMPACT



BOTTOM SURFACE OF THE
PLATE AFTER IMPACT



$v = 100 \text{ IN./SEC}$
SPEC. # 1.5d-

$v = 100 \text{ IN./SEC}$
SPEC. # 1.5d-

Figure 79. Impact Damage in Three-Layer Thornel 300-Kevlar 49-5208 Epoxy Hybrid Composite Plates.

32177
 PANE
 + [50
 52087
 K



v = 100 IN./SEC
 SPEC. # 1.5d-

Figure 79. Continued.

Table XXXVII
INFLUENCE OF CURVATURE ON EXPERIMENTALLY OBSERVED IMPACT DAMAGE (1)

| Specimen | Nominal Cylinder Radius, in. | Impact Velocity, in./sec | Major and Minor Diameters of the Area of Contact, in. | End Fixity | Damage on Back Face (or Front Face) |
|----------|---------------------------------------|--------------------------------|--|---------------|---|
| 2.2a | - | 100 | - | Free | No visible damage |
| 2.2a | - | 100 | - | Free | No visible damage |
| 2.2a | - | 100 | - | Free | No visible damage |
| 2.2a | 3.0 | 100 | 0.12 x 0.16 | Clamped | 3 axial cracks |
| 2.2a | 3.0 | 100 | 0.10 x 0.14 | Clamped | 2 axial cracks; 0.3 in. maximum length [0.061] |
| 2.2a | 3.0 | 100 | - | Clamped | Damage could not be assessed |
| 2.2a | 3.0 | 100 | 0.10 x 0.14 | Clamped | 2 axial cracks |
| 2.2a | 3.0 | 100 | - | Clamped | 2 axial cracks, 0.1 in. and 0.3 in. long |
| 2.2b | - | 100 | 0.10 x 0.12 | Clamped | No visible damage |
| 2.2b | - | 100 | 0.11 x 0.13 | Clamped | 3 circumferential cracks; 0.4 in. maximum length [0.12] |
| 2.2b | 6.0 | 100 | 0.10 x 0.13 | Clamped | 3 circumferential cracks; 0.4 in. maximum length [0.10] |
| 2.2b | 6.0 | 100 | 0.11 x 0.13 | Clamped | 3 circumferential cracks; 0.3 in. maximum length [0.12] |
| 2.2b | 6.0 | 128 | 0.12 x 0.13 | Clamped | 4 circumferential cracks; 0.3 in. maximum length [0.20] |
| 1.3c | ∞ | | | | See Table XXXIII |

(1) See footnotes in Table XXXI.

100-in./sec impact, axial cracks were observed on the inner surface of the cylinder. In the case of the 6-in.-diameter cylinder provided with metal end rings on both ends, impact caused circumferential cracks to form.

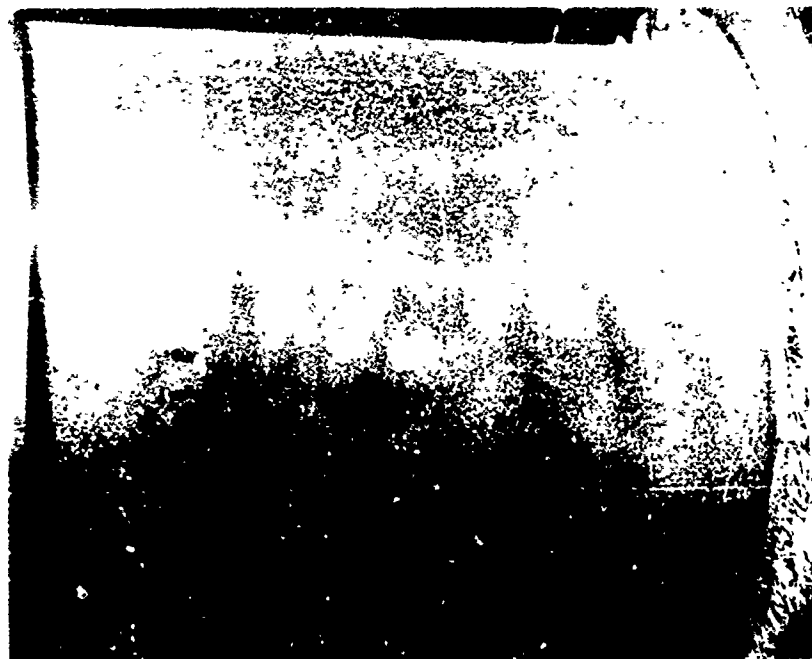
The difference in failure modes between the 3-in.- and 6-in.-diameter cylinders (axial versus circumferential cracks) was caused by the fact that the inner layer in the 3-in.-diameter cylinder consisted of axial fibers, whereas the inner layer in the case of the 6-in.-diameter cylinder consisted of hoop fibers. The difference in construction of the two cylinders resulted from a fabrication error. The shapes of the areas of contact in the 3-in.- and 6-in.-diameter cylinders are shown in Figure 80.

Figure 81 shows the impact damage on the inner surface of the 6-in.-diameter cylinders. Damage on the inner surface of the 3-in.-diameter cylinders could not be photographed readily because the openings in the end rings were small (see Figure 62). Because of the error made during the fabrication of the 3-in.-diameter cylinders, no data are available for a direct comparison of the impact damage versus cylinder diameter. However, from the comparison of test results on the 6-in.-diameter cylinder and on the flat plate (see Table XXXV, Specimen 1.3c), it can be seen that curvature limits the damage caused by impact. Whereas for a given impact velocity the average crack length in flat plates was ≈ 1 in., the average crack length in the 6-in.-diameter cylinders was only ≈ 0.37 in. The average crack length in the 3-in.-diameter cylinders would be expected to be even shorter.

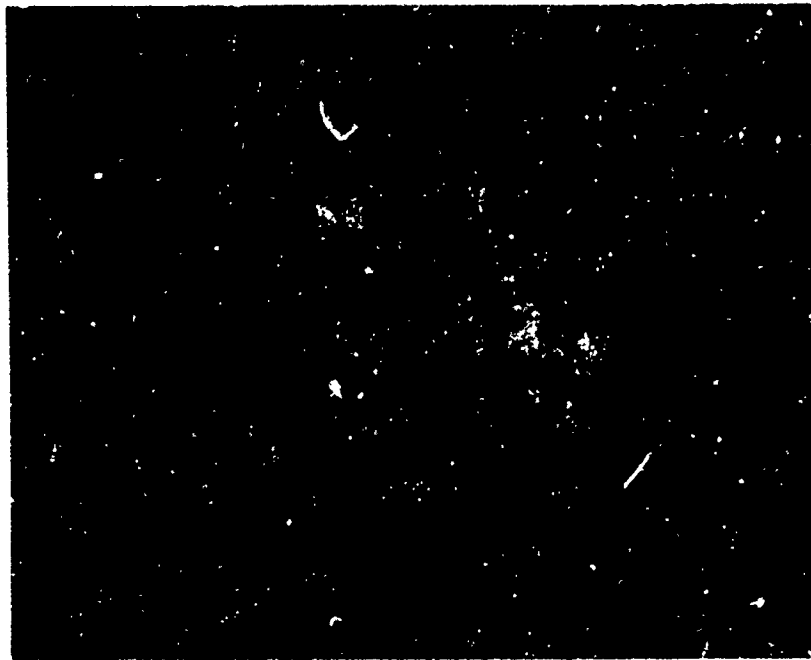
Some additional results on the influence of variables discussed in this section and obtained from instrumented impact tests are presented in the following paragraphs.

RESULTS FROM INSTRUMENTED IMPACT TESTS

Attempts to measure the impact response using specimens instrumented with strain gages and manganin gages were only partially successful. The fact that the areas of contact resulting from impact are small in comparison with the size of manganin gages created difficulties in interpreting the results. To overcome this problem an attempt was made to calibrate the manganin gages by applying known static load (through the impactor) and measuring the resultant strain. This turned out to be a reasonable solution; however, as the static load was increased another problem was encountered - the output from the manganin gage changed sign. This occurred because manganin gages are sensitive both to surface pressure normal to the plane of the gage and to strains in the direction of the plane of the gage. Thus, when the applied static load was low, the strains due to plate bending were small and the output from the manganin gage was governed by applied load. As the surface load increased, the strains due to plate bending increased, so that the manganin gage output was governed by both the normal pressure and the inplane strains. Therefore, direct

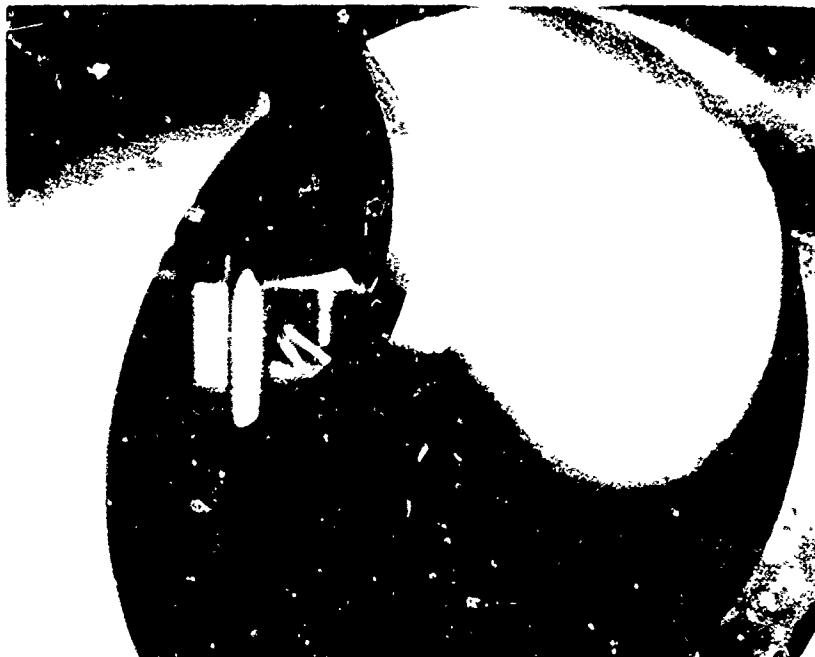


SPECIMEN 2.2a
 DIAMETER = 3-IN.
 $V = 100 \text{ IN./SEC}$

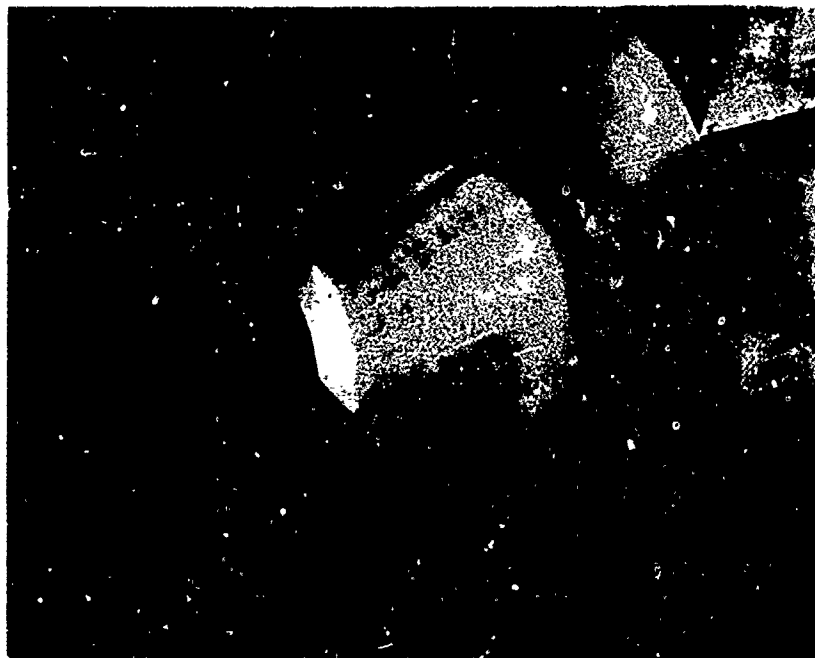


SPECIMEN 2.2b
 DIAMETER = 6-IN.
 $V = 100 \text{ IN./SEC}$

Figure 80. Shape of the Area of Contact Resulting From a 100-In./Sec Impact of a 1.5-In.-Diameter Steel Sphere Into Cylindrical Targets.



$v = 100 \text{ IN./SEC}$



$v = 100 \text{ IN./SEC}$

Figure 81. Impact Damage on the Inner Surface of 6-In -Diameter Cylinders.

measurements of the surface pressure caused by impact could not be made without undertaking an extensive experimental program.

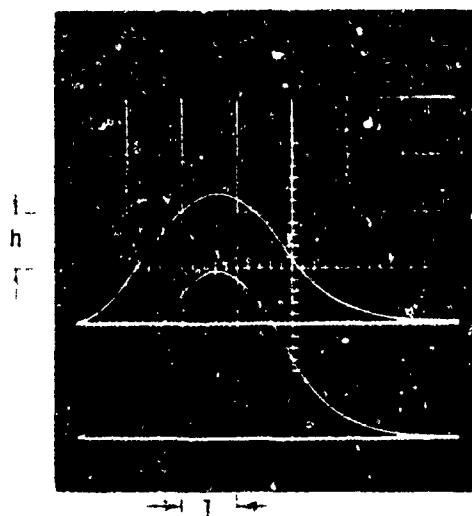
Difficulties were also encountered with the strain-gage instrumentation. The problem of gage size compared to the area of contact was minimized by using small gages (gage length of ≈ 0.62 in.). However, it was found that the gage output was extremely sensitive to the impact site. Moreover, because the strain gages could not be placed directly within the projected area of contact resulting from impact, the experimental results show only an average response in the impact region.

Another factor, which may be important but whose effect could not be assessed readily, is the influence of the gage itself. Presence of the manganin gages at the impact site may affect the impact response; whereas the presence of the strain gages at the backface of the plate could influence the failure mode. The influence of both types of instrumentation could not be established without undertaking a more extensive program than that discussed in Section IV.

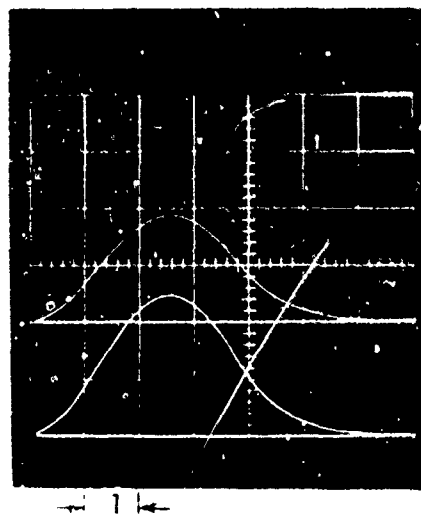
Impact Test Data on Instrumented Composite Plates

Typical results showing oscilloscope traces of strain versus time versus velocity are shown in Figures 82 through 86. Figure 82 shows the strain versus time in Modmor II/5208 pseudo-isotropic plate (Specimen 1.1c) subjected to impact velocities of 30 in./sec, 50 in./sec, and 100 in./sec. The results shown there are on the backface of the plate (opposite the impacted surface) at $r = 0$, that is, at the impact point. Figure 83 shows the radial strains on the backface of the plate in Specimen 1.1c at a distance of $r = R/2$ and $r = R/4$ from the impact point, where R is the inner radius of the support ring. The two curves shown in each portion of Figure 82 represent strains from the two biaxial gages. The differences in strain measured by the two gages are due to the sensitivity of the gage location with respect to the center of impact. Comparison of strains at $r = 0$, $r = R/4$, and $r = R/2$ (Figures 82 and 83) shows that the radial strain decreases rapidly with increasing distance from the center of contact. At $r = R/4$ the radial strain is 14%, while at $r = R/2$ the radial strain is approximately 1.8% of the strain at the impact point.

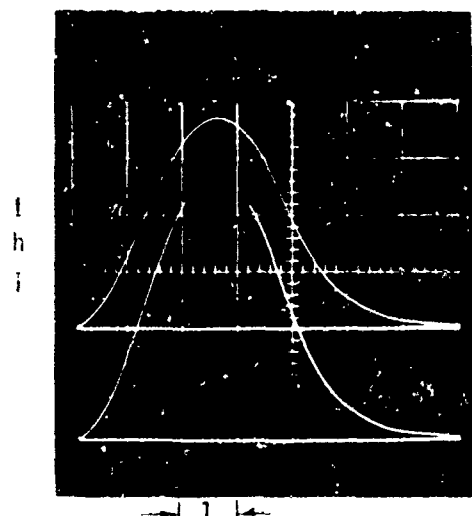
Figure 84 shows results similar to those shown in Figure 82 for the pseudo-isotropic plate made of Thornel 300/5208 (Specimen 1.1b). The influence of repeated impacts of constant velocity at a given point on the strain-time response in Specimen 1.1b is shown in Figure 85. The latter figure shows a flattening of the strain-time curve with increasing impact, which is caused by decrease in modulus of the plate due to local failure. The results presented in Figures 84 and 85 are for two different specimens, which were made identically and were processed at the same time. However, comparison of strains in the two plates shows significant differences. From Figure 84b the maximum strain resulting from 100-in./sec impact was $3100 \mu\text{in}$, whereas for the plate for which the results are shown in Figure 85, the maximum strain on the first impact was $\sim 4000 \mu\text{in}$. The difference in strains is attributed to the gage location with respect to the



$v = 30 \text{ IN./SEC}$
 $h = 500 \text{ } \mu\text{IN./IN./CM}$
 $l = 200 \text{ } \mu\text{SEC./CM}$
 $r = 0$



$v = 50 \text{ IN./SEC}$
 $h = 1000 \text{ } \mu\text{IN./IN./CM}$
 $l = 200 \text{ } \mu\text{SEC./CM}$
 $r = 0$

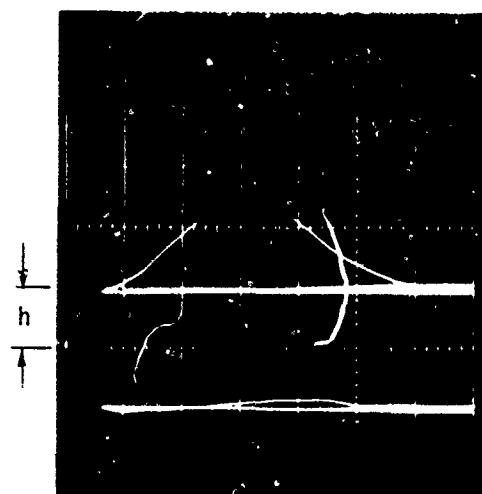


$v = 100 \text{ IN./SEC}$
 $h = 1000 \text{ } \mu\text{IN./IN./CM}$
 $l = 200 \text{ } \mu\text{SEC./CM}$
 $r = 0$

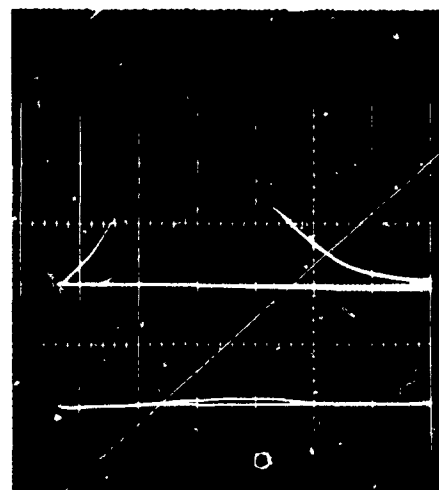
v = IMPACT VELOCITY
 h = VERTICAL SCALE
 l = HORIZONTAL SCALE
 r = IMPACT LOCATION
 $(r = 0 \text{ DENOTES CENTER OF IMPACT})$

NOTE: THE TWO CURVES SHOWN IN EACH PORTION OF THE FIGURE WERE OBTAINED FROM THE BIAxIAL GAGES MOUNTED ON THE SURFACE OPPOSITE THE IMPACT SITE. THE UPPER CURVES GIVE STRAINS IN THE FIBER DIRECTION; LOWER CURVES ARE AT 90° .

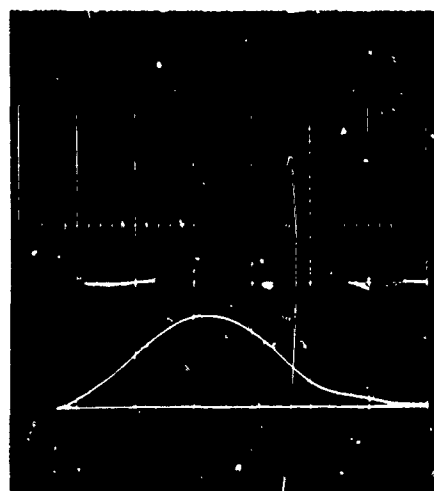
Figure 82. Impact-Induced Strains in Pseudo-Isotropic Modmor II-5208 Composite Plate (Specimen 1.1c) at $r = 0$.



$v = 30 \text{ IN./SEC}$
 $h = 100 \text{ } \mu\text{IN./IN./CM}$
 $l = 200 \text{ } \mu\text{SEC./CM}$
 $r = R/4 \text{ (TOP CURVE)}$
 $r = R/2 \text{ (BOTTOM CURVE)}$



$v = 50 \text{ IN./SEC}$
 $h = 250 \text{ IN./IN./CM}$
 $l = 200 \text{ SEC./CM}$
 $r = R/4 \text{ (TOP CURVE)}$
 $r = R/2 \text{ (BOTTOM CURVE)}$

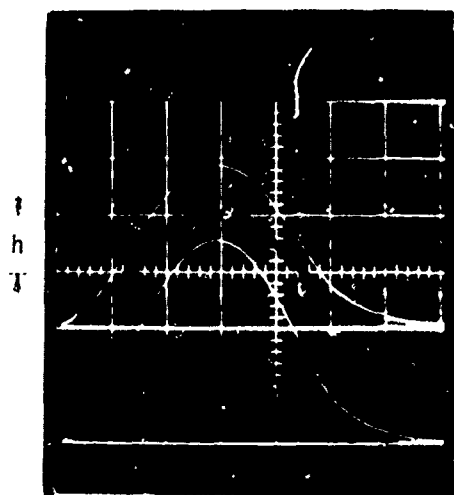


$v = 100 \text{ IN./SEC}$
 $h = 500 \text{ } \mu\text{IN./IN./CM}$
 $l = 200 \text{ } \mu\text{SEC./CM}$
 $r = R/4 \text{ (BOTTOM CURVE)}$
 $r = R/2 \text{ (TOP CURVE)}$

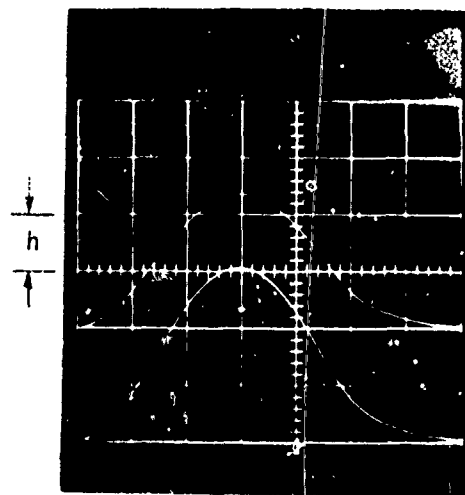
$R/4$ AND $R/2$ LOCATIONS ARE
 QUARTER AND HALF THE
 DISTANCE FROM THE IMPACT
 POINT TO EDGE OF SUPPORT
 RING RESPECTIVELY.

NOTE: THE GAGE GRID WAS
 NORMAL TO THE FIBER
 DIRECTION. SEE
 FIGURE 81 FOR
 ADDITIONAL
 INFORMATION.

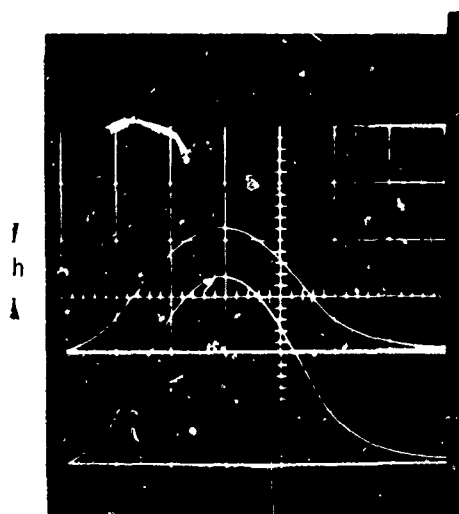
Figure 83. Impact-Induced Strains in Pseudo-Isotropic Modnar II-5208
 Composite Plate (Specimen 1.1c) at $r = R/4$ and $r = R/2$.



$v = 30 \text{ IN./SEC}$
 $h = 500 \mu\text{IN./IN./CM}$
 $l = 200 \mu\text{SEC/CM}$
 $r = 0$

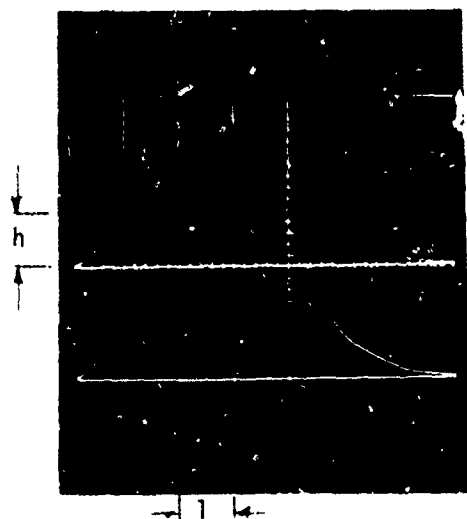


$v = 50 \text{ IN./SEC}$
 $h = 1000 \mu\text{IN./IN./CM}$
 $l = 200 \mu\text{SEC/CM}$
 $r = 0$

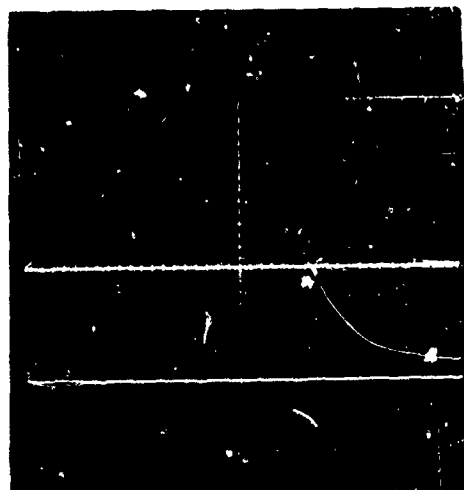


$v = 100 \text{ IN./SEC}$
 $h = 2000 \mu\text{IN./IN./CM}$
 $l = 200 \mu\text{SEC/CM}$
 $r = 0$

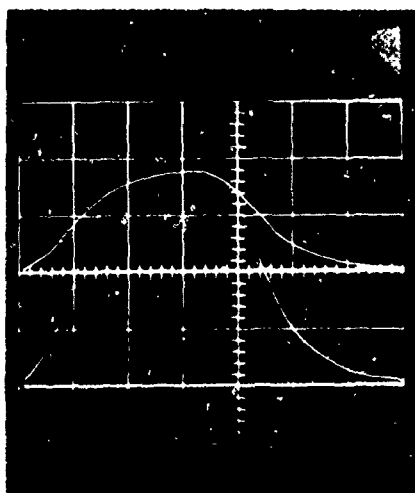
Figure 84. Impact-Induced Strains in Pseudo-Isotropic Thornel 300-5208 Composite Plate (Specimen 1.1b) at $r = 0$.



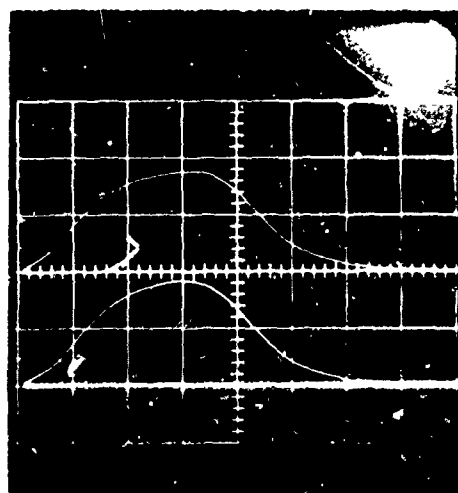
IMPACT #1
 $h = 1000 \text{ IN./IN./CM}$ (TOP CURVE)
 $h = 500 \text{ IN./IN./CM}$ (BOTTOM CURVE)



IMPACT #2
 $h = 1000 \mu\text{IN./IN./CM}$ (TOP CURVE)
 $h = 500 \mu\text{IN./IN./CM}$ (BOTTOM CURVE)



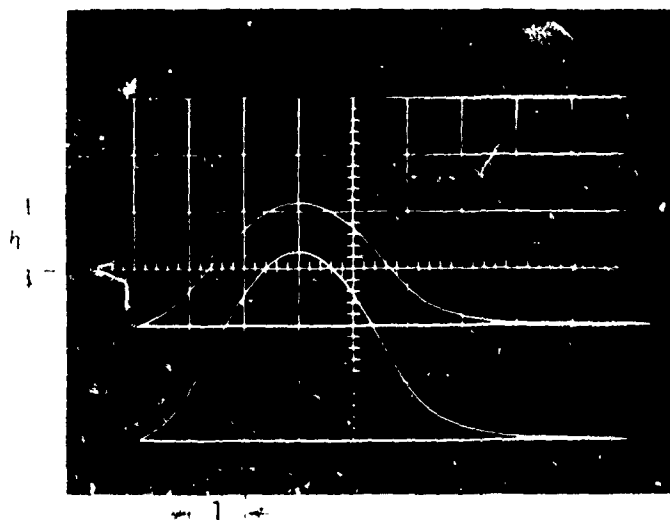
IMPACT #3
 $h = 2000 \mu\text{IN./IN./CM}$ (TOP CURVE)
 $h = 1000 \mu\text{IN./IN./CM}$ (BOTTOM CURVE)



IMPACT #5
 $h = 2000 \mu\text{IN./IN./CM}$ (TOP CURVE)
 $h = 2500 \mu\text{IN./IN./CM}$ (BOTTOM CURVE)

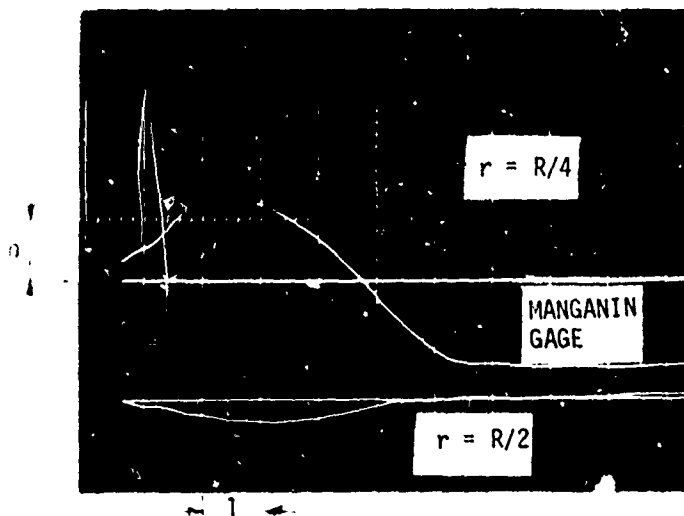
NOTE: IN ALL CASES $v = 100 \text{ IN./SEC}$; $l = 200 \mu\text{SEC/CM}$; $r = 0$

Figure 85. Influence of Repeated Impacts on Strain-Time Response
 (Thornel 300-5203 Pseudo-Isotropic Laminate
 Designated 1.1b).



$h = 2000 \mu\text{IN./IN./CM}$
 $t = 200 \mu\text{SEC/CM}$
 $r = 0$

NOTE: TOP CURVE IS FOR
 DIRECTION 1; BOTTOM
 CURVE IS FOR
 DIRECTION 2. VOLUME
 FRACTION OF FIBERS
 IN DIRECTION 2 WAS
 TWICE AS HIGH AS IN
 DIRECTION 1.



$h = 500 \mu\text{IN./IN./CM}$ FOR
 BOTH STRAIN GAGES
 $h = 0.2 \text{ v/CM}$ FOR
 MANGANIN GAGE
 $t = 200 \mu\text{SEC/CM}$

Figure 86. Impact-Induced Strains in 2:1 Bidirectional Thornel 300-5208
 Composite Plate (Specimen 1.3c) Subjected to 100-In./Sec
 Impact.

impact point and to the influence of the manganin gage. The specimen for which data are presented in Figure 85 contained a manganin gage at the impact point, while the specimen for which data are presented in Figure 84 did not. The impact test results on an instrumented composite plate having 2:1 bidirectional layup at Thornel 300/5208 are presented in Figure 86. The test data obtained from impact tests on instrumented plates are presented in Table XXXVIII.

Impact Tests on Instrumented Composite Cylinders

Tests similar to those described in the preceding section were conducted on the 3-in. - and 6-in. -diameter cylinders. The 6-in. -diameter cylinder was instrumented with a manganin gage at the impact site on the outer surface and biaxial strain gages on the inner surface. Because of the problems discussed at the beginning of this section, direct measurement of the surface pressure resulting from impact could not be made. Moreover, the strain gages located at 180° from the impact site did not show any output because of the low stresses and strains at that location. Consequently, the only strains measured in the cylindrical specimens were the strains at the impact site on the inner surface of the cylinder. Typical results for the axial and circumferential strains in the 6-in. - and 3-in. -diameter cylinders are presented in Figures 87 and 88. Comparison of the ratio of axial to circumferential strains in the two cylinders showed this ratio to be significantly different. In trying to establish the reason for this difference, it was discovered that an error had been in the fabrication of cylinders. The construction of the two cylinders was as follows (see Table XVII):

1. Construction in 3-in. -diameter cylinder: $[0, 90, 90]_8$
2. Construction in 6-in. -diameter cylinder: $[90, 90, 0]_4]_S$

Because of this error, the influence of the cylinder radius on the impact response could not be assessed. However, the influence of curvature can be assessed by comparing the data on a 2:1 bidirectional plate (see Figure 86) with the data on the 6-in. -diameter cylinder. For an impact velocity of 100 in./sec, comparison of results shows the following:

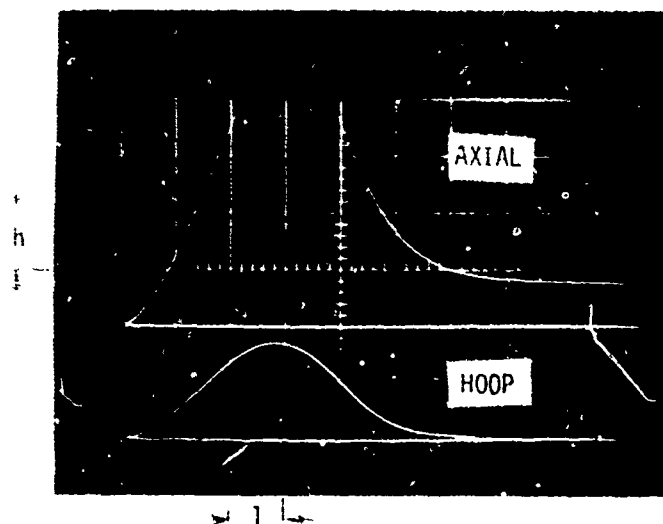
1. Maximum strain in the cylinder was 6800 $\mu\text{in./in.}$, whereas in the flat plate the maximum strain was 6500 $\mu\text{in./in.}$
2. The ratio of the axial to hoop strain in the cylinder was 2.26, whereas the ratio of maximum to minimum strain in the plate was 1.55.
3. The contact duration in flat plate was longer than in the cylinder (1400 μsec vs 1200 μsec).
4. The area of contact resulting from impact was elliptical in the case of the cylinder and nearly circular in the case of the flat plate.

From the above results and the results presented previously in this section, it appears that curvature has an influence on impact response. Moreover, it would be expected that the curvature effects would increase with decreasing cylinder radius.

Table XXX'/'III
(1)
TEST DATA FROM INSTRUMENTED COMPOSITE PLATE TESTS

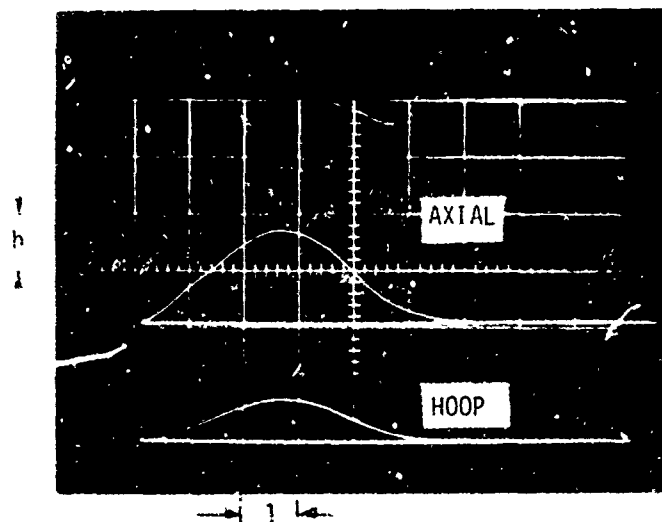
| Specimen | v = 30 in/sec | | | | v = 50 in/sec | | | | v = 100 in/sec | | | |
|----------|---------------|------|-------|-------|---------------|------|-------|-------|----------------|------|-------|-------|
| | Location | | | | Location | | | | Location | | | |
| | r=0 | | r=R/4 | r=R/2 | r=0 | | r=R/4 | r=R/2 | r=0 | | r=R/4 | r=R/2 |
| | A | B | A | A | A | B | A | A | A | B | A | A |
| 1.1(b)-1 | 1750 | 1450 | 290 | -20 | 3100 | 2400 | 325 | -50 | 6800 | 4400 | 850 | -25 |
| 1.1(b)-2 | | | | | | | | | 4500 | 3400 | 750 | 0 |
| 1.1(c)-1 | 1450 | 1150 | 200 | 0 | 2500 | 1900 | 350 | 0 | 4600 | 3700 | 750 | 0 |
| 1.3(c)-1 | | | | | | | | | 6800 | 4400 | 900 | -200 |

(1) A - Radial Direction: In all cases the radial gage direction was normal to the fiber direction.
Strains are given in μin .



$h = 2000 \mu\text{IN./IN./CM}$
 $l = 200 \mu\text{SEC/IN}$
 $v = 100 \text{ IN./SEC}$
 $r = 0$

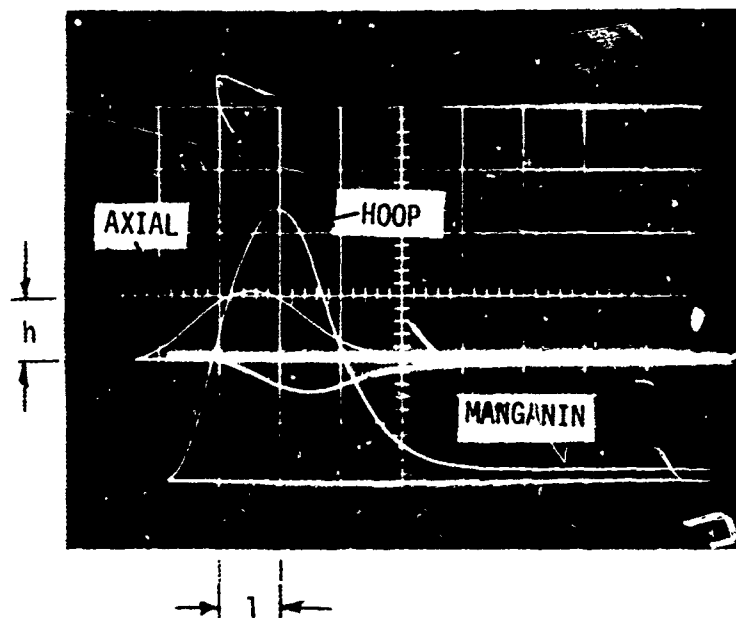
IMPACT SITE #1



$h = 4000 \mu\text{IN./IN./CM}$
 $l = 200 \mu\text{SEC/CM}$
 $v = 100 \text{ IN./SEC}$
 $r = 0$

IMPACT SITE #2

Figure 87. Impact-Induced Strains in 6-In. -Diameter, 2:1 Bidirectional Thornel 300-5208 Composite Cylinder.



$h = 4000 \mu\text{IN./IN./CM}$
 $l = 200 \mu\text{IN./IN./CM}$
 $v = 100 \text{ IN./SEC}$
 $r = 0$

NOTE: MATERIAL LAYUP IN
 THE 3-INCH-DIAMETER
 CYLINDER WAS DIFFERENT
 THAN IN THE 6-INCH-
 DIAMETER CYLINDER.

Figure 88. Impact-Induced Strains in 3-In. -Diameter
 2:1 Bidirectional Thornel 300-5208 Composite
 Cylinder.

SECTION VI

EVALUATION OF RESULTS, CONCLUSIONS, AND RECOMMENDATIONS

Inasmuch as the analytical studies on impact response of composite plates were conducted prior to fabrication and testing of the various plates and, as described in Section IV, the thicknesses of the fabricated plates differed from the thicknesses used in the analysis, a direct test-theory comparison of the threshold impact velocities to initiate damage could not be made for all the plates without making numerous computer runs for the various cases. Only in certain cases could a test-theory comparison be made without making additional computer runs. The results of the latter comparison are used to verify the theory. Further theory verification is obtained by comparing the theoretically predicted and experimentally observed trends in impact response of composite plates made with different fibers and resins and having different fiber orientations and layups, different thicknesses, and different geometries.

TEST-THEORY COMPARISON OF THE THRESHOLD IMPACT VELOCITY TO INITIATE DAMAGE

As noted above, the plate thicknesses used in the analytical studies were 0.125 in., whereas, because of the fabrication constraints discussed in Section IV, the actual thicknesses of the fabricated specimens were somewhat higher (see Table XXIX). Figure 36 shows that even small variations in the plate thickness have a significant influence on the surface pressure, q_o^* , and thereby on the impact velocity at which failure initiates at a point in a plate. Moreover, as shown in Figure 37, changing the radius of the support ring does not have a significant effect on q_o^* . The analytical results shown in Figures 36 and 37 are for pseudo-isotropic composite plates made with Thornel 300 fibers. Additional analytical results on impact damage in this material are presented in Figures 25, 26, 27, 45, and 46. With the information presented in those figures, it is possible to estimate the threshold impact velocity to cause damage in the tridirectional Thornel 300/5208 composite plates. For a 0.125-in.-thick plate it was shown in Figure 46 that significant damage occurred on the bottom surface of the plate when the plate was impacted at 50 in./sec. From the curve labeled No. 6 in Figure 25, the maximum surface pressure corresponding to this impact condition is $q = 102$ ksi. The average thickness of the plate that was tested under impact was $t = 0.1392$ in. (see data for Specimen 1.1b in Table XXIX). The threshold impact velocity to cause significant damage in the 0.1392-in. plate can be estimated from the results shown in Figures 36, 25, and 89. Figure 89 is a replot of the portion of the curve shown in Figure 36,

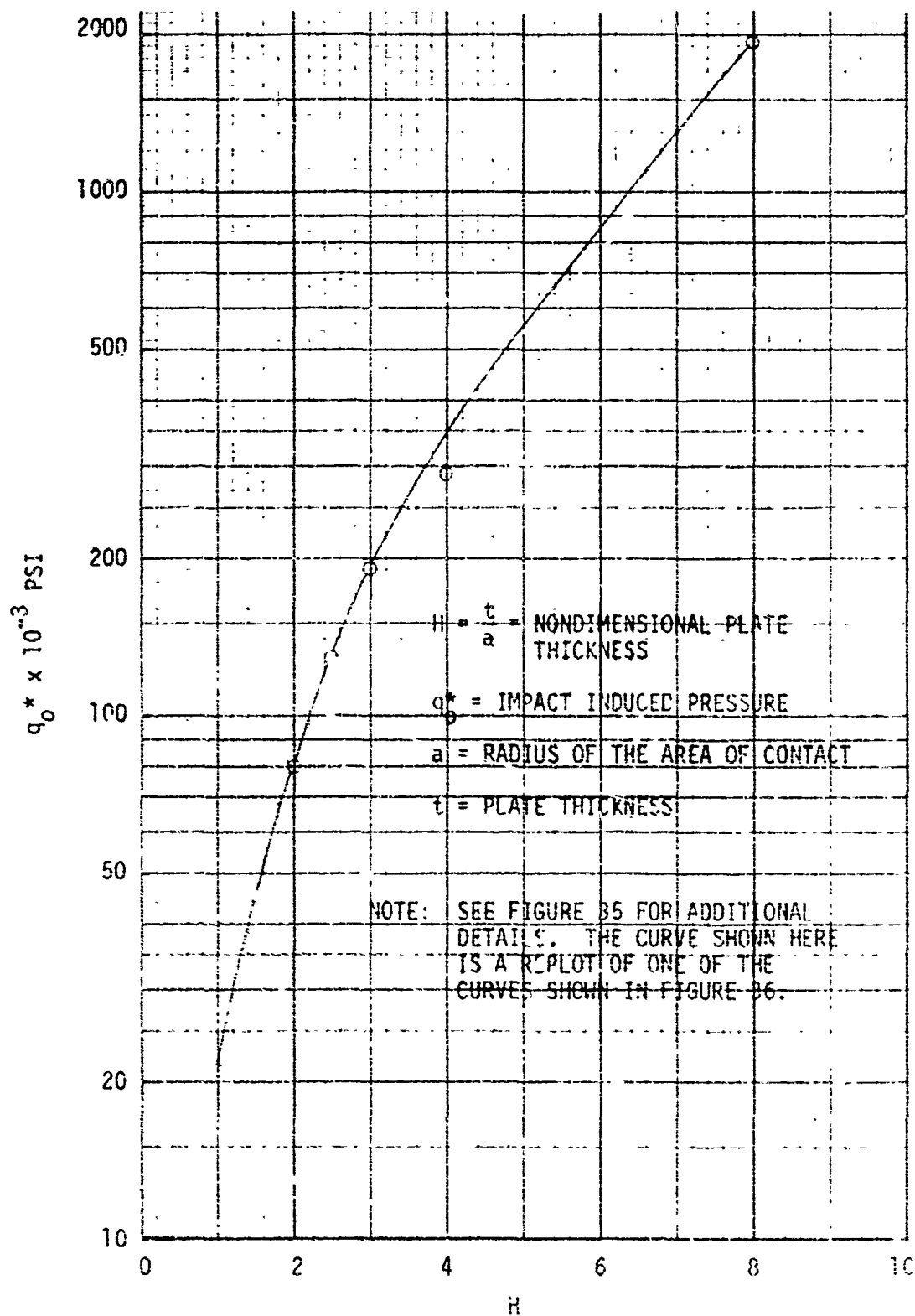


Figure 80. Influence of Plate Thickness on Impact-Induced Pressure Which Initiates Bending Failure at the Back Face of the Plate.

which gives failure on the bottom surface of the plate due to bending stresses. From Figure 89, the value of nondimensional thickness, H , corresponding to $t = 0.125$ in., $v = 50$ in./sec, $q_0 = 102$ ksi is $H = 2.10$. Taking the ratio of the actual plate thickness, $t' = 0.1392$ in., to the plate thickness used in the analysis, $t = 0.125$ in., and multiplying the above-given value of H by the thickness ratio gives the value of H' for the thicker plate

$$H' = \left(\frac{t'}{t} \right) H = \left(\frac{0.1392}{0.125} \right) (2.10) = 2.34$$

The maximum surface pressure to cause damage for the case when $H' = 2.34$ is (from Figure 89)

$$q_0^* = 128 \text{ ksi}$$

whereas from Figure 25 the threshold velocity to initiate significant damage is

$$v = 88 \text{ in./sec}$$

The extent of damage on the bottom surface of the plate can be estimated in a similar manner using the results presented in Figures 27 and 46. The final estimated width of the damaged region on the bottom surface of the plates is $w = 0.224$ in. The experimental results presented in Table XXXI for Specimen 1.1b show that, out of four impact tests conducted at 100 in./sec, failure was observed in one of the tests. Moreover, when the impact velocity was increased to 128 in./sec, two of the specimens did not show any damage, whereas the third specimen showed extensive damage at that impact velocity.

Although no results such as shown in Figures 25, 26, 27, 36, 37, 45, and 46 were generated for other plate specimens, nevertheless the results presented in those figures can be used to obtain a rough estimate of the impact velocities required to cause damage in Specimens 1.1c and 1.3a. Applicability of the above results to Specimen 1.1c is partially justified inasmuch as the properties of Modmor II fibers do not differ significantly from the Thornel 300 fibers (see Tables III and IV). In the case of Specimen 1.3a, unidirectional Thornel 300-5208 composite, results similar to those presented in Figure 45 are given in Figure 43; consequently, Figure 89 is used only to correct for the thickness effect.

In the case of Modmor II-5208 composite plates (Specimen 1.1c), the average plate thickness was 0.1669 in. Using an approach similar to that described above gives the following:

$$H' = 2.80$$

$$q_0^* = 188 \text{ ksi}$$

$$v = 235 \text{ in./sec}$$

For the unidirectional Thornel 300/5208 composite (Specimen 1.3a) the predicted velocity to initiate significant damage in 0.125-in. -thick plate was $v = 30$ in./sec, which corresponds to $q^* \approx 84$ ksi and $H = 1.92$. Estimate of the threshold impact velocity in the actual test specimen ($t = 0.139$ in.) gives

$$H' = 2.14$$

$$q^* = 108 \text{ ksi}$$

$$v = 58 \text{ in./sec}$$

Impact velocities at which damage was observed in Specimens 1.1c were 100 in./sec and 160 in./sec, whereas in the case of unidirectional Thornel 300-5208 composites the impact velocity that caused damage was $50 \text{ in./sec} < V < 100 \text{ in./sec}$, the damage extending through the width of the plate for the 100-in./sec impact velocity (see Tables XXXI and XXXIII).

The results presented above show fair correlation between tests and theory if one recognizes that the theoretical results discussed here were obtained in an approximate manner. Moreover, no account was made in the theory for the influence of the plate deformation on the surface pressure or for the fact that the material properties used in the initial theoretical analyses may have been different from the actual material properties within the various plate specimens. Use of the properties data from actual test specimens would be expected to improve test-theory correlation. The properties data needed is in the direction of the thickness of the specimen. For example, the Young's modulus in the thickness direction of the plate has a significant influence on the impact-induced surface pressure, which in turn affects the internal stresses, the failure mode, and the extent of failure.

As to the influence of the plate flexibility, it too would influence the magnitude and distribution of the surface pressure as well as the contact duration resulting from impact. The contact duration is shown to increase with decreasing E_z , the Young's modulus in the direction of plate thickness (see Table VIII and Figure 26). The plate flexibility could be looked upon as decreasing the Young's modulus of the material, E_z , to some effective modulus, E_z' , where $E_z' < E_z$. Thus, E_z' of the plate would be expected to decrease in comparison to E_z , as the flexural rigidity of the plate increased, which would cause an increase in the contact duration. The experimental results for instrumented specimens (see Figures 82 through 86) do indicate that the contact durations are significantly higher than the theoretically predicted values, which assumed the plate bending effects to have a negligible influence. Whereas for an impact velocity of 100 in./sec, the theoretically predicted contact durations were between 240 μsec and 300 μsec , the experimentally measured contact durations were of the order of 600 μsec . The fact that the flexibility of the specimen influences the contact duration follows

from the comparison of contact durations in flat plates and cylinders. For a composite having bidirectional layup, the contact duration resulting from impact of a 1.5-in. -diameter steel sphere into a cylinder was $\sim 600 \mu\text{sec}$, whereas for the same impact condition into flat plate the impact duration was $700 \mu\text{sec}$.

The results predicted analytically and observed experimentally are briefly compared in sections that follow.

Influence of Fiber Properties on Impact Response

Both test and theory agree on the influence of fiber properties on impact response. The resistance of impact damage increases with increasing fiber strength and decreasing fiber modulus. Impact damage is more sensitive to strength than to modulus.

Influence of Matrix Properties on Impact Response

Both tests and theory show that for a given reinforcing fiber and a given fiber layup, the resistance of the composite to impact damage increases as the Young's modulus of the matrix decreases and its tensile strength increases. Composites made with a polysulfone matrix were shown to be more resistant to impact damage than those made with 5208 epoxy or ERLA 4617. The fact that the composites made with polysulfone were of poorer quality than the other composites (higher void content and lower stiffness and strength) may have altered the mode of failure.

Influence of Target Thickness on Impact Response

Both tests and theory show that by increasing the target thickness the velocities required to cause damage by a given impactor also increase. Theory shows that for thick targets, local or subsurface damage at the impact site will occur first. Moreover, the theory predicts when the damage will be local and when it will be overall. No experimental work was conducted to define the type of subsurface and local damage as a function of target thickness and impact velocity.

Influence of Fiber Orientation on Impact Response

Both theoretical and experimental results show that a composite having a 1:1 bidirectional layup is more resistant to impact damage than a composite with a tridirectional fiber layup. The latter in turn is shown to be significantly superior to a composite with unidirectional fiber layup, as one would expect. Both theory and experiments show that the area of contact in uni-directional composites is elliptical.

Influence of Stacking Sequence on Impact Response

Both theory and experiment show that for a given composite and fiber layup, uniform and complete dispersion of layers through the specimen thickness gives a more impact-damage-resistant material than does a construction in which the fibers are not dispersed but rather are placed in distinct layers. For example, for a 2:1 bidirectional layup in which twice as many fibers are in Direction x as in Direction y , complete dispersion of the x fibers between the y fibers would give a more impact-damage-resistant construction than would a construction in which all the x fibers are placed in the two outer layers and the y fibers are placed in one central layer.

Influence of Hybridization on Impact Response

Neither theoretical results nor experimental results indicate any dramatic improvements in resistance to impact damage due to hybridization (combining different composite materials). In fact, in some cases the experimental threshold velocities to initiate damage in hybrid composites were lower than the threshold velocities required to initiate damage in all graphite-epoxy composites. In the case of graphite-fiberglass-resin hybrid composites, theory shows that a three-layer construction whereby the bidirectional fiberglass layers are placed on both sides of a bidirectional graphite-epoxy layer is more impact resistant than a construction in which the bidirectional fiberglass and bidirectional graphite layers are interspersed. The experimental results were not sufficient to permit an accurate assessment of which type construction is more efficient. Test results on hybrid composites consisting of Thornel 300-fiberglass-resin and Thornel 300-Kevlar 49-resin show that for a given impact velocity the backface damage in the latter composite is less extensive than in the former one. This appears to be in agreement with theoretical predictions.

Influence of Curvature on Impact Response

Both theory and experiments show that the area of contact resulting from an impact of a sphere into a cylinder will be elliptical, with the major axis of the ellipse coinciding with the cylinder axis. The theoretically predicted ratio of the axial-to-circumferential strains at the backface of the impact site was ~ 1.5 , whereas the tests show this ratio to be ≈ 2.3 . (Additional results for the curvature effects are discussed in Section III).

CONCLUSIONS AND RECOMMENDATIONS

In general, the theoretically predicted trends for the influence of fiber properties, matrix properties, fiber layup, stacking sequence, thickness, and curvature effects show fair agreement with the test results.

Further theory refinement appears desirable, however. Among the important items that need to be done to refine the theory are the following two:

1. Determination of how target flexibility influences the surface pressure, internal stresses, and contact duration.
2. Determination of the influence of local compressive yielding under the impactor on the impact-induced surface pressure.

Studies required to make a more accurate assessment of the reliability of the theory should include:

3. Complete characterization of materials, including determination of inplane and through-the-thickness properties of materials.
4. Experimental studies on internal failure modes in composite targets as influenced by impact velocity and target thickness. This should include development of experimental techniques for detecting surface and subsurface damage.
5. Additional experimental studies using instrumented specimens.

In order to establish which type of impact damage is critical, it is recommended that theoretical and experimental work be conducted on specimens impacted at various velocities. This should include determination of reduction in static and fatigue strength and elastic properties as a function of impact velocity. Studies are also recommended on repair techniques for impact-damaged composite materials, including a definition of when it is feasible to repair and when it is necessary to replace a composite structural component damaged by impact. Finally, it is recommended that the refined theory for predicting the impact response of composites be applied and implemented through fabrication and testing of composite materials or combinations of materials that are shown to be resistant to impact damage.

REFERENCES

- 1*. Oplinger, D. W., and Slepetz, J. M., IMPACT DAMAGE TOLERANCE OF GRAPHITE/EPOXY SANDWICH PANELS, U.S. Army Materials and Mechanics Research Center, Watertown, Mass., Sept. 1973.
- 2*. Suarez, J. A., and Whiteside, J. B., COMPARISON OF RESIDUAL STRENGTH OF COMPOSITE AND METAL STRUCTURES AFTER BALLISTIC DAMAGE, Grumman Aerospace Corp., Bethpage, N. Y., Sept. 1973.
- 3*. Lucas, J. J., IMPACT TESTS OF GRAPHITE/GLASS EPOXY HELICOPTER TAIL ROTOR BLADE, Sikorsky Aircraft, Stratford, Conn., Sept. 1973.
- 4*. Potts, J. M., and Gray, W. A., EFFECT OF COMPOSITION AND PROCESSING VARIABLES ON THE RESISTANCE TO IMPACT DAMAGE OF REINFORCED PHENOLIC ABLATORS, Martin Marietta Aerospace, Orlando, Fla., Sept. 1973.
- 5*. Husman, G. E., Whitney, J. M., and Halpin, J. C., RESIDUAL STRENGTH CHARACTERIZATION OF LAMINATED COMPOSITES SUBJECTED TO IMPACT LOADING, U.S. Air Force Materials Laboratory, Wright-Patterson AFB, Ohio, Sept. 1973.
- 6*. Broutman, L. J., Rotem, A., and Zych, J., IMPACT ENERGY OF GLASS FIBER AND GLASS-CARBON FIBER HYBRID COMPOSITES, Illinois Institute of Technology, Chicago, Ill., Sept. 1973.
- 7*. Baumont, P. W., Riewald, P. G., and Zweben, C., THE IMPACT FRACTURE CHARACTERISTICS OF SOME FIBER-STRENGTHENED EPOXY RESIN SYSTEMS, E. I. duPont de Nemours and Co., Inc., Wilmington, Del., Sept. 1973.

*Papers presented at the ASTM Symposium on Foreign Object Impact Behavior of Composites in Philadelphia, Pennsylvania, September 20, 1973, and to be published as ASTM STP 568 in 1975.

- 8*. Cristescu, N., Meivern, L. E., and Sierakowski, R. L., FAILURE MECHANISMS IN COMPOSITE PLATES IMPACTED BY BLUNT-ENDED PENETRATORS, University of Florida at Gainesville, Sept. 1973.
- 9*. Mortimer, R. W., Chou, P. C., and Carleone, J., THE BEHAVIOR OF LAMINATED COMPOSITE PLATES SUBJECTED TO IMPACT, Drexel University, Phila., Pa., Sept. 1973.
- 10*. Greszczuk, L. B., RESPONSE OF ISOTROPIC AND COMPOSITE MATERIALS TO PARTICLE IMPACT, McDonnell Douglas Astronautics Co., Huntington Beach, Calif., Sept. 1973.
- 11*. Sun, C. T., and Sierakowski, R. L., STUDIES OF THE IMPACT STRUCTURAL DAMAGE OF COMPOSITE BLADES, authors from Air Force Materials Laboratory, Wright-Patterson AFB, Ohio, and University of Florida at Gainesville respectively, Sept. 1973.
- 12.* Preston, J. L., Jr., and Cook, T. S., IMPACT RESPONSE OF GRAPHITE-EPOXY COMPOSITES TO SIMULATED AIRCRAFT ENGINE FOREIGN OBJECT DAMAGE ENVIRONMENTS, Pratt and Whitney Aircraft Corporation, Division of United Aircraft, East Hartford, Conn., Sept. 1973.
- 13.** Kubo, J. T., and Nelson, R. B., ANALYSIS OF IMPACT STRESSES IN COMPOSITE PLATES, University of California, Los Angeles, Calif. 1974.
- 14.** Avery, A. G., and Porter, T. R., COMPARISON OF BALLISTIC IMPACT RESPONSE OF METALS AND COMPOSITES FOR MILITARY AIRCRAFT APPLICATIONS, Boeing Aerospace Co., Seattle, Wash. 1974.
15. Chamis, C. C., Hanson, M. P., and Serafini, T. T., IMPACT RESISTANCE OF UNIDIRECTIONAL FIBER COMPOSITES, IN COMPOSITE MATERIALS: TESTING AND DESIGN, American Society for Testing and Materials, ASTM STP 497, February 1972, pp. 324-349.
16. Novak, R. C., and DeCrescente, M. A., IMPACT BEHAVIOR OF UNIDIRECTIONAL RESIN MATRIX COMPOSITES TESTED IN FIBER DIRECTION, IN COMPOSITE MATERIALS: TESTING AND DESIGN, American Society for Testing and Materials, ASTM STP 497, February 1972, pp. 311-323.

*Same as previous page

**To be published in ASTM STP 568 in 1975.

17. Friedrich, A. L., and Preston, J. L., Jr., IMPACT RESISTANCE OF FIBER COMPOSITE BLADES USED IN AIRCRAFT TURBINE ENGINES, Pratt and Whitney Aircraft, Division of United Aircraft Corporation; NASA Technical Report CR-134502, National Aeronautics and Space Administration, NASA Lewis Research Center, Cleveland, Ohio, May 1973.
18. Coppa, A. P., MEASUREMENT OF TURBOFAN BLADE RESPONSE TO SIMULATED BIRD-CARCASS IMPACT, General Electric Report, 71 SD 266, December 1971.
19. Sayers, K. H., and Harris, B., INTERLAMINAR SHEAR STRENGTH OF A CARBON FIBER REINFORCED COMPOSITE MATERIAL UNDER IMPACT CONDITIONS, J. Composite Materials, Vol. 7, January 1973, pp. 129-133.
20. Bradshaw, F. J., Dorey, G., and Sidey, G. R., IMPACT RESISTANCE OF CARBON FIBER REINFORCED PLASTICS, Royal Aircraft Establishment Technical Report 72240, March 1973.
21. Dorey, G., FRACTURE BEHAVIOR AND RESIDUAL STRENGTH OF CARBON FIBER COMPOSITES SUBJECTED TO IMPACT LOADS, Paper B3, presented at the NATO AGARD Meeting, Munich, Germany, October 7-9, 1974.
22. Moon, F. C., THEORETICAL ANALYSIS OF IMPACT IN COMPOSITE PLATES, National Aeronautics and Space Administration Report NASA CR-121110, 1972.
23. Moon, F. C., A CRITICAL SURVEY OF WAVE PROPAGATION AND IMPACT IN COMPOSITE MATERIALS, National Aeronautics and Space Administration Report, NASA CR-121226, May 1973.
24. Chen, W. T., STRESSES IN SOME ANISOTROPIC MATERIALS DUE TO INDENTATION AND SLIDING, International Journal of Solids and Structures, Vol. 5, 1969, P. 191.
25. Willis, J. R., HERTZIAN CONTACT OF ANISOTROPIC BODIES, J. Mechanics and Physics of Solids, Vol. 14, 1966, pp. 163-176.
26. Svelko, V. A., BOUSSINESQ-TYPE PROBLEM FOR ANISOTROPIC SEMISPACE, Prikladnaia Matematika i Mekhanika, Vol. 28, 1964, pp. 908-913.
27. Lekhnitskii, S. G., THEORY OF ELASTICITY OF AN ANISOTROPIC ELASTIC BODY, Holden-Day Inc., San Francisco, 1963.
28. Green, A. E., and Zerna, W., THEORETICAL ELASTICITY, Oxford at the Clarendon Press, 1954.

29. Winsa, E. A., and Petrasek, D. W., PENDULUM IMPACT RESISTANCE OF TUNGSTEN FIBER/METAL MATRIX COMPOSITES, in COMPOSITE MATERIALS: TESTING AND DESIGN, American Society for Testing and Materials, ASTM STP 497, February 1972, pp. 350-362.
30. Chamis, C. C., Hanson, M. P., and Serafini, T. T., DESIGNING FOR IMPACT RESISTANCE WITH UNIDIRECTIONAL FIBER COMPOSITES, National Aeronautics and Space Administration Report, NASA TN D-6463, 1971.
31. Avery, J. F., and Porter, T. R., A PARAMETRIC EVALUATION OF LIGHTWEIGHT METAL AND COMPOSITE STRUCTURES EXPOSED TO GUNFIRE, presented at the Army Symposium on Solid Mechanics, Ocean City, Maryland, 1972.
32. Toland, R. H., FAILURE MODES IN IMPACT-LOADED COMPOSITE MATERIALS, Presented at Symposium on Failure Modes in Composites, AIME Spring Meeting, Boston, Mass., May 1972.
33. Wullaert, R. A., APPLICATION OF THE INSTRUMENTED CHARPY IMPACT TEST, American Society for Testing and Materials, ASTM STP 466, 1970, pp. 148-184.
34. Toland, R. H., INSTRUMENTED IMPACT TESTING OF COMPOSITE MATERIALS, presented at the ASTM Symposium on Instrumented Impact Testing, Philadelphia, Pennsylvania, June 1973.
35. Allen, G., Morley, D. C. W., and Williams, T., THE IMPACT STRENGTH OF POLYCARBONATE, J. of Material Science, Volume 8, No. 10, October 1973, pp. 1449-1452.
36. Brown, H. R., A CRITICAL EXAMINATION OF THE IMPACT TEST FOR GLASS POLYMERS, J. of Material Science, Vol. 8, No. 7, July 1973, pp. 941-948.
37. Marshall, G. P., Williams, J. G., and Turner, C. E., FRACTURE TOUGHNESS AND ABSORBED ENERGY MEASUREMENTS IN IMPACT TESTS ON BRITTLE MATERIALS, presented at the ASTM Symposium on Instrumented Impact Testing, Philadelphia, Pennsylvania, June 1973.
38. Olster, E. F., and Woodbury, H. A., EVALUATION OF BALLISTIC DAMAGE RESISTANCE AND FAILURE MECHANISMS OF COMPOSITE MATERIALS, AVCO Corp., Report AFML-TR-72-79 prepared under Air Force Materials Laboratory Contract F33615-70-C-1570, April 1972.

39. Suarez, J. A., VULNERABILITY OF COMPOSITE AIRCRAFT STRUCTURES, Grumman Corporation, Report AFFDL-TR-72-3 prepared under Air Force Flight Dynamics Contract F33615-71-C-111, February 1972.
40. Tsai, Y. M., A NOTE ON THE SURFACE WAVES PRODUCED BY HERTZIAN IMPACT, J. MECH. PHYS. SOLIDS, Vol. 16, pp. 133-136, 1968.
41. Gupta, B. P., and Davids, N., PENETRATION EXPERIMENTS WITH FIBERGLASS REINFORCED PLASTICS, EXPERIMENTAL MECHANICS, Vol. 6, p. 455, 1966.
42. Askins, D. R., and Schwartz, H. S., MECHANICAL BEHAVIOR OF REINFORCED PLASTIC BACKING MATERIALS FOR COMPOSITE ARMOR, Technical Report, AFML-TR-71-283, Air Force Materials Lab., Dayton, Ohio, 1972.
43. Wrzesien, A., IMPROVING THE IMPACT RESISTANCE OF GLASS-FIBER COMPOSITES, COMPOSITES TECHNOLOGY, Vol. 3, p. 172, 1972.
44. Ross, C. A., and Sierakowski, R. L., STUDIES ON THE IMPACT RESISTANCE OF COMPOSITE PLATES, COMPOSITES TECHNOLOGY, Vol. 4, p. 157, 1973.
45. Sun, C. T., and Sierakowski, R. L., STUDIES ON THE DYNAMIC IMPACT OF JET ENGINE BLADES, BULLETIN 43rd SHOCK AND VIBRATION SYMPOSIUM, 1972.
46. Greszczuk, L. B., MECHANICS OF PARTICLE IMPACT, McDonnell Douglas Astronautics Company Report, MDC G2612, March 1973.
47. Sidey, G. R., and Bradshaw, F. J., SOME INVESTIGATIONS ON CARBON-FIBER-REINFORCED PLASTICS UNDER IMPACT LOADING, AND MEASUREMENTS OF FRACTURE ENERGIES, PROCEEDINGS AT THE INTERNATIONAL CARBON FIBER CONFERENCE, London, 1971.
48. Dorey, G., and Sidey, G. R., RESIDUAL STRENGTH OF CFRP LAMINATES AFTER BALLISTIC IMPACT, Proceedings, Mechanical Properties of Materials at High Strain Rates, Oxford Conference Institute of Physics Conference Series No. 21, 1974.
49. Simon, R. A., IMPACT STRENGTHS OF CARBON FIBER COMPOSITES, Proceedings 28th Annual Technical Conference of the Society of Plastics Industry, 1973, p. 17-C.

50. Dory, G., and Sidey, G. R., ON USE OF EPOXY RESIN CF84 AS A MATRIX FOR CFRP LAMINATES - IMPACT PROPERTIES, RAE Technical Report 74071, 1974.
51. Rogers, K. F., Sidey, G. R., and Lingstone-Lee, D. M., BALISTIC IMPACT RESISTANCE OF CARBON-FIBER LAMINATES, Composites Vol 2, 1971, pp. 237-241.
52. Timoshenko, S., THEORY OF ELASTICITY, McGraw Hill Book Company, New York, 1934.
53. Belajef, W. M., MEMOIRS ON THEORY OF STRUCTURES, Izdatelstvo Puti (St. Petersburg), 1924. See also Belajef, STRENGTH OF MATERIALS, Gosudarstvennoje Izdatelstvo Tekh. - Teor. 1945 (In Russian).
54. Conway, H. D., THE PRESSURE DISTRIBUTION BETWEEN TWO ELASTIC BODIES IN CONTACT, Zeitschrift fuer Angewandte Mathematik und Physik, Vol. VII, 1956, pp. 460-465.
55. Crose, J. G., and Jones, R. M., SAAS III, FINITE ELEMENT STRESS ANALYSIS OF AXISYMMETRIC AND PLANE SOLIDS WITH DIFFERENT ORTHOTROPIC, TEMPERATURE-DEPENDENT MATERIAL PROPERTIES IN TENSION AND COMPRESSION, TR-0059 (S6816-53)-The Aerospace Corporation, San Bernadino, California, June 1971.
56. Crose, J. G., ASAAS - ASYMMETRIC STRESS ANALYSIS OF AXISYMMETRIC SOLIDS WITH ORTHOTROPIC, TEMPERATURE-DEPENDENT MATERIAL PROPERTIES THAT CAN VARY CIRCUMFERENTIALLY, The Aerospace Corporation Report TR-0172(S2816-15)-1, December 1971.
57. Timoshenko, S. P., THEORY OF PLATES AND SHELLS, McGraw-Hill Book Company, New York, 1940, p. 60.
58. Hearmon, R. F. S., APPLIED ANISOTROPIC ELASTICITY, Oxford University Press, Oxford, 1961, p. 126.
59. Chane, H. L., ELASTIC PLASTIC ASYMMETRIC TRANSIENT RESPONSE OF ORTHOTROPIC CYLINDRICAL SHELLS SUBJECTED TO MECHANICAL AND THERMAL LOADS, McDonnell Douglas Astronautics Company/Western Division, Report MDC G3750 (in preparation).
60. Sanders, Jr., J. L., NONLINEAR THEORIES FOR THIN SHELLS, Quarterly Applied Mathematics, Vol. 21, No. 1, April 1963, pp. 21-36.

61. Leech, J. W., PETROS I: FINITE-DIFFERENCE CALCULATION METHOD FOR LARGE ELASTIC-PLASTIC DYNAMICALLY-INDUCED DEFORMATIONS OF GENERAL THIN SHELLS, MIT, AFFDL-TR-66-171, December 1966.
62. Franke, R. H., CYLINDER: A COMPUTER PROGRAM FOR THE INELASTIC DYNAMIC RESPONSE OF ORTHOTROPIC CYLINDRICAL SHELLS, Kaman Nuclear, KN-67-533(R), September 1967.
63. Hubka, W. F., FURTHER RESULTS IN THE INELASTIC DYNAMIC ANALYSIS OF CYLINDRICAL SHELLS, Kaman Nuclear, KN-67-452(R), September 1967.
64. Greszczuk, L. B., FAILURE CRITERIA FOR THREE-DIMENSIONAL ORTHOTROPIC SOLIDS, Douglas Aircraft Company Report DAC 60869, October 1967.
65. Greszczuk, L. B., THEORETICAL AND EXPERIMENTAL STUDIES ON PROPERTIES AND BEHAVIOR OF FILAMENTARY COMPOSITES, Proceedings of the 21st Annual Technical Conference of the Society of Plastics Industries, Chicago, Illinois, February 1966.
66. Greszczuk, L. B., MICROMECHANICS FAILURE CRITERIA FOR COMPOSITES, Final Summary Report prepared under Naval Air Systems Command Contract No. N00019-72-0221, May 1973.
67. Greszczuk, L. B., MECHANICS OF FAILURE OF COMPOSITES, Final Summary Report prepared under Naval Air Systems Command Contract No. N00019-73-0405, May 1974.

BIBLIOGRAPHY

Ashkenazi, E. K., ANISOTROPY IN THE STRENGTH OF CONSTRUCTION MATERIAL, C. M. Kirov Wood Technology Academy, Leningrad, Vol. 31, No. 5, May 1961.

Ashkenazi, E. K., THE CONSTRUCTION OF LIMITING SURFACES FOR BIAXIAL STRESSED CONDITION OF ANISOTROPIC MATERIALS, Zavodskaya Laboratoriya, Vol. 30, No. 2, Leningrad Forestry Academy, February 1964.

Ashkenazi, E. K., PROBLEMS OF THE ANISOTROPY OF STRENGTH, Mekhanika Polimerov, Vol. 1, No. 2, 1965, p. 79 (English translation: Polymer Mechanics, Vol. 1, 1966, p. 60).

Ashkenazi, E. K., ON THE PROBLEM OF STRENGTH ANISOTROPY OF CONSTRUCTION MATERIALS, The S. M. Kirov Forest Products Academy, Chair of Construction Mechanics, Leningrad.

Azzi, V. D., Tasi, S. W., ANISOTROPIC STRENGTH OF COMPOSITES, Experimental Mechanics, Vol. 5, September 1965, pp. 283-288.

Bogue, D. C., THE YIELD STRESS AND PLASTIC STRAIN THEORY FOR ANISOTROPIC MATERIALS, ORNL-TM-1869, Oak Ridge National Laboratory, Oak Ridge, Tennessee, July 1967.

Caddell, R. M., Raghara, R. S., and Atkins, A. G., A YIELD CRITERION FOR ANISOTROPIC AND PRESSURE DEPENDENT SOLIDS SUCH AS ORIENTED POLYMERS, J. of Materials Science, Vol. 8, No. 11, November 1973, pp. 1641-1646.

Chamis, C. C., FAILURE CRITERIA FOR FILAMENTARY COMPOSITES, Composite Materials: Testing and Design, ASTM STP 460, ASTM, 1969.

Cherry, J. T., Larson, D. B., and Rapp, E. G., A UNIQUE DESCRIPTION OF THE FAILURE OF A BRITTLE MATERIAL, Int. J. Rock Mech. Min. Sci., Vol. 5, 1968, pp. 455-463.

Chou, P. C., McNamee, B. M., and Chou, D. K., THE YIELD CRITERION OF LAMINATED MEDIA, J. Composite Materials, Vol. 7, January 1973, pp 22-35.

Cooper, G. A., ORIENTATION EFFECTS IN FIBRE-REINFORCED METALS, J. Mech. Phys. Solids, Vol. 14, 1966.

Fisher, L., HOW TO PREDICT STRUCTURAL BEHAVIOR OF RP LAMINATES, Modern Plastics, June 1960, p. 120.

Fisher, L., OPTIMIZATION OF ORTHOTROPIC LAMINATES, Journal of Engineering for Industry, August 1967.

Frank, F. C., and Lawn, B. R., ON THE THEORY OF HERTZIAN FRACTURE, Proc. Roy. Soc., Vol. A299, July 1967, pp. 291-306.

Franklin, H. G., CLASSIC THEORIES OF FAILURE OF ANISOTROPIC MATERIALS, Fiber Science Technology, Vol. 1, 1968

Geogdzhayev, V. O., SOME QUESTIONS IN THE THEORY OF ELASTO-PLASTIC DEFORMATIONS OF ANISOTROPIC MATERIALS, Trudi Mosk, Fiz., -Tekh In-Ta, Nol. 1, 1958, pp. 69-96.

Goldenblat, I. I., and Kopnov, V. A. STRENGTH OF GLASS-REINFORCED PLASTICS IN COMPLEX STRESS STATE, Mekhanika Polimerov, Vol. 1, 1965, p. 70.

Grassi, R. C., and Cornet, I., FRACTURE OF GREY-CAST-IRON TUBES UNDER BIAXIAL STRESSES, Journal of Applied Mechanics, June 1949, pp. 178-182.

Greszczuk, L. B., FAILURE CRITERIA FOR THREE DIMENSIONAL ORTHOTROPIC SOLIDS, Douglas Aircraft Co., Report DAC 60869, October 1967.

Greszczuk, L. B., MICROMECHANICS FAILURE CRITERIA FOR COMPOSITES, Presented at the AIAA/ASME 12th Structures, Structural Dynamics and Materials Conference, Anaheim, California, April 1971.

Greszczuk, L. B., MICROMECHANICS FAILURE CRITERIA FOR COMPOSITES, McDonnell Douglas Astronautics Company Report, prepared under Naval Air Systems Command Contract N00019-72-0221, Washington, D. C., May 1973.

Greszczuk, L. B., MECHANICS OF FAILURE OF COMPOSITES, McDonnell Douglas Astronautics Company Report, prepared under Naval Air System Command Contract N00019-72-0405, Washington, D. C., May 1974.

Greszczuk, L. B., CONSIDERATION OF FAILURE MODES IN THE DESIGN OF COMPOSITE STRUCTURES, Presented at the NATO AGARD Meeting, Munich, Germany, October 7-9, 1974.

Griffith, J. E., and Baldwin, W. M., FAILURE THEORIES FOR GENERALLY ORTHOTROPIC MATERIALS, Developments in Theoretical and Applied Mechanics, Vol. 1, 1962.

Hershey, A. V., THE PLASTICITY OF AN ISOTROPIC AGGREGATE OF ANISOTROPIC FACE CENTERED CUBIC CRYSTALS, J. Appl. Mech., Vol. 21, No. 3, 1954, pp. 241-249.

Hill, R., A THEORY OF THE YIELDING AND PLASTIC FLOW OF ANISOTROPIC METALS, Proceedings of the Royal Society, Series A. Vol. 193, 1948, pp. 281-297.

Hoffman, O., THE BRITTLE STRENGTH OF ORTHOTROPIC MATERIALS, J. Composite Materials, Vol. 1, 1967, pp. 200-206.

Hu, L. W., MODIFIED TRESCA'S YIELD CONDITION AND ASSOCIATED FLOW RULES FOR ANISOTROPIC MATERIALS AND APPLICATION, Journal of the Franklin Institute, 1958.

Jackson, P. W., and Cratchley, D., THE EFFECT OF ORIENTATION ON THE TENSILE STRENGTH OF FIBRE-REINFORCED METALS, J. Mech. Phys. Solids, Vol. 14, 1966.

Jenkins, C. F., REPORT ON MATERIALS OF CONSTRUCTION USED IN AIRCRAFT AND AIRCRAFT ENGINES, Great Britain Aeronautical Research Committee, 1920.

Kaminski, B. E., and Lantz, R. B., STRENGTH THEORIES OF FAILURE FOR ANISOTROPIC MATERIALS, in COMPOSITE MATERIALS: TESTING AND DESIGN, American Society for Testing and Materials, ASTM STP 460, Dec. 1969.

Lance, R. H., Robinson, D. N., A MAXIMUM SHEAR STRESS THEORY OF PLASTIC FAILURE OF FIBER-REINFORCED MATERIALS, J. Mech. Phys. Solids, Vol. 19, 1971.

Mair, W. M., FRACTURE CRITERIA FOR CAST IRON UNDER BIAXIAL STRESSES, Journal of Strain Analysis, Vol. 3, No. 4, 1968, pp. 254-263.

Malmeister, A. K., GEOMETRY OF THEORIES OF STRENGTH, Mekhanika Polimerov, Vol. 2, No. 4, 1966.

Marin, J., THEORIES OF STRENGTH FOR COMBINED STRESSES AND NON-ISOTROPIC MATERIALS, Journal Aeronautical Sciences, Vol. 24, No. 4, April 1957.

McLaughlin, P. V., Majumdar, S., and Phillips, J. W., ELASTIC BEHAVIOR, BRITTLE FAILURE AND PLASTIC FLOW OF FILAMENTARY MATERIALS, Int. J. Solids and Structures, Vol. 9, No. 8, August 1973, pp. 937-950.

Norris, C. B., STRENGTH OF ORTHOTROPIC MATERIALS SUBJECTED TO COMBINED STRESS, Forst Products Laboratory, Report 1816, 1962.

Norris, C. B., ELASTIC THEORY OF WOOD FAILURE, Trans. ASME, April 1939.

Oh, A. L., and Finnie, I., ON THE LOCATION OF FRACTURE IN BRITTLE SOLIDS DUE TO STATIC LOADING, Int. J. of Fracture Mechanics, Vol. 6, No. 3, Sept. 1970, pp. 287-300.

Oh, A. L., and Finnie, I., THE RING CRACKING OF GLASS BY SPHERICAL INDENTERS, J. Mech. Phys. Solids, Vol. 15, 1967, pp. 401-411.

Olszak, W., and Urbanowski, W., THE PLASTIC POTENTIAL AND THE GENERALIZED DISTORTION ENERGY IN THE THEORY OF NON-HOMOGENEOUS ANISOTROPIC ELASTIC-PLASTIC BODIES, Arch. Mech. Stos., Vol. 8, 1956, pp. 671-694.

Olszak, W., and Urbanowski, W., PLASTIC NON-HOMOGENEITY - A SURVEY OF THEORETICAL AND EXPERIMENTAL RESEARCH, Proc. IUTAM Symposium on Non-Homogeneity in Elasticity and Plasticity, Pergamon Press, 1959.

Prager, W., PLASTIC FAILURE OF FIBER-REINFORCED MATERIALS, Trans. American Society of Mechanical Engineers, E 36, September 1969.

Priddy, T. G., A FRACTURE THEORY FOR BRITTLE ANISOTROPIC MATERIALS, Sandia Laboratories Report, November 1971.

Protasov, V. D., and Kopnov, V. A., STUDY OF THE STRENGTH OF GLASS-REINFORCED PLASTICS IN THE PLANE STRESS STATE, Mekhanika Polimerov, Vol. 1, No. 5, pp. 39-44, 1965.

Puppo, A. H., Evensen, H. A., STRENGTH OF ANISOTROPIC MATERIALS UNDER COMBINED STRESSES, AIAA/ASME 12th Structures, Structural Dynamics and Materials Conf., Anaheim, California, April 19-21, 1971.

Puppo, A. H., GENERAL THEORY OF FAILURE FOR ORTHOTROPIC MATERIALS, Engineering Report 69-E1, Whittaker Corp., April 1969.

Roesler, F. C., BRITTLE FRACTURES NEAR EQUILIBRIUM, Proc. Phys. Soc., Vol. 69, 1956, pp. 981-992.

Sandhu, R. S., A SURVEY OF FAILURE THEORIES OF ISOTROPIC AND ANISOTROPIC MATERIALS, Air Force Flight Dynamics Laboratory, Technical Report AFFDL-TR-72-71, January 1972.

Sawczuk, A., SOME PROBLEMS ON LOAD CARRYING CAPACITIES OF ORTHOTROPIC AND NON-HOMOGENEOUS PLATES, Arch. Mech. Stos., Vol. 8, 1956, pp. 549-563.

Sendeckyj, G. P., A BRIEF SURVEY OF EMPIRICAL MULTIAXIAL STRENGTH CRITERIA FOR COMPOSITES, TESTING AND DESIGN (Second Conference), ASTM STP 497, April 1971, pp. 41-51.

Sendeckyj, G. P., ON EMPIRICAL STRENGTH THEORIES, Presented at ASTM-NMAB Symposium on Predictive Testing, Atlantic City, N. J., June-July 1971.

Stowell, E. Z., and Liu, T. S., ON THE MECHANICAL BEHAVIOR OF FIBER-REINFORCED CRYSTALLINE MATERIALS, J. Mech. Phys. Solids, Vol. 9, 1961.

Tetelman, A. S., FRACTURE PROCESSES IN FIBER COMPOSITE MATERIALS, in COMPOSITE MATERIALS: TESTING AND DESIGN, American Society for Testing and Materials, ASTM STP 460, December 1969, pp. 473-502.

Tsai, S. W., STRENGTH CHARACTERISTICS OF COMPOSITE MATERIALS, NASA CR-224, April 1965.

Tsai, S. W., and Wu, E. M., A GENERAL THEORY OF STRENGTH FOR ANISOTROPIC MATERIALS, Journal of Composite Materials, Vol. 5, January 1971.

Tsai, Y. M., and Kolsky, H., A STUDY OF THE FRACTURE PRODUCED IN GLASS BLOCKS BY IMPACT, J. Mech. Phys. Solids, Vol. 15, 1967, pp. 263-278.

LIST OF SYMBOLS

| | |
|--------------------------|--|
| a | Major radius of the area of contact, in. |
| A_{11}, A_{12}, A_{22} | Terms which are a function of elastic properties of material (see Equation 17). |
| b | Minor radius of the area of contact, in. |
| C_R | Term which takes into account curvature effect (see Equation 3). |
| d | Diameter of a circular plate, in. |
| D | Nondimensional diameter of a circular plate $D = \frac{h}{a}$ |
| E | Young's modulus |
| F | Allowable strength of material, psi |
| G | Shear modulus, psi |
| h | Thickness of target, in. |
| H | Nondimensional thickness of a circular plate ($H = \frac{h}{a}$) |
| k_1, k_2 | Stiffness parameter for the impactor and the target, respectively, psi^{-1} |
| L | Length of cylinder, in. |
| m, n, s | Parameters which are functions of the principal radii of curvature of the impactor and the target (see Figure 2) |
| m_1, m_2 | Mass of the impactor and the target, respectively, $\text{lb-sec}^2/\text{in.}$ |
| N, N_1 | See Equations (8) and (9) |
| q | Surface pressure resulting from impact, psi |

LIST OF SYMBOLS (Continued)

| | |
|------------------|---|
| q_0 | Maximum surface pressure resulting from impact, psi |
| r | Radial coordinate or radius of plate |
| R | Nondimensional radius of the circular plate ($R = \frac{r}{a}$) (or radius of a cylinder, in.) |
| R_{1m}, R_{1M} | Principal radii of curvature of the impactor |
| R_{2m}, R_{2M} | Principal radii of curvature of the target |
| t | Time, sec |
| t_0 | Contact duration, sec |
| v_1 | Velocity of the impactor, in. /sec |
| v_2 | Velocity of the target, in. /sec |
| v | Approach velocity ($v = v_1 + v_2$), in. /sec |
| \bar{Y} | Average radius of the damage zone, in. |
| Y_R | Half width of the damage zone, in. |
| Y_Z | Depth of damage zone, in. |
| α | Displacement under impactor, in. |
| α_1 | Maximum displacement under an impactor, in. |
| $\dot{\alpha}$ | Derivative of α with respect to t |
| ϵ | Strain, in. /in. |
| ν | Poisson's ratio |
| ρ | Density of material, lb/in. ³ |
| σ | Normal stress, psi |
| τ | Shear stress, psi |

LIST OF SYMBOLS (Continued)

SUBSCRIPTS

| | |
|-----------------|--|
| x, y, z | Denote properties in rectangular coordinates |
| θ , r, z | Denote properties in cylindrical or polar coordinates |
| L, T, Z | Denote fiber, transverse and through-the-thickness (transverse) direction in filamentary composite |
| t, c | Denote tensile and compressive properties |
| 1, 2, 3 | Properties in principal coordinates of the material. If used with k, m, or R subscripts, 1 and 2 refer to the impactor and the target, respectively. |